

**Nanoparticulate silica: new adsorbents for  
PTE from aqueous media and VOCs from  
indoor air**

**Salah Ali Mahgoub Idris**

**May 2012**

**Nanoparticulate silica: new adsorbents for PTE  
extraction from aqueous media and VOCs from  
indoor air**

**Salah Ali Mahgoub Idris**

**Supervisor: Dr Lorraine T. Gibson**

**Department of Pure and Applied Chemistry**

**University of Strathclyde**

A thesis submitted to the Department of Pure and Applied Chemistry, University of Strathclyde, in part fulfilment of the regulations for the degree of Doctor of Philosophy (Ph.D).

**May 2012**

The copyright of this thesis belongs to the author under the terms of the United Kingdom Copyrights Acts as qualified by University of Strathclyde Regulation 3.51. Due acknowledgement must always be made of the use of any material contained in, or derived from, this thesis.

## Abstract

Mesoporous silica samples were synthesised and used as sorbents for VOCs. 4 VOCs were extracted from polluted air streams; toluene, ethylbenzene, cumene and dichlorobenzene. Extraction efficiencies were compared to a commercially available sorbent (Tenax TA) at different relative humidity (25 or 80 % RH) and at different flow rates (25, 50, 100, 150 or 200 cm<sup>3</sup> min<sup>-1</sup>). Silica adsorbents showed efficient performance at low RH, whereas Tenax-TA performed better at high RH.

A room temperature method of MCM-41 was developed producing a silica product which exhibited an ordered hexagonal mesostructure, large pore volume (up to 0.99 cm<sup>3</sup>/g), and unusually large pore size (up to 6.7 nm). Diethylenetriamine functionalised MCM-41 was used to extract Pb (II) ions from solution and showed significant adsorption capacity (up to 1000 μmol g<sup>-1</sup>). The sorbent was regenerated, and Pb (II) ions recovered, allowing reuse of the sorbent. Mercaptopropyl (MP) functionalised MCM-41 showed extremely efficient and selective adsorption for the removal of Hg (II) ions from water samples doped with a wide range of metal ions. Additionally a method was developed to remove Hg (II) ions from loaded MP-MCM-41. Finally, speciation and separation of Cr (VI) and Cr (III) ions from aqueous solutions was achieved using amino-propyl functionalised MCM-41. The maximum adsorption capacity at 111.1 mg g<sup>-1</sup> was calculated according to the Langmuir isotherm model. Silica materials with different pore sizes were used to extract Cr (VI) ions from water and the results were examined using kinetics models. Different adsorption behaviours were observed; of which the most significant conclusion was that MWD-samples of MCM-41 had a 2 step adsorption process; the first related to the diffusion of ions through the liquid to the sorbent surface and the second being the diffusion of ions through the large functionalised pores which explains the increased adsorption performance of MWD-MCM-41.

## Acknowledgments

First of all, I would like to express my deepest sense of gratitude to my supervisor Dr. Lorraine Gibson for her patient guidance, encouragement and excellent advice throughout this study.

I am thankful to Dr. Claire Robertson for her generous assistance during the first stage in this study. To the analytical chemistry staff: Dr. Christine Davidson, Dr. Alison Nordon and Prof. David Littlejohn for their useful discussions and advises during the course of this study. To Dr. Alan Kennedy for his assistance with powder X-ray diffractions (PXRD) results and to Dr. John Reglinski who was involved in the initial heavy metals work. To Dr. Pamela Allan and Craig King for their assistance of using the flame atomic absorption instrument and for allowed me use their lab. To Gavin Bain for his assistance of BET isotherms analysis. To Denise Gilmour for doing the micro analysis and her very nice welcome when always bring the samples to analysis. To Margaret Wilson who always kindly look after our chemicals orders. I am really very grateful to all the staff who mentioned above as they helped me a lot in this project. And to all people of pure and applied chemistry department for their technical assistance throughout the project.

I would like to thank all prof. Michael Morris, research group at Chemistry Department, University College Cork, Ireland (UCC) who made my visit there so worthwhile and for allowing me use their instruments for MCM-41 characterisation. Especially to Dr. Colm Mc Manamon for his assistance of BET isotherms results interpretations.

Thanks to everyone work at Scottish Environmental Technology Network (SETN), for allowed me use their ICP-AES instrument. Especially for Dr. Tanya Peshkur and Dr. Peter Anderson for their assistance with ICP-AES.

I also thank all members of the analytical chemistry postgraduate group for sharing experiences and knowledge and the excellent working atmosphere.

Finally, I take this opportunity to express my profound gratitude to my beloved parents (Ali Mahgoub Idris and Khadija Hamad Al-Musrati), my wife (Fariha Almadani), my daughters (Hanna, Monia and Asma) and my son Abu-Baker.

## Table of Contents

<b>Abstract</b> .....	<b>iii</b>
<b>Acknowledgments</b> .....	<b>iv</b>
<b>Chapter 1: Introduction to Mesoporous Materials</b> .....	<b>1</b>
<b>1.1 Porous Adsorbent Materials</b> .....	<b>2</b>
<b>1.2 Conventional sorbents used to extract pollutants from the environment</b> .....	<b>3</b>
1.2.1 Silica gel.....	3
1.2.2 Activated alumina .....	4
1.2.3 Activated Carbon .....	5
1.2.4 Molecular sieve zeolites.....	5
<b>1.3 M41S Adsorbent Materials: The Self Assembly Mechanism</b> .....	<b>6</b>
1.3.1 MCM-48 .....	9
1.3.2 MCM-50 .....	10
1.3.3 MCM-41: general preparation of ‘as-made’ material .....	10
1.3.4 Functionalisation of mesoporous silica materials .....	16
<b>1.4 SBA-15</b> .....	<b>19</b>
<b>1.5 Mesoporous silica material applications</b> .....	<b>20</b>
<b>1.6 Aim and objectives</b> .....	<b>23</b>
<b>Chapter 2: Theory of Instrumental Techniques</b> .....	<b>24</b>
<b>2.1 Techniques used for Material Characterisation</b> .....	<b>25</b>
2.1.1 Gas/N <sub>2</sub> adsorption technique.....	25
2.1.2 Powder X-ray diffraction (PXRD).....	31

2.1.3 Fourier Transform Infrared Spectroscopy (FT-IR) .....	33
2.1.4 Carbon, Hydrogen, Nitrogen, Sulfur (CHNS) Elemental Analysers .....	37
<b>2.2 Techniques used for analyte measurement.....</b>	<b>37</b>
2.2.1 Thermal desorption-gas chromatography-mass spectrometry .....	37
2.2.2. Flame atomic absorption spectrometry (FAAS) .....	46
2.2.3. Inductively Coupled Plasma - Atomic Emission Spectrometry ICP-AES.....	52
<b>Chapter 3: Experimental and Safety.....</b>	<b>62</b>
<b>3.1 Preparation of mesoporous materials .....</b>	<b>63</b>
3.1.1 MCM-41 preparation .....	63
3.1.2 SBA-15 preparation .....	63
<b>3.2 Characterisation of mesoporous silica material.....</b>	<b>64</b>
3.2.1 Power X-ray diffraction .....	64
3.2.2 BET isotherms .....	64
3.2.3 FTIR spectra.....	64
<b>3.3 Generation of known concentration of volatile organic compounds (VOCs) using a dynamic atmospheric chamber.....</b>	<b>65</b>
3.3.1 Determination of the theoretical concentration of VOCs produced in the sampling system. . . . .	67
3.3.2 Dynamic sampling experiments to collect VOCs from atmospheric chamber .....	67
3.3.3 Preparation of sorbent packed sampling tubes.....	68
3.3.4 Experiments used to collect analytes in a 100 cm <sup>3</sup> volume of air.....	70
3.3.5 Alteration of humidity of diluent air .....	70
3.3.6 Extraction efficiency experiments .....	70
3.3.7 Dynamic capacity (breakthrough) experiments .....	71

3.3.8 Analysis of sampling tubes by thermal desorption unit– gas chromatography – mass spectrometry (TDU-GC-MS).....	72
3.3.9 Preparation of calibration solutions for TDU-GC-MS instrument.....	74
3.3.10 Injection of calibration solutions into sampling tube by direct injection method .....	74
<b>3.4 Silica materials used for environmental remediation of polluted waters .....</b>	<b>76</b>
3.4.1 Functionalisation of MCM-41 procedure .....	76
3.4.2 Determination of the adsorption capacity of materials for metal ion removal from aqueous solution.....	77
3.4.3 The sorbent extraction efficiencies for metal ions mixed with multi element or real water samples.....	78
3.4.4 Determinations of metals ions in water using FAAS.....	79
3.4.5 Determination of metal ion concentrations in aqueous solution using ICP-AES .....	80
<b>3.5 Determinations of Cr specious in water using colorimetric method and inductively coupled plasma atomic emission spectroscopy (ICP-AES) .....</b>	<b>81</b>
3.5.1 Determination of chromium (VI) in water samples using the colorimetric method .....	81
3.5.2 Determination of total chromium Cr <sub>(Total)</sub> in water samples using ICP-AES .....	82
<b>3.6 Safety .....</b>	<b>83</b>
3.6.1 The analysis of heavy metals .....	83
3.6.2 The analysis of VOCs .....	83
<b>Chapter 4: MCM-41 synthesis using a novel preparation method.....</b>	<b>85</b>
<b>4.1 Introduction: Summary of conventional procedure used to prepare MCM-41.....</b>	<b>86</b>
<b>4.2 Experimental: Development of new laboratory method for the production of MWD-MCM-41.....</b>	<b>88</b>
<b>4.3 Results and discussion .....</b>	<b>89</b>
4.3.1 MCM-41 characterisation by XRD and N <sub>2</sub> adsorption isotherm .....	89



4.3.2 FTIR and elemental analysis of MCM-41 samples.....	93
<b>4.4 Conclusion .....</b>	<b>95</b>
<b>Chapter 5: Extraction of VOCs from indoor air using mesoporous silicate .....</b>	<b>96</b>
<b>5.1 Introduction: Volatile organic compounds in indoor air .....</b>	<b>97</b>
5.1.1 Sources of indoor VOCs .....	98
5.1.2 Sampling methods for indoor VOCs.....	98
5.1.3 Sorbents used for VOC sampling.....	100
5.1.4 Characterisation of indoor VOCs.....	102
5.1.5 Typical VOCs in indoor air.....	103
5.1.6 Using mesoporous silicates as a sorbent of VOCs from indoor air .....	104
5.1.7 Factors effecting the adsorption of VOCs onto sorbents .....	106
<b>5.2 Experimental .....</b>	<b>107</b>
5.2.1 Calculation of VOC emission rates from permeation vials and theoretical atmospheric concentrations generated inside exposure chamber .....	108
5.2.2 Calculation of atmospheric concentrations .....	109
5.2.3 Characterisation of mesoporous silicates .....	112
5.2.4 Calibration of TD-GC-MS .....	112
<b>5.3 Results and Discussion.....</b>	<b>117</b>
5.3.1 Comparison of experimentally calculated VOC masses with theoretically derived values .....	117
5.3.2 Comparison of collected analyte masses using different sorbents and a standard set of operating conditions at 25 % RH or 80 % RH.....	119
5.3.3 Dynamic adsorption capacity of sorbents (Breakthrough).....	120
5.3.4 Calculation of sorbent capacities .....	122
5.3.5 The relationship between RH and air sampling flow rate on VOC adsorption.....	124

<b>5.4 Conclusions</b> .....	<b>127</b>
<b>Chapter 6: Extraction of lead (II) ions from water samples using functionalised MCM-41</b> .....	<b>129</b>
<b>6.1 Introduction: The extraction of heavy metals from water</b> .....	<b>130</b>
6.1.1 The analysis of heavy metals in water using FAAS .....	130
6.1.2 Current methods used for the removal of heavy metals from water .....	131
6.1.3 Mesoporous silica sorbents for the removal of heavy metals .....	132
<b>6.2 Experimental</b> .....	<b>136</b>
6.2.1 Instrument Calibration .....	136
6.2.2 Preparation of silica materials for Pb (II) extraction.....	136
6.2.3 Experiments used to assess the extraction of Pb (II) from water .....	137
6.2.4 Regeneration of Functionalised MCM-41 .....	137
<b>6.3 Results and discussion</b> .....	<b>138</b>
6.3.1 The lead calibration data .....	138
6.3.2 Characterisation of materials .....	140
6.3.3 Lead adsorption extraction capacities of functionalised MCM-41 materials .....	142
6.3.4 Reutilisation of DETA-MCM-41 for repeated sorbent use and further removal of Pb (II) from contaminated water .....	145
6.3.5 Assessment of DETA-MCM-41 extraction efficiencies in real water samples .....	145
6.3.6 Assessment of DETA-MCM-41 extraction efficiencies in multi-elements samples ..	146
<b>6.4 Conclusions</b> .....	<b>149</b>
<b>Chapter 7: Selective extraction of mercury (II) from water using mercapto functionalised-MCM-41 and regeneration of the sorbent using microwave digestion</b> .....	<b>150</b>
<b>7.1 Introduction</b> .....	<b>151</b>

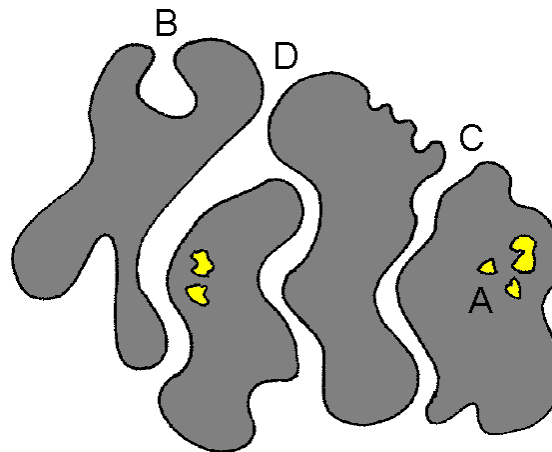
<b>7.2 Experimental .....</b>	<b>152</b>
7.2.1 Preparation of MCM-41 and functionalised-MCM-41 .....	152
7.2.2 Calibration data.....	152
7.2.3 Extraction of Hg (II) from solution using functionalised-MCM-41 .....	155
7.2.4 Experiments used to assess the selectivity of MP-MCM-41 towards Hg (II) in contaminated water samples .....	156
7.2.5 Recovery of Hg (II) from loaded sorbents using microwave digestion .....	156
<b>7.3 Results and discussion .....</b>	<b>158</b>
7.3.1 Parent Material characterisation.....	158
7.3.2 Mercury (II) extraction and adsorption capacities using spiked solutions of distilled water.....	160
7.3.3 The selectivity of MP-MCM-41 towards Hg (II) in the presence of other heavy metal ions.....	163
7.3.4 Removal of Hg (II) from loaded samples of MP-MCM-41 or DETA-MCM-41 and regeneration of the sorbent.....	165
<b>7.4 Conclusions.....</b>	<b>169</b>
<b>Chapter 8: Removal of Chromium (VI) from aqueous solutions .....</b>	<b>170</b>
<b>8.1 Introduction.....</b>	<b>171</b>
8.1.1 Adsorption of chromium species from water samples.....	171
8.1.2 Effect of pH on Cr (VI) adsorption.....	172
8.1.3 Adsorption kinetics study .....	172
8.1.4 Adsorption isotherms to study the maximum adsorption capacity .....	174
<b>8.2 Experimental .....</b>	<b>176</b>
8.2.1 Determination of Cr (VI) in water samples by colourimetry .....	176
8.2.2 Determination of total chromium (Cr <sub>Total</sub> ) in water samples using ICP-AES .....	177
8.2.3 Extraction of Cr from polluted water and regeneration of sorbent .....	180

<b>8.3 Results and discussion .....</b>	<b>181</b>
8.3.1 Extraction of Cr (III) and Cr (VI) from water: the effect of solution pH on the extraction efficiency.....	181
8.3.2 Kinetic study of Chromium (VI) adsorption onto AP-MCM-41 .....	183
8.3.3 Adsorption isotherms .....	188
8.3.4 Fourier-transform infrared spectroscopy.....	190
8.3.5 Preconcentration of Cr (VI) removed from water samples .....	192
8.3.6 Adsorption of Cr (VI) from real water samples .....	194
8.3.7 Selectivity of AP-MCM-41 towards Cr (VI) in the presence of other heavy metal ions.....	195
<b>8.4 Effect of meso-silica pore size distribution on extraction of Cr (VI).....</b>	<b>196</b>
8.4.1 Material characteristics .....	196
8.4.2 Adsorption study.....	199
8.4.3 Kinetic study .....	201
8.4.4 FTIR study .....	203
<b>8.5 Conclusions.....</b>	<b>205</b>
<b>Chapter 9: Conclusions and further work.....</b>	<b>206</b>
<b>9.1 Extraction of VOCs from indoor air .....</b>	<b>207</b>
<b>9.2 New method of MCM-41 preparation.....</b>	<b>208</b>
<b>9.3 Extraction of heavy metals from water using MWD-MCM-41 .....</b>	<b>209</b>
<b>9.4 Future work.....</b>	<b>210</b>
<b>References:.....</b>	<b>213</b>
<b>Publications from this work .....</b>	<b>230</b>

# **Chapter 1: Introduction to Mesoporous Materials**

## 1.1 Porous Adsorbent Materials

The design, synthesis and characterisation of ordered porous materials have been the subject of intense research for several decades now. Porous materials have the advantage of having a large surface area per unit weight. A qualitative description of porosity has been defined by the International Union of Pure and Applied Chemistry (IUPAC) Committee as that of a solid containing structure such as cavities, channels or interstices, which are deeper than they are wide. [1] A corresponding diagram is shown in Figure 1.1.



**Figure 1.1: Cross section of a hypothetical porous particle presenting various examples of porosity: closed pores (A); blind pores (B); through pores (C); and interconnected pores (D). [1]**

Materials consisting of cracks, cavities and channel networks of varying size, shape and connectivity can all be grouped under the large banner of ‘porous materials’. IUPAC had classified these porous materials depend on the size dimension. According to the standards, set IUPAC [1] definitions of porous materials can be divided into:

- Microporous materials, if their pore size is below 2 nm,
- Mesoporous materials, if their pore size is between 2 and 50 nm,
- Macroporous materials, if their pore size is bigger than 50 nm.

## **1.2 Conventional sorbents used to extract pollutants from the environment**

There are many materials have been used for extraction of pollutants air and also from water. The most important commercial adsorbents are:

- Silica gel,
- Activated alumina,
- Activated carbon, and
- Molecular sieve zeolites.

The uses of those sorbents is usually depends on their physicochemical properties and also on the properties of the target element or compound. For example silica gel and activated alumina were used widely for volatile organic compounds (VOCs) adsorption while zeolite has been used mainly for separation application due to a narrow pore size distribution.

Also the polarity of the surface usually was playing very important roles. Polar sorbents (hydrophilic) used to trap polar compounds and nonpolar sorbents (hydrophobic) are used for nonpolar compounds adsorbents.

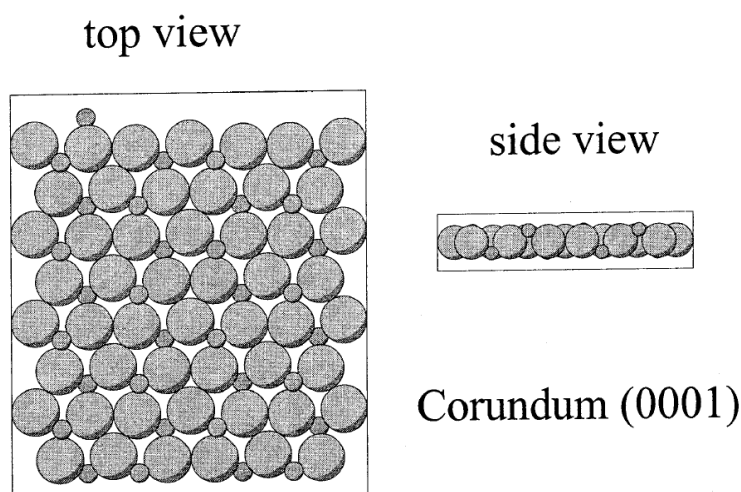
### **1.2.1 Silica gel**

Silica gel ( $\text{SiO}_2$ ) can be used as catalyst support [2] and a sorbent for heavy metals and VOCs [3-5]. The structure of silica gel consists of tetrahedral units of  $\text{SiO}_4$  connected by siloxane bridges  $\text{Si-O-Si}$  [2, 6].

The silica gel is a material of high superficial area, resistant, porous, formed of irregular particles (amorphous) [7]. The silica surface under normal conditions is covered with reactive hydroxyl groups  $\text{SiOH}$ , called silanol groups [7]. Silica gel is thermally stable (up to  $1000\text{ }^\circ\text{C}$ ) due to its structure (tetrahedron units) which hardly to be collapsed [8]. It is commercially available at relatively low costs and with dimensions of areas and varied pores.

### 1.2.2 Activated alumina

Activated aluminas are classified as porous materials which contain water and alumina with various concentrations. Activated aluminas are amorphous (or non-crystalline) in nature which make its structure less uniform. The pore system of Activated alumina consists of both mesopores and macropores. Alpha alumina, the only thermally stable oxide of aluminium, which has the corundum structure. Therefore, corundum is usually taken as a model system used to analyse the performance of different experimental or theoretical techniques.(Figure 1.2) [9].



**Figure 1.2: Top and Side view of the Al-terminated corundum surface. [9]**

Alumina has a unique combination of useful electrical and mechanical properties. Electrically, it possesses high resistivity (around  $10^{17} \Omega \text{ cm}$  at room temperature). Mechanically, alumina has very good hardness. The main feature for alumina is inert against attack from most chemicals and can be used in various environments. Alumina maintains these characteristics to high temperatures; the working temperature can be up to  $1500 \text{ }^\circ\text{C}$  [9].



### 1.2.3 Activated Carbon

Activated carbon (AC) is a synthetic carbon modification containing very small graphite crystallites and amorphous carbon. The pore diameters are usually less than 1 nm and form a very large surface area up to  $3000 \text{ m}^2 \text{ g}^{-1}$ .

AC is prepared from carbon-rich organic precursors by a thermal method (dry distillation) to form carbonised organic precursors, which can be activated to increase the pore volume either thermally or chemically:

**Thermal method:** Treatment at  $\sim 700\text{--}1000 \text{ }^\circ\text{C}$  in the presence of oxidising gases such as steam,  $\text{CO}_2$ , steam/ $\text{CO}_2$  mixtures, or air [10].

**Chemical method:** Treatment at  $\sim 500\text{--}800 \text{ }^\circ\text{C}$  in the presence of dehydrating substances such as  $\text{ZnCl}_2$ ,  $\text{H}_3\text{PO}_4$ , or  $\text{KOH}$ , which are leached out afterwards [10].

### 1.2.4 Molecular sieve zeolites

Zeolite molecular sieves are crystalline, highly porous materials, which belong to the class of aluminosilicates (Figure 1.3).

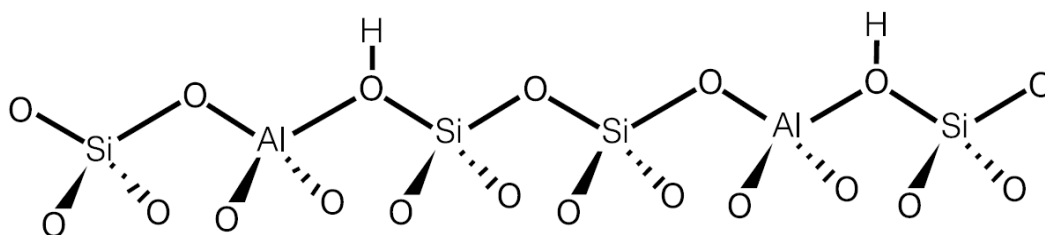
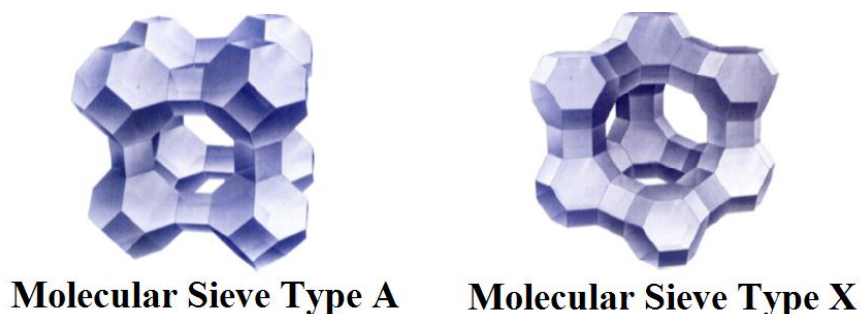


Figure 1.3: Schematic representation of a zeolite in the H form. [7]

These crystals are characterised by a three-dimensional pore system, with pores of precisely defined diameter. The corresponding crystallographic structure is formed by tetrahedras of (AlO<sub>4</sub>) and (SiO<sub>4</sub>). These tetrahedras are the basic building blocks for various zeolite structures, such as zeolites A and X; the most common commercial adsorbents (see Figure 1.4).



**Figure 1.4: The most common zeolite structures. [11]**

Due to the presence of alumina, zeolites exhibit a negatively charged framework, which is counter balanced by positive cations resulting in a strong electrostatic field on the internal surface. These cations can be exchanged to fine-tune the pore size or the adsorption characteristics.

### **1.3 M41S Adsorbent Materials: The Self Assembly Mechanism**

In recent years, silica based M41S adsorbents have been receiving more attention as adsorbents due to their high mechanical strength, low cost and ease of material preparation. Silica materials contain silanoxy bridges ( $\equiv\text{Si-O-Si}\equiv$ ) in their framework and silanol functional groups ( $\equiv\text{Si-OH}$ ) distributed on the surface as a result of incomplete condensation.

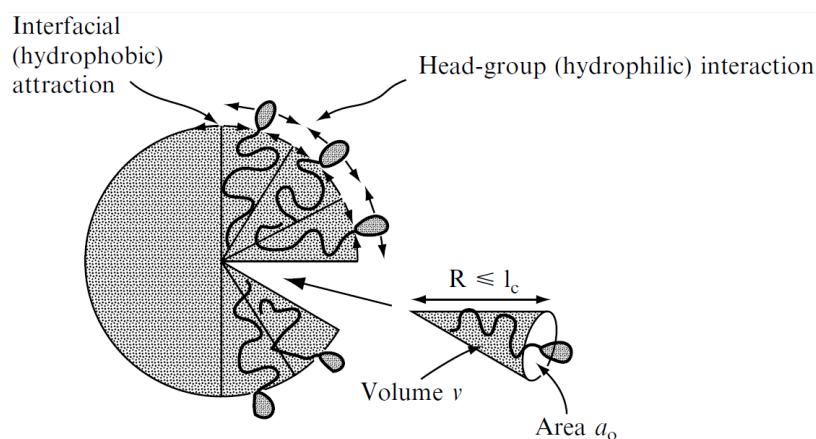
The number of silanol groups present on the surface of the material is controllable: a decrease in silanol groups is achieved by thermal treatment which causes increased condensation of silanol groups. The condensation reaction is reversible and silanol groups can be reintroduced by hydration [12].

With silica mesoporous materials, the general mechanism of formation involves the arrangement of silica around a surfactant template. Beck and co-workers [13, 14] suggested a liquid-crystal templating (LCT) mechanism for the formation of silica mesoporous materials. In the LCT mechanism, the condensation of a silica precursor was not the driving factor for the formation of the mesoporous structure [15]. The amphiphilic molecules organized themselves in liquid crystal phases independently of the inorganic crystallization, and the polymerization of the silica precursor took place around the self-assembled template [16]. The LCT was the important mechanism when the surfactant concentration was so high that the liquid crystals were already formed when the inorganic precursor starts organizing itself around them [17]. Surfactants may be classified into four different groups, depending on the nature of the polar head group: anionic surfactants, cationic surfactants, zwitterionic surfactants and non-ionic surfactants [18]. However the most common surfactants used to generate M41S materials are quaternary ammonium ions with long alkyl chains (generally a hexadecyl group).

The shape of micelle produced in water depends on the surface packing:[19]

$$v/al$$

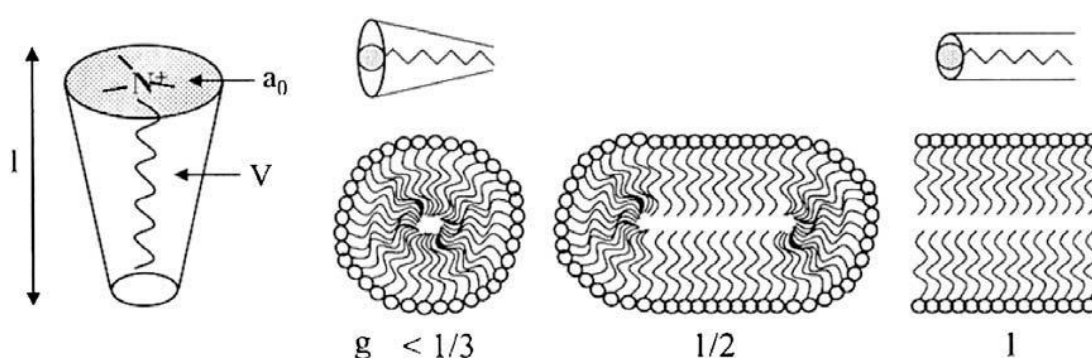
where  $v$  is surfactant tail's volume,  $a$  is the surfactant head group area and  $l$  is the length of surfactant tail, (see Figure 1.5)



**Figure 1.5: illustration of the surfactant packing parameter. [20]**

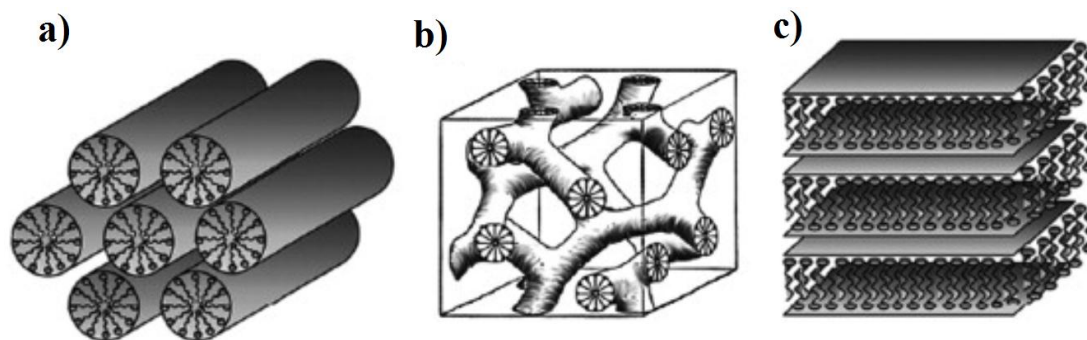
The size of the surfactant tail and the head group play important roles in packing the surfactant together to form micelles of different shape [18, 20]. Therefore changing the surfactant tail to head ratio will result different micelle geometry as can be seen in Figure 1.6. When the packing parameter is below  $1/3$ , spherical micelles are found in solution. By increasing the concentration of the surfactant the spherical micelles arrange themselves in solution to produce a three-dimensional, cubic form. By increasing the  $v/al$  ratio greater than  $1/3$  the formation of a rod-like shape will take place. As the surfactant concentration continues to increase these rod-shaped micelles will assemble together into a hexagonal array to produce a hexagonal liquid crystal. When the  $v/al = 1$  (the size of the head group and tail are equal), the surfactants form a sheet-like, three-dimensional liquid crystal, with lamellar cubic structures. And finally if  $v/al$  is more than 1, the surfactants form reversed systems.

Chiola et al.[21], first reported a procedure to synthesis mesoporous materials in 1969. Di Renzo et al.[22] prepared a solid by following the instructions given by Chiola et al, and found that it led to a mesoporous material which Beck et al.[13, 14] and co-workers had already produced in 1992 at the laboratories of Mobil Oil Corporation. This new family of mesoporous materials, which was called M41S, has many advantages including, large pores (from 2 to 100 nm) and high surface areas (above  $1000 \text{ m}^2 \text{ g}^{-1}$ ).



**Figure 1.6: Schematic representation of the values of the packing parameters.**  
[23]

MCM-41 was denoted to the material possessing a hexagonal phase consisting of long cylindrical channels. MCM-48 was denoted for the cubic phase of the mesoporous material and consists of a three-dimensional channel structure that is arranged in a gyroid minimal surface, and MCM-50 was denoted for a meso-lamellar phase. See Figure 1.7.



**Figure 1.7: M41S family: a) MCM-41, b) MCM-48 and c) MCM-50. [24]**

### 1.3.1 MCM-48

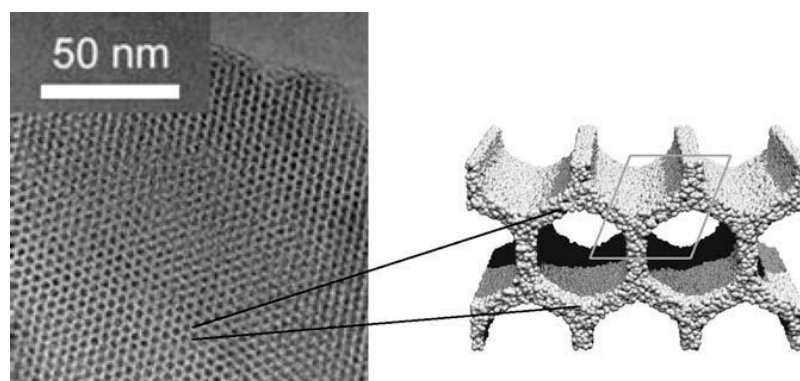
MCM-48, the second important member behind MCM-41 in the M41S family, contains two independent three-dimensional pore systems, which are interweaved and situated in a mirror-plane position to each other [25]. The special pore systems provide favourable mass transfer kinetics in catalytic and separation applications than MCM-41 with a one-dimensional hexagonal directional pore system [26]. However, the formation of MCM-48 requires critical synthesis conditions and large amount of surfactant (molar ratio of CTAB/SiO<sub>2</sub>=0.55–1.5) while using single cationic surfactant as template. In order to overcome the synthetic difficulties, much effort has been made to develop its synthesis methods, such as the use of mixed or surfactants [27, 28] and adding organic additive into the initial solution [29]. However, still the reproducibility the main concern about MCM-48 preparation and also the cost is a bit higher than MCM-41 which still makes the MCM-41 more economical and large-scale production.

### 1.3.2 MCM-50

Lamellar MCM-50 was included as a member of the original M41S family of surfactant-templated silicas. But according to the difficulty associated with the template removal by losing the mesoporous structure (pore collapse), MCM-50 has not been well studied as other M41S members [30, 31]. However, recently a few papers have described new methods for preparing MCM-50 materials with stable mesoporous structure, even after removing the template. For example by using,  $\alpha$ , $\omega$ -diamine bolaamphiphiles as templates [32], demonstrated that as-made lamellar framework structures were stable and the surfactant removal can be obtained through direct supramolecular assembly processes owing to cross-linking of the lamellae by laterally spaced pillars and also it has been found that the electrically neutral EO<sub>20</sub>PO<sub>70</sub>EO<sub>20</sub> block co-polymer (Pluronic 123) is capable of templating a lamellar framework, but only when this surfactant is used in conjunction with a co-surfactant such as an aliphatic [33, 34] or aromatic hydrocarbon [35], or a mixture of anionic and cationic surfactants [36].

### 1.3.3 MCM-41: general preparation of ‘as-made’ material

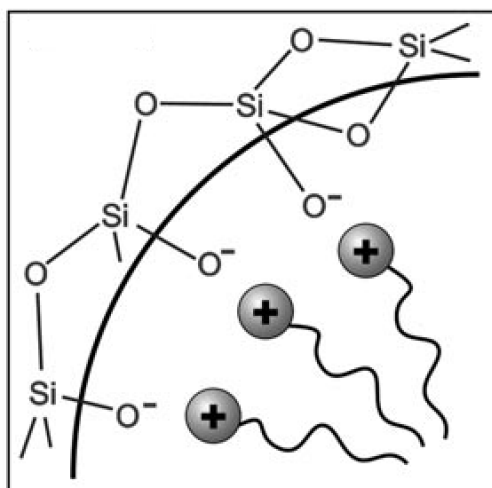
MCM-41 (see Figure 1.8) is the most famous member of the M41S family. It has an ordered structure with uniform mesopores which are arranged into a hexagonal (honeycomb-like) porous structure separated by thin silica pore walls of approximately 1 – 1.5 nm. MCM-41 can be obtained using surfactants which are amphiphilic molecules consisting of a hydrophilic, polar, head group and a hydrophobic, non-polar tail.



**Figure 1.8: TEM image of the honeycomb structure of MCM-41 and a schematic representation of the hexagonal shaped one-dimensional pores. [23]**

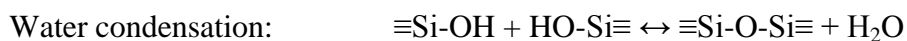
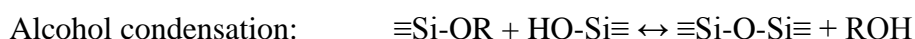
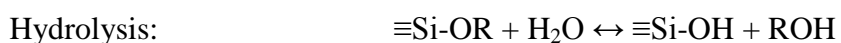
Various sources of silica can be used for MCM-41 preparation, for example the organic silicon alkoxides. After the micelles are obtained and rod-shaped micelles are created the silicate source is added, where it will diffuse on the surface of the micelles because of an electrostatic attraction between the surface of the surfactant micelle and the silicate source (see Figure 1.9).

The concentration of silicate anions on the surface of the micelles will increase very quickly and start to condense creating a monolayer of silicate around the micelles. At this stage the silica "coated" micelles start to cluster together by condensation reactions between the silica layers of individual micelles, thus generating the classic 'MCM-41' framework.

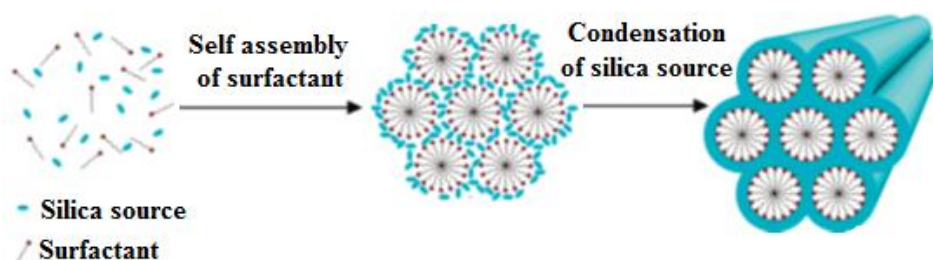


**Figure 1.9: The diffusion of silicate anions on the surface of the micelles. [24]**

General reaction mechanisms that describe the condensation of silicon alkoxides (hydrolysis and condensation) are given below [37, 38]:



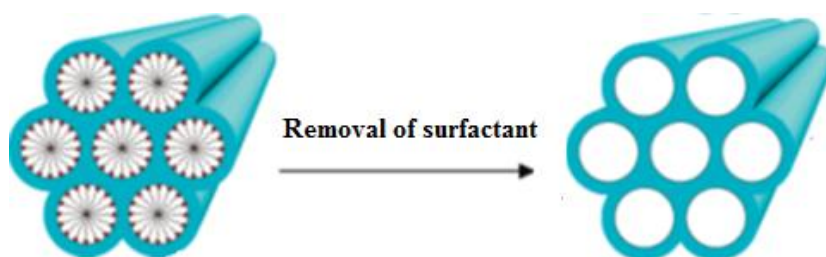
MCM-41 produced by this reaction method always have amorphous pore walls and two or three silica monolayers on the surface of the micelles [39]. The processes described above can take place over a wide range of synthesis conditions including different, gel composition (surfactant: silica ratio), pH, reaction time, temperature and pressure. A simplified procedure for typical MCM-41 synthesis is shown in Figure 1.10, and this material is generally referred to as ‘as-made MCM-41’. At this stage in the process the pores are still filled with the organic surfactant micelles.



**Figure 1.10: The typical MCM-41 synthesis procedure. [40]**

### ***1.3.3.1 Removing the organic template from ‘as-made’ MCM-41***

In order to obtain a material that contains mesoporous the micelles, or the organic template, must be removed [15-17] as illustrated in Figure 1.11.



**Figure 1.11: The last step in the MCM-41 preparation (template removal).**



Removal of the organic template is usually performed by calcination [41], solvent extraction [42] or microwave digestion [43].

Calcination is arguably the most common method of template removal and this step usually takes place under thermal conditions using a muffle furnace at temperatures between 500 and 700 ° C, under an air atmosphere [41, 44-47]. This procedure will remove the template completely although it is decomposed and therefore cannot be reused.

An alternative procedure for removing the template is by solvent extraction using low temperature refluxing [48, 49]. The main advantage of the solvent extraction procedure is to allow the surfactant to be removed without decomposition, giving the opportunity for the surfactant to be reused, [50, 51]. Disadvantages however include the use of liquid solvents and the need to perform the extraction more than once to ensure complete removal of the template.

Other researchers have used less common techniques such as supercritical fluid extraction (SFE) with CO<sub>2</sub> in the presence of solvents [52-55].

More recently, Bozhi et al.[56] and Gu et al.[43] used microwave digestion to remove an organic template with a mixture of HNO<sub>3</sub> and H<sub>2</sub>O<sub>2</sub> as the oxidative agents.

A literature review of MCM-41 preparation has shown that almost all research groups refer to the original preparation method published in 1992 [13, 14], but some modifications also have been reported to enhance the physicochemical properties for MCM-41. Table 1.1 summarises the wide range of different conditions used to prepare MCM-41 and indicates the type of mesoporous silica obtained.

**Table 1.1: Modifications used to prepare M41S materials.**

No.	Surfactant	pH adjustment	Silica source	Condensation time and temperature	Method of template removing	Characterisation			Mesoporous Silica Obtained	Ref.
						$S_{\text{BET}}$ ( $\text{m}^2 \text{g}^{-1}$ )	$V_p$ ( $\text{cm}^3 \text{g}^{-1}$ )	Pore size (nm)		
1	CTAB	TMAS	TEOS	48 h at 150 °C	Calcination at 540 °C for 7 h	1040	-----	3.70	MCM-41	[14]
2	CTAB	diethylamine	TEOS	72 h at 100 °C	Calcination at 550 °C for 6 h	1012	0.91	2.73	MCM-41	[57, 58]
3	CTAB	aqueous ammonia	TEOS	12 h at 90 °C	Calcination at 550 °C for 5 h	1070	0.85	3.19	MCM-41	[59]
4	CTAB	sodium hydroxide	TEOS	72 h at 110 °C	Calcination at 550 °C for 6 h	1000	1.0	3.50	MCM-48	[60-62]
5	CTAB	TAAB & sulfuric acid	fumed silica	168 h at 100 °C	Calcination at 550 °C for 6 h	1136	0.61	2.26	MCM-41	[63]
6	CTAB	HCl	soluble glass	24 h at 120 °C	Calcination at 550 °C for 6 h	-----	-----	-----	MCM-41	[64]

7	MTAB	sodium hydroxide	sodium silicate	1 h Microwave at 100 °C	Calcination at 550 °C for 6 h	1020	0.745	2.10	MCM-41	[65]
8	DDAB	methanol	TMOS	0.5 h at pH=3	Without removing the template	-----	-----	-----	MCM-50	[30]
9	CTMACl	aqueous ammonia	TEOS	24 h at 100 °C	Solvent extraction ethanol/HCl	1003	0.35	2.50	MCM-41	[66]
10	CTAB	sodium hydroxide	TEOS	72 h at 100 °C	Solvent extraction ethanol/80 °C	950	0.31	2.28	MCM-48	[67]
11	HDTMAB	sodium hydroxide	TEOS	10 h at 100 °C	Solvent extraction ethanol/HCl	1070	0.664	2.42	MCM-41	[68]
12	CTAB	sodium hydroxide	TEOS	96 h at 100 °C	supercritical fluid	destroyed after applying supercritical fluid			MCM-48	[69, 70]
13	CTAB	TEAOH	sodium silicate	96 h at 96 °C	supercritical fluid	1332	0.81	2.92	MCM-41	[69, 70]

### Abbreviations used in table 1.1:

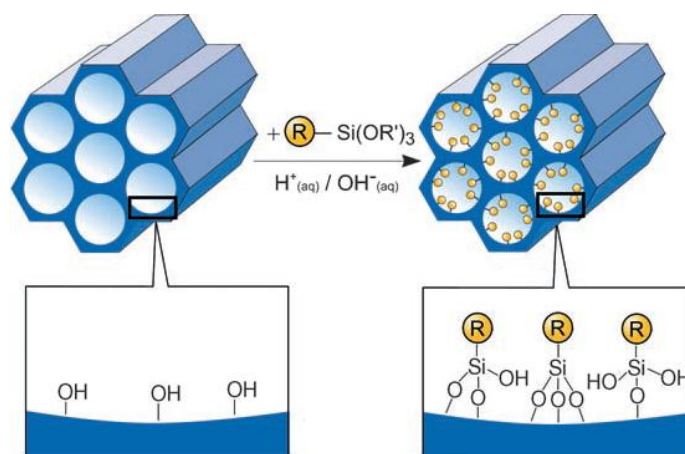
BET surface area	:	$S_{\text{BET}}$
pore volume	:	$V_p$
Cetyl trimethyl ammonium bromide	:	CTAB
Tetramethylammonium silicate	:	TMAS
Tetraethyl orthosilicate	:	TEOS
tetraalkylammonium bromide	:	TAAB
soluble glass	:	SiO <sub>2</sub> :28.2%, Na <sub>2</sub> O:8.7%
didodecyldimethylammonium bromide	:	DDAB
silicon tetramethoxide	:	TMOS
cetyl trimethylammonium chloride	:	CTACl
hexadecyltrimethylammonium bromide	:	HDTMAB
Tetraethylammonium hydroxide	:	TEAOH
Myristyltrimethylammonium bromide	:	MTAB

### **1.3.4 Functionalisation of mesoporous silica materials**

Mesoporous silica materials are often modified by the addition of chelates onto the surface of the material to increase their use in adsorption and catalysis. In general, two basic approaches for organic moiety incorporation have been used and include (i) post-synthesis grafting and (ii) co-condensation methods [71].

#### ***1.3.4.1 Post-synthesis grafting [24, 71-73]***

Mesoporous silica functionalisation has been widely achieved by grafting the functional organic moiety onto the surface and/or pore walls. Grafting is a method of covalently linking reactive organosilane species with surface silanol groups (free and terminal silanols), as shown in Figure 1.12.



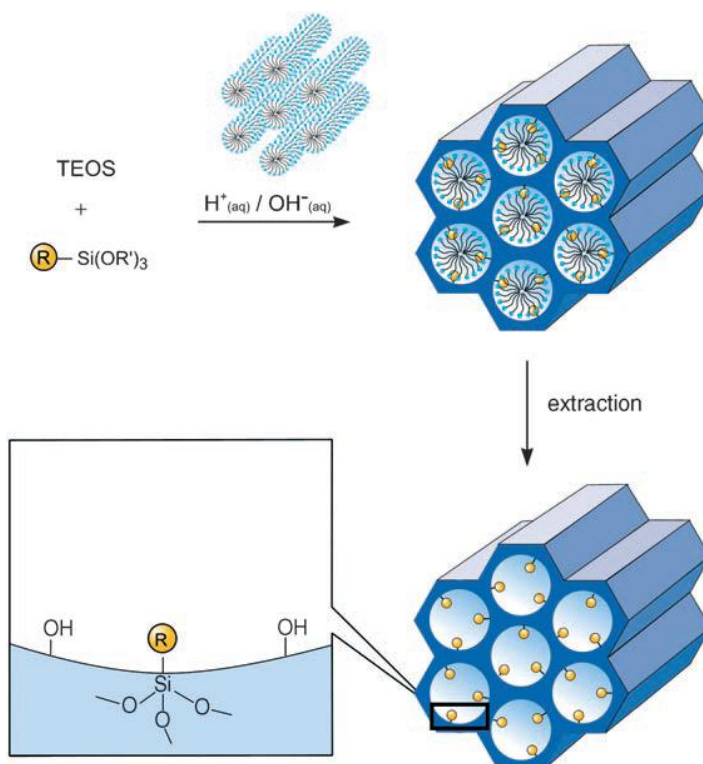
**Figure 1.12: Schematic diagram illustrate functionalization of MCM-41 by the grafting method. [24]**

The typical synthesis involves two steps, obtaining mesoporous silicates and grafting functional groups. The first step should involve the removal of physically-adsorbed water from hollow-out mesoporous silicates by heating at 100~130 ° C in a vacuum. The material is then dipped in an inert organic solvent to react the functional groups with the organosilane via a covalent condensation reaction. The organic functional mesoporous silicates are finally achieved by washing, filtering and drying [71]. The main advantage of this method of functionalisation is the possibility to choose a wide variety of organic functional groups (R) without any restriction. In addition, one batch of MCM-41 can be used to obtain a wide range of functionalised mesoporous silica materials. The main disadvantage of this method is that the size of functional group needs to be taken into account to prevent functionalization on the outer surface of the material only and not inside the pores. There is also the possibility of pore closure (pore blocking). When functionalised-MCM-41 is prepared in this way and the material is used as an adsorbent this process is normally referred to as immobilisation [74].

#### **1.3.4.2 Co-condensation functionalization (direct synthesis) [24, 71-73, 75]**

Co-condensation is a synthetic approach in which silane (R'O)<sub>4</sub>Si and organosilane (R'O)<sub>3</sub>Si-R (where R' is Et or Me and R is non-hydrolysable ligand) precursors co-

assemble with amphiphilic surfactants, as shown in Figure 1.13. Different organic functional groups can then be readily introduced into the mesoporous silica [76, 77]. This approach allows anchorage organic functional ligands on the mesopore walls in a single step, enabling a higher and more homogenous surface coverage of organosilane functionality. Inorganic silane  $(R'O)_4Si$  is used to construct the pore wall because the three-connected organosilane itself cannot build the infinite framework. Selective removal of the surfactant by extraction with solvents such as methanol, ethanol, THF, etc., generates the mesoporous silicate with controlled pore surface functionalisation. In the co-condensation method pore blocking is not a problem and furthermore the organic functional groups are generally more homogeneously distributed on the surface compared with grafting method. However, the co-condensation method has also some disadvantages: in general, an increase in the concentration of the organic functional group is limited as high concentrations could lead to micelles destruction. Moreover, over-loading of the incorporated organic groups can lead to a reduction in the pore diameter, pore volume, and surface area of the material.



**Figure 1.13: Organically functionalised mesoporous silicates using co-condensation procedure. [24]**

## 1.4 SBA-15

There have been growing demands for new types of mesoporous silica materials after the discovery of the M41S family of materials [13, 14]. A novel material, SBA-15, was first synthesized by the research group lead by Stucky [50, 51] at UC-Santa Barbara. SBA-15 earned much attention over the last decade owing to its excellent thermal stability, variable pore sizes, and tailored particle morphology. The pore topology consists of a two dimensional mesoporous network of uniform dimensions formed by microporous walls.

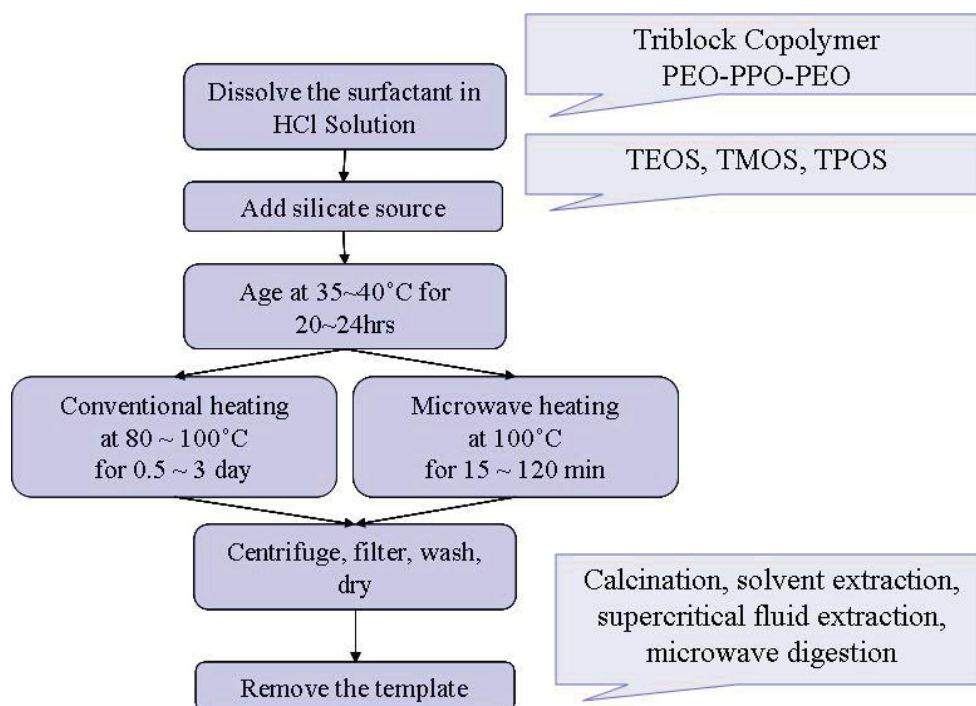
Compared to zeolites which have pores in the micro-range (4~14Å), SBA-15 material is a new type of mesoporous material with micropores, hence it is expected to lower the diffusion limitation that a microporous material typically experiences. Zeolites are crystalline while SBA-15's pore walls are essentially amorphous; however, the mesopores of SBA-15 material are regularly spaced due to the templates liquid crystal micelle arrangement [78].

The two most prevalent block lengths used for templating are Pluronic P123 (EO<sub>20</sub> PO<sub>70</sub>EO<sub>20</sub>) and Pluronic F127 (EO<sub>106</sub> PO<sub>70</sub>EO<sub>106</sub>). The external PEO blocks are the more hydrophilic portions and the internal PPO is more hydrophobic. The micelle is constructed with a hydrophobic PPO core surrounded by the hydrophilic PEO blocks. The length of the PEO block mainly determines the phase mesostructure and the silica wall thickness. The pore size can be tailored by varying the length and hydrophobicity of this block, and these surfactants can produce some of the largest pore diameters [51].

The aqueous silica cations locate themselves within the hydrophilic regions of the self-assembled system and associate preferentially with the PEO blocks. Removal of the polymer results in a mesoporous solid due to the hexagonal arrangement of cylindrical polymer aggregates and also microporosity generated by PEO segments [78]. Using these non-ionic block copolymers as surfactants, ordered mesoporous silica materials with large pore diameters (4-30 nm) can be obtained.

The process to obtain solid powder SBA-15 (Figure 1.14) involves dissolution of the template polymer in acidic solution, adding a silica source, which is typically tetraethyl orthosilicate (TEOS), tetramethyl orthosilicate (TMOS), or sodium silicate.

The mixed solution is aged at a temperature slightly above room temperature for 20 to 24 h and heated up to 80 to 100 ° C either in a conventional oven or in a microwave oven for an appropriate amount of time. Precipitated solids are centrifuged, washed and dried. Finally, the organic polymer is removed using one of the methods as outlined for M41S materials in Section 1.3.3.1 and can be functionalised as discussed in Section 1.3.4.



**Figure 1.14: A simplified procedures to obtain SBA-15.**

## 1.5 Mesoporous silica material applications

MCM-41 material has been used extensively for adsorption or separation applications. Functionalised MCM-41 has been used to extract mercury and cadmium from different gas streams [79], or heavy metal ions from waste water [80-82]. Functionalised MCM-41 also showed the ability to be regenerated in many cases, and the regeneration process was carried out using simple techniques like washing with alkaline or acid solutions [83-87].



A mesoporous silica material was also used to selectively adsorb/desorb biomolecules [88-90]. Zhao et al.[91] reported the use of MCM-41 as an adsorbent for removing of VOCs from indoor air even at high humidity and it was found that its performance was better than the reported values for zeolites or activated carbon. This increase in performance was attributed the larger pore size and surface areas of the silica mesoporous materials. Mesoporous silica has also been used to separate peptides and proteins [92] and CO<sub>2</sub> from CH<sub>4</sub> in the gas mixture [93].

Using unmodified MCM-41 as a catalyst is of limited use because the material is electrically neutral. However, when elements such as aluminium [94], titanium [95], zirconium [96], vanadium [97] or cobalt [98] has been incorporated into MCM-41, various catalytic applications have been reported which showed compatible properties to commercially porous material. Trivalent metals, such as Al<sup>3+</sup> or Fe<sup>3+</sup> ions have been incorporated onto the channel walls of MCM-41 leaving a negatively charged framework [96], providing acidic sites for catalysis. On the other hand if the silicon atoms are substituted with tetravalent metal ions, like Ti<sup>4+</sup>, V<sup>4+</sup>, or Zr<sup>4+</sup>, the charged material can be used in the oxidation of organic compounds [99]. MCM-41 incorporated with aluminium, have been used as supports for acidic catalytic reactions [100].

Over the last 20 years mesoporous silica has been used for various other applications such as; ion conductors for batteries or fuel cells [101], electron conductors [102] or sensors [103]. Li and Nogami [104] reported the importance of a cubic mesostructure for proton conductivity. Huang et al.[105] succeeded in synthesising silver nanowires inside the channels of mesoporous silica. Since the first report on the M41S family of silica based mesoporous materials in 1992 an extensive number of studies have been performed using MCM-41. Many reports have focussed on material synthesis with the aim of further improving the bulk properties of the material.

Using the Science Direct search engine, it was noted that a total of 17810 papers were published with MCM-41 as a keyword, between 1992 and 2012. For SBA-15, the number of papers reported was approximately 8300 papers; publication date started from 1998. Figure 1.15 illustrates the continued interest in both MCM-41 and SBA-15 as the numbers of publications in this field are still increasing year to year.

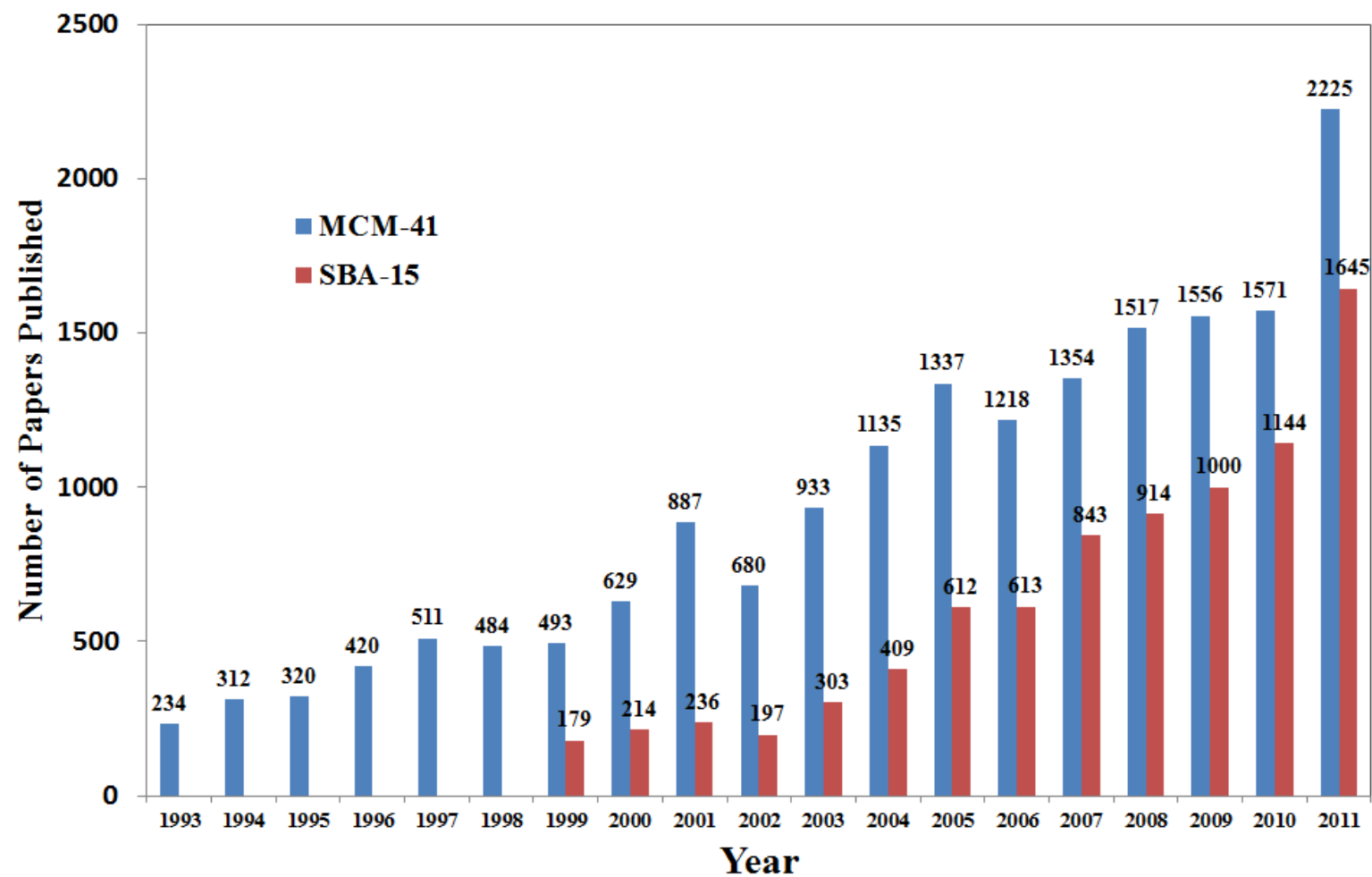


Figure 1.15: The number of papers published verses year for MCM-41 and SBA-15.

## 1.6 Aim and objectives

The aim of this work described here was to develop a method of MCM-41 production which is faster, more economical and provides larger masses of sample in batch production. Moreover, the target application areas in this research were adsorption studies: extraction of potentially toxic elements (PTE) from water samples and extraction of volatile organic compounds (VOCs) from indoor air. Hence the ultimate aim of this work was to obtain a fast method of MCM-41 production (as-made MCM-41 and template removal) with larger pores, wide pore size distribution and increased surface silanol groups that could be functionalised significantly enhancing the material's adsorption properties. The objective was to determine if the novel sorbents synthesised could have improved capacities than those previously reported in the literature, providing a new possible approach for the removal of heavy metals from aqueous solution. Also in order to compare the efficiency of MCM-41 with commercial sorbents for extraction VOCs from indoor air, there are main objectives associated with this research which is study the effect of relative humidity (25 and 80 %RH) and flow rate to adsorb VOCs onto the sorbents and Compare the adsorption capacity (5% breakthrough) and adsorption rate (dynamic adsorption capacity) of sorbents at different relative humidities.

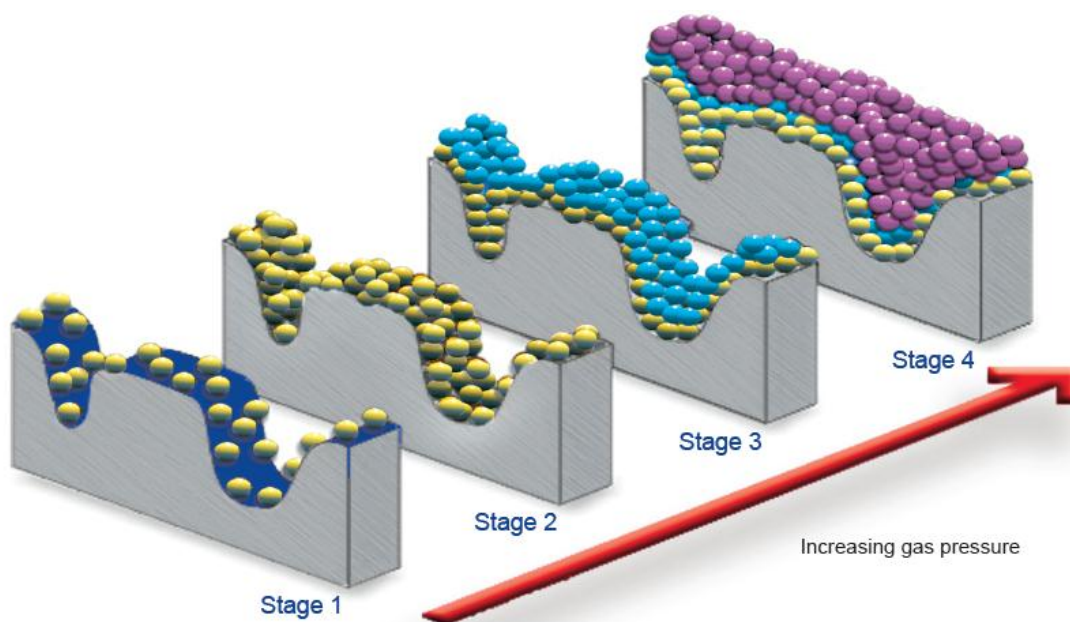
Therefore the thesis has divided into 9 chapters. Chapter 1 provides an overview of the literature on synthesis, properties, functionalisation and applications of mesopores silicate materials. Chapter 2 and 3 present an overview of instrumental and experimental methods employed in this work. Chapter 4 gives full details about new method to prepare mesoporous silicate based on the preparation of MCM-41 and using microwave digestion for organic template removal. Chapter 5 demonstrates that mesoporous silicate materials outperform a commercially available sorbents (Tenax TA) in trapping VOCs from air samples under low humidity conditions. Chapter 6, 7 and 8 highlight the benefit of using functionalised mesoporous materials for extraction Pb(II), Hg(II) and Cr(III)/(VI) ions from aqueous solutions including environmental samples. Chapter 9 presents the thesis conclusions and the future work.

## **Chapter 2: Theory of Instrumental Techniques**

## 2.1 Techniques used for Material Characterisation

### 2.1.1 Gas/N<sub>2</sub> adsorption technique

The Gas/N<sub>2</sub> adsorption technique, especially Brunauer-Emmett-Teller isotherm model (BET isotherm) is normally used for the determination of surface area and pore size of porous materials. To understand the principle of this technique, the gas adsorption theory should be known. This theory describes the dependence of the surface coverage of an adsorbed gas on the pressure of the gas above the surface at a fixed temperature. Whenever a gas is in contact with a solid there will be an equilibrium established between the molecules in the gas phase and the corresponding adsorbed species (molecules or atoms) which are bound to the surface of the solid. Figure 2.1 shows the four stages which can occur on the surface of porous materials during the adsorption process [106].



**Figure 2.1: Adsorption stages on porous material. [106]**

Briefly, at stage 1 the isolated sites on the adsorbent start to adsorb the molecules at low pressure. And by increasing the pressure (stage 2), all isolated sites will be covered to produce one layer of molecules on the adsorbent surface (monolayer). At stage 3, increasing the gas pressure will result in multi-layer coverage. At this stage

the surface area can be calculated according to the BET equation. Finally at stage 4, a further increase of the gas pressure will cause complete coverage of the sample and fill all the pores. At this stage, the Barret-Joyner-Halenda (BJH) calculation can be used to determine pore diameter, volume and distribution.

### 2.1.1.1 General classification of adsorption isotherms

Adsorption isotherms are divided into six different categories according to IUPAC [107] (Figure 2.2). Type I is associated with microporous solids, type III, V and VI are uncommon isotherms, but still obtained in special cases. Type II refers to a non-porous or macroporous material and Type IV isotherms are typical for mesopores. Hysteresis loops are seen in the isotherms of type IV and V. The different hysteresis corresponds to the different pore shapes: H1: spheres of approximately the same size, H2: ‘ink bottle’ pores, larger pores connected via smaller pores, H3: slit-shaped pores and H4: narrow slit-like pores [107].

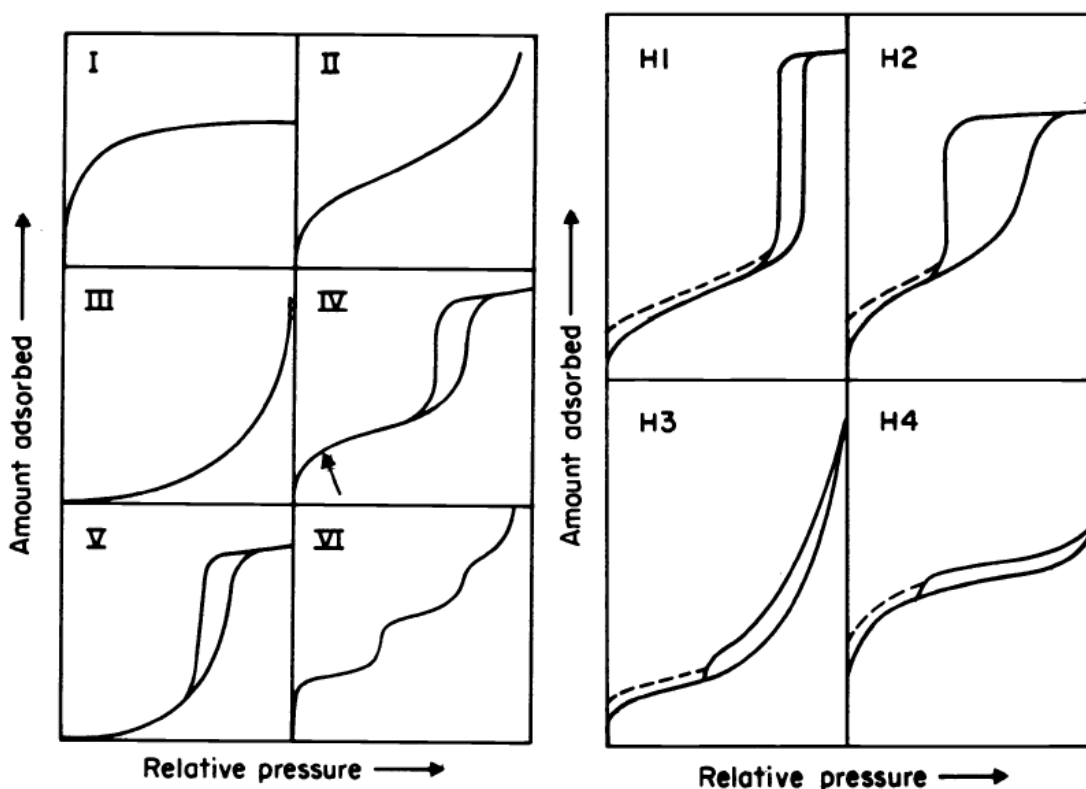
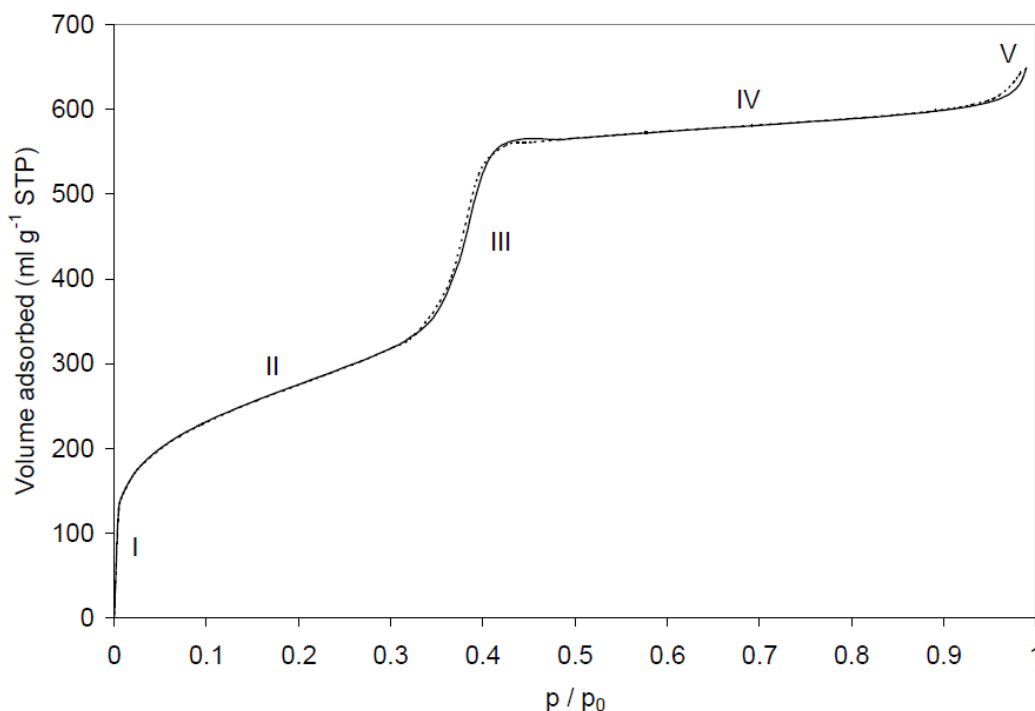


Figure 2.2: Different types of isotherms and hysteresis loops. [107]

### 2.1.1.2 Interpretation of nitrogen isotherms obtained from MCM-41[108-110]

A typical nitrogen isotherm for MCM-41 is shown in Figure 2.3. Both the adsorption (straight line) and desorption (dotted line) curves are shown. Five distinct regions can be discerned in this graph.



**Figure 2.3: A typical nitrogen isotherm for mesoporous MCM-41.**

At very low relative pressures ( $p/p_0$ ) a very large amount of nitrogen becomes physisorbed (region I). This region can be assigned to a monolayer adsorption of nitrogen on both on the external surface and inside the mesopores. A large amount of nitrogen starts to be adsorbed at region II, which can be assigned to the formation of multilayers and those multilayers take place both internally (in the pores) and on the external surface. Data collected at this stage can be used for surface area calculations. At region III the volume of nitrogen adsorbed increasing sharply can be assigned to the condensation of nitrogen inside the mesopores; this capillary condensation can be applied to determine the pore volume and pore size distribution. If the desorption curve is too close to the adsorption curve (narrow hysteresis) that implies that pore shapes are similar, which is the case here in Figure 2.3. If the hysteresis is broad this means that the pores have different shapes. Region IV is

associated with multilayer adsorption of nitrogen at the external surface of MCM-41. The very shallow slope of this region indicates that the external surface area of MCM-41 is small. Finally, at relative pressures close to 1 a volume of nitrogen adsorbed with a small hysteresis loop (region V). This can be assigned to condensation of nitrogen within the interstitial voids of the porous material.

### 2.1.1.3. Determination of specific surface area using BET isotherms

The determination of specific surface areas ( $\text{m}^2 \text{g}^{-1}$ ) of MCM-41 is based on the BET equation (Equation 2.1) proposed in 1938 by Brunauer, Emmett and Teller [111]:

$$\frac{V}{V_m} = \frac{C\left(\frac{P}{p_0}\right)}{\left[1+(C-1)\left(\frac{P}{p_0}\right)\right]\left[1-\left(\frac{P}{p_0}\right)\right]} \quad \text{Equation 2.1}$$

The BET equation is considered classical in the original meaning of this word, i.e. every possible proposed improvement of methodology, or calculations, in the determination of specific surface areas will use BET as a reference. Equation 2.1 is not linear and for the determination of  $V_m$  it is used in its linear form as shown in Equation 2.2.

$$\frac{\left(\frac{P}{P_0}\right)}{V\left(1-\left(\frac{P}{P_0}\right)\right)} = \frac{1}{CV_m} + \frac{(C-1)\left(\frac{P}{P_0}\right)}{CV_m} \quad \text{Equation 2.2}$$

where:

$V$  = moles of gas adsorbed per gram of adsorbent at vapour pressure  $P$ .

$V_m$  = the monolayer capacity of the surface.

$P^o$  = the saturation gas pressure at the temperature used.

$C$  = constant.

Plots in the form  $(P/P_o) / [V (1-(P/P_o))] = f (P/P_o)$  provide straight lines at a low pressure range, usually  $0.05 < (P/P_o) < 0.25$  depending on the sample. From such linear plots, with slope  $s = (C-1)/CV_m$  and intercept  $t = 1/CV_m$ , two unique values of  $C$  and  $V_m$  can be estimated. Derivation of the monolayer capacity ( $V_m$ ) from the above



equation allows the subsequent calculation of the surface area,  $S$ , by estimation the volume of the adsorbed monolayer  $V_m$ , if  $N_2$  is used as the adsorptive gas, which is usually the case, then according to reference [112].

$$S (\text{m}^2 \text{g}^{-1}) = 4.356 V_m (\text{cm}^3 \text{g}^{-1}) \quad \text{Equation 2.3}$$

#### 2.1.1.4 Determination of pore size

The Barrett-Joyner-Halenda (BJH) method [113] for calculating pore size distributions is based on a model of the adsorbent as a collection of cylindrical pores. The theory accounts for capillary condensation in the pores using the classical Kelvin equation [114], for a cylindrical pore the Kelvin equation is given by:

$$\ln\left(\frac{P}{P_0}\right) = \frac{2\gamma\bar{V}}{rRT} \quad \text{Equation 2.4}$$

where  $\gamma$  is the surface tension of the liquid and  $\bar{V}$  is the molar volume of the condensed liquid contained in a narrow pore of radius  $r$ .  $R$  is the gas constant and  $T$  is the temperature. Using nitrogen as adsorptive gas at its boiling temperature (-77 K). The Kelvin equation can be written as:

$$r_k = \frac{4.15}{\log\left(\frac{P}{P_0}\right)} \text{ \AA} \quad \text{Equation 2.5}$$

where  $r_k$  indicates the radius into which condensation occurs at the required relative pressure. This radius, called the Kelvin radius or the critical radius, is not the actual pore radius since some adsorption has already occurred on the pore wall prior to condensation, leaving a centre core of radius  $r_k$ . Conversely, an adsorbed film remains on the wall during desorption, when evaporation of the centre core takes place. Barrett-Joyner-Halenda (BJH) [113] takes this under consideration and produces another equation based on the thickness of the adsorbed film when condensation or evaporation occurs, then the actual pore radius  $r_p$ , is given by:

$$r_p = r_k + t \quad \text{Equation 2.6}$$

where:

$r_p$  = actual radius of the pore.

$r_k$  = Kelvin radius of the pore.

$t$  = thickness of the adsorbed film.

#### ***2.1.1.5 Determination of pore volume and average pore radius [115]***

The total specific pore volume is defined as the liquid volume at a certain  $P/P_o$  ratio (usually at  $P/P_o = 0.95$ : after the condensation step). In this case, the amount of adsorbed gas reflects the adsorption capacity and the total specific pore volume can be calculated by converting the amount adsorbed into a liquid volume assuming that the density of the adsorbate is equal to the bulk liquid density at saturation. Then the pore volume,  $V$ , is given by:

$$V_p = \frac{W_a}{\rho_l} \quad \text{Equation 2.7}$$

where  $W_a$  is the adsorbed amount (g), and  $\rho_l$  is the liquid density at saturation. Assuming, that no surface exists, other than the inner walls of the pores and that the pore is of cylindrical geometry, the average pore radius (*a.p.r*) can be calculated from the ratio of the total pore volume and the BET surface area from the following equation:

$$a.p.r = \frac{2V_p}{S_{BET}} \quad \text{Equation 2.8}$$

The total surface area  $S_{BET}$  can then be calculated from the BET method described above.

### 2.1.2 Powder X-ray diffraction (PXRD) [116, 117]

X-ray diffraction is an important and powerful method for the investigation of materials. This method is based on the scattering of X-rays by the electrons of atoms. The wavelengths of X-rays are similar to interatomic distances, and so the X-rays scattered by different atoms will interfere destructively or constructively, in the latter case giving rise to diffracted beams. In the case of crystalline samples, sharp diffraction phenomena result.

The geometry of the corresponding diffraction events can be described by Bragg's law, which combines a measure of the lattice of the crystal structure, namely the distance  $d$  between lattice planes, the wavelength  $\lambda$  of the X-ray radiation and the diffraction angle  $\theta$ :

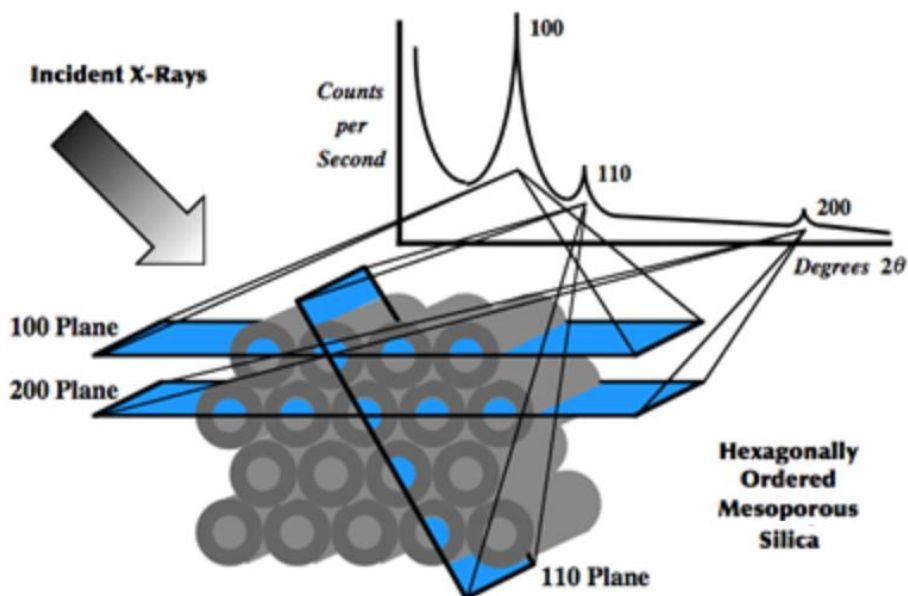
$$2d \sin \theta = \lambda$$

**Equation 2.9**

The Bragg equation treats diffraction as the reflection of X-rays at the lattice planes; correspondingly, a diffraction event is usually called a reflection. By analysing the geometry of the diffracted beams, information can be gained on the geometry of the lattice of the structure under investigation. By further analysing the intensity distribution of the reflections, information on the positions of the atoms can be obtained. This is usually carried out by measuring X-ray reflections on a single-crystal and forms the basis of X-ray single-crystal structural analysis [23].

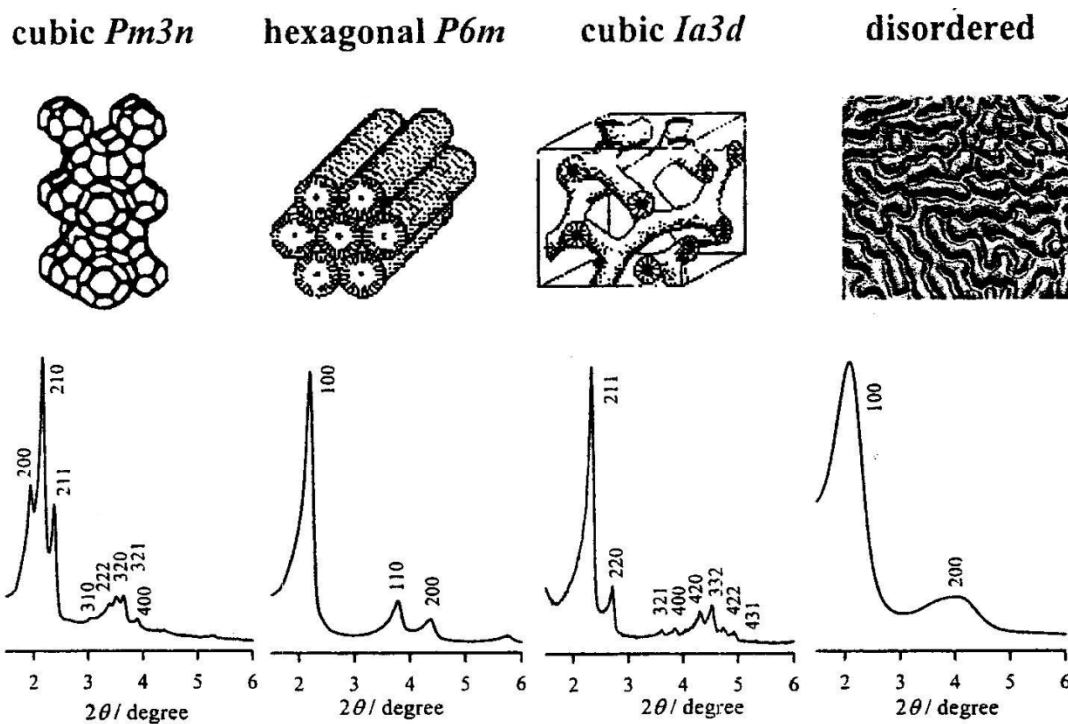
X-ray diffraction can also be carried out on powders, and this is the way it is typically applied to mesoporous materials. An X-ray beam with an exact angle is directed onto a smooth surface of the sample. If the material has any long range periodicity the X-ray beam will, at some angles, be reflected and collected by a detector. X-ray diffraction literature studies of MCM-41 indicate that the material has long-range structural ordering [118-120] and it can be seen in Figure 2.4 that

MCM-41 presents a well-ordered lattice. Moreover, because of the geometry of its lattice MCM-41 can be indexed with a hexagonal unit cell, with  $a = b$  and  $c = \infty$ . Because the parameters  $a$  and  $b$  are in the order of nanometres instead of tenths of nanometers, as usually encountered in crystals, X-rays are diffracted over small angles only. Therefore, characterisation of MCM-41 with X-ray diffraction yields a diffractogram with a limited number of reflections, all situated at low angle.



**Figure 2.4: X-ray diffraction peaks of hexagonal mesoporous silica. [121]**

Generally only three diffractions are well-resolved, corresponding to the (100), (110) and (200) reflections. A fourth diffraction peak with a notably lower intensity, corresponding to the (210) reflection can also be observed. From the reflection angles the size of the hexagonal unit cell of MCM-41 can be calculated (i.e. the parameters  $a$  and  $b$ ). With these values and the pore diameter (determined by nitrogen isotherms) the thickness of the silica pore walls can be calculated. Figure 2.5 illustrates the different mesostructures and associated X-ray diffraction patterns obtained.



**Figure 2.5: Mesostructures for MCM-41 with PXRD-pattern for each particular shape. [122]**

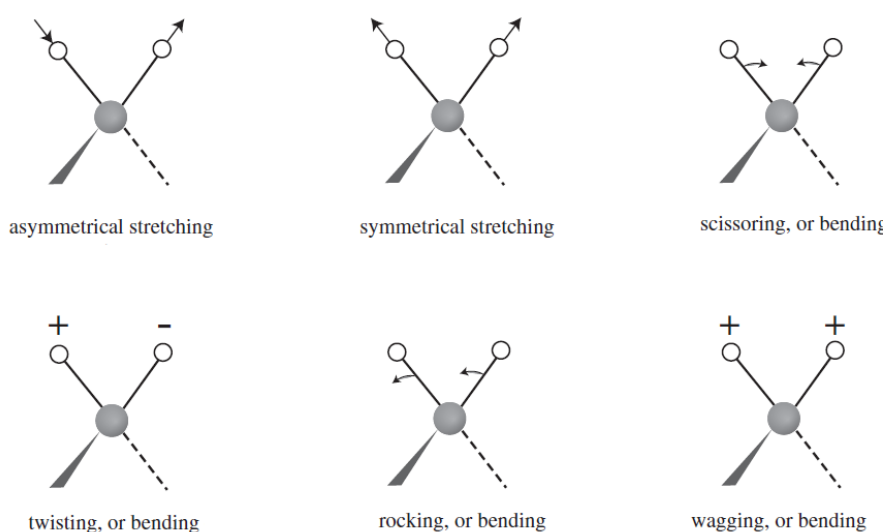
### 2.1.3 Fourier Transform Infrared Spectroscopy (FT-IR) [123, 124]

Electromagnetic (EM) radiation can be absorbed by a material and this process can cause a number of physical processes to occur according to the quantum energy of the radiation. Although IR radiation does not have enough energy to induce electronic transitions as seen with UV and visible light, absorption of IR radiation will cause changes in the vibrational and rotational states of a molecule. As alteration of a molecule's rotational state needs low energy this process occurs at the far IR region of the EM spectrum.

Absorption of IR radiation can either be transformed into kinetic energy, as a result of collisions, or released again as a photon. A spectrometer is used to measure the radiation intensity as a function of the wavelength of the light behind a sample. At the vibrational frequencies of the molecules an intensity decrease is obtained and a transmittance, or absorbance, spectrum is measured.

### 2.1.3.1 Number of vibrational modes

A molecule can vibrate in many ways, and each vibration is referred to as a vibrational mode. For molecules which contain  $N$  atoms, the number of expected vibrational modes can be calculated. For example, linear molecules demonstrate  $3N - 5$  degrees of vibrational modes, whereas nonlinear molecules have  $3N - 6$  degrees of vibrational modes (also called vibrational degrees of freedom). For example the  $\text{CH}_2$  group, commonly found in organic compounds, can vibrate in six different ways: symmetric and asymmetric stretching, scissoring, twisting, rocking and wagging:



**Figure 2.6: Stretching and bending vibrational modes for a  $\text{CH}_2$  group. [125]**

### 2.1.3.2 Stretching Vibrations

The stretching of a bond in a molecule, caused by absorption of IR radiation, can be understood by the use of a model which was suggested by Hooke and is known as Hooke's Law. In this approximation, two atoms and the connecting bond are treated as a simple harmonic oscillator composed of 2 masses (atoms) joined by a spring:



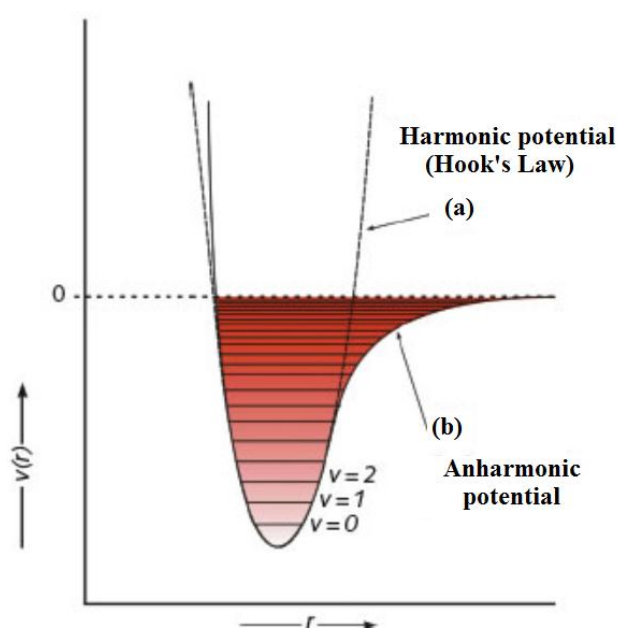
**Figure 2.7: Hooke's law models. [126]**

According to Hooke's law, the frequency of the vibration of the spring is related to the mass and the force constant of the spring,  $k$ , by the following equation:

$$v = \frac{1}{2\pi} \sqrt{\frac{k}{m}} \quad \text{Equation 2.10}$$

where  $k$  is the force constant,  $m$  is the mass and  $v$  is the frequency of the vibration.

Some limitations apply to this theory because the bond in the molecule does not behave exactly as a spring, as it cannot be compressed beyond a certain point. Removing this limitation leads to a molecule following an anharmonic oscillating as seen in Figure 2.8.



**Figure 2.8: Effect of increasing energy on the bond length ( $r$ ) and energy levels ( $v$ ). [126]**

In this case, the molecule's energy levels become more closely spaced as the interatomic distance of the atoms increase. This allows transitions to occur at smaller energy. Therefore, overtones can be different, (lower) in energy, to those obtained by the harmonic oscillator theory. The following equation has been derived from Hooke's law. For the case of a diatomic molecule:

$$\bar{\nu} = \frac{1}{2\pi c} \sqrt{\frac{f(m_1+m_2)}{m_1m_2}} \quad \text{Equation 2.11}$$

where  $\bar{\nu}$  is the vibrational frequency ( $\text{cm}^{-1}$ ).

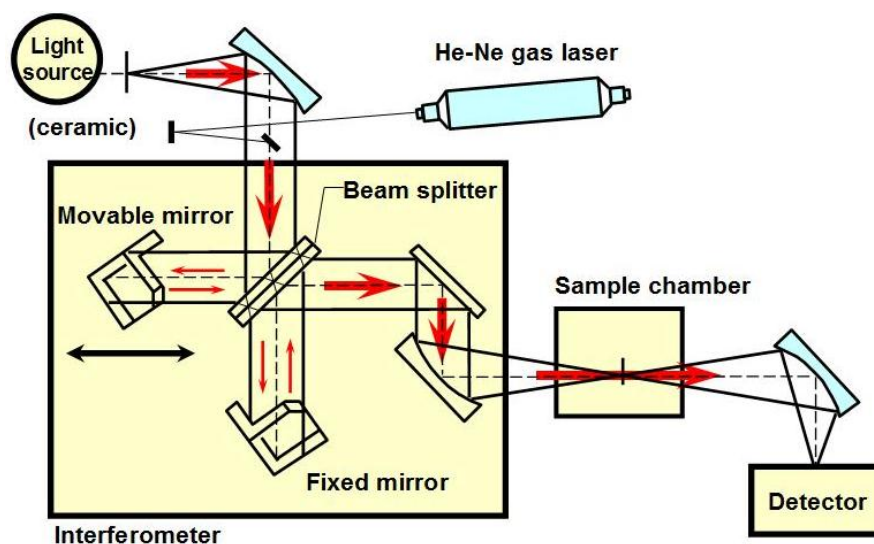
$m_1$  and  $m_2$  are the mass of atoms 1 and 2, respectively, in g.

$c$  is the velocity of light (cm/s).

$f$  is the force constant of the bond (dyne/cm).

### 2.1.3.3 FTIR spectroscopy

FTIR spectroscopy is an analytical techniques widely used for the identification of organic compounds. In most cases the FTIR spectra obtained can be used as a characteristic finger print of the whole compound, or features of the FTIR spectrum can be used to assign chemical structures to the observed molecule. An FTIR spectrometer normally contains an interferometer which causes interference in the incident beam using a moving mirror and beam splitter (Figure 2.9). The beams then recombine to produce a complex model of frequencies which can be measured by a suitable detector to produce a signal (interferogram). Fourier transform is used to convert the interferogram into the conventional FTIR spectrum,



**Figure 2.9: Diagram of the Michelson Interferometer used in an FTIR Spectrophotometer. [123]**



### **2.1.4 Carbon, Hydrogen, Nitrogen, Sulfur (CHNS) Elemental Analysers [127, 128]**

A CHNS elemental analyser is a fast technique which is used to estimate the quantities (%) of carbon, hydrogen, nitrogen or sulfur in a sample. The basic principle of the technique is based on applying very high temperature to the sample (1000 °C) causing combustion. During the combustion process, any carbon, hydrogen, nitrogen or sulfur present in the sample will be converted to carbon dioxide; water, nitrogen oxides or sulfur dioxide, respectively. Any other elements present in the sample will also be converted to their corresponding combustion products, for example chloride will be converted to hydrogen chloride.

The combustion products are introduced into a combustion chamber (furnace) using an inert gas and they are passed over very high purity copper at a temperature of approximately 600 °C. The main function of the heated copper is to remove any extra oxygen gas remained in the sample after combustion and to convert nitrogen gas into nitrogen dioxide. All gases produced flow over sorbent traps and all gases other than CO<sub>2</sub>, H<sub>2</sub>O, NO<sub>2</sub> and SO<sub>2</sub> are removed. To determine the identities of adsorbed gases, the sorbent traps are heated and the effluent is introduced into the gas chromatography (GC) column for separation. A thermal conductivity detector can be used to detect the eluted analytes. Quantification of the elements requires calibration and is achieved using high purity 'micro-analytical standard' compounds such as acetanilide and benzoic acid.

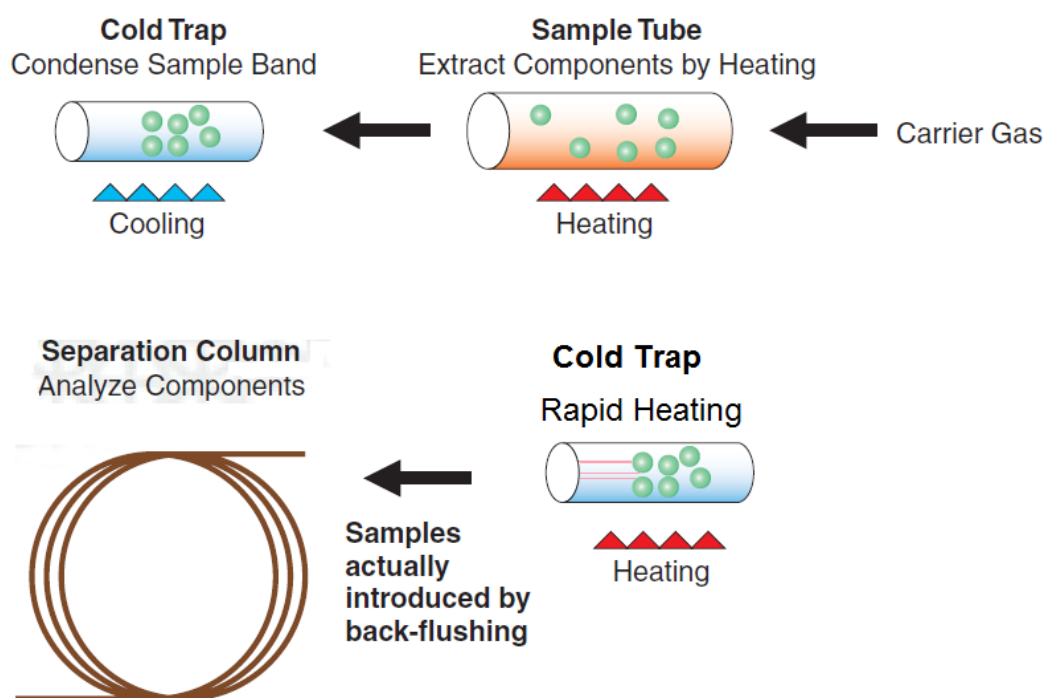
## **2.2 Techniques used for analyte measurement**

### **2.2.1 Thermal desorption-gas chromatography-mass spectrometry**

#### ***2.2.1.1 Thermal Desorption [129, 130]***

Thermal desorption is a technique used as a sample introduction method for GC. The principle of this technique is to adsorb volatile organic compounds from an air sample onto a cold trap (-30 °C) which is subsequently heated rapidly to a temperature of 300 °C. During this process analytes collected in the cold trap are desorbed and transferred rapidly into a GC column for separation.

Figure 2.10 explains the basic mechanism of the sample path through a typical thermal desorption process.



**Figure 2.10: Two stages desorption mechanism used in the Thermal desorption unit (TDU). [130]**

### **2.2.1.2 Gas chromatography (GC) [131, 132]**

Chromatography is a term used to define the process of separating a mixture of compounds (solutes) into separate components. By separating the sample into individual components, it is easier to identify and measure the quantities of the various sample components. There are numerous chromatographic techniques and corresponding instruments. It is estimated that 10-20 % of known compounds can be analysed by GC. To be suitable for GC analysis, a compound must have sufficient volatility and thermal stability. If all or some of a compound or molecules are in the gas or vapour phase at 400-450 °C, and they do not decompose, the compound can probably be analysed by GC. One or more high purity gases, called the carrier gas,

flows into the GC injection port carrying an injected sample with it onto the column and then into the detector.

Liquid or gaseous samples are conventionally introduced into the injection port using a syringe (in manual or automatic injection mode). In the case of air samples collected onto sorbent tubes, they are introduced into the chromatography by heating the sorbent tube in a thermal desorption unit (TDU) as discussed in Section 2.2.1.1. The column is held in a temperature controlled oven and solutes travel through the column at a rate that is primarily determined by their physical properties, the temperature and the composition of the column. The fastest moving solute exit (or elute) from the column first, followed by the remaining solutes in a specific order. As each solute elutes from the column it is transferred to a detector.

Although the word 'chromatography' is used to describe several systems and techniques, common to all systems is the use of a stationary and mobile phase. The mobile phase is a gas or a liquid that is used to carry a sample mixture through, or over, the stationary phase. The stationary phase usually contains small silica particles, ranging from 1 to 150  $\mu\text{m}$  in diameter given rise to a large surface area that can interact with the analytes in the injected sample. The particles are typically modified by chemical reactions to give a column which contains a stationary phase with a large surface of specific properties. When analytes (solute molecules) are introduced into the chromatographic system they will distribute between the two phases. Whilst interacting with the stationary phase, the analytes remain immobile and do not move. As such analyte mobility is dictated, to a large extent, by the interaction of the analyte with the chosen stationary phase: those analytes with a strong interaction with the stationary phase take a long time to move through the column and so are eluted last.

### ***Mobile phase in the GC [133]***

The mobile phase in GC is usually known as a carrier gas. As noted above, the carrier gas is responsible for carrying the sample from the injection port through the column (for separation) and onto the detector. The carrier gas is usually an inert gas like helium or nitrogen and should not interact with the stationary phase or be involved in the separation process. The flow rate used will have an effect on the

solute bandwidth as it moves through the chromatographic system and the eventual width of the measured analyte peak.

### ***Selection of stationary phase used in the column***

The separation principle of the column is based on the basic theory of “like likes like.” In other words, non-polar stationary phases are used for the analyses of non-polar compounds and polar stationary phases provide the most effective separation of polar compounds. Interaction between non-polar compounds and a nonpolar is by physical adsorption (Van der Waals forces) and this interaction is increased by the increasing the size of analyte which mean more retention time for larger molecules. The polar molecules can interact with the stationery phase in the column by three different interactions: dipole ( $\pi$ - $\pi$ ), acid-base interactions and physical adsorption (Van der Waals forces). Separations are determined by differences in the overall effects of these interactions. Generally the separation in GC column is following one of two methods:

- ***Normal-phase chromatography (NPC)*** the stationary phase in this type is non-modified silica or alumina with a hydrophilic surface chemistry and a stronger affinity for polar compounds.
- ***Reversed-phase chromatography (RPC)*** includes any chromatographic method that uses a non-polar stationary phase. Or by other words introduction of alkyl chains bonded covalently to the support surface reversed the elution order. This hydrophobic stationary phase will have more affinity to non-polar molecules.

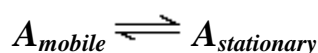
### ***Type of columns in the GC [134]***

There are two main types of column in common use in GC; the conventional packed column or the capillary column. Packed columns, usually made of glass or stainless steel, have an internal diameter of 2 to 4 mm, are 1 to 4 m long and are packed with particles containing the stationary phase. Packed column are commonly used in gas sample analysis because they have a very large sample capacity compared to capillary columns. Packed columns are also used for analysis of liquid samples but they have significantly lower resolving powers than capillary columns and as a result the latter are more commonly used in industrial and research applications.

Capillary columns are made of fused silica, which can be coiled easily, and so the length of capillary columns ranges from 10 - 100 m. They have a smaller internal diameter than packed columns, approximately 100 - 500  $\mu$ m. They are not packed with particles and the stationary phase is normally coated onto the internal wall of the column as a film of 0.2 - 1  $\mu$ m thickness. Such columns are called wall coated open tubular columns (WCOT) columns.

### ***Chromatographic separation and selectivity factors [135]***

When an analyte is injected onto a column equilibrium occurs and the analyte is distributed between two phases. Essentially the analyte partitions between the mobile and stationary phases:



The equilibrium constant,  $K$ , in this case is known as the *partition coefficient*; which can be defined as the molar concentration of analyte in the stationary phase divided by the molar concentration of the analyte in the mobile phase. The time required for the separation, or the time between analyte injection and detection, is known as the analyte *retention time* ( $t_R$ ). Each analyte will have a specific retention time according to its interaction with the stationary phase and the flow rate of the carrier gas. This time should be longer than the time taken for the mobile phase to pass through the column, the so-called void time ( $t_M$ ). The *retention factor*,  $K_A$  is used to describe the rate of analyte through the column and this factor can be expressed as given in equation 2.12:

$$K_A = \frac{t_R - t_M}{t_M} \qquad \text{Equation 2.12}$$

The *retention factor* ( $K_A$ ) value is useful to estimate the capability of the column for the separation of target analytes. For example if the  $K_A$  value is less than one, this means that the analyte will pass too fast through the column and when the  $K_A$  value is

too high (about 20) the analyte will take a very long time to pass the column. Usually the preferable  $K_A$  values lie in the range 1 - 5 [133].

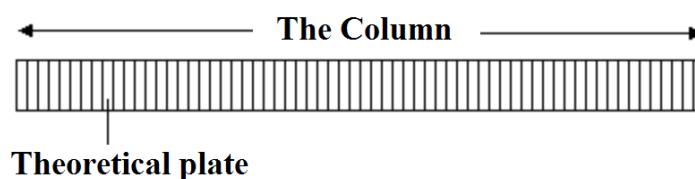
In addition to the retention factor there is another important term, normally used to describe the separation between two species (A and B) on the column, called the *selectivity factor* ( $\alpha$ ):

$$\alpha = \frac{K_B}{K_A} \qquad \text{Equation 2.13}$$

where  $K_B$  and  $K_A$  are the retention factors for the two species (B and A). For efficient separation the selectivity factor should be greater than 1 [133].

### ***The Theoretical Plate Model of Chromatography [133]***

This model assumes that the column consists of a large number of separate layers, called theoretical plates. The separation equilibrium of the sample between the stationary and mobile phase occur in these "plates". The assumption is based on the molecules move into the column according to the equilibrium occurred in the plate and then the molecules will pass to the next plate and so on.



**Figure 2.11: The assumption of theoretical plates inside the column.**

In fact those plates do not really exist but the information which could be got from this assumption is very useful to estimate the column efficiency by calculating the number of theoretical plates in a column,  $N$  (the more plates the better), or by stating The Height Equivalent to a Theoretical Plate (*HETP*)

$$N = \frac{5.55 t_R^2}{w_{0.5}^2} \quad \text{Equation 2.14}$$

$$HETP = L / N \text{ (the smaller the better)} \quad \text{Equation 2.15}$$

where  $w_{0.5}$  is the peak width at half-height.  $L$  is the column length.

### ***Column temperature and temperature program [135]***

Usually the columns used in GC instruments are placed in a controllable temperature oven. The analytes migration rate is directly related to the column temperature, it therefore plays an important role in the speed of analysis and also for the efficiency of the separation. In some samples, which contain analytes of similar physical properties, use of a high column temperature could lead to very poor separation. Equally if column temperatures are too low analytes may take too long to elute from the column and so a compromise is required. Therefore a procedure known as temperature programming is used to analyse samples which contain a large number of analytes of different polarity. By altering the oven temperature during the chromatographic process, best analyte resolution can be obtained.

Low temperatures are used initially to resolve analytes with low strengths of interaction with the stationary phase and the temperature increases thereafter to increase the rate of migration of analytes which interact more strongly with the stationary phase. The temperature change during the chromatographic process (the ramp rate) has to be optimised for each chromatographic system.

### 2.2.1.3 Detection the analyte by mass spectrometry [131, 136, 137]

#### *The Mass Spectrometer*

Mass spectrometry is a technique which is normally used in analytical chemistry to determine the molecular weight of an analyte or to identify unknown organic compounds in a sample. The instrument contains 3 main components described below and shown later in Figure 2.12.

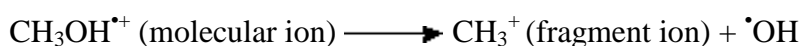
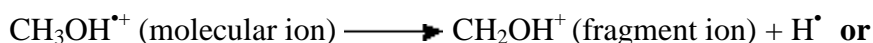
- The Ion Source: here the analyte is ionised to cations by losing an electron.
- The Mass Analyser the ions obtained from the ion source are separated due to their mass to charge ratio.
- The Detector: the quantity of ions will be measured.

#### **The ion source: Formation of molecular ions and fragments [136]**

Molecules separated by a GC can be introduced into a mass spectrometer where it is identified and detected. The molecule is introduced into the ion source where a high-energy electron beam (70 eV) is applied. The electron beam will strike the molecule removing an electron. An example of the ionisation process for methanol in the ion source is given below.



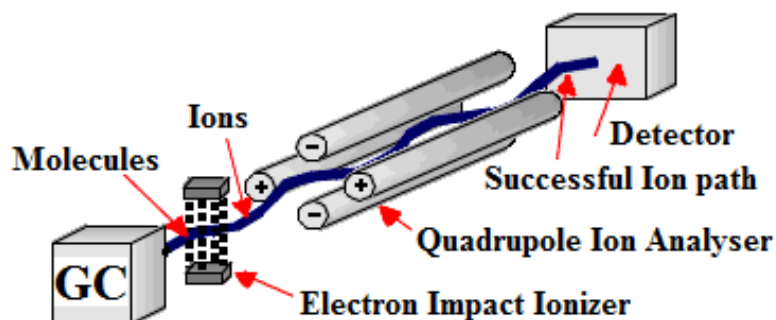
The charged methanol ion, which contains an unpaired electron, is normally unstable and will breakdown into smaller pieces (fragments).



The positively charged ions that are created will pass through the MS and uncharged atoms will be removed before reaching the detector.



The ion source normally operates at  $2 \times 10^{-5}$  Torr with  $1.0 \text{ cm}^3 \text{ min}^{-1}$  helium flowing into the manifold for electron ionisation or  $3 \times 10^{-4}$  Torr for chemical ionisation. This large pressure change between the end of the chromatographic column and the inside of the ion source causes the gas to expand to a flow equivalent to several litres per minute. Therefore, large pumps are required to remove the excess gas and maintain the vacuum inside the source near optimum pressure for ionisation.



**Figure 2.12: General schematic of a mass spectrometer. The blue line illustrates ions of a particular mass/charge ratio which reach the detector at a certain voltage combination. [138]**

**The mass analyser:**

In the ion analyser molecular ions and fragment ions are accelerated by manipulation of the charged particles through the mass spectrometer. Uncharged molecules and fragments are pumped away. Ions travel down the path based on their mass to charge ratio ( $m/z$ ). EI ionisation produces singly charged particles, so the charge ( $z$ ) is 1. Therefore an ion's path will depend on its mass. There are many types of detectors, but most work by producing an electronic signal when struck by an ion. Timing mechanisms which integrate those signals with the scanning voltages allow the instrument to report which  $m/z$  strikes the detector. The mass analyser sorts the ions according to their  $m/z$  ratio and the detector records the abundance of each.

The mass analyser used throughout the course of this investigation was the quadrupole mass analyser. The quadrupole uses the stability of the trajectories in oscillating electric fields to separate the ions based upon their  $m/z$  ratio. Quadrupole analysers are made up of four rods with circular or hyperbolic section [136]. These rods are arranged in pairs to which an alternating RF and DC potential is applied. The oscillating field allows a range of  $m/z$  ratios to pass through, while any ions with a  $m/z$  ratio higher or lower than this preselected range are unable to pass through and collide with the poles, see Figure 2.12.

### **The Detectors:**

Once the ion beam has passed through the mass analyser it is detected and transformed into a usable signal by the detector. There are a number of different detectors for use with the mass spectrometer; however they can generally be divided into two categories [136]. The first of which involves the direct measurement of the charges which reach the detector, for example photographic plate and Faraday cage detectors. The other category of detectors involves increasing the intensity of the signal such as the array detector and the photomultiplier detector [136].

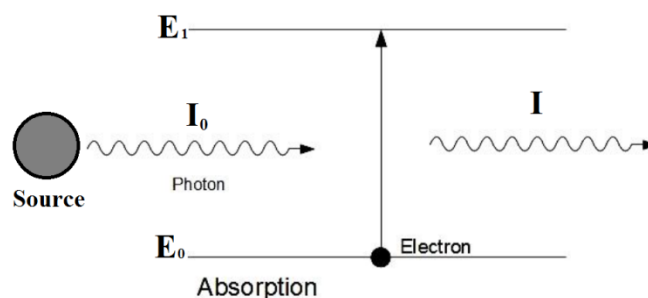
During the course of this investigation the photomultiplier detector was used. The photomultiplier detector consists of two conversion dynodes, a photomultiplier and a phosphorescent detector. This detector enables the detection of both positive and negative ions. When operated in the positive mode the secondary ions are accelerated towards the negatively charged dynode, while in negative mode the ions are accelerated towards the dynode which carries the positive potential. The secondary electrons given off are then accelerated towards the phosphorescent screen, which is coated in a thin layer of aluminium conductor to avoid the accumulation of a charge. At the phosphorescent screen the electrons are converted to photons, which are then detected by the photomultiplier [136].

### **2.2.2. Flame atomic absorption spectrometry (FAAS) [132, 139, 140]**

FAAS is an analytical technique that is used to measure the concentrations of elements in an aqueous solution. The detection limits of this technique are usually in the range of parts per million (ppm) volume. While for some elements it can be lower and reach parts per billion (ppb) volume.

### ***Basic theory of atomic absorption [141]***

The ability of an atom to absorb light depends on the energy of the light applied. An atom has several energy levels and when light interacts with this atom, an electronic transition, from the ground state ( $E_0$ ) to the excited state ( $E_1$ ) will occur if the difference in energy between  $E_0$  and  $E_1$  matches the energy of the incoming light (see Figure 2.13).



**Figure 2.13: Schematic representation of absorption of radiation.**

If the energies match a portion of the light is absorbed and an electronic transition occurs. The intensity of light passing through the species will be decreased and that decrease in intensity is proportional to the number of atoms present in the material. In other words the change in intensity from the incoming ( $I_0$ ) and transmitted ( $I$ ) light can be used to determine the concentration of the species.

Experimental measurements are usually made in terms of transmittance ( $T$ ), which is defined as:

$$T = I / I_0 \quad \text{Equation 2.16}$$

where  $I$  is the light intensity after it passes through the sample and  $I_0$  is the initial light intensity. The relation between  $A$  and  $T$  is:

$$A = -\log T = -\log (I / I_0) \quad \text{Equation 2.17}$$

This relationship is known as the Beer-Lambert law and can be written as follows:

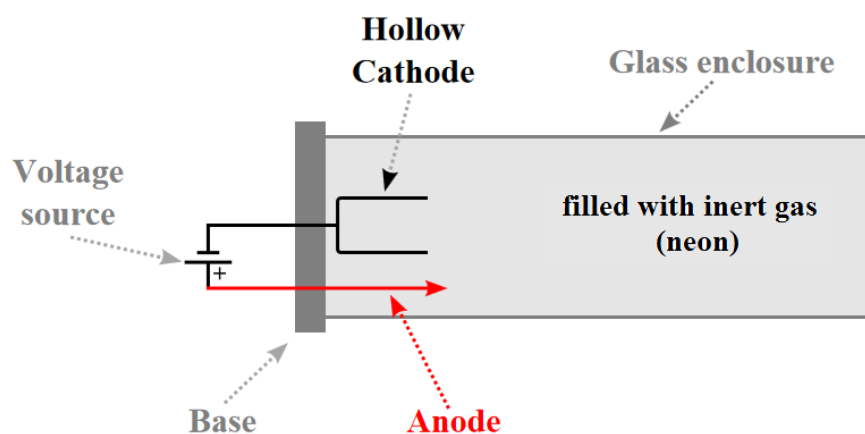
$$A = \varepsilon \cdot l \cdot c \qquad \text{Equation 2.18}$$

where  $A$  is absorbance,  $\varepsilon$  is the molar absorptivity,  $l$  is the path length and  $c$  is the concentration. Beer's law is a linear relationship and therefore allows the absorption principle to be used as a quantitative analytical technique.

There is limitation of using Beer-Lambert law in high concentration solutions because the derivation of the equation assumes that every absorbing particle behaves independently with respect to the light and is not affected by other particles (some particles are in the shadow of others). But this was not the case in highly concentrated solutions [142]. In practice, when large absorption values are measured, dilution is required to achieve accurate results. Measurements of absorption in the range of  $(I/I_0) = 0.1$  to 1 are less affected by shadowing. At higher absorbance, concentrations will be underestimated due to this shadow effect and the results will be inaccurate [142].

### ***The operating principle of FAAS***

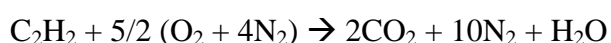
FAAS is a technique based on the Beer-Lambert law described above. The source of light used is an important component of the instrument as the transition of the electron is dependent upon the energy of the incoming light. To ensure that the source of light will produce the desired wavelength required the analyte of interest, different hollow cathode lamps (HCLs) are used. Figure 2.14 gives a schematic diagram of a HCL.



**Figure 2.14: General schematic diagram of a hollow-cathode lamp [140].**

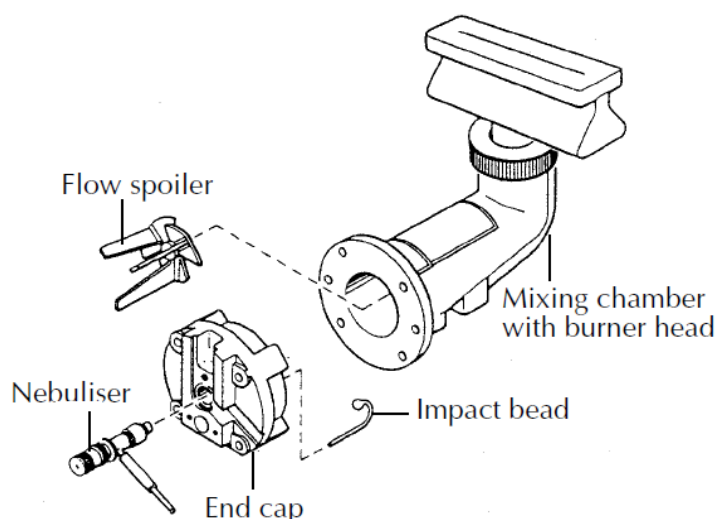
A HCL contains a tungsten anode and a cylindrical hollow cathode made of the element to be determined. A high voltage is applied across the electrodes causing ionisation of the fill-gas, in the schematic above Ne gas would be ionised. These gaseous ions attach the cathode releasing atoms which collide with the metal-stable fill gas and become excited. The excited atoms subsequently relaxed and emit photons. The light produced has a wavelength that will be absorbed by the element of interest. Before the resulting beam of light produced by HCL interacts with the species of interest, the analytes must be in the atomic state.

The most common atomisation system used in AAS is the combustion flame, involving a mixture of either air and acetylene, or nitrous oxide and acetylene. The air-acetylene flame is cooler, 2125-2400 °C, and is satisfactory for the majority of elements determined by atomic absorption. However, the hotter nitrous oxide-acetylene flame, 2600-2800 °C, is often required for many refractory-forming elements. Although the nitrous oxide-acetylene flame gives better atomisation efficiencies it also gives a more intense background emission signal, which gives it poorer precision. Throughout the course of this investigation the air-acetylene flame was used, the combustion reaction of which is shown below;



In general the atomisation process can be described as shown below:

- Desolvation (drying) – dryness the solvent from the sample.
- Vaporisation (transfer to the gaseous phase) – in this stage the solid particles will be converted to gas.
- Atomisation – in this stage the molecules will be dissociated to free atoms. The molecules are dissociated into free atoms.



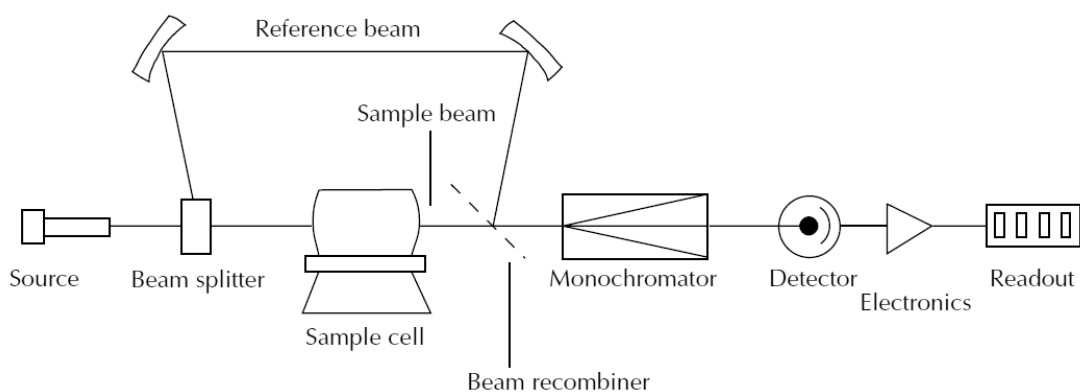
**Figure 2.15: A typical burner and spray chamber. [140]**

Samples are therefore introduced in the FAAS using a spray chamber system, see Figure 2.15. A capillary tube connects the sample solution to a nebuliser where the solution will become broken-down into very small droplets. These fine aerosol droplets ( $< 10 \mu\text{m}$ ) will pass to a burner (1%) to be vaporised and atomised in a flame.

Flames can be classified into several types depending on fuel/oxidant used. However when ratio between fuel/oxidant is high (flame-rich) the fuel tends to reduce MO and MOH to M so can get better signal. Rich flames are cooler, so not as many M atoms are excited state. On the other hand when this ratio is low (flame lean) by increase the oxidant percentage, more tendency to oxidise metals, but hotter flame so more M

in excited state but this also can increase the background signal associated with absorption. Therefore choosing the type of flame is such an important step as the best sensitivity could be produced would be according to the type of flame chosen. The electromagnetic beam produced by the HCL will be passed through the sample vapour; some of this light will be absorbed by the target element atoms in the sample. The more concentrated the analyte species introduced into the system the more light is absorbed.

The transmitted light that passed through the sample is directed to a monochromator which separates the desired wavelengths of light and focuses it on to a photomultiplier device to convert the light signal into an electrical signal for data production. To avoid any loss of the sensitivity, the original beam obtained by the HCL is split into two beams. One of them is directed to the sample and the other is used as reference. This can be useful when the light source is unstable. So by using double beam systems (a schematic is given in Figure 2.16) absorption monitoring will be improved.



**Figure 2.16: General schematic diagram of the FAAS. [140]**

### 2.2.3. Inductively Coupled Plasma - Atomic Emission Spectrometry ICP-AES [143, 144]

ICP-AES is used, similar to absorption spectroscopy, to determine the concentrations of elements in an aqueous solution. This technique has become one of the most commonly used, sensitive, techniques for metal ion determination since 1969 [145].

The main advantages of using ICP-AES over FAAS includes the ability to perform multi-element analysis in a rapid analysis time and a higher level of high sensitivity [146]. Figure 2.17 demonstrates the main components of an ICP-AES instrument. The main steps for using ICP-AES are sample introduction, production of emission, collection and detection of emission, these steps will be discussed below.

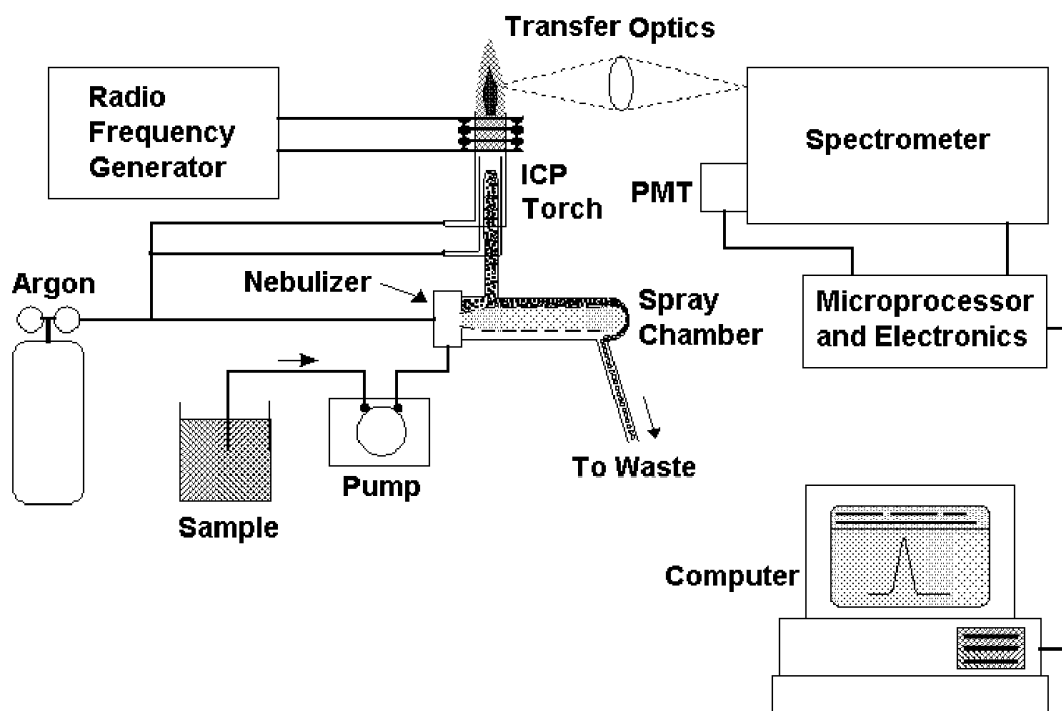


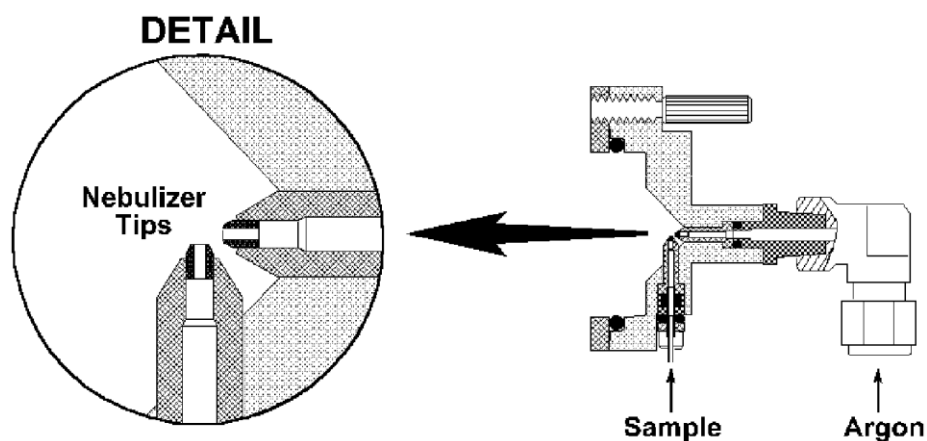
Figure 2.17: Major components and layout of a typical ICP-AES instrument. [143]



### 2.2.3.1. Sample Introduction

#### *Nebulisers*

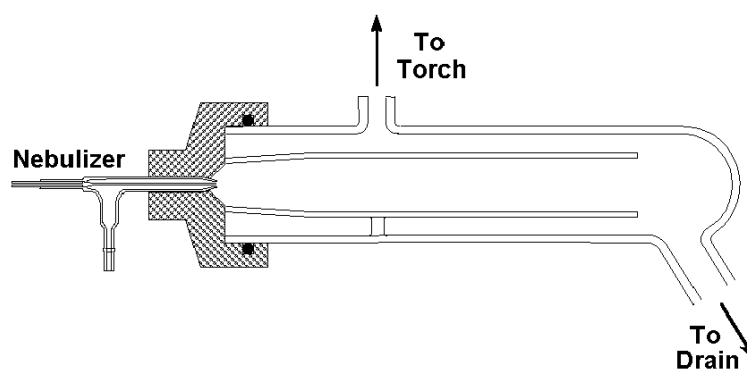
Nebulisers are devices which transform the samples from a liquid to very fine droplets which are known as an aerosol. The most common Nebuliser used the cross-flow Nebuliser (Figure 2.18), where argon gas with a high flow rate is applied perpendicular to the tip of tube containing the liquid sample moving at low pressure. Therefore when the argon gas travelling at high speed contacts the liquid sample stream, the liquid will break up to produce small droplets (aerosol).



**Figure 2.18: A cross-flow Nebuliser. [143]**

#### *Spray chambers*

Spray chambers are used to transport the droplet produced in the Nebuliser to the torch. Only the very fine sized droplets will be transferred to the plasma whilst any others will be passed to drain. A range of spray chambers can be used for ICP-AES, but all of them follow the same operating principles. A typical ICP spray chamber design is shown in Figure 2.19.



**Figure 2.19: A typical ICP spray chamber. [143]**

All the spray chambers designed for ICP-AES allow only the droplets with diameters less than 10  $\mu\text{m}$  to pass to the plasma. As droplets of this size constitute approximately 1 to 5 % of the total number of droplets obtained from the Nebuliser, 95 % of the sample introduced into the ICP-AES will be drained to waste.

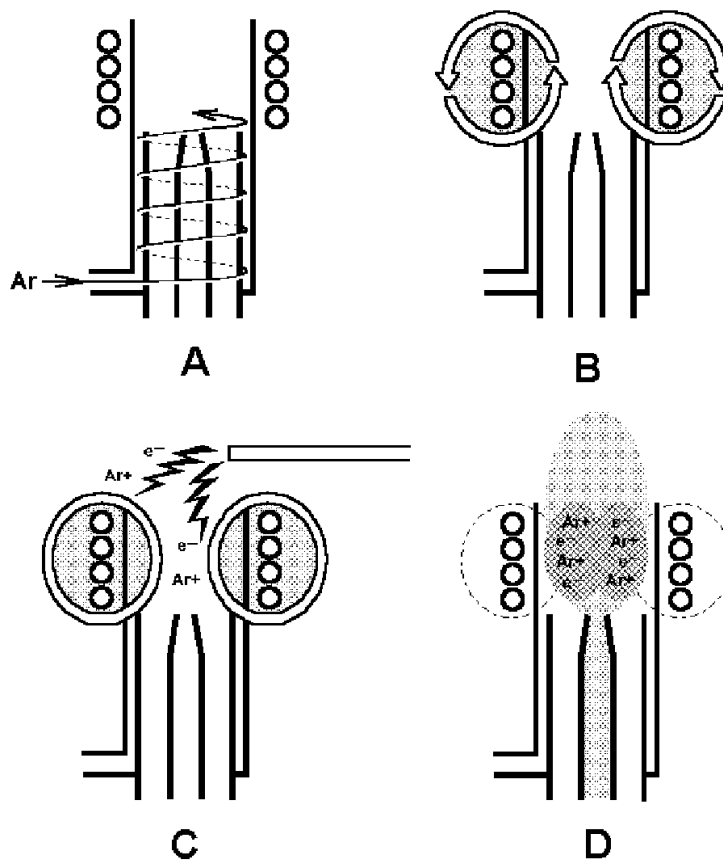
### ***2.2.3.2. The Inductively Coupled Plasma Torch***

Torch used for ICP-AES are similar in design and function to those originally reported by Fassel in 1969 [145]. The main function for the torch is to produce the plasma.

#### ***The Plasma Formation***

In the torch, which consists of three concentric tubes made from the quartz, there is a radio frequency (RF) generator connected to a copper coil located at the top of the torch. The RF power (about 1000 watts) is applied to the copper coil to produce a current with a frequency of 7 or 40 MHz. Here an electromagnetic field will be obtained and cover the area at the top of the torch. By passing argon gas through this area and applying a spark, electrons will be removed from the argon atoms. These electrons, which are present in the magnetic field, will be accelerated and collisions with other argon atoms will occur causing more electron be released and more argon

ions to be produced. Chain reactions will occur and a huge numbers of ions will be produced which will form a plasma. Figure 2.20 demonstrates the four steps to plasma production.



**Figure 2.20: the steps for plasma formation: A: Argon gas is introduced to the torch. B: RF power is applied to the copper coil. C: a spark is applied to release some electrons from argon gas. D: formation of the plasma by producing more argon ions as a result of the collisions of the accelerated electrons with argon atoms. [143]**

### ***Ionisation of analytes in the plasma***

The spray chamber is used to direct the small droplets to the torch which will be directed to the centre of the plasma. In the plasma the species will go through a range of processes until the element of interest is excited and ionised as described in Figure 2.21.

At the first step desolvation is achieved because of the high temperature of the plasma transforming the sample to very small solid particles which are then vaporised and atomised as particles dissociate. Desolvation, vaporisation and atomisation all take place in the so-called preheating zone (PHZ) of the plasma, Figure 2.22. Excitation and ionisation processes occur in the initial radiation zone (IRZ) and the normal analytical zone (NAZ). The NAZ is the region of the plasma from which analyte emission is typically used for measurements.

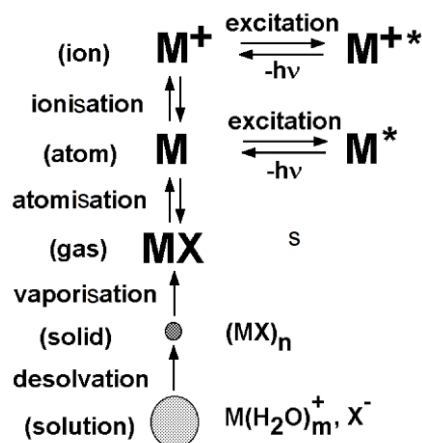


Figure 2.21: description to the process happen to the droplet when it's introduced to the plasma. [143]

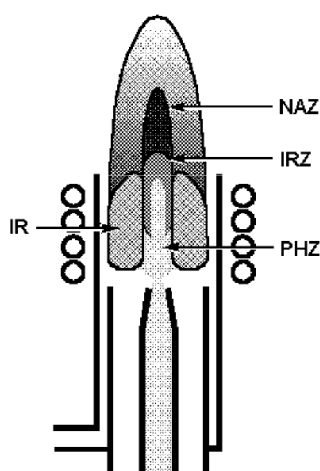
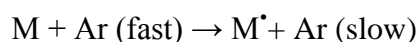
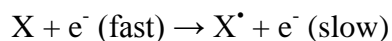


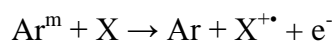
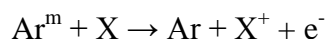
Figure 2.22: Zones of the ICP. IR: Induction Region, PHZ: Preheating Zone, IRZ: Initial Radiation Zone, NAZ: Normal Analytical Zone. [143]

Several different mechanisms have been proposed to explain the populations of the various excited atomic and ionic states. The main mechanisms are as follows [142]:

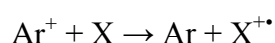
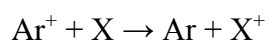
- a) Thermal excitation or ionisation caused by collisional energy exchange between atoms, ions and electrons:



- b) Penning ionisation or excitation caused by collisions between ground-state atoms and argon metastable species:



- c) Charge-transfer ionisation or excitation caused by the transfer of charge between ions and atoms,



### ***2.2.3.3. Detection of emission***

After absorbing energy to produce excited atoms, ions or excited ions, the electrons will transfer back to a lower energy state, or to the original ground state. This will cause emission of radiation of different frequencies (as described in Figure 2.23). Each element will emit characteristic frequencies of light that can be used to identify the element. As the emitted light is proportional to the concentration of analyte the measured signal can also be used to determine analyte concentration.

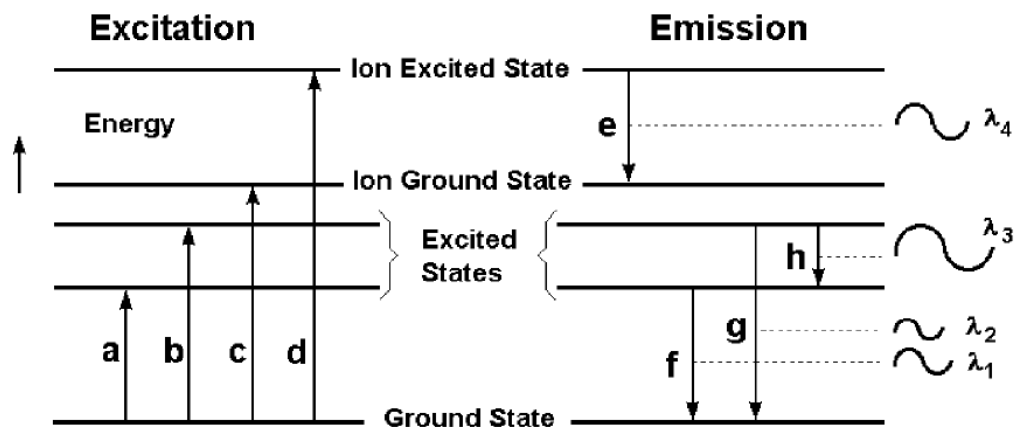


Figure 2.23: The energy transitions of the electrons after absorbing the energy where a and b represent excitation, c is ionisation, d is ionisation/excitation, e is ion emission, and f, g and h are atom emission.

### *Transfer Optics*

The emitted radiation from the plasma, produced from the excited analyte atoms or ions will be directed to a detector using optics. Two types of optics are used in the ICP-AES, either using side-on or end-on viewing (Figure 2.24).

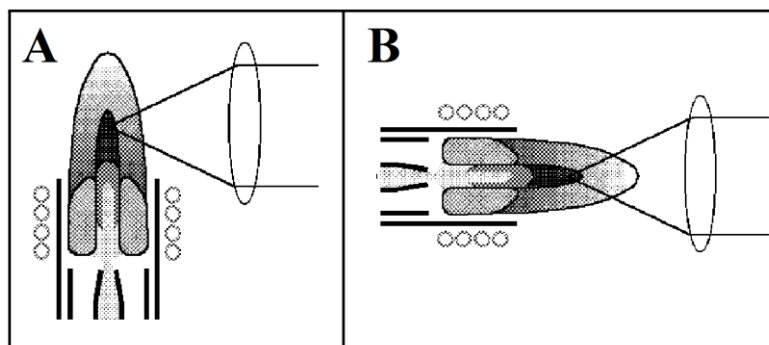


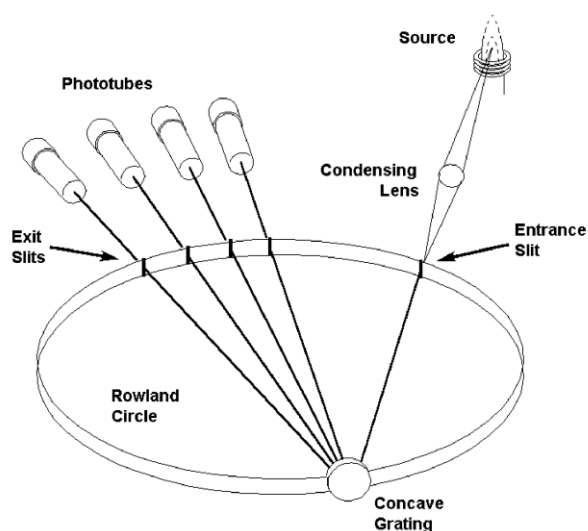
Figure 2.24: Types of optics used in ICP-AES. Side-on (A) and end-on viewing (B). [143]

In recent instruments both optic types are used and can be combined (in a dual system) to produce an instrument with higher analyte sensitivity. Regardless of the type used, the main function of the optic device is to focus radiation into an entrance slit of the wavelength dispersing device or the spectrometer.

### ***Wavelength Dispersive Devices***

The radiation obtained from the plasma consists of a mixture of different wavelengths. To select the desired wavelength, a wavelength dispersive device should be used. These devices use a diffraction grating to reflect the proper wavelength to certain angles which then can be collected by a detector (and blocking out other undesired wavelengths).

As ICP-AES instruments are able to measure samples containing multi-elements, the conventional wavelength dispersive devices were modified using a polychromator. Each exit slit in a polychromator is located to an atomic or ionic emission line for a specific element to allow simultaneous multielement analyses. A number of detectors are required to simultaneously measure the number of emission lines separated by this device. The most popular design is the Paschen- Runge mount (Figure 2.25).



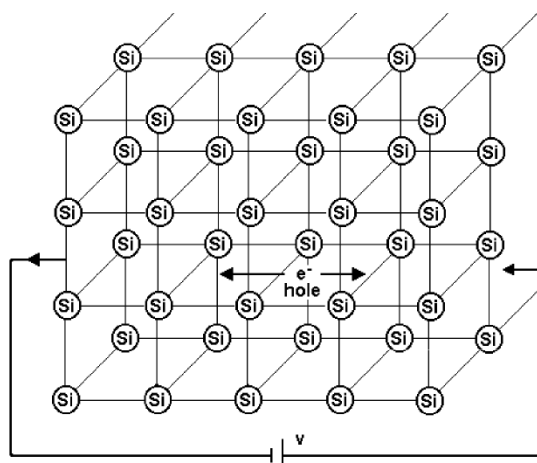
**Figure 2.25: Paschen-Runge mount used in multielement analyses. [143]**

## Detectors

The most widely used detector for ICP-AES is the photomultiplier tube or PMT. The PMT is a vacuum tube that contains a photosensitive material, called the photocathode, which ejects electrons when it is struck by light. These ejected electrons are accelerated towards a dynode which ejects 2 to 5 secondary electrons for every 1 electron which strikes its surface. The secondary electrons strike another dynode, ejecting more electrons which strike yet another dynode, causing a multiplicative effect along the way.

Recently, advanced solid-state detectors with high sensitivity and resolution for spectroscopic applications are used [147]. The charge-coupled device (CCD) is mostly used with recent instrument.

The CCD device is based on the light-sensitive properties of solid-state silicon which sometimes known as charge transfer devices (CTD). The basic principle of this device is to transform the photons to electricity using a block of very high purity crystalline silicon which is simply a layer of  $\text{SiO}_2$  as shown in Figure 2.26. Each silicon atom is bonded to two silicon atoms in a three dimensional lattice.



**Figure 2.26: Photon absorption by silicon crystalline lattice and the formation of electron-hole pairs.**



The silicon-silicon bond can be broken by absorbing the light, which has a frequency range in the visible or ultraviolet region, and that creates a hole (electron-hole pairs) in the silicon crystalline structure. If a voltage is applied to the silicon layer the free electrons will be moved in the opposite direction of the electrical field creating a positive charge in the place of the hole. This electron movement will create a current. The intensity of this produced current is proportional to the number of holes or a number of photons absorbed, which in turn is related to the concentration of the measured species.

## **Chapter 3: Experimental and Safety**

## **3.1 Preparation of mesoporous materials**

### **3.1.1 MCM-41 preparation**

MCM-41 used in the chapter 5 (VOCs extraction from indoor air) was prepared according to the method reported by Xia et al.[148]. Briefly, 4.4 g of cetyltrimethylammonium bromide (CTAB, 98%, BDH) was dissolved in 32 cm<sup>3</sup> of distilled water and 3.5 g of tetramethyl ammonium hydroxide (TMAOH, 97 %, Sigma). The solution was heated to 35 °C with constant stirring for 30 min before the drop wise addition of 10 g of tetraethylorthosilicate (TEOS, 98%, Aldrich). The solution was stirred for a further hour at 38 °C then stirred for a further 2 h at room temperature.

The solution was transferred without filtration or washing to a steel bomb for autoclaving at 100 °C for 24 h. Removal of the surfactant was achieved by acidified solvent extraction: 1 g of silicate material was added to 25 cm<sup>3</sup> of hydrochloric acid (HCl, 37 %, Sigma Aldrich) and 300 cm<sup>3</sup> of ethanol (Sigma Aldrich). The mixture was then refluxed for 24 h. Once the solution was cooled the silicate material was collected by gravity filtration.

### **3.1.2 SBA-15 preparation**

SBA-15 was prepared by modifying the original method reported by Zhao et al.[50]. A surfactant tri-block copolymer solution of 4 g pluronic P123, PEO<sub>20</sub>PPO<sub>70</sub>PEO<sub>20</sub> (BASF Corporation, 3000 Continental Drive), was dissolved in 120 cm<sup>3</sup> of 2 M HCl and 60 cm<sup>3</sup> of distilled water in a glass bottle at room temperature and the mixture was magnetically stirred at 330 rpm. The surfactant solution was heated to 40 °C and 11.3 g of TEOS was added and left for 24 h at 40 °C.

The mixture was then placed in an oven for 5 days at 60 °C. The material was filtered and washed with water and dried overnight at 60 °C before calcination at 550 °C for 24 h.

## **3.2 Characterisation of mesoporous silica material**

### **3.2.1 Power X-ray diffraction**

Powder X-ray diffraction (PXRD) profiles were recorded on a Philips X'Pert diffractometer, equipped with a Cu K $\alpha$  radiation source and accelerator detector. Incident and reflected Stöller slits of 0.2° were used with a programmable divergent slit (a constant 10 mm sample footprint) and the weight of sample was about 0.5 g.

### **3.2.2 BET isotherms**

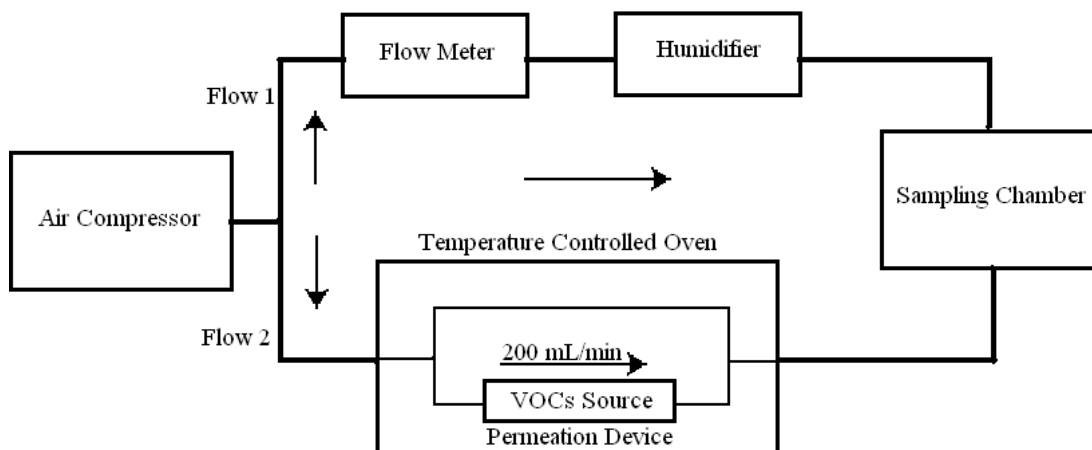
The surface area of silica materials were measured using nitrogen physisorption isotherms on a Micromeritics Gemini 2375 volumetric analyser. Each sample (300 – 400 mg in weight) was accurately weighed, transferred to a gas adsorption sampling tube. The sample tube weight was recorded before and after the addition of silica material. The sample tube was attached to the degas port of a gas adsorption instrument and degassed prior to analysis for 6 h at 200 °C. The Brunauer–Emmett–Teller (BET) surface areas were calculated using experimental points at a relative pressure ( $P/P_0$ ) of 0.05–0.25. The total pore volume was calculated from the N<sub>2</sub> amount adsorbed at the  $P/P_0$  of 0.99 for each sample and the average pore size distribution of the materials was calculated using the Barrett–Joyner–Halenda (BJH) model from a 30-point BET surface area plot. Desorption isotherms were used to calculate the pore diameters.

### **3.2.3 FTIR spectra**

Infrared spectra of samples were obtained using samples ground with KBr to produce pellets which were analysed over the wavelength range of 4000–400 cm<sup>-1</sup> region and a resolution of 4 cm<sup>-1</sup>. An average spectrum was produced by accumulating 64 scans using an ATI Mattson FTIR spectrophotometer. The sample FTIR disc was prepared by mixing approximately 0.1 g of the solid sample with about 0.25-0.50 g of KBr. This mixture was placed in the press machine to cover bottom in pellet die and the pressure used was about at 5 KN and then the pressed sample was carefully removed from the die and place in the FTIR sample holder for analysis.

### 3.3 Generation of known concentration of volatile organic compounds (VOCs) using a dynamic atmospheric chamber

Dynamic atmospheric chambers [149, 150] were used to provide a constant and controlled polluted air stream of VOCs. The sampling chamber consisted of a VOC source, two flow streams and a 20 dm<sup>3</sup> sampling chamber as shown in Figure 3.1:



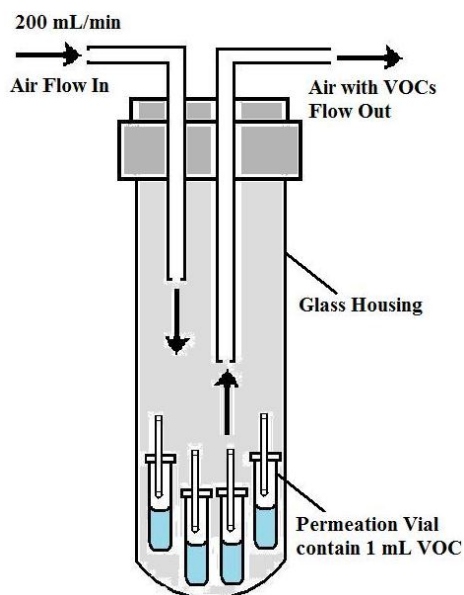
**Figure 3.1: Atmospheric chamber system.**

The initial air stream was obtained using an air compressor (Jun Air 12-50) and was split into two main flows. Flow 1 passed through a humidification system to provide the sample chamber with either high-relative humidity (H-RH) air at 80 % RH or low-relative humidity air (L-RH) at 25 % RH. The second flow stream entered a temperature controlled oven (Kin-Tek Laboratories Inc. Model 491 M-B) and passed over a VOC source. In this set-up four GC auto-sampler vials (with silicon-seal tops) were used to store 1 cm<sup>3</sup> each of toluene, ethylbenzene (EB), cumene or dichlorobenzene (DCB) (see Table 3.1). To provide a controlled permeation source each vial was pierced with a GC syringe needle (18 gauge) and the vials, complete with needle, were placed inside the oven in a glass housing unit which was o-ring sealed (see Figure 3.2).

The emission rates of the VOCs were controlled by the oven temperature and flow rate of air passing through the glass housing unit. Both flows (humidified air and polluted air) were recombined in the sampling chamber.

**Table 3.1: Some physical properties of VOCs studied. [151]**

VOCs	Liquid Density g/cm <sup>3</sup> at 25 °C	Boiling Point / °C	Vapour Pressure mmHg at 20 °C	Molecular Weight	Manufacturer
Toluene	0.87	111	22	92.14	Fisher Scientific (99.5%)
EB	0.87	136	10	106.17	Sigma-Aldrich (99%)
Cumene	0.86	154	8	120.2	ACROS Organics (99%)
DCB	1.3	180	1.2	147	Aldrich Chemical (99%)



**Figure 3.2: Permeation Device (VOCs Source).**

### 3.3.1 Determination of the theoretical concentration of VOCs produced in the sampling system

The theoretical concentrations of VOCs generated in the chamber were calculated using Equation 3.1.

$$C = \frac{K_o E}{F} \quad \text{Equation 3.1}$$

where  $C$  is the VOC concentration (ppm),  $E$  is the emission rate ( $\text{ng min}^{-1}$ ) and  $F$  is the flow rate of the air stream passing through the VOC source ( $\text{cm}^3 \text{min}^{-1}$ ). The  $K_o$  value is used to convert the gas units to a convenient term quoted in parts per million (ppm or  $\mu\text{g g}^{-1}$ ). The value of  $K_o$  ( $\text{L g}^{-1}$ ), which is the inverse density of the gas, depends on temperature. Often a nominal temperature of  $25^\circ\text{C}$  is used to convert gas units and this temperature is used in this research. At  $25^\circ\text{C}$  the  $K_o$  value is then the molar volume of the gas at  $25^\circ\text{C}$  divided by its molecular weight, see Equation 3.2.

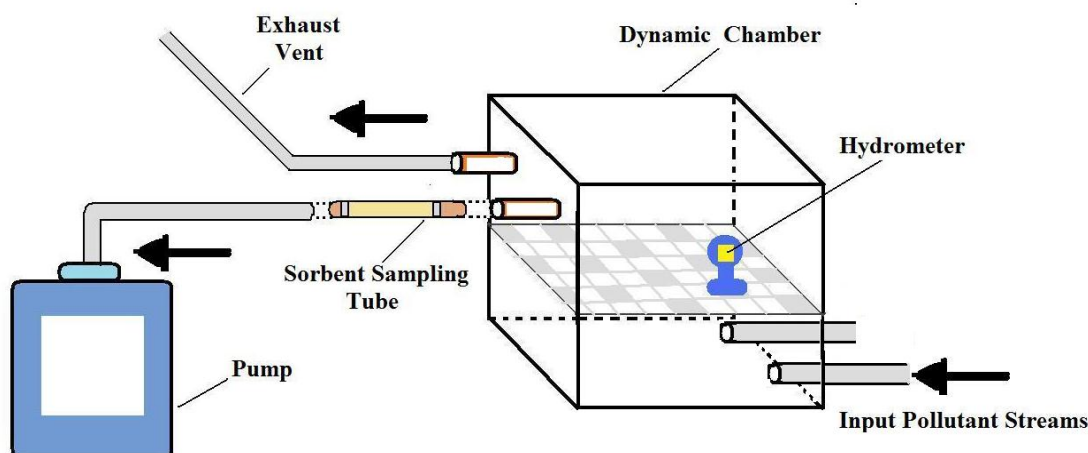
$$K_o = \frac{24.46 (L)}{MW (g)} \quad \text{Equation 3.2}$$

Thus,  $K_o$  values were calculated for toluene, ethylbenzene, cumene or dichlorobenzene as 0.265, 0.230, 0.204 or  $0.166 \text{ L g}^{-1}$ , respectively.

### 3.3.2 Dynamic sampling experiments to collect VOCs from atmospheric chamber

The dynamic sampling chamber, described in section 3.4 was used to generate a known concentration of VOCs. The atmospheres were then actively sampled using a specific flow rate of  $100 \text{ cm}^3 \text{min}^{-1}$ . The front end of the sampling tube was connected to the chamber and the back end was connected to an SKC sidekick sampling pump (see Figure 3.3). The flow rate of the SKC sidekick pump was calibrated to  $100 \text{ cm}^3 \text{min}^{-1}$  using a bubble meter. Sampling tubes (containing various

sorbents – see Section 3.5.1) were used to sample a 100 cm<sup>3</sup> aliquot of contaminated air from the experimental chamber.



**Figure 3.3: Sampling set up to collect VOCs from atmospheric chamber**

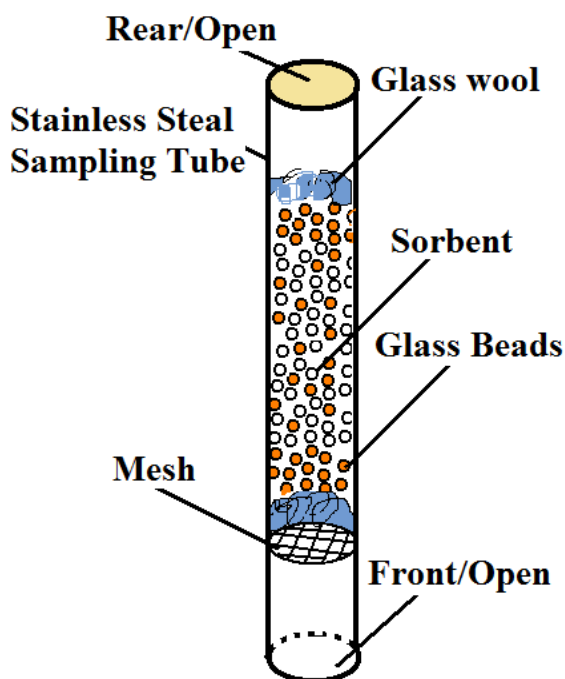
### 3.3.3 Preparation of sorbent packed sampling tubes

Different sorbents were packed into sampling tubes. Three sets of tubes were prepared containing Tenax TA (2,6-diphenylene-oxide polymer resin), MCM-41 or SBA-15. Tenax TA tubes used in this study were of 2 types. Type one was commercially available (Perkin Elmer) and type 2 was laboratory prepared where 100 mg of Tenax TA was loaded into stainless steel sampling tubes (Markes, Unit D3, Llantrisant Business Park Pontyclun, UK). All tubes were 8.89 cm (3.5 inches) in length with dimensions of 5 mm internal diameter. When sampling an aliquot of air, both sampling tubes (commercially available or laboratory prepared) gave statistically similar results. No differences in absorption efficiencies for all VOCs under study were observed.



In-house sampling tubes were also prepared containing MCM-41 or SBA-15 using the same stainless steel sampling tubes (Markes). Before the sorbents were loaded into the tubes they were pressed into a disc, crushed and sieved between 40 - 60 mesh. Each sampling tube was then packed with 100 mg of sorbent inter-dispersed with 1.5 g of glass beads (750-1000  $\mu\text{m}$ ), contained within two plugs of glass wool as shown Figure 3.4. The glass beads were incorporated within the sampling tubes to reduce the backpressure and enable the air flow rate required [152].

The 'rear/open' end of the sampling tube was then connected to a nitrogen cylinder via a mass flow controller. Nitrogen was passed through the filled tube for 5 min at flow rate of  $100 \text{ cm}^3 \text{ min}^{-1}$ . After the in-house sampling tubes were prepared the tubes were conditioned by heating under a flow of He using a thermal desorption unit (TDU) at  $320 \text{ }^\circ\text{C}$  for 15 min.



**Figure 3.4: Inter-dispersed of Sorbent and glass beads into sampling tubes.**

### **3.3.4 Experiments used to collect analytes in a 100 cm<sup>3</sup> volume of air**

To test the extraction efficiency of each sorbent for the 4 VOCs generated in the chamber, a 100 cm<sup>3</sup> aliquot of air was sampled. The initial sampling conditions chosen were 100 cm<sup>3</sup> min<sup>-1</sup> for 1 min and the masses of VOCs trapped onto the 3 sorbents were measured. To examine the effect of different flow rates on sampling efficiency the conditions were altered by using flow rates of 25, 50, 100, 150, or 200 cm<sup>3</sup> min<sup>-1</sup> with sampling time of 4, 2, 1, 0.667 or 0.5 min, respectively. The concentration of VOCs in the chamber remained the same and in each case a 100 cm<sup>3</sup> aliquot of air was sampled.

### **3.3.5 Alteration of humidity of diluent air**

The relative humidity (RH) of polluted air produced by the atmospheric dynamic chamber system was controlled by passing the stream through a humidifying system (a dreschel bottle which contained either distilled water or air). This system allowed the atmosphere to generate either 80 % (with water) or 25 % (with air) RH. When conditions were altered the system had to be left to equilibrate for 72 h period prior to sampling. A hydrometer (ETI.UK) was placed inside the sampling chamber to indicate the actual and accurate % RH value. The two RH conditions (80 or 25 % RH) were used to investigate the effect of relative humidity on VOC adsorption by each of the three sorbents.

### **3.3.6 Extraction efficiency experiments**

Three different sorbents were used (Tenax TA, MCM-41 or SBA-15) to sample 100 cm<sup>3</sup> of air from the experimental chamber using identical condition (a sampling flow rate of 100 cm<sup>3</sup> min<sup>-1</sup> for 1 min). The concentrations of analytes generated in the chamber were 34.1, 18, 12.4, or 7.8 mg m<sup>-3</sup> of toluene, ethylbenzene, cumene or dichlorobenzene respectively. The VOCs were thermally desorbed from the sampling tubes using a TDU and then diverted into the GC/MS for analysis. Internal standard calibration curves were used to determine the amount of masses trapped by each

sorbent and the extraction efficiency of each sorbent for the analytes under study was determined using Equation 3.3.

$$\text{Extraction Efficiency} = \frac{\text{Weight of analyte trapped on sorbent}}{\text{Theoretical Weight of analyte applied onto sorbent}} \times 100 \%$$

**Equation 3.3**

### 3.3.7 Dynamic capacity (breakthrough) experiments

Breakthrough experiments were carried out using 2 sampling tubes set up as shown in Figure 3.5. The principle of this experiment was to determine when breakthrough occurred for each sorbent using one set of VOC concentration. Here breakthrough is defined as the point at which 5 % of the analyte was trapped by the second sampling tube. The first experiment undertaken was to sample an atmosphere containing 34.1, 18, 12.4, or 7.8 mg m<sup>-3</sup> of toluene, ethylbenzene, cumene or dichlorobenzene, respectively at 100 cm<sup>3</sup> min<sup>-1</sup> for 1 min. The masses (M<sub>1</sub>) of each VOC trapped in tube 1 by three sorbents were then measured for the 100 cm<sup>3</sup> aliquot air.

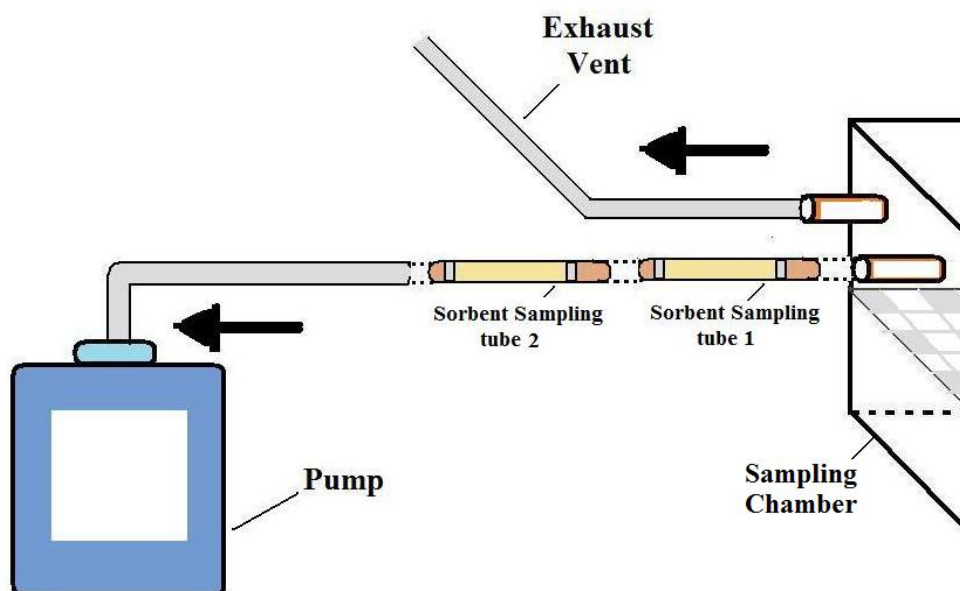
To introduce higher masses of analyte to each sorbent, the sampling times were increased to 2, 3, 5, 10, 15, 20, 30, 40, 50 or 60 min. For these experiments it was not possible to directly measure the VOCs trapped by tube 1 because the detector would have become swamped, particularly for the latter experiments. Instead the masses of VOC expected to be trapped by each sorbent were estimated by multiplying the masses trapped in the first experiment by the sampling time (M<sub>1</sub> × time). These will be referred to as mass expected (M<sub>E</sub>).

To determine breakthrough, the VOCs trapped by tube 2 were measured (M<sub>2</sub>) and the percentages of VOCs trapped were calculated using:

$$\text{Percentage of VOCs trapped on tube 2} = \frac{M_2}{M_E} \times 100 \%$$

**Equation 3.4**

Breakthrough was reported when the percentage of VOC measured on tube 2 exceeded 5 %.



**Figure 3.5: Schematic of breakthrough set up.**

### **3.3.8 Analysis of sampling tubes by thermal desorption unit– gas chromatography – mass spectrometry (TDU-GC-MS)**

The analytical instrument used to desorb, identify and quantify the VOCs trapped in the sampling tubes incorporated a thermal desorption unit, gas chromatograph (GC) and a mass spectrometer. The thermal desorption unit (TDU) was a Perkin Elmer Turbo Matrix TD. The operating conditions used when analysing VOC samples are outlined in Table 3.2. The TDU was coupled to a Perkin Elmer GC and Turbo Mass Gold Mass spectrometer (MS). The operating conditions for the GC and MS are outlined in Tables 3.3 and 3.4, respectively.

**Table 3.2: Operating conditions of the TDU for the desorption VOCs.**

<b>Desorb flow</b>	19 cm <sup>3</sup> min <sup>-1</sup>
<b>Desorb temperature</b>	300 °C
<b>Cold trap sorbent</b>	Tenax TA
<b>Cold trap temperature</b>	Held at -30 °C, Ramped at 99 °C s <sup>-1</sup> to 300 °C, Held at 300 °C for 5 min
<b>Split ratio</b>	1 %

**Table 3.3: Operating conditions of the GC for the separation of analytes.**

<b>Inlet Line temperature</b>	180 °C
<b>Oven Temperature</b>	65 °C
<b>Heating Rate</b>	65 °C for 5 min, Ramped to 90 °C for 8 °C min <sup>-1</sup> held 90 °C for 1.87 min
<b>Column</b>	Perkin Elmer, SMS Elite, (dimethylpolysiloxane (5%diphenyl)) 30 m 0.25 mm i.d.
<b>Carrier Gas</b>	Helium
<b>Carrier Gas Flow</b>	1 cm <sup>3</sup> min <sup>-1</sup>

**Table 3.4: Operating conditions of the MS for the detection of analytes.**

<b>Electron Energy</b>	<b>Trap Emission</b>	<b>Multiplier</b>	<b>Scan Run Time</b>	<b>Scan Time</b>	<b>Inter Scan Delay</b>	<b>m/z range (amu)</b>	<b>Solvent Delay</b>
70 eV	70 eV	350 V	10 min	0.2 s	0.1 s	50-300	2 min

### 3.3.9 Preparation of calibration solutions for TDU-GC-MS instrument

To calibrate the TDU-GC-MS for the quantification of analytes detected standard solutions were used. Methanolic solutions containing toluene, ethylbenzene, cumene and dichlorobenzene (see Supplier and purity information in Table 3.1) were prepared in 100 cm<sup>3</sup> volumetric flasks to prepare a stock solution where the final analyte concentrations were 60 ng μL<sup>-1</sup>. A second methanolic solution of o-xylene (99 %, Sigma Aldrich) was also prepared at the same concentration, to be used as an internal standard. An example calculation for the preparation of a 60 ng μL<sup>-1</sup> stock solution of toluene is given below.

*The desired concentration is 60 ng μL<sup>-1</sup> ≡ 60 μg cm<sup>-3</sup>*

$$\begin{aligned} \text{Required mass in volumetric flask is} &= V_f \text{ cm}^3 \times 60 \mu\text{g cm}^{-3} \\ &= 100 \times 60 \\ &= 6000 \mu\text{g} \equiv 6 \text{ mg} \end{aligned}$$

*Liquid density of toluene* = 0.87 g cm<sup>-3</sup> ≡ 870 mg cm<sup>-3</sup>

*The volume of toluene required to deliver 6 mg of toluene to the volumetric flask is then 6 mg / 870 mg cm<sup>-3</sup> = 6.9 μL.*

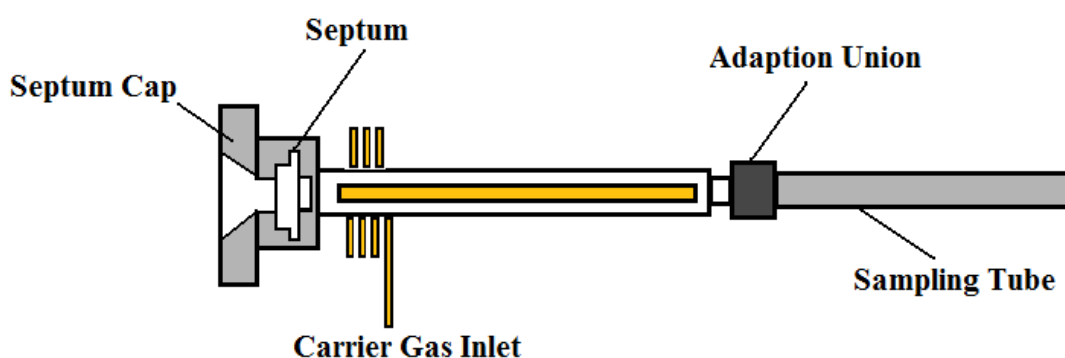
Thus, 6.9 μL of toluene was transferred into a 100 cm<sup>3</sup> volumetric flask and methanol (99 %, Fluka) was added to the 100 cm<sup>3</sup> mark. Similar calculations were obtained to calculate the volumes required preparing 60 ng μL<sup>-1</sup> of ethylbenzene, o-xylene, cumene, or dichlorobenzene, giving volumes of 6.9, 6.8, 7.0, or 4.6 μL respectively.

### 3.3.10 Injection of calibration solutions into sampling tube by direct injection method

To calibrate the instrument standard solutions containing known masses of each analyte were introduced onto conditioned sampling tubes containing Tenax, MCM-41 or SBA-15. The sorbent-type used for calibration was chosen to match the sorbent type used during the experimental procedure.

For each sorbent-type a different set of calibrant tubes were prepared by injecting 2, 4, 6, 8 or 10  $\mu\text{L}$  of the  $60 \text{ ng } \mu\text{L}^{-1}$  stock solution into the tube using the direct injection method discussed below. Before any tube was analysed (calibrant or experimental sampling tubes) a  $5 \mu\text{L}$  aliquot of o-xylene ( $60 \text{ ng } \mu\text{L}^{-1}$ ) was also injected into the tube to act as an internal standard. Sampling tubes were then taken through the full thermal desorption-gas chromatographic analysis.

A Perkin Elmer GC 8000 injection port was modified as shown in Figure 3.6 to permit efficient liquid sample introduction into sorbent tubes. An adaption union was used to connect the sampling tube to the injection port of the GC. Helium was used to connect the sampling tube to the injection port of the GC. Helium was used as a carrier gas permitting the transport of the injected analytes onto the sampling tube. The GC oven was controlled at  $25 \text{ }^\circ\text{C}$ . After injection of the standard solution, helium was passed over the sampling tube for 2 min at a flow rate of approximately  $100 \text{ cm}^3 \text{ min}^{-1}$ . The sampling tubes were then removed, capped and analysed by TD-GC-MS immediately after injection. The peak area ratios of analyte: internal standard were obtained and used to prepare calibrations for each analyte under investigation.

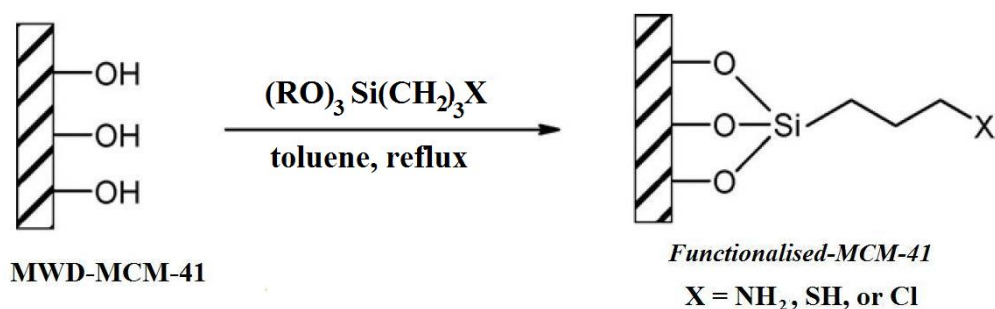


**Figure 3.6: Schematic of the modified Perkin Elmer GC 8000 injection port.**

### 3.4 Silica materials used for environmental remediation of polluted waters

#### 3.4.1 Functionalisation of MCM-41 procedure

Chemical modification of MCM-41 started with a condensation reaction containing the organosilane of choice and approximately 5 g of MCM-41 (Figure 3.7). The silica material was pre-treated at 140 °C for 2 h and then immersed into 50 cm<sup>3</sup> of toluene and 10 cm<sup>3</sup> of 3-aminopropyltrimethoxysilane APTMS (Sigma Aldrich, 99%) or 3-mercaptopropyltrimethoxysilane (Sigma Aldrich, 99%) MPTMS in a 250 cm<sup>3</sup> flask. The mixture was refluxed for 4 h and the solid produced was filtered, washed with 100 cm<sup>3</sup> of ethanol (Sigma Aldrich), and oven-dried at 80 °C for 1 h to produce an aminopropyl-functionalised (AP-MCM-41) or mercaptopropyl-functionalised (MP-MCM-41) sorbent, respectively.

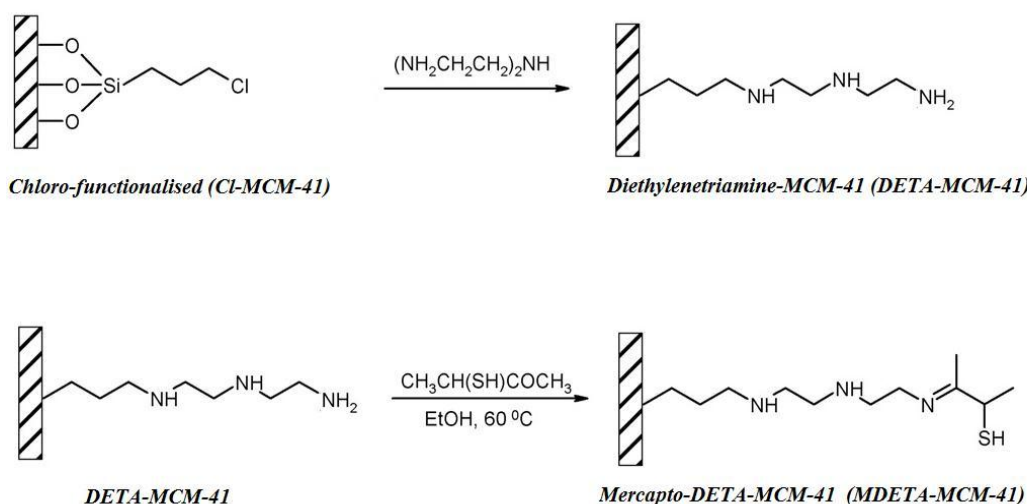


**Figure 3.7: Modification of activated silica using trialkoxysilanes.**

A similar procedure was used to prepare chloro-functionalised MCM-41 (Cl-MCM-41) using 3-chloropropyltrimethoxysilane, CPTMS (Sigma Aldrich, +97 %), which was further reacted to produce diethylenetriamine-MCM-41 (DETA-MCM-41) or mercaptodiethylenetriamine (MDETA-MCM-41). For DETA functionality 10 cm<sup>3</sup> of diethylenetriamine, DETA (Sigma Aldrich, 99 %), was added to 2 g of Cl-MCM-41 under reflux for 18 h. It was also prepared directly following the procedure discussed for AP- or MP-MCM-41 above using N-(3-trimethoxysilylpropyl) diethylenetriamine, DETA-TMS (Sigma Aldrich, +99 %). Both methods produced a



solid material that was filtered, washed with 100 cm<sup>3</sup> of ethanol and oven-dried at 80 °C for 1 h. To produce MDETA-MCM-41, 1.5 g of 3- mercaptobutanone (Sigma Aldrich, 99%), was dissolved in ethanol (50 cm<sup>3</sup>) and added to a 3 g subsample of DETA-MCM-41. The reaction mixture was refluxed for 16 h at 60 °C, cooled, filtered and washed with ethanol and dried at 80 °C, producing MDETA-MCM-41. Figure 3.8 illustrates the functionalising processes thought to occur via reaction at surface hydroxyl sites.



**Figure 3.8: Schematic representation of DETA- and MDETA-MCM-41**

### 3.4.2 Determination of the adsorption capacity of materials for metal ion removal from aqueous solution

The initial adsorption capacity experimental procedure used to test the silica materials potential to remove metal ions from aqueous solution was adapted from Burke et al.[153]. Approximately 10 mg of functionalised MCM-41 was suspended in a 20 cm<sup>3</sup> solution containing 20 µg cm<sup>-3</sup> of the metal ion of interest and the solution was stirred (250 rpm) for approximately 2 h. After this time a 5 cm<sup>3</sup> aliquot of solution was removed and analysed by flame atomic absorption spectrometry (FAAS) or inductively coupled plasma atomic emission spectroscopy (ICP-AES). The sorbent was recovered from the solution by vacuum filtration, dried and then re-immersed in another solution containing the metal ion of interest and the

concentration of the solution after sorbent addition was measured by FAAS or ICP-AES. This procedure was repeated until saturation of the sorbent as indicated by identification of the target analyte in the solution after sorbent addition. The extraction was repeated at various pH values (between 3 and 10) with solution modification achieved via the addition of small amounts of 1 M ammonium hydroxide (Sigma Aldrich, 30 %).

The amount of metal ion adsorbed by each material was calculated and the initial adsorption capacity values were determined using equation 3.5. [154]

$$q_e = \frac{(C_0 - C_e) V}{W \times \text{metal atomic weight}} \quad \text{Equation 3.5}$$

where  $q_e$  is the adsorption capacity ( $\mu\text{mol g}^{-1}$ ) of the adsorbent at equilibrium;  $C_0$  and  $C_e$  are the initial and equilibrium concentrations of solute ( $\mu\text{g cm}^{-3}$ ), respectively;  $V$  is the volume of the aqueous solution ( $\text{cm}^3$ ) and  $W$  the mass (g) of adsorbent used in the experiments. To check the results of the repeated adsorption capacity experiments, solutions containing larger concentrations of metal ions,  $200 \mu\text{g cm}^{-3}$ , were added to the sorbent to ensure the capacity of the sorbent was reached more quickly.

### 3.4.3 The sorbent extraction efficiencies for metal ions mixed with multi element or real water samples

To demonstrate the potential environmental performance of the sorbents when exposed to solutions containing mixed metal ions, a river water sample (collected from the Bothlin River in Glasgow. Sampling method is BS 6068-6.4:1987. The sample was stored in the sealed container at  $4^\circ\text{C}$ ) and a tap water sample (taken from a building in the Drygate campus in Glasgow. The water had lift running for 15 min before sampling taken place and then sample was stored in the sealed container at  $4^\circ\text{C}$ ) were analysed. Prior to addition of sorbents, both samples were analysed to determine the concentration of the target metal ions in solution used in this study. As the three case studies focus on extraction of lead, mercury or chromium ions from

water, both solutions were spiked with those metal ions individually to produce solutions containing each metal ion at a concentration of  $25 \mu\text{g cm}^{-3}$ . Multi elements experiments were carried out using standard solutions containing selected metals (Cd, Co, Cr, Cu, Fe, Hg, Mn, Ni, Pb, and Zn) diluted to a  $1 \mu\text{g cm}^{-3}$  concentration using non-buffered  $\text{H}_2\text{O}$  as a solvent. In each experiment 0.025 g of functionalised MCM-41 was added to solutions which were stirred for 2 h.  $5 \text{ cm}^3$  aliquots were removed and filtered (Fisherbrand QL100) prior to analysis by FAAS or ICP-AES.

### 3.4.4 Determinations of metals ions in water using FAAS

The concentrations of metal ions were measured in the water samples using an AAnalyst 200 (Perkin Elmer Instrument, Beaconsfield, Bucks, UK) flame atomic absorption spectrometer. Each set of sample solutions, and associated procedural blanks, were analysed using an integration time of 3 s. The absorbance values for three repeat measurements were used to determine the average measured concentration of each solution. HCL currents and absorption line wavelengths used are summarised in Table 3.5.

**Table 3.5: Flame atomic absorption spectrometer parameters.**

PTE	HCL Current /mA	HCL Wavelength / nm	Fuel
Ni	12	232	Air-Acetylene
Cr	8	357.87	Air-Acetylene
Cd	6	228.8	Air-Acetylene
Zn	8	213.86	Air-Acetylene
Hg	4	253.65	Air-Acetylene
Pb	8	283.31	Air-Acetylene

The specific metal hollow cathode lamp (HCL, Cathodeon, Burke Analytical) was used with each metal. The lamp was used at approximately 75 % of its maximum current. The combustion flame was comprised of an air-acetylene mixture.

In order to determine what effect, if any, the sample matrix had on the measured calibration; solutions for heavy metal were prepared in water, ammonium hydroxide and hydrochloric acid at 1, 5, 10, 15 or 20  $\mu\text{g cm}^{-3}$ . The solutions were prepared in 100  $\text{cm}^3$  volumetric flasks by the addition of 100  $\mu\text{L}$ , 500  $\mu\text{L}$ , 1  $\text{cm}^3$ , 1.5  $\text{cm}^3$  and 2  $\text{cm}^3$ , respectively, of analyte 1000  $\mu\text{g cm}^{-3}$  stock solutions.

Linear regression analysis experiments for the target metals were carried out using different matrix solutions at different pH conditions to identify any interference effects that may occur as a result of the presence of ammonium hydroxide or hydrochloric acid in sampled solutions. To determine if altering the solution, during the extraction experiments, would affect the measured the metal ions result, calibration graphs were measured with solution pHs of 4, 7 or 10. The solution pH was altered by the drop wise addition of either hydrochloric acid or ammonium hydroxide and measured using a PW9421 pH meter (Philips).

### **3.4.5 Determination of metal ion concentrations in aqueous solution using ICP-AES**

Metals ions were measured in water samples using a Perkin Elmer Optima 5300DV instrument (Perkin Elmer, UK) at an RF power of 1300 W, plasma, auxiliary and nebuliser argon gas flows of 15, 0.2 or 0.75  $\text{L min}^{-1}$ , respectively, and a pump flow rate of 1.5  $\text{cm}^3 \text{min}^{-1}$ . Multi-element calibration standards in the concentration range 0.02 - 1  $\mu\text{g cm}^{-3}$  were used and the emission intensity measured at appropriate wavelengths. For all elements, analytical precision (RSD) was typically 1-5 % for individual aliquots (n=3). Table 3.6 summarise the wavelength for heavy metals used in this research.

**Table 3.6: Wavelengths Used in ICP-AES.**

<b>Analyte</b>	As	Ca	Cd	Co	Cr
<b>Wavelength (nm)</b>	193.696	317.933	226.502	230.786	267.716
<b>Analyte</b>	Cu	Fe	Hg	Mg	Mn
<b>Wavelength (nm)</b>	324.572	239.562	194.168	279.077	257.610
<b>Analyte</b>	Ni	Pb	Zn		
<b>Wavelength (nm)</b>	231.604	220.353	213.857		

### **3.5 Determinations of Cr specious in water using colorimetric method and inductively coupled plasma atomic emission spectroscopy (ICP-AES)**

#### **3.5.1 Determination of chromium (VI) in water samples using the colorimetric method**

A method used was a slight modified to the method reported in ref. [140, 155]. 1000 ppm of Cr (VI) ions was used as stock solution (0.2828g of potassium dichromate was dissolved in 100 cm<sup>3</sup> distilled water). Six different levels of calibration standards were prepared in the range from 0.1 µg cm<sup>-3</sup> to 1.0 µg cm<sup>-3</sup> with reagent blank as first level. Results showed linearity with a good correlation co-efficient of 0.9986. A 1 cm<sup>3</sup> of diphenylcarbazide solution (250 mg of 1,5-diphenylcarbazide was dissolved in 50 cm<sup>3</sup> acetone and stored in a brown bottle) was added to 1 cm<sup>3</sup> of the water sample and the pH of the solution was adjusted to be in the range of 1-2 by adding 0.2 cm<sup>3</sup> hydrochloric acid (1 M) and allowed to stand 15 min for full colour development. An appropriate portion was transferred to a 1 cm absorption cell and measured the absorbance at 540 nm with the blank as a reference. The analysis was carried out using SI Photonics (M-420) CCD Array UV-Vis spectrophotometer.

### 3.5.2 Determination of total chromium Cr<sub>(Total)</sub> in water samples using ICP-AES

The Thermo Scientific iCAP 6200 ICP-AES was used for the analysis. Calibration standards were prepared in 5 % HNO<sub>3</sub> at the following concentrations: 0.1, 0.5, 1, 5, and 10 µg cm<sup>-3</sup>. A QC check solution was prepared at 1 µg cm<sup>-3</sup> to check recovery and test the stability of the method and repeatedly analysed after each 20 samples. The Environmental Method Template was opened within the Thermo Scientific iTEVA Software. Method parameters are shown in table 3.7.

**Table 3.7: ICP-AES instrumental parameters employed for chromium determination.**

---

RF Power	1150 W
Auxiliary gas flow	0.5 L/min
Nebuliser argon gas flows	0.5 L/min
Nebuliser	Glass concentric
Spray chamber	Glass cyclonic
Coolant gas flow	12 L/min
Flush pump rate	100 rpm
Analysis pump rate	50 rpm
Pump Stabilisation	5 sec
Pump tubing	Sample tygon orange/white; Drain tygon white/white
Sample repeats	3
Sample Flush time	30 sec
Analysis maximum	Radial 15 sec
Integration times	Radial 5 sec
Wavelength rang	Low

---

To determine the total chromium in water samples, study the difference in the calibration curves between Cr (III) and Cr (VI) standard solutions was necessary. Three sets of standard solutions of both chromium species were prepared at the range 0.1-1  $\mu\text{g cm}^{-3}$  and the third set was a mixed between Cr (III) and Cr (VI) using two different wavelengths (267.7 and 283.6 nm) and that was to see the differences in the results in case a sample contained both chromium species and the possibility to apply one set of standard curve to calculate the total chromium concentration in water samples.

### **3.6 Safety**

All work involving apparatus and chemical substances were performed in a safe and controlled manner in accordance with experimental risk assessments. In this work several substances were used (Table 3.8) which are classified as hazardous to health in relation to the 'Control of Substance Hazardous to Health' regulation.

#### **3.6.1 The analysis of heavy metals**

During all stages of analysis appropriate PPE was worn, including lab coat, safety glasses and gloves. The chemicals used during this stage of analysis were classified as harmful, irritant and oxidising. The solutions were prepared in a fume cupboard and stored either in the fridge or within the fume cupboard. Training on the use of the FAAS and ICP-AES were given before the project commenced, throughout the course of the investigation the FAAS and ICP-AES were used in the presence of other staff or students.

#### **3.6.2 The analysis of VOCs**

During all stages of the analysis lab coat, safety glasses and gloves were worn. The chemicals used during this stage of analysis were classified as toxic, harmful, irritant, flammable, carcinogenic and sensitising. All solutions were prepared in a fume cupboard and stored in a refrigerator. A risk assessment was carried out and the appropriate training on the GC-MS and modified injection port were given before the project commenced.

**Table 3.8: Hazardous substance associated with experimental methods.**

Substance	Very Toxic	Toxic	Carcinogenic	Mutagenic	Harmful	Flammable	Corrosive	Irritant
Toluene			√		√	√		√
Ethybenzene			√		√	√		√
Cumene			√					√
Dichlorobenzene			√		√			√
o-Xylene			√			√		√
Tetraethylthosilicate (TEOS)					√	√		√
Tetramethylammomium hydroxide (TMAOH)					√		√	
Cetyltrimethylammounim bromide (CTAB)								√
Hydrochloric Acid							√	√
Ethanol						√		
Methanol		√				√		
Lead nitrate		√	√		√			√
Mercury nitrate		√			√			√
Chromium (III) nitrate								√
Potassium dichromate	√		√	√				√



**Chapter 4: MCM-41 synthesis using a novel preparation  
method**

## **4.1 Introduction: Summary of conventional procedure used to prepare MCM-41**

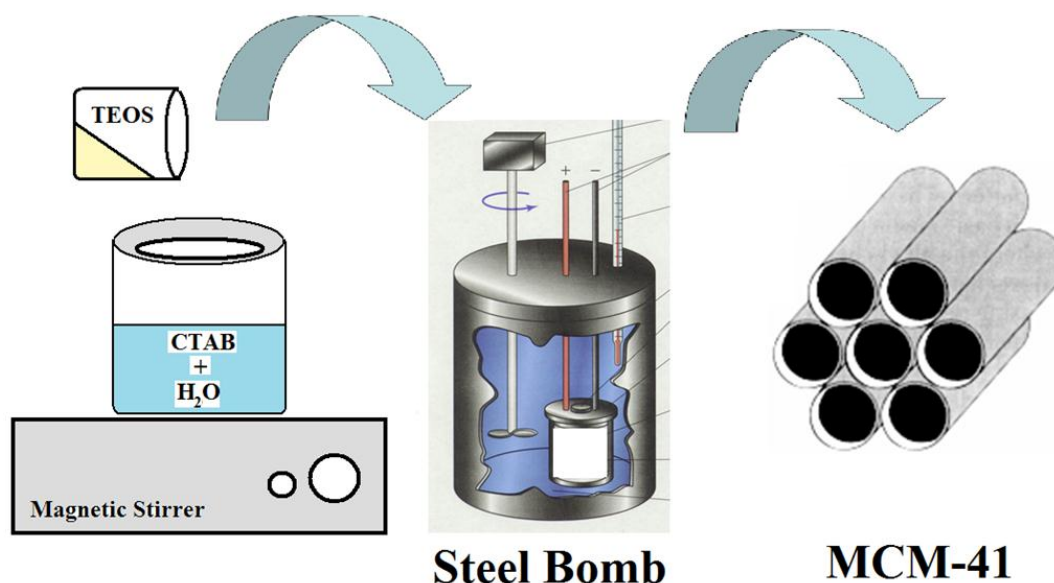
MCM-41 is a mesoporous silicate which can be synthesised following the original preparation method reported in reference [13], or by modification of this method to enhance the material's physicochemical properties (summary details of different preparation methods were given in Table 1.1, Section 1.3.3, p. 14-15). In general terms the material is produced by coating an organic template with silica using an aqueous solution of silica. The porous material can then be obtained by removing the organic template from the nanochannels of the synthesised material. Despite the ever increasing attention of researchers studying the potential applications of MCM-41, it is postulated here that there are three main disadvantages in the current MCM-41 preparation which lead to its limited use in industrial applications:

- 1- Most published preparation times are long (2 – 7 days).
- 2- Small quantities of MCM-41 are normally produced at a time (few grams).
- 3- The pore diameter of the final material is limited to a maximum size of approximately 5 nm.

Most research groups focus on enhancing the physicochemical properties of MCM-41 and chemically modifying its surface. There are only a few papers which focus on alteration of as-made MCM-41 method. Of these, most groups have tried to reduce the preparation time. For example Climent et al.[156] reported shorter synthesis times of the production of basic of MCM-41. Inagaki et al. reported a fast two-step method including aging prior to drying [157].

Tang et al. used ultrasound irradiation for synthesis of highly ordered MCM-41 in a short time [158]. Finally, Liu et al. introduced a rapid method for the synthesis of highly ordered MCM-41 using silica gel as the silica source [159]. Undoubtedly shorter preparation time is a distinct advantage, but without increasing the quantity of material per batch, use of MCM-41 material in industrial applications may still be limited.

Most reported MCM-41 laboratory preparation procedures follow the conventional method which involves the use of a steel bomb to control hydrolysis and condensation of the silica framework (Figure 4.1). The long preparation time and limits to the quantities of material produced are due to the use of a steel (or Teflon) bomb at the intermediate stage (condensation stage) to control pressure and temperature. The mass of MCM-41 produced in each synthetic batch is always limited according to the capacity of the steel bomb.



**Figure 4.1: The conventional procedure to produce MCM-41 in the lab.**

More recently attention has been focussed on the production of increased quantities of material. Ritter et al.[160] recently reported a scale-up, room temperature procedure for the production of unmodified MCM-41, with template removal by calcination. Removing previous necessary steel bomb allowed higher masses of material to be produced. Finally, Wan et al.[161] recently discussed a new procedure for template removal by microwave digestion. In addition to being faster than the traditional calcination method, there was an additional benefit: the mesoporous material produced had larger amounts of surface silanol groups.

This was also observed by Gu et al.[43] who used microwave digestion to increase the pore size of SBA-15 (from 6 nm using a conventional method of template removal to approximately 23 nm); here it was hypothesised that the increased pore size obtained was due to the joining of 2 or 3 pores together after pore wall teardown.

The research aims of this chapter were to develop a method of MCM-41 production which is faster, more economical and provides larger masses of sample in batch production. Moreover, the target application areas in this research were adsorption studies: environmental remediation after functionalisation of MCM-41 with an appropriate chelate. Hence the ultimate aim of this chapter was to obtain a fast method of MCM-41 production (as-made MCM-41 and template removal) with larger pores and increased surface silanol groups that could be functionalised significantly enhancing the material's adsorption properties. It was thought that the inclusion of larger mesopores (or even mesotunnels) in an adsorbent material would be highly desirable if it were to be surface functionalised and used to provide a higher number of chelating groups that could extract analytes (vapour or liquid) from a contaminated matrix.

## **4.2 Experimental: Development of new laboratory method for the production of MWD-MCM-41**

The synthesis method used was adapted from Ritter et al.[160]. Approximately 8.8 g of CTAB was dissolved under slight warming (35 °C) in a mixture of 208 cm<sup>3</sup> of distilled H<sub>2</sub>O and 96 cm<sup>3</sup> of aqueous NH<sub>3</sub>. To this clear solution, 40 cm<sup>3</sup> of TEOS was slowly added under stirring. After further stirring for 3 h, the gel was aged at room temperature for 24 h in a closed container.

The product was obtained by filtration, washed with 600 cm<sup>3</sup> of distilled H<sub>2</sub>O, and air dried at room temperature. To remove the surfactant microwave digestion (MWD) was performed by modifying the method reported by Gu et al.[43]. A MARS 5 microwave digestion system (CEM Corporation, Buckingham, UK) was used at an operating power of approximately 1600 W. The pressure and temperature inside the microwave were controlled to be lower than 1.3 MPa and 200 °C. Samples (approx. 0.3 g) were added to multiple Teflon vessels to which 5 cm<sup>3</sup> of HNO<sub>3</sub>

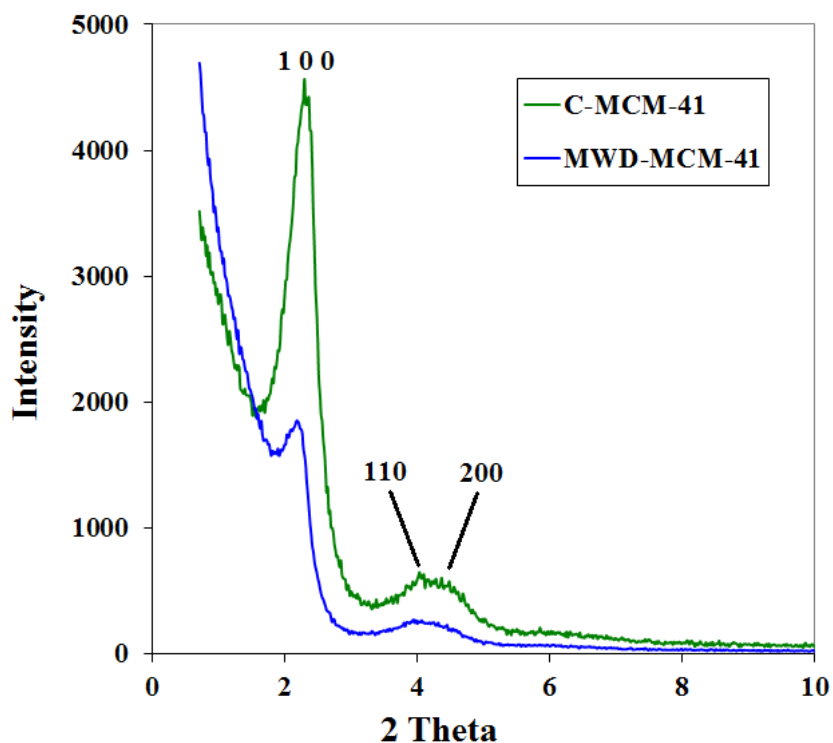
(Fisher Scientific, 65 wt.%) and 2 cm<sup>3</sup> of H<sub>2</sub>O<sub>2</sub> (Sigma Aldrich, 30 wt. %) were added. Microwave digestion was operated at a working frequency of 2450 MHz and 220 V for 15 min. The product (to be hereafter referred to as ‘MWD-MCM-41’) was filtered, washed with copious amounts of distilled H<sub>2</sub>O and dried at 100 °C for 2 h. For comparison a second batch of MCM-41 was produced where template removal was performed using a conventional calcination rig by heating in air at 550 °C for 8 h. This material will be referred to as ‘C-MCM-41’.

### **4.3 Results and discussion**

The room temperature method of preparation was used to produce as-made MCM-41 material that was subsequently treated to or microwave digestion (MWD-MCM-41), or high temperature (C-MCM-41) to remove the organic template. As steel bombs were not used to control the silica hydrolysis the mesoporous material was produced on the bench, in large quantities, providing approximately 100 g of material each batch while about 2 g only can be produced when the conventional method was used.

#### **4.3.1 MCM-41 characterisation by XRD and N<sub>2</sub> adsorption isotherm**

XRD patterns of MWD-MCM-41 or C-MCM-41 samples, shown in Figure 4.2, indicated that the adsorbent materials possessed a hexagonal mesophase structure with a clear (100) peak and weaker reflections assignable to (110) or (200) reflections. The first indication of that the two methods have produced different order materials was from the intensity of the (100) peak. It was clear that the C-MCM-41 has wide range of ordinary compared with MWD-MCM-41 which indicates that something happen to the pores of MWD-MCM-41 causing a reduction of the (100) reflection peak. Analysis of materials by BET provided the physicochemical material properties summarised in Table 4.1.



**Figure 4.2: XRD patterns of the MWD-MCM-41 and C-MCM-41.**

**Table 4.1: Physicochemical properties of microwave digested and calcined MCM-41.**

Sample Name	BET Surface Area (m <sup>2</sup> g <sup>-1</sup> ) <sup>a</sup>	Pore Size (nm) <sup>b</sup>	Pore Volume (cm <sup>3</sup> g <sup>-1</sup> ) <sup>c</sup>	d-Space (Å) <sup>d</sup>
MWD-MCM-41	760	6.7	0.99	42.20
C-MCM-41	813	2.53	0.69	38.48

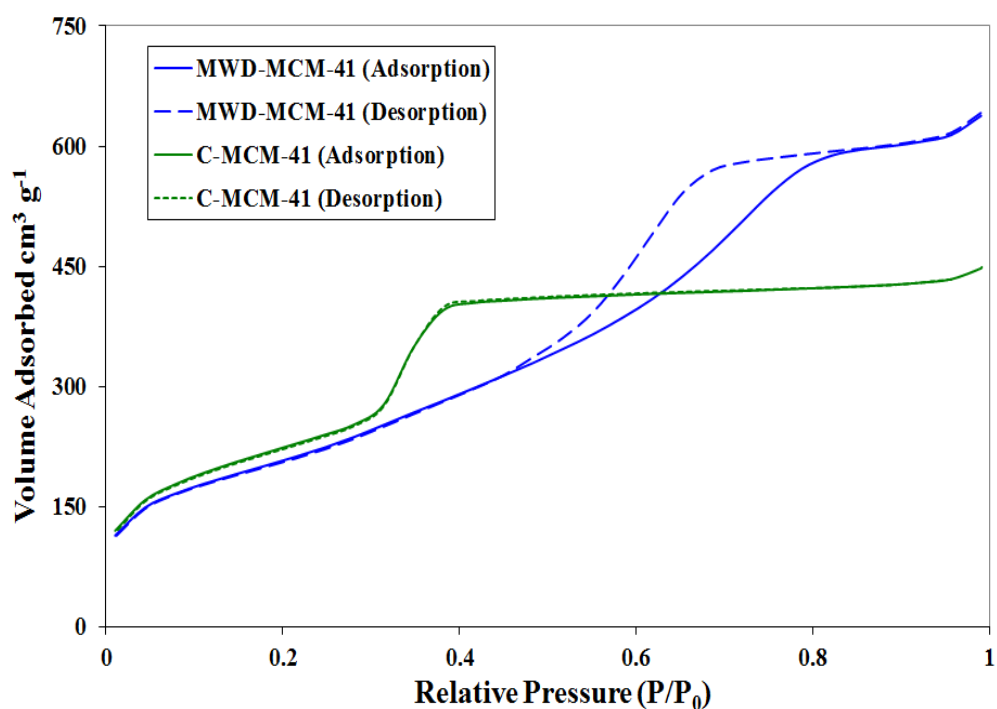
<sup>a</sup> Calculated by the BJH model from sorption data in a relative pressure range from 0.05–0.25.

<sup>b</sup> Calculated by the BJH model from the adsorption branches of isotherms.

<sup>c</sup> Calculated from N<sub>2</sub> amount adsorbed at a relative pressure P/P<sub>0</sub> of 0.99.

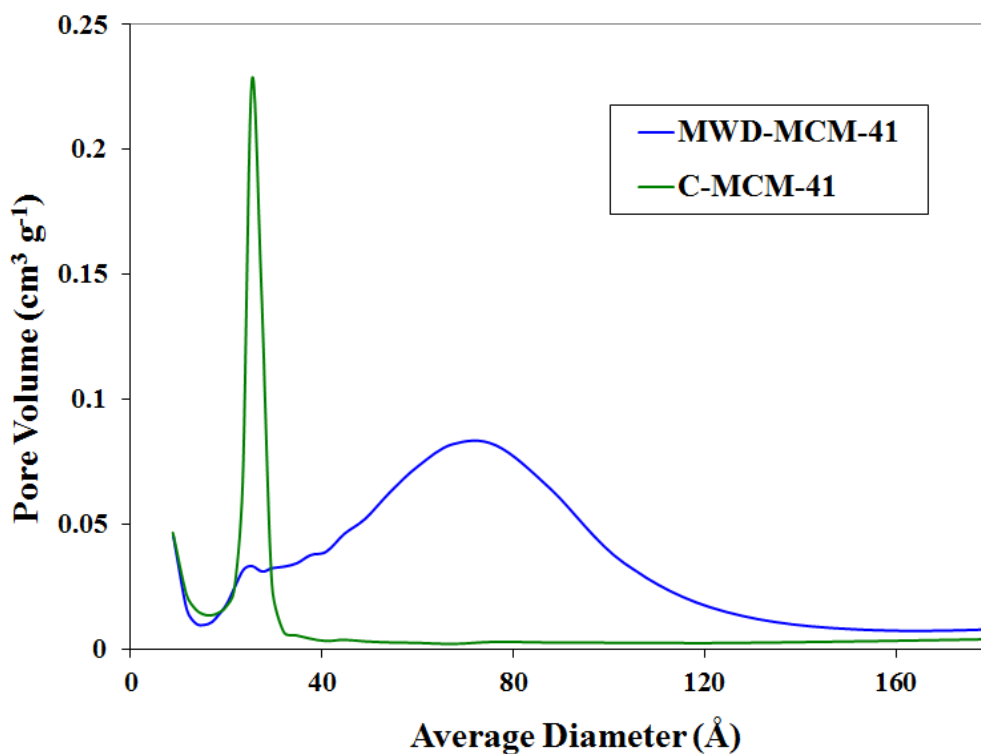
<sup>d</sup> Calculated from PXRD data.

It was shown that the surface area of MCM-41 reduced slightly (from 813 to 760  $\text{m}^2 \text{g}^{-1}$ ) when the template was removed by MWD compared to calcination. More importantly however there a significant increase in average pore size from 2.5 to 6.7 nm (pore size distribution was in range from 2-12 nm) when microwave digestion was used to remove the organic template. This larger pore size is not common for mesoporous silica materials as MCM-41, which typically demonstrate a pore size range between 2.5-4.5 nm. A significant increase in pore volume and d-spacing was also demonstrated. The  $\text{N}_2$  sorption isotherms obtained (Figure 4.3) were of IUPAC type IV confirming their mesoporous nature, however slightly different capillary condensation steps were noted at relative pressures of 0.31–0.38 and 0.55-0.69 for the calcined and microwave-treated products, respectively, as expected as the microwave digestion method induced larger pores in the material. The hysteresis loop was also broader for MWD-MCM-41 suggesting that this material contained pores of different shape and size.



**Figure 4.3: Nitrogen adsorption isotherms of MCM-41 after the template removal by calcination and by MWD.**

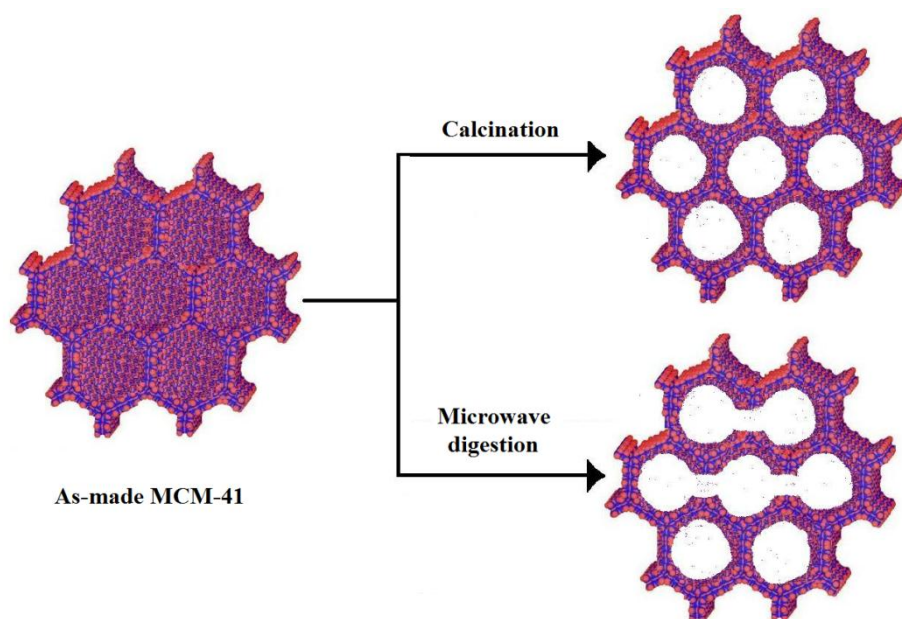
Whereas there was no deviation of the adsorption and desorption traces for C-MCM-41 indicating a narrow range of well-defined pores. This was confirmed by examination of the pore distribution plots (Figure 4.4). The increased surface area of C-MCM-41 was further evidence that smaller, well-defined, pores are obtained by this method of surfactant removal.



**Figure 4.4: BET pore size distribution patterns of the MWD-MCM-41 and C-MCM-41.**

It is suggested here that these results provide further evidence of a hypothesis, first discussed by Gu et al.[43] for SBA-15, that the pores in SBA-15 joined together during an applied microwave digestion procedure (Figure 4.5).



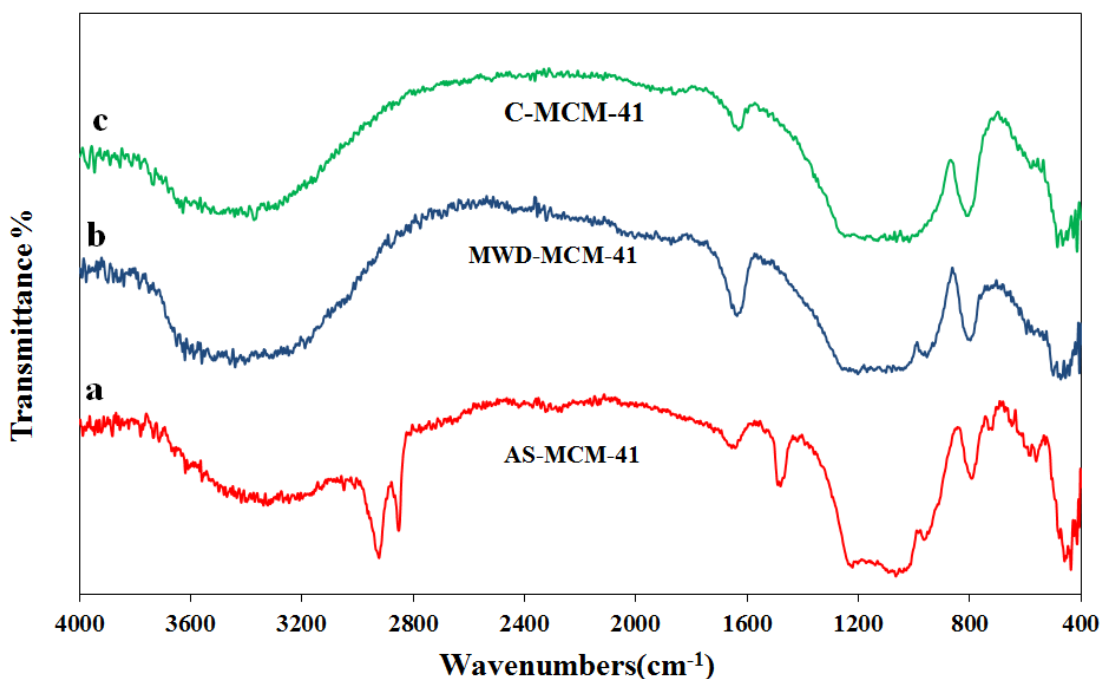


**Figure 4.5: Schematic representation of the procedure for template removal by calcination and microwave digestion.**

### 4.3.2 FTIR and elemental analysis of MCM-41 samples

The FTIR spectra of all samples (Figure 4.6) contain similar features expected of a silica containing material associated with the inorganic backbone such as (i) a large broad band between 3500 and 3200  $\text{cm}^{-1}$  which is assigned to the O–H stretching mode of silanol groups and also to some adsorbed water, (ii) several absorption bands at around 1030-1240  $\text{cm}^{-1}$  which can be assigned to the Si–O–Si stretching and (iii) the water bending mode band around 1650  $\text{cm}^{-1}$  [162]. In addition to those peaks the spectrum of the as-made MCM-41 sample contained extra bands at 2850 and 2930  $\text{cm}^{-1}$  which were assigned to the C-H stretching of  $\text{sp}^3$  carbon, and a band at 1490  $\text{cm}^{-1}$  was assigned to a C-N stretching mode. The presence of these bands (due to the surfactant template in the as-made sample) were absent in both spectra for C-MCM-41 or MWD-MCM-41 confirming that both methods successfully removed the organic template. It was also noted that the intensity of MWD-MCM-41 Si-OH bands at around 970  $\text{cm}^{-1}$  were comparable to those of the as-made MCM-41 bands; whereas the peak was considerably smaller in the C-MCM-41 spectrum. Again these

results confirm the theory of increased silanol groups on the surface of the material after microwave digestion. Successful template removal was confirmed by microanalysis (see Table 4.2); no carbon or nitrogen atoms were detected in the final products.



**Figure 4.6: FT-IR spectra of (a) MCM-41 (as-made), (b) MWD-MCM-41, and (c) C-MCM-41.**

**Table 4.2: Elemental analysis data recorded for the MCM-41 samples.**

Silica	% C	% H	% N	% S
As-made MCM-41	22.48	5.14	1.26	0.00
C-MCM-41	Trace/Nil	0.50	Trace/Nil	0.00
MWD-MCM-41	Trace/Nil	0.52	Trace/Nil	0.00

This data indicated that the MCM-41 samples treated with nitric acid, hydrogen peroxide and microwave digestion produced a material that had a larger number silanol groups, increased pore size and pore volume. Should this be the case then it is suggested that a higher degree of functionalisation would be possible for samples of MWD-MCM-41 compared to C-MCM-41. This set of results, supported by the FTIR data, confirmed that the new combined method of analysis for MCM-41, not reported before, can produce larger quantities of an optimised material for adsorptive or catalytic applications (mesoporous channels, larger pores, more silanol groups available for functionalisation) using a simple procedure in the laboratory.

Very little information has been published to date discussed the ability to increase the pore size and pore size distribution [163, 164]. However pore size control has been a critical issue in the synthesis of M41S type materials. This was the biggest limitation of M41S type materials and also was the first reason to produce material with larger pore size (SBA-15) [165]. Therefore the successful in this chapter to produce MCM-41 with large pore size and moreover with broad pore size distribution will open a new window of possibility of using MCM-41 with the application when the large pore size and also pore distribution required.

#### **4.4 Conclusion**

A new method of MCM-41 production using room temperature hydrolysis and condensation conditions together with microwave and nitric acid/hydrogen peroxide digestion of the organic template has resulted in the production of mesoporous silica with higher silanol group availability and a larger pore distribution. This is a new preparation method for MCM-41 that is faster, provides larger quantities of material per batch and is more economical than conventional approaches.

**Chapter 5: Extraction of VOCs from indoor air using  
mesoporous silicate**

## 5.1 Introduction: Volatile organic compounds in indoor air

Volatile organic compounds (VOCs) are one of the most common air pollutants that need to be controlled according to increasingly stringent environmental regulations. VOCs are emitted as gases from certain solids, or liquids, which include a variety of chemicals, some of which may have short- and long-term adverse health effects. As many people spend the greater part of their lives indoors the risks to health may be greater due to indoor air pollution than the outdoor air.

Classification of VOCs can be made according to, their chemical character (alkanes, aromatic hydrocarbons, aldehydes, etc.), their physical properties (boiling point, vapour pressure, carbon number, etc.), or their potential health effects (irritants, neurotoxics, carcinogens, etc.). Following the classification given by the World Health Organisation (WHO) working group on organic indoor air pollutants (WHO, 1989 ) [166], it has become common practice to divide organic chemicals into 4 main categories (Table 5.1) according to the molecule's boiling point.

**Table 5.1: Classification of indoor organic pollutants (WHO, 1989). [166]**

Category	Description	Abbreviation	Boiling-point range*	Sampling media typically used in field studies
1	Very volatile (gaseous) organic compounds	VVOC	< 0 to 50-100	Batch sampling; adsorption-on charcoal
2	Volatile organic compounds	VOC	50-100 to 240-260	Adsorption on Tenax TA, graphitised carbon black or charcoal
3	Semivolatile organic compounds	SVOC	240-260 to 380-400	Adsorption on polyurethane foam or XAD-2
4	Organic compounds associated with particulate matter or particulate organic matter	POM	> 380	Collection on filters

\* Polar compounds appear at the higher end of the range.

Several hundred organic compounds have been detected in indoor air [167], most of which belong to the VOC classification. Many of these compounds are aromatic hydrocarbon, alkenes, alcohols, aliphatic hydrocarbons, aldehydes, ketones, esters, glycols, glycolethers, halocarbons, cycloalkanes or terpenes [106].

### **5.1.1 Sources of indoor VOCs**

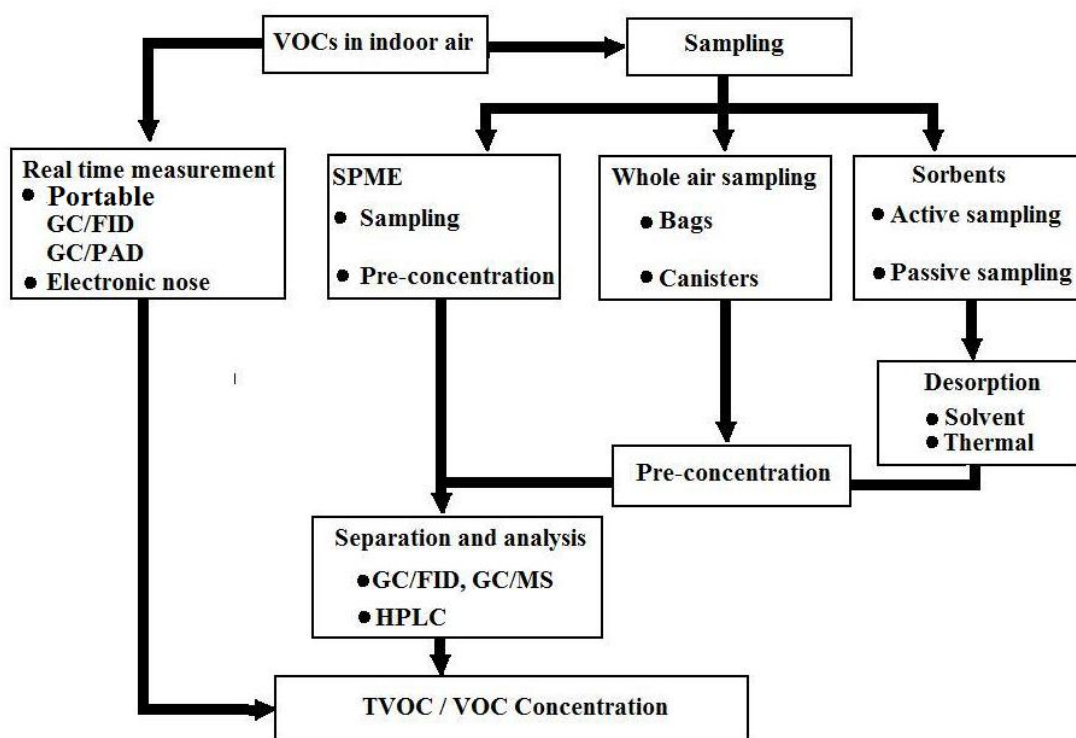
Potential indoor VOC sources include human activities such as cooking, cleaning, building renovation and tobacco, which all generate high levels and wide varieties of VOCs. Other emissive sources include household and consumer products, furnishing and building materials, office equipment, air fresheners, paints, paint strippers, household solvents. Apart from these indoor sources, intrusions of VOCs from outdoor traffic as well as biogenic and industrial emissions contribute significantly to the overall indoor VOCs level [168]. While some common indoor VOCs originate exclusively from indoor sources, others have multiple indoor and outdoor sources. Consequently, the indoor level of a particular VOC is the total of its different indoor and outdoor sources.

### **5.1.2 Sampling methods for indoor VOCs**

The general analytical procedures described in Figure 5.1 can be applied to most air monitoring exercises.

To select the most appropriate sampling method for each monitoring campaign, the purpose of the monitoring exercise must be clearly set out. Then an appropriate method of sampling (typically one of the methods in Figure 5.1 will be used) must be chosen, by choice of suitable methods for sampling storage, sample preparation and sample separation technique. Lastly, identification and quantification of the components are performed [169].

The choice of the sampling method depends on the objective of the investigation and the VOCs of interest. A significant disturbance of the indoor environment while collecting the samples, such as increased air circulation or different behaviour of the occupants, must be avoided otherwise this could lead to biased analytical results. The most two commonly used air sampling methods (active and passive) used to sampling VOCs from indoor air are discussed below [169, 170].



**Figure 5.1: Summary of the steps involved in the characterisation of indoor volatile organic compounds (VOCs). [170]**

### *Active air sampling methods*

The method of active sampling involves the use of a pump, to draw a specified volume of the air to be sampled through an adsorbent tube, with a specified, usually low, air flow rate. Some sampling pumps allow the collection of long term average samples intermittently, or sampling at a very low air flow rate. However, active sampling is usually performed when short-term averages are needed [171]. Short-term samples are preferred when increased or variable concentrations are to be expected and time resolution is needed [172]. There is a wide range of adsorbents available for sampling indoor VOCs which can be classified into three broad categories: porous polymer-based sorbent (e.g. Tenax TA and Chromosorb), carbon-based sorbents (activated charcoal, graphitised carbon blacks, carbotraps, anasorb, carboxens and carbosieve) and silica gels. Porous polymer and carbon-based sorbents are the most widely used for indoor VOC sampling.

### ***Passive air sampling methods***

Passive sampling may be defined as any sampling technique that is based on the free flow of analyte molecules from a sampling medium to a collecting medium. The driving force of analyte collection is the concentration difference between the analyte in the indoor air and the analyte at the collecting medium (which should be zero) [173]. Advantages of passive sampling over active sampling methods include lower cost and greater worker acceptability; it does not require bulky and expensive pumps that are subjected to regular checking and possible error in flow rate. A layer of adsorbent, which may collect a range of analytes or be specific, is covered with a barrier material whose outer surface is exposed to the contaminated air when sampling commences. The diffusion barrier is a known volume of air inside a tube, a semi-permeable membrane or a layer of plastic drilled with many small parallel holes. The barrier prohibits bulk flow of air to the surface of the adsorbent. Since the adsorbent has a strong affinity for the contaminant, a concentration gradient will be established which favours diffusion of the contaminant from the air to the adsorbent.

The rate of diffusion, determined by the properties of the compounds and sampler geometry, must be determined by previous calibration. The critical limitations are sorbent capacity and uptake rate in the case of high dosages, the response time and sensitivity in the case of low dosages [174].

#### **5.1.3 Sorbents used for VOC sampling**

The type of sorbent used for VOC collection depends on the nature of compounds in the air mixture to be measured. An overview of the available solid sorbents for VOC sampling is given in Table 5.2.

Only adsorbents which are commonly used in indoor studies are included and most of them are used for active sampling. Some of them may also be used for passive sampling.[168]

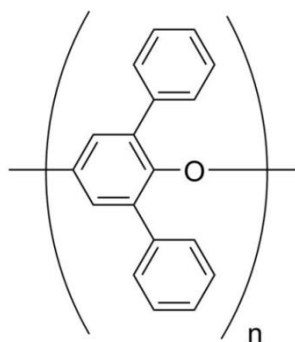


**Table 5.2: Sorbents used to collect VOCs from indoor air [168, 173, 174].**

<b>Sorbent</b>	<b>Compounds Sampled</b>	<b>Main Advantages and Disadvantages</b>
Tenax TA	<ul style="list-style-type: none"><li>- most non-polar VOCs</li><li>- terpenes</li><li>- slightly polar VOCs</li><li>- aldehydes &gt; C5</li><li>- (acids &gt; C3)*</li></ul>	<ul style="list-style-type: none"><li>- low background</li><li>- well investigated</li><li>- some decomposition products (benzaldehyde, acetophenone)</li></ul>
Carbotrap	<ul style="list-style-type: none"><li>- most non polar VOCs</li><li>- slightly polar VOCs</li></ul>	<ul style="list-style-type: none"><li>-low background</li><li>-reactions of some compounds (i.e. aldehydes, terpenes)</li></ul>
Activated carbon	<ul style="list-style-type: none"><li>- most non-polar VOCs</li><li>- slightly polar VOCs</li></ul>	<ul style="list-style-type: none"><li>-high capacity</li><li>-reactions of some compounds</li></ul>
Porapak Q	<ul style="list-style-type: none"><li>- most non-polar VOCs</li><li>- slightly polar VOCs</li></ul>	<ul style="list-style-type: none"><li>-high background</li><li>-low thermal stability</li></ul>
Organic molecular Sieves (e.g. Carboxen 563, 564, Carbosieve-S 111)	<ul style="list-style-type: none"><li>- polar and non-polar VOCs</li></ul>	<ul style="list-style-type: none"><li>-water adsorption</li></ul>

\* can be used (mainly low recoveries).

In literature Tenax TA (Poly-2,6-diphenylphenylene oxide), with high thermal stability up to 350 ° C, is the most often used and best evaluated sorbent for VOCs sampling; thus it tends to be the default choice for most research groups monitoring indoor air [169]. The monomeric unit of Tenax TA is illustrated in Figure 5.2.



**Figure 5.2: Tenax TA.**

To monitor a large mixture of VOCs multiple sorbents are required to cover the wide range of VOC boiling points. VOCs can be desorbed from solid sorbents thermally using a thermal desorption unit which uses a flow of an inert carrier gas, e.g. helium.

#### **5.1.4 Characterisation of indoor VOCs**

Analyses of indoor VOCs are usually performed with gas chromatographs (GCs), which are coupled with a flame ionisation detector (FID), an electron capture device (ECD) or mass spectrometry (MS). Alternatively high-performance liquid chromatography (HPLC) is used. Of these techniques, GC/MS provides the most conclusive qualitative and quantitative information, although a combination of FID and ECD has also been reported to permit the identification of compounds with widely different properties [175]. Nonetheless, GC/MS remains the most widely used technique for the characterisation of indoor VOCs [176]. A total ion chromatogram is usually measured to obtain information on the ranges of compounds present and selected ion monitoring is performed to identify and monitor particular analytes.

### 5.1.5 Typical VOCs in indoor air

Numerous studies have measured VOC concentrations in various types of buildings over the last 20 years. Several hundred VOCs have been detected in indoor air and Brown et al.[177] have compiled a list of VOCs that can affect humans. Table 5.3 shows monoaromatic hydrocarbons that appeared in most of the published literature studying VOC concentrations in indoor air. Monoaromatic hydrocarbons (MAHCs), including benzene, toluene, ethylbenzene, xylene (BTEX), cumene and dichlorobenzene (DCB), form an important group of air pollutants in urban areas [178]. Among them, benzene is a well-known carcinogen (Group A), while ethylbenzene has been classified as potential carcinogens to humans (Group 2B) by the International Agency for Research on Cancer [86, 179].

**Table 5.3: The average concentrations ( $\mu\text{g m}^{-3}$ ) of monoaromatic hydrocarbons monitored in selected studies.**

Compound	Ref.[180]	Ref.[181]	Ref.[182]	Ref.[183]	Ref.[184]	Ref.[185]
	Finland	Canada	USA	Australia	Hong Kong	UK
Benzene	2.2	17.0	4.8	7.0	8.1	13.9
Toluene	20.4	49.0	15.3	14.0	52.8	38.4
Ethylbenzene	2.9	.....	9.7	1.8	7.3	2.3
o-Xylene	2.5	33.0	11.2	8.9	5.1	1.9
Cumene	0.8	16.0	.....	.....	.....	.....
DCB	.....	11.5	4.8	31.0	10.2	0.1

### **5.1.6 Using mesoporous silicates as a sorbent of VOCs from indoor air**

Mesoporous silica materials have great potential for application as adsorbents for the removal of VOCs given their uniform pore size, open pore structure, and in particular, reliable desorption performance [186].

The high surface area of mesoporous silica can be used to adsorb VOCs at room temperature with great capacity. The saturated sorbent can be reactivated with hot air (120 - 150 °C) and the recovered VOCs can be concentrated by 3-10 times. This process does not require the use of an air steam for adsorbent reactivation and is flexible for the recovery of various kinds of VOC [187].

Tung-Min et al.[188] compared the efficiency of sorption of VOCs from the environment using mesoporous silica and compared the results with other widely used commercial carbon-based molecular sieves of micro-porosity. The results indicated that carbon sorbents quantitatively trapped a wide range of VOCs from C<sub>3</sub> to C<sub>12</sub> at room temperature whereas MCM-41 trapped considerably larger molecules from C<sub>8</sub> to C<sub>12</sub> with the potential to go beyond C<sub>12</sub>. The desorption temperatures used were different with trapped VOCs being released from mesoporous silica at low temperature, approximately 150 °C, whereas the microporous carbon sorbents required higher desorption temperatures of 300 °C for good recovery[188].

Further, recent modifications in the preparation methods of MCM-41 and SBA-15 presents several major advantages including low temperature synthesis, broad ranged and controllable pore widths and thermal stability. Functional groups can be introduced onto the silica surface to increase the adsorption performance of mesoporous silica for specific targets.

Functionalisation provides two main advantages for VOC adsorption: first, the functional groups increase the affinity of the solids towards vapour molecules. Second, the functional groups modify the solid pore and the surface area becomes more vapour adsorbent [189].

Table 5.4 lists some physical properties of mesoporous silica materials used to adsorb VOCs from indoor air.

**Table 5.4: Physical properties of mesoporous silica used to adsorb VOCs from indoor air.**

Sorbent	$S_{\text{BET}}$ ( $\text{m}^2 \text{g}^{-1}$ )	$V_p$ ( $\text{cm}^3 \text{g}^{-1}$ )	BJH Dp (nm)	Functional Group	Adsorbates	Ref.
MCM-41	1065	0.73	2.3	Pure Silica	Toluene, isopentane	[190]
MCM-41	1310	0.66	1.8	Al-MCM-41	Water	[190]
MCM-41	1030	----	----	Pure Silica	C7–C12	[188]
MCM-41	1060	0.87	----	Pure Silica	Benzene, n-hexane	[91]
MCM-41	1086	0.86	3.5	Pure Silica	Dichloromethane, benzene	[191]
MCM-41	734	0.76	----	Pure Silica	Ethane, Ethylene	[192]
SBA-15	594	0.85	6.4	Pure Silica	Toluene, isopentane	[193]
SBA-15	501	1.14	8.2	Pure Silica	Cyclohexane, benzene	[194]
SBA-15	577.1	1.03	5.6	Me-SBA-15	Cyclohexane, benzene	[194]
SBA-15	794.5	0.87	4.4	Ph-SBA-15	Cyclohexane, benzene	[194]
SBA-15	279.1	0.34	----	Ph-SBA-15	Benzene, n-hexane	[189]
SBA-15	353.5	0.41	----	Vinyl-SBA-15	Benzene, n-hexane	[189]
SBA-15	698	1.2	----	Pure Silica	Benzene	[195]

### 5.1.7 Factors effecting the adsorption of VOCs onto sorbents

Factors which could affect the adsorption efficiency of VOCs from indoor air onto building materials are reported in many literature studies. However, not one study reports on the influence of factors which affect the adsorption of VOCs from indoor air onto sorbents. Table 5.5 summarises the results of previous studies on the effects of various factors on sorption.

**Table 5.5: Factors affecting adsorption of VOCs on sorbents.**

<b>Factor</b>	<b>Effect of adsorption</b>	<b>Ref.</b>
1 Physical properties of VOCs	Adsorption of VOCs increased with increased vapour pressure and decreased boiling point.	[196, 197]
2 Physical properties of sorbent	The greater the specific area, the larger the VOCs adsorption.	[198]
3 Air temperature	The adsorption and desorption rate at 35 °C was higher than at 23 °C. Desorption rate increased more rapidly than the adsorption rate, the VOCs adsorption decreased with an increase in temperature of 23 °C to 35 °C.	[199]
4 Air velocity	The higher air velocity, the higher desorption rate.	[200]

The relative humidity (RH) of the sampled air is also known to affect the adsorption of VOCs. However conflicting results are reported in the literature with respect to how the change in RH affects the adsorption rate; the influence of water vapour appears to be a complicated phenomenon. For example, one report concluded that there was no significant influence of RH on VOCs (cyclohexane, toluene, ethyl acetate, isopropyl alcohol) adsorption onto a ceiling tile [201].

Corsi et al.[202] found no apparent impact of relative humidity on the sorption of seven VOCs (methyl tert-butyl ether, cyclohexane, toluene, tetrachloroethene, ethylbenzene, o-dichlorobenzene, and 1,2,4-trichlorobenzene) on various materials (carpet, vinyl and wood flooring, upholstery and fiberglass shower stall). In contrast, Kirchner et al.[198] found that the sorption strength of 2-butoxyethanol on gypsum board was weaker under higher humidity levels (40 % RH) compared to 0 % RH. Finally, Zhang et al.[203] showed that the presence of water vapour may decrease the adsorption of dodecane, but increase the adsorption of benzaldehyde when the RH is increased from 50 % to 80 %.

Silica materials have recently been used as trapping methods for VOCs in indoor air. As a sustainable material with the potential for functionalisation, silica adsorbents are potentially ideal materials for VOC determination in indoor air. However there is still conflicting results regarding the effects of humidity and calibration performance of the sampling method. The key aims of this chapter were then to (i) validate an air system to generate known concentrations of VOCs in air (ii) study the use of silica adsorbents for VOC extraction, compare performance to Tenax TA, (iii) to examine calibration variability and (iv) the effects of RH on adsorbance performance using silica materials prepared at the University of Strathclyde.

## **5.2 Experimental**

A VOC chamber was set up, as described in Section 3.3, p 65. To create air environments contaminated with known concentration of selected VOCs. The air generated inside the chamber was sampled using an active sampling method. Sorbents were packed into sampling tubes and the trapped VOCs by TD-GC-MS using the operating conditions described in Section 3.3.8, p. 73. The volatiles were generated using a permeation device as the pollutant source, prior to examination of sorbents for extraction of VOCs from indoor air.

### 5.2.1 Calculation of VOC emission rates from permeation vials and theoretical atmospheric concentrations generated inside exposure chamber

Four permeation vials containing a 1 cm<sup>3</sup> aliquot of each VOC standard were weighed before being placed inside the permeation oven. The temperature of the oven was set to 25 °C and the air passing through the glass housing unit was set to 200 cm<sup>3</sup> min<sup>-1</sup>. To determine the emission rate of each VOC under the chosen conditions, the vials were removed after set periods of time, cooled to room temperature, weighed and then re-inserted back into the oven.

The emission rates (ng min<sup>-1</sup>) of the in-house permeation devices were determined by dividing the masses (ng) of VOC lost from the permeation device over time (min), see Equation 5.1. The weights were measured weekly on 6 occasions and the resulting average weight losses (ng min<sup>-1</sup>) are given in Table 5.6.

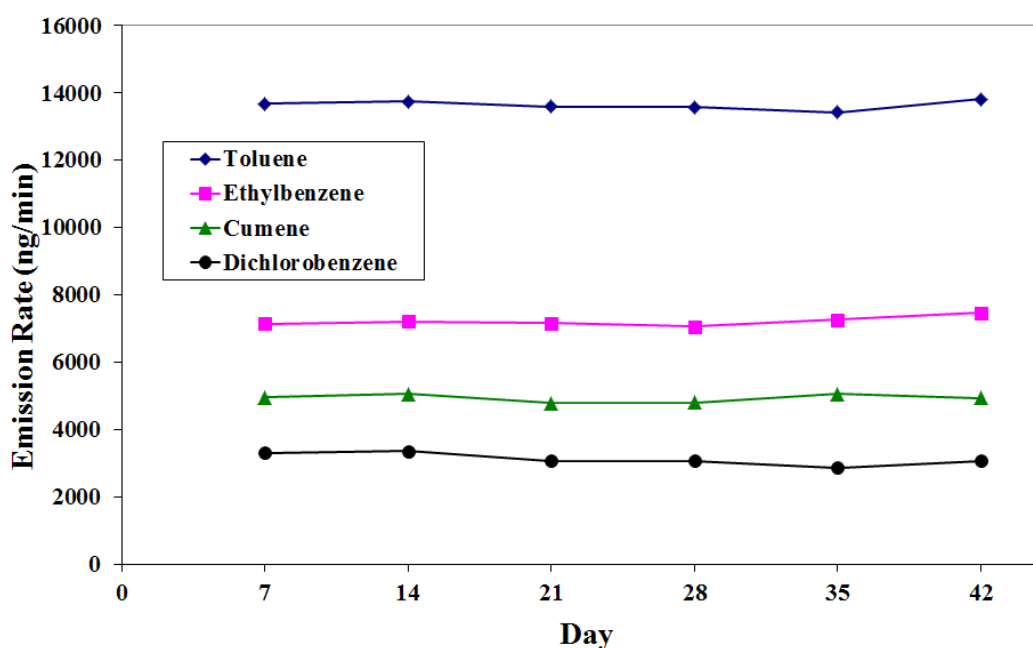
$$E = \frac{\text{mass loss}}{\text{time}} \quad \text{Equation 5.1}$$

**Table 5.6: Permeation vial emission rates of VOCs determined through weight loss.**

VOC	Weight Loss (g/week)						Average of Weight Loss (g/week)	Average of Weight Loss (ng/min)
	Week 1	Week 2	Week 3	Week 4	Week 5	Week 6		
Toluene	0.1380	0.1386	0.1370	0.1369	0.1353	0.1393	0.1375	13643
Ethylbenzene	0.0720	0.0727	0.0722	0.0712	0.0733	0.0753	0.0728	7221
Cumene	0.0500	0.0510	0.0483	0.0485	0.0511	0.0498	0.0498	4939
Dichlorobenzene	0.0334	0.0339	0.0310	0.0310	0.0290	0.0310	0.0316	3130



The constant weight loss of analytes from the permeation devices (see Figure 5.3) confirmed the stability of the in-house prepared permeation devices and the ability to produce stable streams of contaminated air using the exposure chamber system. These results also confirmed that the 1 cm<sup>3</sup> aliquot of analyte inserted into the permeation system provided stable emission rates for at least 42 days before they had to be replenished. It was also observed that, for the same exposure chamber conditions, the emission rates of VOCs in this study were indirectly proportional to the boiling points of the analytes as expected with toluene at 110.6 °C, ethylbenzene at 136 °C, cumene at 152 °C and dichlorobenzene at 180.5 °C.



**Figure 5.3: Emission rates of VOCs over a period of 42 days based on weight loss.**

### 5.2.2 Calculation of atmospheric concentrations

Using the average emission rates of each analyte, given in Table 5.6, the theoretical atmospheric concentration ( $\mu\text{g g}^{-1}$  or ppm) of VOCs generated in the polluted air stream were calculated using Equation 3.1, p. 67. Since the polluted air stream was combined with the humidified air stream the final concentration of pollutants in the atmospheric chamber were divided by a factor of 2 (see Table 5.7).

**Table 5.7: Theoretical concentrations of VOCs generated in the air stream**

VOCs	Calculated Emission Rate ng min <sup>-1</sup>	K <sub>0</sub> L g <sup>-1</sup>	Flow cm <sup>3</sup> min <sup>-1</sup>	Concentration of pollutants in air stream / ppm	Concentration of pollutants in chamber / ppm
Toluene	13643	0.265	200	18.077	9.038
Ethylbenzene	7221	0.230	200	8.304	4.152
Cumene	4939	0.204	200	5.038	2.519
DCB	3130	0.166	200	2.598	1.299

In addition to units of ppm ( $\mu\text{g g}^{-1}$ ), gases are often given in the literature in terms of a mass per volume unit ( $\text{mg m}^{-3}$ ). To convert ppm ( $\mu\text{g g}^{-1}$ ) to  $\text{mg m}^{-3}$ , the density of the gas must be considered, and again a temperature of 25 °C will be used. To calculate the gaseous density of each pollutant, the ideal gas equation was used (Equation 5.2) where the gas constant ( $R$ ,  $0.0821 \text{ L atm mol}^{-1} \text{ K}^{-1}$ ), temperature ( $T$ , 298 K) and pressure ( $P$ , 1 atm) were used to calculate the gaseous density ( $D$ ,  $\text{g L}^{-1}$ ), see Equation 5.3.

$$PV = nRT \quad \text{Equation 5.2}$$

$$D = \frac{PMW}{RT} \quad \text{Equation 5.3}$$

Using the calculated densities; the concentrations given in ppm ( $\mu\text{g g}^{-1}$ ) were converted to  $\mu\text{g L}^{-3}$  (see Table 5.8), which is equivalent to  $\text{mg m}^{-3}$ . Thus to convert from ppm to  $\text{mg m}^{-3}$ , gaseous concentrations are multiplied by their respective gas densities.

All practical work undertaken during the course of this work involved the determination of VOCs present in a 100 cm<sup>3</sup> aliquot of the contaminated air. Based on the theoretical concentrations, the masses (ng) of each analyte expected to be trapped from a 100 cm<sup>3</sup> aliquot of polluted air were calculated (see Table 5.8).

The system described was then used to determine the efficiency of three different sorbent materials as a scavenger for the pollutants in the atmospheric chamber. One of the sorbents examined was commercially available, whereas the other two sorbents were prepared in-house (see Section 3.3.2, p. 67, for a description of the experimental set up).

**Table 5.8: Theoretical concentrations of VOCs generated in the chamber and expected mass of analyte in a 100 cm<sup>3</sup> aliquot of air.**

VOCs	Concentration of pollutants in chamber (ppm)	Gaseous density (g L <sup>-1</sup> ) at 25 °C	Concentration of pollutants in chamber (mg m <sup>-3</sup> )	Mass (ng) of analyte trapped in 100 cm <sup>3</sup> aliquot of air
Toluene	9.038	3.767	34.046	3405
Ethylbenzene	4.152	4.340	18.020	1802
Cumene	2.519	4.914	12.378	1238
DCB	1.299	6.010	7.8070	781

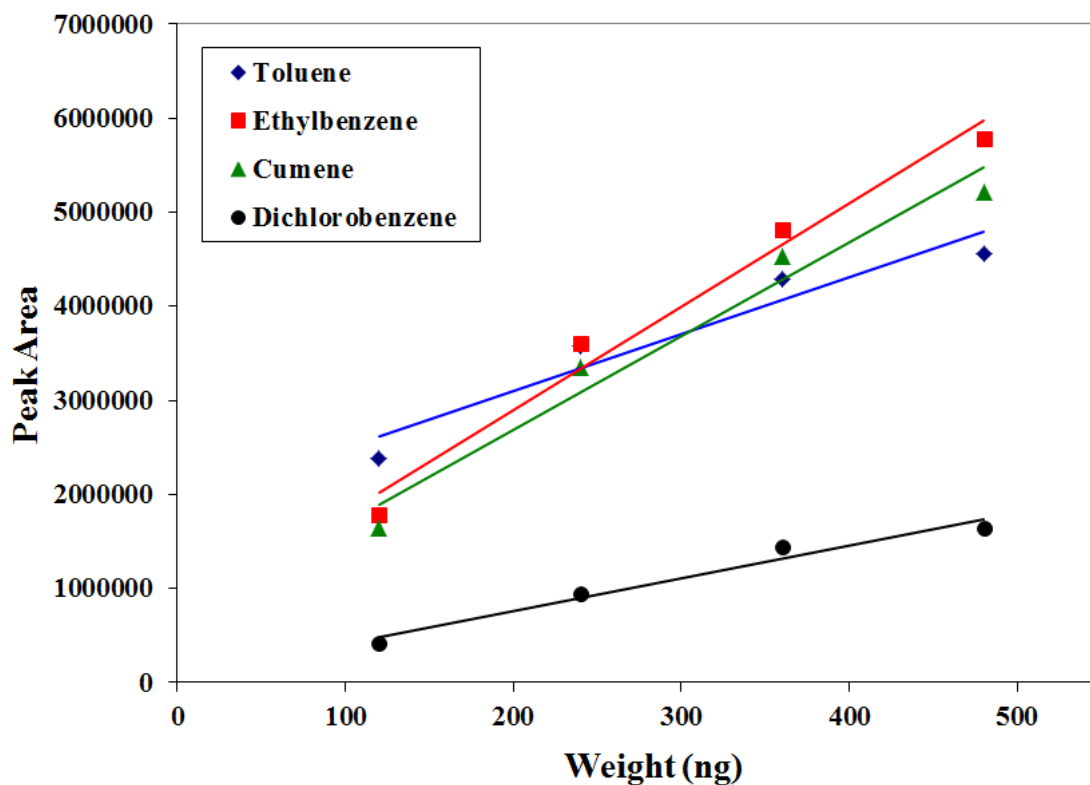
### 5.2.3 Characterisation of mesoporous silicates

Mesoporous silicates were prepared as outlined in Section 3.1.1 and 3.1.2 and characterised using the techniques discussed in Section 3.2. The nitrogen adsorption/desorption isotherms for the calcined SBA-15 and solvent extracted MCM-41 samples were measured at liquid nitrogen temperature using a micrometric Gemini BET analyser. The nitrogen adsorption isotherm obtained demonstrated a type IV isotherm for SBA-15 and MCM-41.

A full description of the characterisation of the materials can be found in much details in reference [149, 150]. The MCM-41 material had a BET surface area of  $644 \text{ m}^2 \text{ g}^{-1}$  and a BJH pore volume of  $0.670 \text{ cm}^3 \text{ g}^{-1}$ . The calculations from power X-ray diffraction (PXRD) pattern for MCM-41 gave a  $d$  spacing of  $44 \text{ \AA}$  and repeating unit ( $a_0$ ) unit  $50 \text{ \AA}$ . The repeating unit includes the pore diameter and pore wall distance therefore given the BJH pore diameter the pore wall was determined to be  $18 \text{ \AA}$ . The BET surface area of the SBA-15 material was  $849.5 \text{ m}^2 \text{ g}^{-1}$ , with a BJH pore volume of  $1.01 \text{ cm}^3 \text{ g}^{-1}$  and a micropore volume of  $0.1346 \text{ cm}^3 \text{ g}^{-1}$ . The pore wall thickness was determined as  $47 \text{ \AA}$  as repeating unit was  $116 \text{ \AA}$ .

### 5.2.4 Calibration of TD-GC-MS

Before the sorbents were examined as pollutant scavengers, the TD-GC-MS instrument used was calibrated for quantification of toluene, ethylbenzene, cumene and dichlorobenzene. The calibrant standard solutions used are described in Section 3.3.9 and solutions were loaded onto sampling tubes as discussed in Section 3.3.10. For the sampling method to be valid for VOCs in air, it was recognised that the chromatographic response (peak area) of each analyte should increase linearly with increased analyte mass. Using a set of calibrant sampling tubes, loaded with Tenax TA, the peak area obtained for each analyte was taken from the SIR chromatograms and plotted against mass of VOCs injected onto the sampling tubes. The results obtained are given in Figure 5.4.



**Figure 5.4: Peak area obtained from the SIR chromatogram when the masses of VOCs injected by direct injection were altered.**

Linear regression analysis was performed and the results obtained are shown in Table 5.9. The correlation coefficients (0.9257 – 0.9781) produced were below the accepted criteria of 0.9900. The slope ratios (the value of the slope divided by the value of the standard deviation of the slope) produced for VOCs were below the accepted criteria of 20: with toluene, ethylbenzene, cumene or dichlorobenzene ratios of 5.0, 9.5, 7.3 or 7.5, respectively. Additionally none of the VOC calibrations, apart from DCB, had an intercept confidence interval that included zero, therefore the data were deemed non-linear.

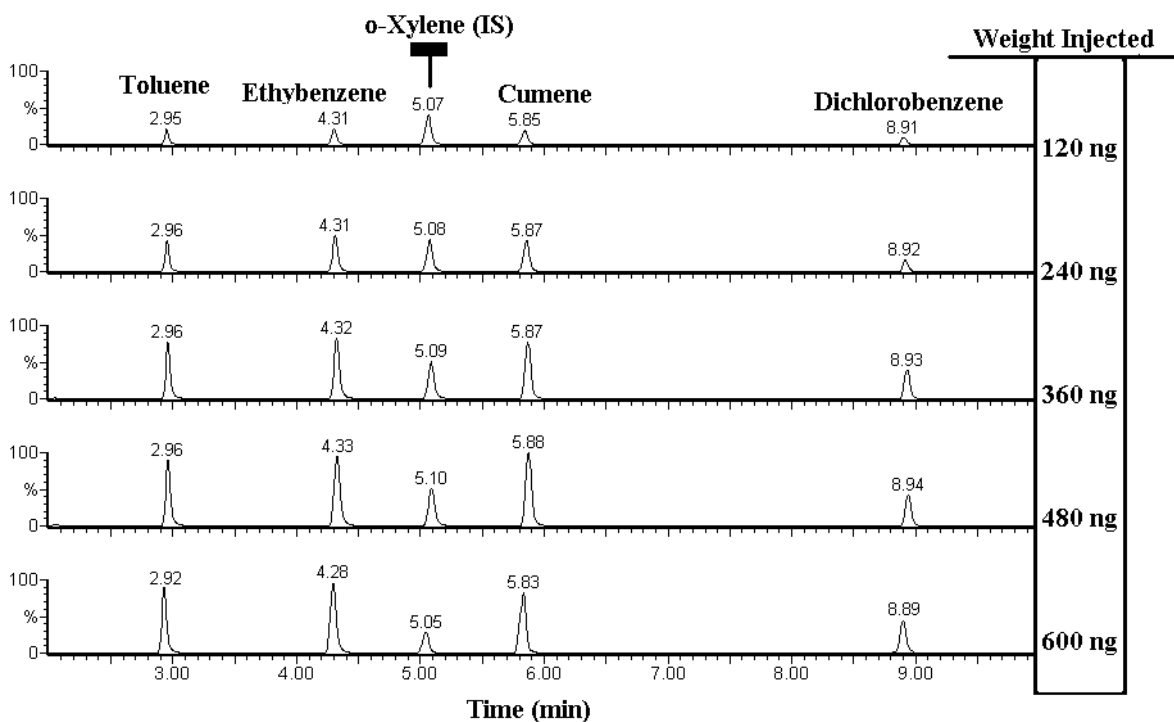
**Table 5.9: Statistical evaluation for the VOCs linearity with respect to different concentrations injected.**

VOCs	Slope	Intercept	Correlation Coefficient	Error on Slope	Error on Intercept
Toluene	6043	1888873	0.9257	1210	397778
Ethylbenzene	10990	700689	0.9781	1162	381792
Cumene	9945	702893	0.9640	1358	446406
Dichlorobenzene	3483	67961	0.9655	466	152995

#### ***5.2.4.1 Internal standard calibration curves***

To improve the calibration an internal standard method was used to account for any variability in injected sample volume or split ratios used in the instrument. The peak areas for each analyte mass obtained from the resultant SIR chromatograms were divided by the peak area of the internal standard. The mass of internal standard injected onto the sampling tubes was constant at 300 ng, whereas the masses of injected analytes increased from 120 to 600 ng. The chromatograms obtained for sampling tubes containing Tenax TA are shown in Figure 5.5. Internal standard calibration curves were obtained for sampling tubes loaded with Tenax TA, SBA-15 or MCM-41. Linear regression analysis was performed on the data (see Table 5.10).

The correlation coefficients for the analytes were improved (table 5.10) compared to the previous peak area calibrations and now were in the accepted criteria of  $> 0.9900$ . Equally for all analytes on each of the three sorbents the internal standard calibrations had a confidence interval of the intercept which included zero. Moreover, for most analytes the slope: standard deviation ratio was greatly improved.



**Figure 5.5: Chromatograms illustrating internal standard chromatograms: analyte masses of 120 ng to 600 ng.**

From table 5.10 data collected indicate that less sensitive calibrations were measured for toluene, ethylbenzene and cumene for the silica adsorbents, compared to Tenax TA. Analyte recovery values were calculated for each sampling tube and it was shown that Tenax TA had almost 100 % recovery for all analytes of interest whereas the silica based adsorbents retained < 50 % of toluene, ethylbenzene or cumene.

The lower analyte recovery values were only observed when tubes were spiked with methanolic VOC solutions as a calibration technique and indicated that methanol competed with the VOCs for the surface of the silica. Calibration by spiked solutions therefore could only be accurately performed using Tenax TA and not with silica adsorbents. All further quantitative experiments used Tenax TA sampling tubes to calibrate the instrument regardless of the sorbent used in sampling tubes.

**Table 5.10: Statistical evaluation for the calibration curves of the VOCs with different sorbents**

VOCs	Slope	Intercept	Correlation Coefficient	Error on Slope	Error on Intercept
<b>Tenax TA</b>					
Toluene	0.0042	0.4567	0.9932	0.00020	0.0802
Ethylbenzene	0.0065	-0.0890	0.9951	0.00026	0.1054
Cumene	0.0059	-0.0365	0.9983	0.00014	0.0552
Dichlorobenzene	0.0021	-0.1048	0.9942	0.00009	0.0373
<b>SBA-15</b>					
Toluene	0.0021	-0.0975	0.9951	0.00009	0.0341
Ethylbenzene	0.0039	-0.1708	0.9962	0.00014	0.0559
Cumene	0.0034	0.0187	0.9940	0.00015	0.0615
Dichlorobenzene	0.0022	-0.0393	0.9944	0.00010	0.0383
<b>MCM-41</b>					
Toluene	0.0013	0.3202	0.9968	0.00004	0.0165
Ethylbenzene	0.0016	0.6539	0.9927	0.00008	0.0313
Cumene	0.0024	0.5019	0.9958	0.00009	0.0366
Dichlorobenzene	0.0022	-0.0276	0.9949	0.00009	0.0365



## **5.3 Results and Discussion**

### **5.3.1 Comparison of experimentally calculated VOC masses with theoretically derived values**

The permeation chamber was set to generate an atmosphere containing approximately 9.0, 4.1, 2.5 or 1.3 ppm of toluene, ethylbenzene, cumene or dichlorobenzene. The polluted environment was then sampled at  $100 \text{ cm}^3 \text{ min}^{-1}$  for 1 min and the theoretical masses of each analyte expected to be trapped in the sample of air were 3405, 1802, 1238 or 781 ng, respectively. Two sets of experiments were conducted with the atmosphere conditioned to 80 % RH or 25 % RH. In each set of experiments the VOCs were trapped onto 3 Tenax TA sampling tubes and the masses trapped were determined by TD-GC-MS. The results obtained (see Tables 5.11 and 5.12) indicated that repeatable results were achieved. The % RSD values were all below 14 %. Comparison of the average masses indicated that a higher mass of analyte was trapped when the humidity of the atmosphere was 80 % RH (H-RH) compared to 25 % RH (L-RH), even though the concentration of analytes were unaltered. The differences were significant for toluene (T), ethylbenzene (EB), cumene (C) and dichlorobenzene (DCB) at 50, 40, 30 or 14 %, respectively. This set of experiments therefore indicated that the humidity of the test site may affect the adsorption efficiency of VOCs onto Tenax TA with higher efficiencies being obtained at higher relative humidity.

In both sets of experiments it was noted that the masses of VOCs trapped by Tenax TA were significantly lower than the theoretically expected values. The sampling was therefore repeated a further three times over a period of three months to ensure that the experiment was conducted correctly. Each time similar experimental results were obtained, ensuring that the sampling was both repeatable and reproducible. It was therefore thought that leaks in the system, or loss of VOCs into walls or tubing caused the differences observed between theoretically determined and experimentally measured values. Therefore, the concentrations generated in the chamber could not be determined theoretically but were determined experimentally.

**Table 5.11: Masses trapped of VOCs on Tenax TA from H-RH air. Standard deviation and % RSD values for VOCs.**

<b>VOCs</b>	<b>T</b>	<b>EB</b>	<b>C</b>	<b>DCB</b>
Weight of VOCs Adsorbed S1	429 ng	200 ng	145 ng	227 ng
Weight of VOCs Adsorbed S2	424 ng	193 ng	139 ng	219 ng
Weight of VOCs Adsorbed S3	502 ng	224 ng	157 ng	231 ng
Standard Deviation	43.8	16.2	9.2	6.2
% RSD	9.7	7.9	6.3	2.7
Average Weight Trapped	451 ng	206 ng	147 ng	225 ng
Theoretical Mass Applied	3405 ng	1802 ng	1238 ng	781 ng

**Table 5.12: Masses trapped of VOCs on Tenax TA from L-RH air.**

<b>VOCs</b>	<b>T</b>	<b>EB</b>	<b>C</b>	<b>DCB</b>
Weight of VOCs Adsorbed S1	330 ng	152 ng	113 ng	203 ng
Weight of VOCs Adsorbed S2	251 ng	120 ng	98 ng	185 ng
Weight of VOCs Adsorbed S3	314 ng	143 ng	112 ng	200 ng
Standard Deviation	41.5	16.8	8.6	9.5
% RSD	13.9	12.2	8.0	4.9
Average Weight Trapped	298 ng	138 ng	107 ng	196 ng
Theoretical Mass Applied	3405 ng	1802 ng	1238 ng	781 ng

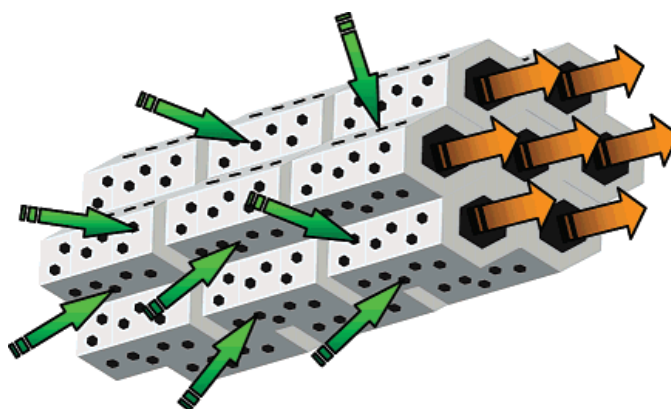
### 5.3.2 Comparison of collected analyte masses using different sorbents and a standard set of operating conditions at 25 % RH or 80 % RH

The same conditions outlined for Tenax TA sampling tubes in Section 3.3.8 were applied to the other sorbents MCM-41 and SBA-15. The average (n = 3) masses of analytes trapped by each sorbent at low relative humidity, 25 % RH (L-RH) or high relative humidity, 80 % RH (H-RH) is given in Table 5.13. The different masses trapped by MCM-41 and SBA-15, despite sampling the same vapour concentration, were observed, especially at the L-RH conditions, confirming the results obtained by Rodrigo et al.[191], who concluded that the adsorption of aromatic compounds on mesoporous silicate in dry conditions is higher than in humidified conditions. It is postulated that strong interactions between the silica surface and the  $\pi$ -electrons of aromatic hydrocarbons strongly influences the adsorption capacity for aromatic compounds.

**Table 5.13: Average masses trapped of VOCs on Tenax TA , SBA, and MCM-41 at different %RH.**

Sorbent	%RH	Toluene		EB		Cumene		DCB	
		Mass Trapped (ng)	%RSD	Mass Trapped (ng)	%RSD	Mass Trapped (ng)	%RSD	Mass Trapped (ng)	%RSD
Tenax TA	80	452	9.7	206	7.9	147	6.3	225	2.7
	25	298	13.9	138	12.2	108	8	196	4.9
SBA-15	80	252	0.20	165	2.7	142	0.8	156	0.2
	25	621	2.0	402	1.5	344	4.9	473	1.7
MCM-41	80	517	2.3	327	1.5	258	1.9	154	5.5
	25	708	2.9	423	3.5	328	2.7	224	6.2

The results given in Table 5.13 provided some initial information required for understanding the adsorption behaviour of VOCs by mesoporous materials. For example it appeared that H-RH conditions were favourable for adsorption onto Tenax TA but not the silica materials. The effect of water vapour was greater on SBA-15 than MCM-41, perhaps due to the presence of a bimodal pore system in this material [204]. SBA-15-type mesoporous materials with a bimodal pore system (see Figure 5.6) are expected to be ideal sorbents. The high performance of SBA-15 is likely derived from the intrinsic pore connections between long 1D-mesopore channels and complementary micropores. A pore network of this nature leads to the strong adsorption of VOCs by the micropores (green arrows) and, moreover, results in additional diffusivity of the adsorbed VOCs through the mesoporous (light brown arrows).



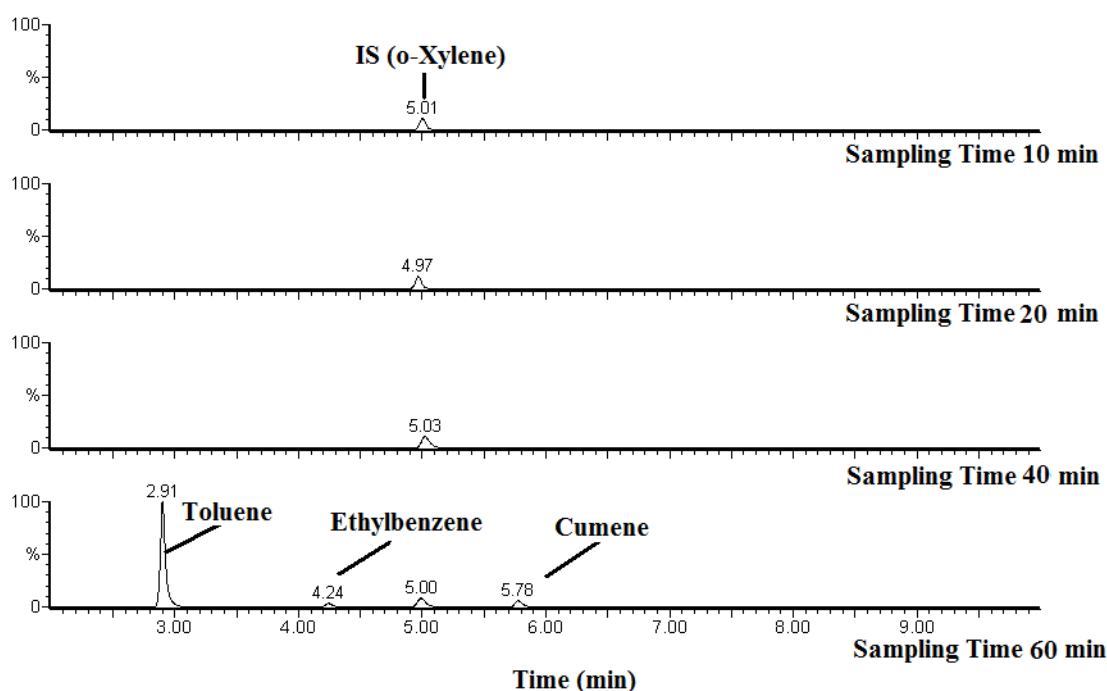
**Figure 5.6: Schematic representation showing the effect of the bimodal pore system on VOC adsorption. [204]**

### **5.3.3 Dynamic adsorption capacity of sorbents (Breakthrough)**

A breakthrough measurement is a direct method designed to clarify the dynamic performance of VOC adsorption [194]. It is known that sorbents have a limited capacity for absorption of a given analyte, either by saturation or chemical displacement. Once this capacity has been reached the analyte will pass through the sorbent unabsorbed. This is commonly referred to as ‘breakthrough’.

The point of breakthrough is identified when the concentration of analyte in the outlet stream is equal to 5 % of that in the inlet stream [205].

The dynamic adsorbent capacity of each sorbent was examined at 25 or 80 % RH as outlined in Section 3.3.7 p.71. The first sampling tube was connected to a sampling port on the permeation chamber and a second sampling tube was connected in line immediately after the first sampling tube. The flow rate was kept constant at  $100 \text{ cm}^3 \text{ min}^{-1}$ . Figure 5.7 illustrates example chromatograms obtained from desorption of VOCs from the second sampling tube containing Tenax TA at 10, 20, 40 or 60 min when sampling at H-RH.



**Figure 5.7: Chromatograms from the second Tenax TA tube illustrating analyte breakthrough in the 60 min sample time using H-RH conditions.**

The emergence of a significant analyte peaks after a sampling time of 60 min indicated that breakthrough had occurred for toluene when the masses trapped by tube 1 were approximately 17,140 ng. Figure 5.8 indicates the percentage of toluene breakthrough on different sorbents (Tenax TA, SBA-15, or MCM-41) at 25 or 80 % RH.

The breakthrough volume for toluene was greater for Tenax TA than for SBA-15, and SBA-15 was larger than for MCM-41. The results indicated that at a sampling flow rate of  $100 \text{ cm}^3 \text{ min}^{-1}$ , and with set concentrations of VOCs, Tenax TA can sample approximately 4 times the volume of contaminated air compared to SBA-15 or MCM-41 before breakthrough occurs. Moreover for every sorbent studied, higher masses of VOCs were retained at L-RH conditions compared to H-RH conditions indicating that water vapour may be involved in chemical displacement when VOC masses increased.

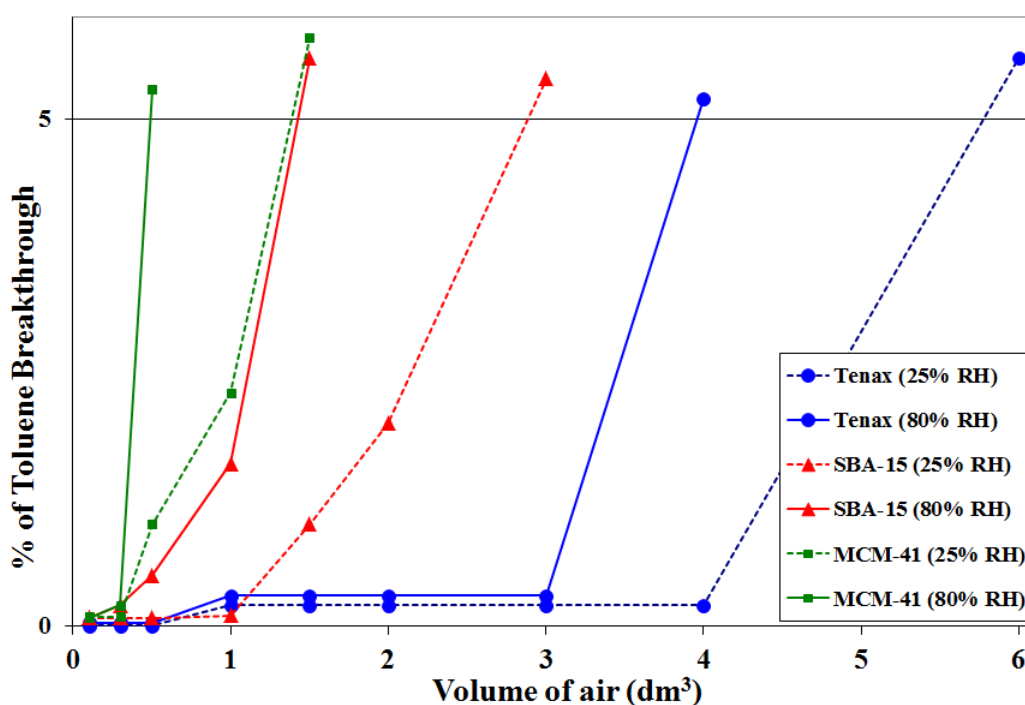


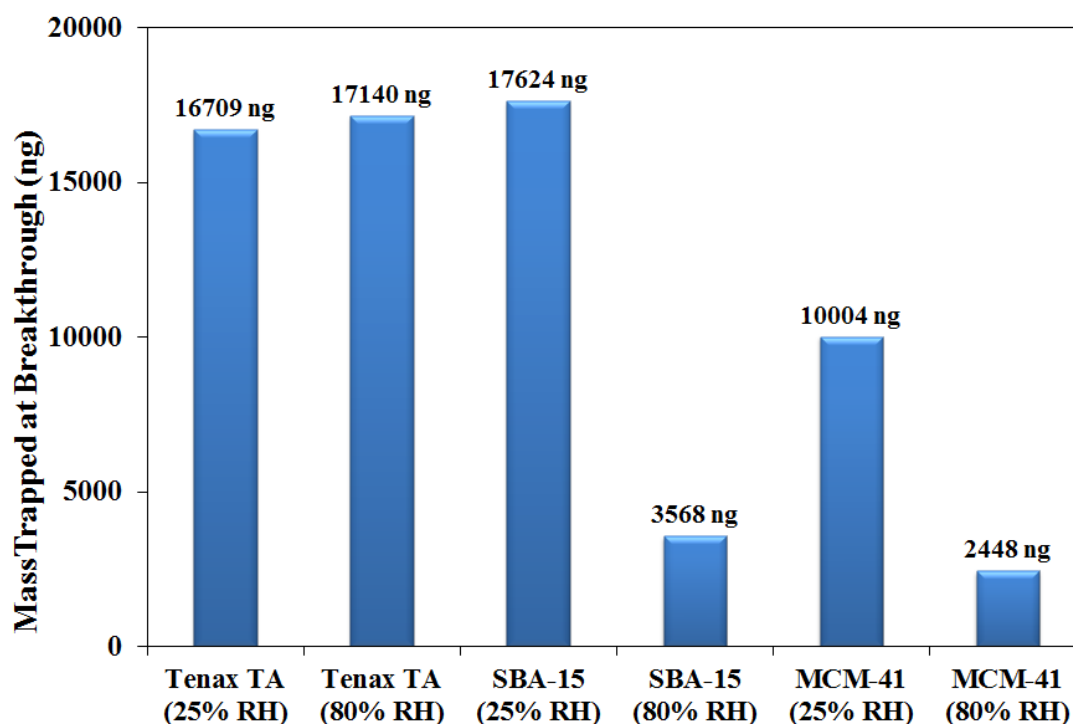
Figure 5.8: Dependence of breakthrough on adsorbent type and % RH.

### 5.3.4 Calculation of sorbent capacities

In addition to examination of breakthrough volumes it was also important to assess the masses of VOCs retained by each sorbent when breakthrough occurred (i.e., the capacity of the sorbents). Figure 5.9 indicates the masses of toluene trapped on each sorbent at L-RH or H-RH. The first observation was that Tenax TA trapped the highest mass of toluene (approximately 17000 ng) before breakthrough occurred and that the masses trapped were similar regardless of the humidity of the contaminated

air stream. This implied that Tenax TA had the highest capacity for toluene compared to SBA-15 or MCM-41. A similar performance to Tenax TA was observed for SBA-15 at L-RH (a toluene mass of 17,624 ng, which was the largest adsorption weight capacity in the study). However, when the amount of water vapour in the sample increased from 25 % RH to 80 % RH the capacity of the sorbent decreased by a factor of 5 for the silica sorbents. MCM-41 showed the lowest adsorption weight capacity of approximately 10,000 or 2,500 ng with L-RH or H-RH, respectively.

Finally the air volume sampled at breakthrough must be considered (see Table 5.14). When the concentration of analyte was considered (mass trapped per unit volume of air sampled) MCM-41 showed the best dynamic adsorption capacity at L-RH, even more than SBA-15 or Tenax TA. It would appear therefore that the silicate sorbents performed better than the commercially available material for the VOCs examined in this study.



**Figure 5.9: Mass trapped at 5% breakthrough.**

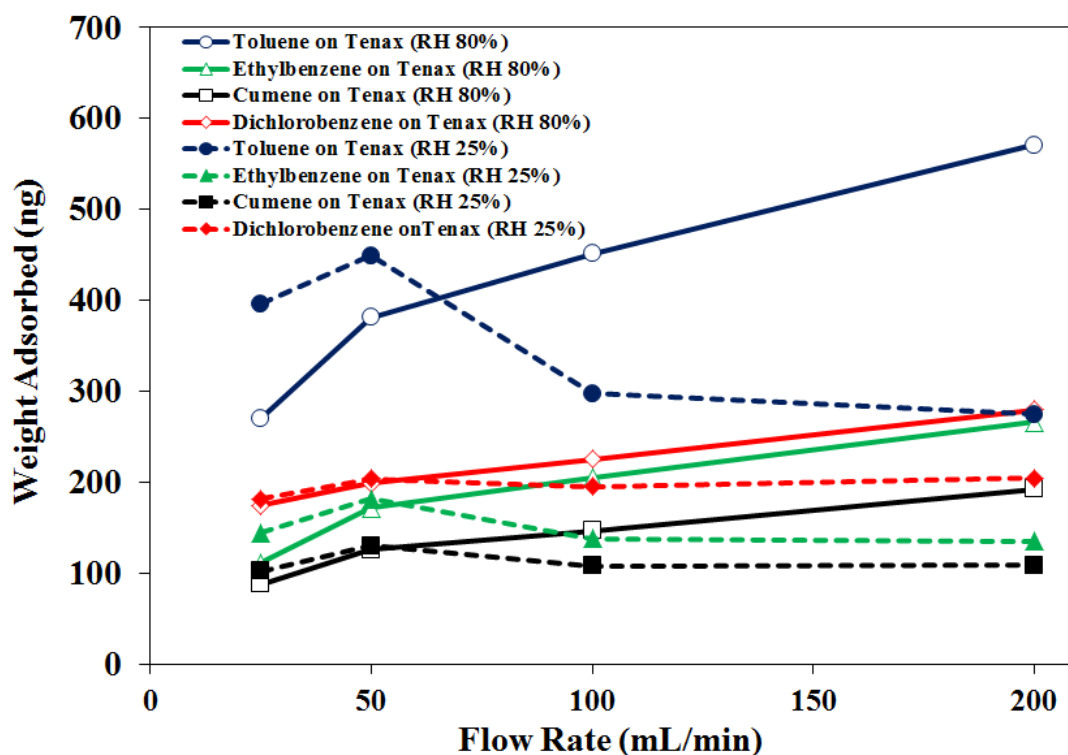
**Table 5.14: Effect of Relative humidity and sorbent type on toluene mass trapped at 5% breakthrough.**

Adsorbents	Relative Humidity (% RH)	Air Volume at Breakthrough (dm <sup>3</sup> )	Mass trapped at Breakthrough (ng)	Mass trapped/Air Volume at Breakthrough (ng/cm <sup>3</sup> )
Tenax TA	25	6.0	16709	2.8
Tenax TA	80	4.0	17140	4.3
SBA-15	25	3.0	17624	5.9
SBA-15	80	1.5	3568	2.4
MCM-41	25	1.5	10004	6.7
MCM-41	80	0.5	2448	4.9

### **5.3.5 The relationship between RH and air sampling flow rate on VOC adsorption**

When the RH of the polluted stream was set to 80 %, the VOC masses trapped onto Tenax TA increased when air sampling flow rates were increased from 25 cm<sup>3</sup> min<sup>-1</sup> to 200 cm<sup>3</sup> min<sup>-1</sup>, see Figure 5.10 (note: sampling times were reduced accordingly to ensure constant air volumes were sampled). This effect was not observed for ethylbenzene, cumene or dichlorobenzene when the air sampling flow rates were increased similarly at L-RH conditions as measured masses were relatively stable when sampling flow rates were altered. However at L-RH the mass of toluene adsorbed by Tenax TA appeared to have been significantly increased when the air flow rate was reduced below 100 cm<sup>3</sup> min<sup>-1</sup>.





**Figure 5.10: Comparison between VOCs Adsorption on Tenax TA at different flow rate.**

In general higher masses of VOCs were retained by Tenax TA when the humidity of the polluted air stream was altered from 25 % to 80 % RH and sampling flow rates greater than  $50 \text{ cm}^3 \text{ min}^{-1}$  were used. A different picture was observed for the silica based adsorbents where, in general, higher VOC masses were obtained at L-RH conditions particularly when sampling flow rates above  $50 \text{ cm}^3 \text{ min}^{-1}$  were used (Figures 5.11 and 5.12).

The effect of changing RH conditions on VOC masses adsorbed was most pronounced for SBA-15 compared to MCM-41 which favoured lower RH conditions for best adsorption performance, perhaps due to the presence of a bimodal pore system in SBA-15 and also the difference in surface area between SBA-15 ( $849.5 \text{ m}^2 \text{ g}^{-1}$ ) and MCM-41 ( $644.6 \text{ m}^2 \text{ g}^{-1}$ ).

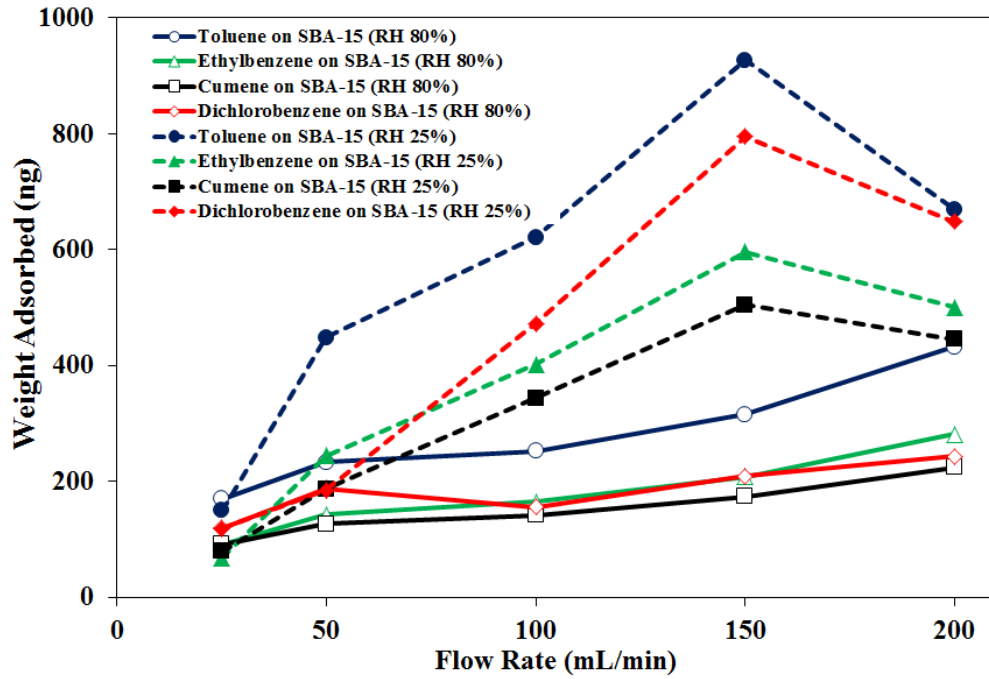


Figure 5.11: Comparison between VOCs Adsorption on SBA-15 at different flow rate.

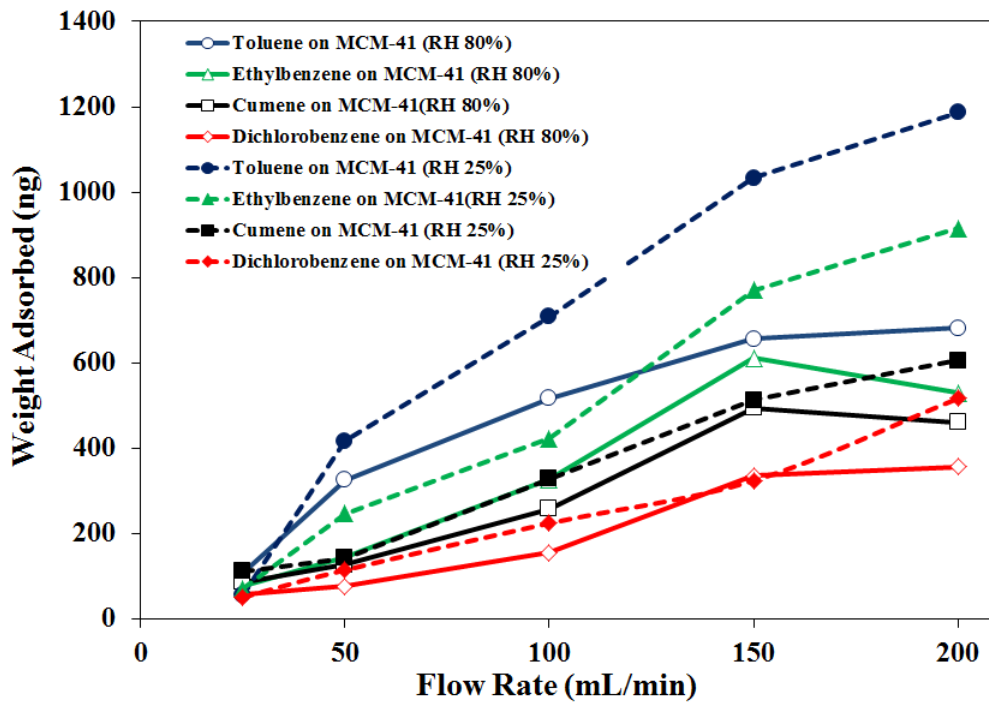


Figure 5.12: Comparison between VOCs Adsorption on MCM-41 at different flow rate.

These results suggest that, as expected, the presence of water molecules had a large influence on the performance of the silica-based adsorbents when used to trap VOCs from polluted air, apparently competing with the VOCs for adsorption sites leading to lower measured VOC masses. These results suggested that the adsorption of aromatic compounds on mesoporous silicate in dry conditions is higher than humidified conditions; presumably as a result of monolayer water coverage on the surface of the silica.

## 5.4 Conclusions

The overall aim of this work was to produce mesoporous silicate adsorbents to remove pollutants from indoor air and determine their efficiency compared with commercial sorbents (Tenax TA). This comparison included the influence of humidity and sampling flow rate. The results indicated that the adsorption of VOCs using adsorbent tubes was complicated and care needed to be taken to ensure accurate results were obtained. There were perhaps 3 main questions that could be addressed from this study:

- What sorbent type can be used for quantitative air sampling campaigns?
- How are sampling tubes calibrated?
- Which adsorbent would be a useful scavenger to reduce the concentration of indoor air pollutants?

If accurate results are to be achieved from indoor air sampling campaigns and the humidity of the sampling environment is unknown, sampling tubes should be filled with Tenax TA as this material was affected less by changing the humidity of the sampling environment from 25 % to 80 % RH or by altering flow rates from 25 to 200 cm<sup>3</sup> min<sup>-1</sup>. The silica based sorbents were strongly influenced by the presence of water vapour leading to decreasing amounts of VOCs adsorbed onto MCM-41 or SBA-15 at H-RH. Moreover, it was shown that a simple calibration method of spiking sampling tubes with methanolic solutions of VOCs can be achieved with

Tenax TA. To calibrate silica tubes it would be necessary to provide a range of atmospheres of known VOC concentration at the same humidity as the sampling site. In general the masses of VOCs trapped by Tenax TA sampling tubes were also affected less when sampling flow rates were altered, compared to silica, although it was interesting to note that different masses were measured for the same volume of air passing over the Tenax TA sorbent bed especially at 80 % RH. Thus the interaction between RH and sampling flow rate on accuracy of the VOC masses collected by Tenax TA needs further study. Nonetheless this material was more reliable than MCM-41 or SBA-15 when quantification was required.

**Chapter 6: Extraction of lead (II) ions from water samples  
using functionalised MCM-41**

## **6.1 Introduction: The extraction of heavy metals from water**

“Heavy metals” are chemical elements with a specific gravity that is at least 5 times the specific gravity of water [151]. The specific gravity, or relative density, is the ratio of the density of a given amount of a solid substance when compared to an equal amount of water; the specific gravity of water at 4 °C is 1.

In the environment, there are 35 metals identified as causing health concerns, due to occupational or residential exposure. Of these 23 are heavy metals; such as antimony, arsenic, cadmium, chromium, copper, gold, iron, lead and mercury [206]. During the course of this investigation lead, was chosen as a target analyte as it is ranked second in the 2007 CERCLA (comprehensive environmental response, compensation and liability act) priority list of hazardous substances. [206]

Heavy metals can enter the human body through food, water, air or absorption through the skin [151]. The MACs (The maximum allowed concentration) of lead is 10 µg/L; if water contaminated with this heavy metals is consumed kidney damage may result.

### **6.1.1 The analysis of heavy metals in water using FAAS**

Due to the serious health problems associated with heavy metal toxicity, the analysis and determination of heavy metals in environmental samples is an area of great interest within the scientific community. There are a number of analytical methods that are available for use within this field including inductively coupled plasma atomic emission spectroscopy (ICP-AES) [207, 208], and flame atomic absorption spectrophotometry (FAAS) [209, 210]. During this work, the method of choice for the determination of Pb (II) in water solutions was FAAS and the ICP-AES was used for multi-elements samples analysis. FAAS has been utilised successfully for many years for the determination of heavy metal ions present in water. In 1989, Sarmani et al.[211] reported the results of a six month investigation into the distributions of heavy metals in the Langat River, Malaysia. The investigation determined the concentrations of heavy metals, such as; arsenic, cadmium, cerium, cobalt, chromium, caesium, lanthanum, rubidium, antimony, scandium, thorium and zinc, present in water, suspended materials and sediment samples. Instrumental neutron

activation analysis was used in the determination of 12 trace elements in the sediments and suspended matter. While, atomic absorption spectrometry was used for the analysis of arsenic, cadmium, cobalt, copper, mercury, lead and zinc in the soluble fraction of the river water samples. The investigation determined that by comparison to the WHO drinking water standards, the river water was not suitable for drinking without treatment; highlighting the importance of the analysis of heavy metals in environmental samples and demonstrating the need for an efficient and reliable method of heavy metal removal [211].

In 2007, Obiri et al [212] presented the results of an investigation in the determination of heavy metals in water from boreholes in Dumasi, in the Wassa west district of western region of Republic of Ghana. The aim of the investigation was to determine the concentrations of heavy metal ions in water from the boreholes in Dumasi township and compare the extent of contamination to the permissible background concentrations in underground water. The concentrations of the heavy metals of interest, including; zinc, cadmium, lead, chromium, manganese, iron, arsenic and cobalt, were determined using FAAS. The investigation showed that the water had significantly high levels of a number of heavy metals, specifically cadmium, arsenic and lead.

Usually FAAS is used for heavy metal determination when analytes are present at the low ppm concentration range as this technique has reasonable detection limits and provides reliable results in this concentration range. For example FAAS has been used in different heavy metals determination methods like preconcentration [213, 214], chromium speciation [215] and solid phase extraction [216].

### **6.1.2 Current methods used for the removal of heavy metals from water**

Environmental pressure has resulted in a major focus on waste treatment and clean-up research, in order to produce economic and effective methods for the removal of selected metal ions from water [153]. There are a number of methods currently in practice for the removal of heavy metals in water, such as; chemical precipitation, ion exchange, solvent extraction, reverse osmosis and adsorption [217]. However, there are a number of drawbacks with some of these methods, for example chemical precipitation is often not suitable for the removal of trace amounts of contamination,

and in addition this method often produces large amounts of sludge [217]. The efficient extraction of trace level impurities from a large volume of aqueous phase by a small volume of an organic, such as in solvent extraction, can be hampered by the mutual solubility of the phases leading to difficulties in their separation [218]. While, ion exchange and reverse osmosis, although effective, can often be considered as relatively expensive techniques for the removal of heavy metals from water [217].

The adsorption process has become one of the preferred methods for the removal of toxic contaminants, such as heavy metals, from water [219]. Adsorption has been found to be highly effective, versatile, economical and relatively simple. In addition to being applicable at very low concentrations, in both batch and continuous processes. Adsorption has the advantage of producing very little sludge and, depending on the material, it is often possible to regenerate and reuse the material [220]. The process of adsorption has acquired global attention for the minimisation of the problems associated with the contamination of water and air [217].

Guet al.[221] reported the development of an innovative iron-containing ordered mesoporous carbon, which was used as an effective sorbent for contaminants such as arsenic. Due to its carbon-based properties, the material overcame some of the problems associated with other arsenic absorbents, such as the build-up of high headloss and weak mechanical strength [221]. The biggest advantage of using this ordered mesoporous carbon adsorbent was found to be its fast adsorption kinetics [221].

### **6.1.3 Mesoporous silica sorbents for the removal of heavy metals**

A sorbent used for the removal of heavy metals from water should have a good sorption capacity, chemical stability under the experimental conditions and an especially high capacity [218]. Previously, a number of low-cost adsorbents were reviewed for their feasibility within this area. The materials reviewed included commercial activated carbon, chitosan, zeolites, peat moss, fly ash, coal and aluminium oxide [217]. In addition to these materials two common clays, kaolinite and montmorillonite, together with silica gel, were assessed for their applicability in



this field [217, 218]. It was determined that the adsorption capacities of the adsorbents tested depended on the characteristics of the individual adsorbents, the extent of any chemical modifications and the concentration of the adsorbate [217].

Development of synthetic routes of preparation of mesoporous materials has greatly expanded the possibilities for adsorbent design; with better control of the open pore structures; the surface areas, the well-defined pore size and shape. It has been recognised that these materials have great potential in both environmental and industrial processes [222]. Recently, these materials have received great interest for application as host materials in adsorption, in addition to being used in protein sequestration and release, enzyme immobilisation, drug delivery and catalysis [160].

Key to the success of silica adsorbents is the large pore size and the presence of silanol groups which can be chemically modified to provide adsorption sites for target analytes [223, 224]. By introducing additional molecular functionality in a controlled way, it is possible to adjust many of the key properties of these materials, including; hydrothermal stability, surface polarity and the density of the attached organic moieties [225]. Surface functionalisation leads to sorbents with unique characteristics and the desired properties for applications in adsorption [221, 226]. For example, modified ordered mesoporous materials have been designed to selectively remove selected metal ions from aqueous and organic systems [153]. The choice of which functionalisation agent is used can be derived from the Irving-Williams stability series, which associates particular ligands with particular metal ions to form a stable complexes [153]. Aminopropyl ligands (-NH) are identified as being attracted to “hard” metals, for example Ni, Cr, Mn and Fe, while mercaptpropyl ligands are identified as being attracted to “soft” metal ions such as Pd and Hg [153]. Other alternatives are also used with an Fe/Al coordinated mesoporous silica materials acting as a strong adsorbent for arsenic [221].

The use of mesoporous silica materials as a sorbent for the removal of heavy metal ions in water has been reported in the literature for a number of years. In 1997, Feng et al. [222] reported the use of mesoporous silica materials containing functionalised organic monolayers for the removal of mercury and other heavy metals, such as lead

and silver, from water. The formation of the organic monolayers within the ordered mesoporous silica conferred specific adsorption behaviour for the heavy metal ions. The material was found to have a high metal loading capacity due to the densely populated thiol groups on the large surface area of the mesoporous oxides. The functionalised material was found to be highly selectively for heavy metals against background electrolytes, such as sodium, barium and zinc [222].

Lee et al.[227] prepared a functionalised mesoporous silica material for the removal of copper ions from water. The functionalising agent used in this work was 3-(2-aminoethyl-amino) propyltriethoxysilane (AAPTS). AAPTS was chosen due to its ability to selectively bind with the silica surface via covalent bonding, in addition; it is hydrophobic which enables external mass-transfer resistance to be avoided [227]. The functionalised mesoporous silica was found to successfully remove copper ions from aqueous solution, with the removal capacity being over 10 times larger than that of commercial silica. The mass transfer rate was found to be fast due to little resistance of external mass transfer and diffusion [227].

In 2003, Yoshitake et al.[224] investigated the adsorption properties of cation-anchored functionalised mesoporous silicas by comparing two types of mesoporous framework structures, MCM-41 and MCM-48 in addition to comparing the cation centers;  $\text{Fe}^{3+}$ ,  $\text{Co}^{2+}$ ,  $\text{Ni}^{2+}$ ,  $\text{Cu}^{2+}$  or  $\text{H}^+$ [224] The transition metal cations,  $\text{Fe}^{3+}$ ,  $\text{Co}^{2+}$ ,  $\text{Ni}^{2+}$  and  $\text{Cu}^{2+}$  were captured by both the diamino-functionalised MCM-41 and the diamino-functionalised MCM-48. The largest absorption capacity was achieved with Fe/NN-MCM-48, in which it was found that  $\text{Fe}^{3+}$  bound to 2.7 arsenate anions. It was also determined that the absorption capacity of the functionalised MCM-48 was higher than that of the functionalised MCM-41, which was attributed to the larger cation incorporations in NN-MCM-48 than in NN-MCM-41 [224].

In 2008, Yang et al.[228] presented a new approach for preparing mesoporous absorbents, by using TMAOH as the subsidiary structure-directing agent and ethanol as the organic solvent. The adsorption of copper, zinc, lead, iron, silver and manganese ions on the absorbent obtained was investigated. It was found that the

absorbent had a great adsorption capacity, which was believed to be due to the uniform distribution of amine inside channels as well as the large and well-proportioned pore size [228]. The order of the adsorption capacity for the six metal ions investigated was  $Mn^{2+} < Zn^{2+} < Cu^{2+} < Fe^{2+} < Pb^{2+} < Ag^{+}$  [228].

In 2003 also Chen et al. [223] investigated the use of 3-(2-aminoethylamino) propyltrimethoxysilane (AAPTS) modified ordered mesoporous silica for use as a solid phase extraction material for the preconcentration/separation of As(III) and As(V). As(V) was quantitatively adsorbed by the material, while As(III) was not retained and passed through the column. It was found that the AAPTS modified ordered mesoporous silica was stable and enabled more than 50 loading and elution cycles to be performed without loss of analytical performance [223].

In 2009, Burke et al. [153] synthesised aminopropyl (Si-NH) and mercatopropyl (Si-SH) functionalised mesoporous silica in addition to a bi-functionalised (both aminopropyl and mercatopropyl) material. It was believed that, as most environmental samples will contain a mixture of metal ions, the bi-functionalised material would allow effective removal of both hard and soft metallic ions, through interaction with the aminopropyl and mercatopropyl groups respectively [153]. The Si-NH material showed a high extraction capacity for zinc, lead, cadmium, nickel, iron, chromium, manganese and copper ions, while the Si-SH material showed increased extraction of magnesium, vanadium and calcium ions [153]. When the bi-functionalised material was used as a sorbent for mixed metal solutions it had a higher affinity for each of the metal ions when compared to the mono-functionalised mesoporous silica [153]. The results demonstrated that environmental samples containing relatively high concentrations of mixed metal ions can be reduced to low concentrations using a simple procedure and functionalised mesoporous silica sorbents.

A comparison between the absorption properties of functionalised silica gel and MCM-41 has been carried out by Puannagam et al. [86]. The adsorbents for mercury were prepared using (3-(2-aminoethylthio) propylthioethanamine) as the ligand, due

to the presence of both sulfur and nitrogen donor atoms. The sorbents were found to have a high selectivity towards Hg(II) ions over other metal ions, with the functionalised MCM-41 showing a higher binding ability compared to the functionalised amorphous silica gel due to its uniform structure [86]. The research carried out in this field, highlights the potential of mesoporous silica materials as sorbents for the removal of heavy metal ions from water. In particular, functionalised MCM-41 appears to be a very promising compound for use in this field. Heavy metals, such as lead, are important environmental pollutants, threatening the health of human populations and natural ecosystems. Removal of these species from the environment is thus a major focus of waste treatment and clean-up efforts [229]. However, amino-functionalised mesoporous silica was found in literature have a good efficiency for the removal of a wide range of toxic metal ions and the used absorbents can be regenerated through a simple process of acid washing [83, 230, 231]. Therefore in this chapter we will focus on the ability of functionalised MCM-41 to extract lead ions from water samples.

## **6.2 Experimental**

### **6.2.1 Instrument Calibration**

FAAS and ICP-AES instruments were used to determine the concentration of Pb (II), and other metal ions, in solution. Details of the instrument used, and operating parameters are given in Sections 3.4.4 and 3.4.5, p.79-82.

### **6.2.2 Preparation of silica materials for Pb (II) extraction**

The prepared MCM-41 which outlined in section 4.2 and functionalised as summarised in section 3.4.1 has characterised using N<sub>2</sub> adsorption isotherms, XRD, elemental analysis and FTIR has shown high surface area, large pore volume, broad pore size distribution and also more hydroxyl groups were remained in the surface. The ability of aminopropyl-MCM-41 (AP-MCM-41), mercaptopropyl-MCM-41 (MP-MCM-41), diethylenetriamine-MCM-41 (DETA-MCM-41) or mercapto-diethylenetriamine MCM-41 (MDETA-MCM-41) to remove Pb (II) from water samples was investigated in this chapter.

### **6.2.3 Experiments used to assess the extraction of Pb (II) from water**

The extraction ability of each sorbent was investigated at five different pH values: 3, 5, 7, 9 or 11, to assess what effect, if any, the pH of the solution plays in the extraction process.

In each extraction experiment 10 mg of sorbent was added to 20 cm<sup>3</sup> of a 20 µg cm<sup>-3</sup> Pb (II) aqueous solution. The pH of the solution was then adjusted to the desired pH through the drop wise addition of hydrochloric acid or ammonium hydroxide. A stirrer bar was then placed in the solutions which were left to stir on a magnetic stirrer for 2 h. After this time, 5 cm<sup>3</sup> solution aliquots were removed and filtered, to remove particles from the solution and recover the sorbent. The filtrate was then analysed by FAAS to determine whether Pb (II) remained in solution. If the FAAS absorbance reading was zero, indicating that no Pb (II) ions were present in the aliquot, the sorbent was introduced back into the solution after the addition of 5 cm<sup>3</sup> of 80 µg cm<sup>-3</sup> Pb (II), to return the solution to its original concentration of 20 µg cm<sup>-3</sup>. Note that the filter paper was flushed during addition of the aliquot to return any sorbent held by the filter paper. The solution was then stirred for a further 2 h. The solution was re-examined for Pb (II) and the extraction the process repeated until the sorbent reached capacity, as indicated by the presence of Pb (II) in solution.

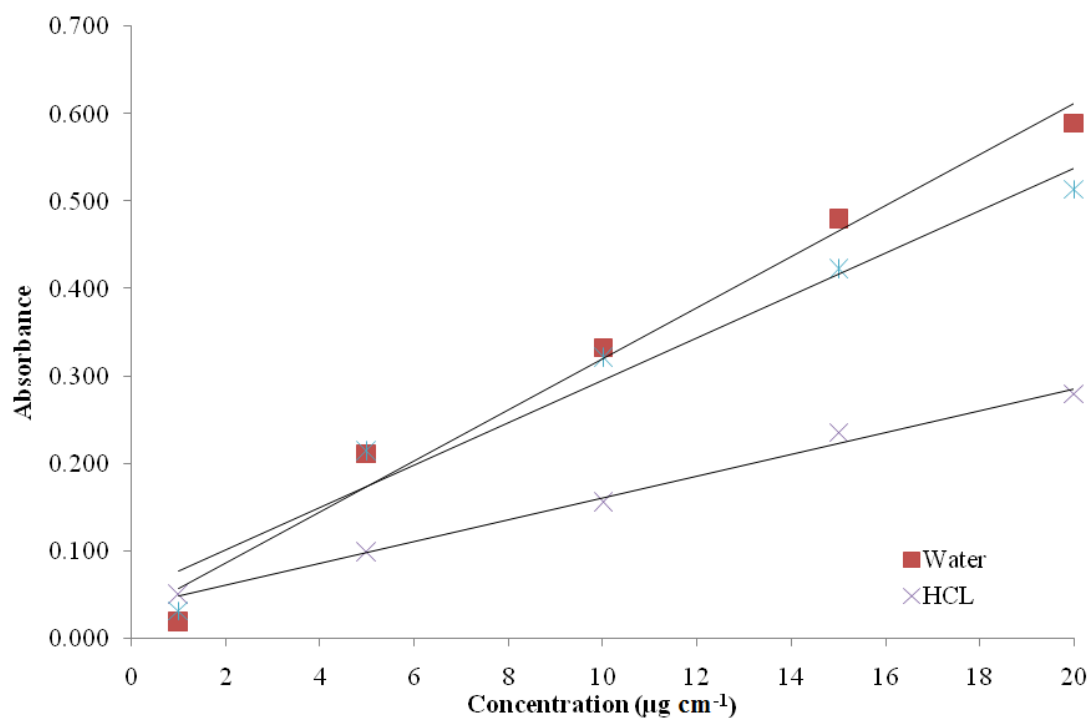
### **6.2.4 Regeneration of Functionalised MCM-41**

Regeneration of the functionalised MCM-41 material after adsorption of lead ions from water was examined. A 20 cm<sup>3</sup> solution containing 20 µg cm<sup>-3</sup> metal ions were added to a conical flask containing 100 mg of functionalised MCM-41. After stirring for 2 h at room temperature, the suspension was separated by filtration. The filtrate was measured by FAAS or ICP-AES to determine whether metal ions were removed from water and trapped by the sorbent. The filter paper containing the recovered sorbent was then immersed into 20 cm<sup>3</sup> of a 1 mol L<sup>-1</sup> solution of HCl for 2 h at room temperature. The solution was filtered and the metal ions concentration of the acid filtrate was measured by FAAS or ICP-AES. The sorbent was then dried at 80 °C for 2 h and the extraction repeated to examine the capacity of the regenerated sorbent.

## 6.3 Results and discussion

### 6.3.1 The lead calibration data

Calibration solutions were prepared in water, hydrochloric acid or ammonium hydroxide and the calibration curves obtained are given in Figure 6.1.



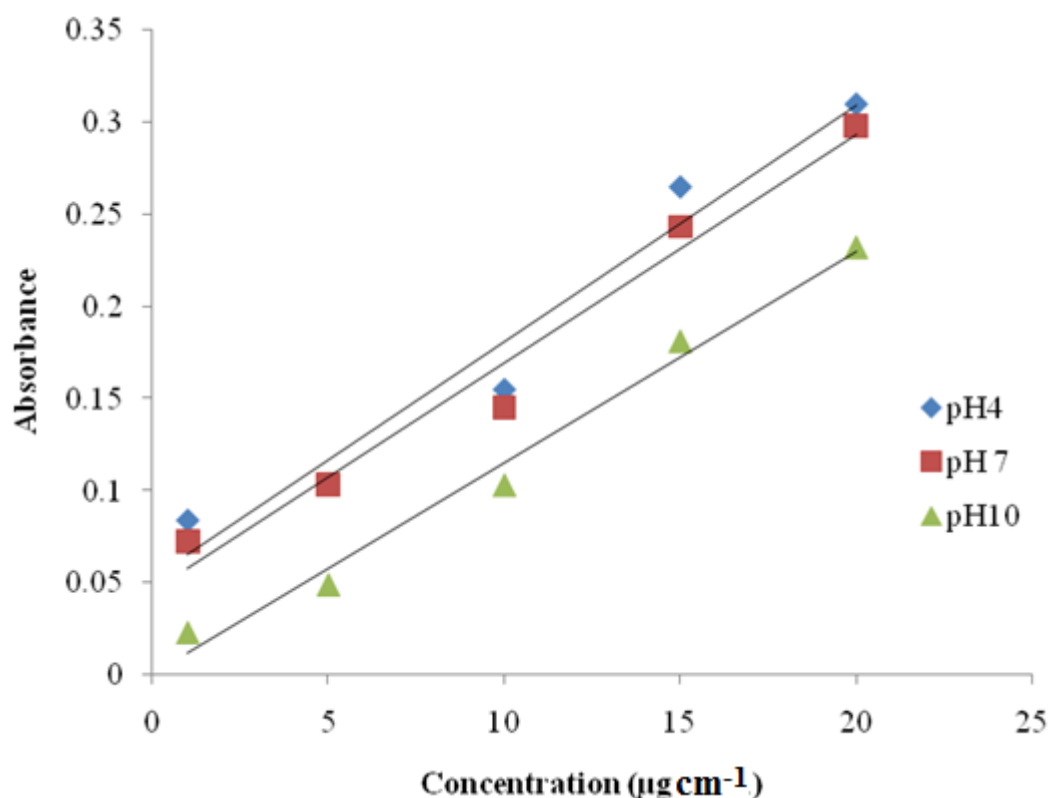
**Figure 6.1: Calibration curves for Pb (II) solutions in; water, HCL or NH<sub>4</sub>OH.**

Reasonable linearity was obtained for each set of calibrants, with  $r^2$  values greater than 0.9652 in all cases. The regression analysis results (Table 6.1) demonstrated that there was no significant difference between the calibration results obtained for the water or NH<sub>4</sub>OH solutions; however, there was a significant difference for the solutions prepared in HCl. Although these experiments were looking at extreme conditions they suggested that if an extraction was to be carried out in hydrochloric acid, matrix matched calibration solutions would need to be used. However if an extraction was to be carried out in ammonium hydroxide, aqueous calibration solutions could be used. In order to determine how the pH of the solution would affect the calibration, further experiments were then carried out, because the pH of the solution was adjusted throughout the experiment by using drop wise addition of

HCl or NH<sub>4</sub>OH. The purpose was to enable the solutions to be consistent with those used during the extraction experiments; the results are given in Figure 6.2.

**Table 6.1: The results of linear regression analysis for Pb (II) calibrants prepared in; water HCl or NH<sub>4</sub>OH.**

Matrix	$r^2$ value	Slope	Intercept	Error on slope	Error on intercept
Water	0.9811	0.029231	0.02824	0.002343	0.028714
HCl	0.9652	0.012462	0.036689	0.00576	0.007063
NH <sub>4</sub> OH	0.9936	0.024226	0.053493	0.002655	0.032539



**Figure 6.2: Regression lines for Pb (II), prepared at pH 4, 7 or 10.**

For each calibrations a reasonable degree of linearity was achieved with  $r^2$  greater than 0.9603. Linear regression analysis was then performed on the results obtained, see table 6.2. A significant difference was observed for the calibrants prepared at pH 10 compared to pH 4 or 7, suggesting that a separate calibration is required when pH 10 is used. It is interesting to note that although the results for the calibration carried out under extreme acidic conditions suggested that a separate calibration would be needed under these conditions, this was not observed for the calibration measured here using a solution at pH4.

**Table 6.2: Linear regression analysis for Pb (II) calibrants at pH 4, 7 or 10.**

pH	$r^2$ value	Slope	Intercept	Error on slope	Error on intercept
4	0.9603	0.012848	0.052547	0.001509	0.018494
7	0.9733	0.024782	0.091627	0.002369	0.029035
10	0.9863	0.011505	0.000247	0.000783	0.009594

According to the results mentioned above a separate calibration is required. Therefore for more accurate results, the results were obtained according to the specific calibration curve for each experiment.

### 6.3.2 Characterisation of materials

Features that combine to suggest that the chosen method of preparation is ideal for a sorbent used in analytical research include the: (i) ability to synthesis large quantities (100 g) of material in a simple batch process, (ii) large mesopores which favour functionalisation, (iii) wide pore size distribution, (iv) long range order of the pores and (v) ease at which the material was prepared without expensive laboratory kit. The MCM-41 base material, prepared in ambient conditions and using microwave digestion to extract the surfactant from the pores (see Table 6.3).



**Table 6.3: Physicochemical properties MCM-41 used.**

Sample Name	BET Surface Area (m <sup>2</sup> g <sup>-1</sup> )	Pore Size (nm)	Pore Volume (cm <sup>3</sup> g <sup>-1</sup> )	d-Space (Å)
MWD-MCM-41	760	6.7	0.99	42.20

**6.3.2.1 Elemental analysis for functionalised-MCM-41 materials**

Elemental analyses was used to estimate the amount of molecules ( $L_o$ ) attached to functionalised samples (AP-, MP-, DETA- or MDETA-MCM41) from the percentage of nitrogen, or sulfur, in the functionalised mesoporous silica [179], using equation (6.1) as an example for nitrogen:

$$L_o = \frac{\% N}{\text{nitrogen atomic weight}} \times 10 \quad \text{(Equation 6.1)}$$

From Table 6.3 it can be seen that the calculated  $L_o$  values were above those typically reported in the literature [232-234] with the DETA sample giving the highest  $L_o$  value published to date. This high degree of functionality observed with DETA-MCM-41 was the first proven of the success of producing new MCM-41 with high silanol groups in the surface which remain the material with high ability to be functionalised.

**Table 6.3: Elemental analysis data recorded for functionalised-MCM-41**

Silica	% C	% H	% N	% S	$L_o$ (mmol/g) <sup>a</sup>
AP-MCM-41	8.20	2.32	2.79	0.00	1.99
MP-MCM-41	11.43	2.17	0.00	9.46	2.96
DETA-MCM-41	17.13	4.15	10.08	0.00	7.2
MDETA-MCM-41	12.10	2.39	3.61	2.62	2.57

<sup>a</sup>Functionalisation degree = millimoles of ligand per gram of functionalised silica.

### **6.3.3 Lead adsorption extraction capacities of functionalised MCM-41 materials**

Samples of MCM-41 and functionalised MCM-41 (AP-MCM-41, MP-MCM-41, DETA-MCM-41 or MDETA-MCM-41) were each added to aqueous solutions containing known amounts of Pb (II). Solution pH was altered (to 3, 5, 7, 9 or 11), to test the materials' extraction efficiencies over a wide pH range. The results, summarised in Figure 6.3, illustrate that all functional groups were successful in removing Pb (II) from solution. To ensure that the functionality of the material was responsible for extraction, control experiments were run using 0.01 g of non-functionalised MCM-41. No Pb (II) was removed from solution in each case, regardless of the solution pH.

Lower Pb (II) adsorption capacities were observed for the mono-functional groups (AP-MCM-41 and MP-MCM-41) compared to DETA- or MDETA- where multi co-ordination sites led to a significant improvement in extraction performance; presumably because lead prefers a trigonal chelation geometry. A strong dependence on pH was observed for co-ordination with DETA or MDETA ligands with highest capacities achieved when the solution pH was adjusted to values of 9 and above.

Although adsorption capacity values for 3 of the materials were only comparable to what had been previously cited in the literature (Table 6.4), the DETA ligand in particular illustrated a tremendous improvement in adsorption capacity ( $960 \mu\text{mol g}^{-1}$ ), at double the previously reported maximum value.

This improvement in performance was in-line with expectations due to the unique character of the products produced by the microwave digestion method (larger pores to incorporate longer non-linear ligand conformation and higher degree of functionalisation due to the microwave digestion procedure).

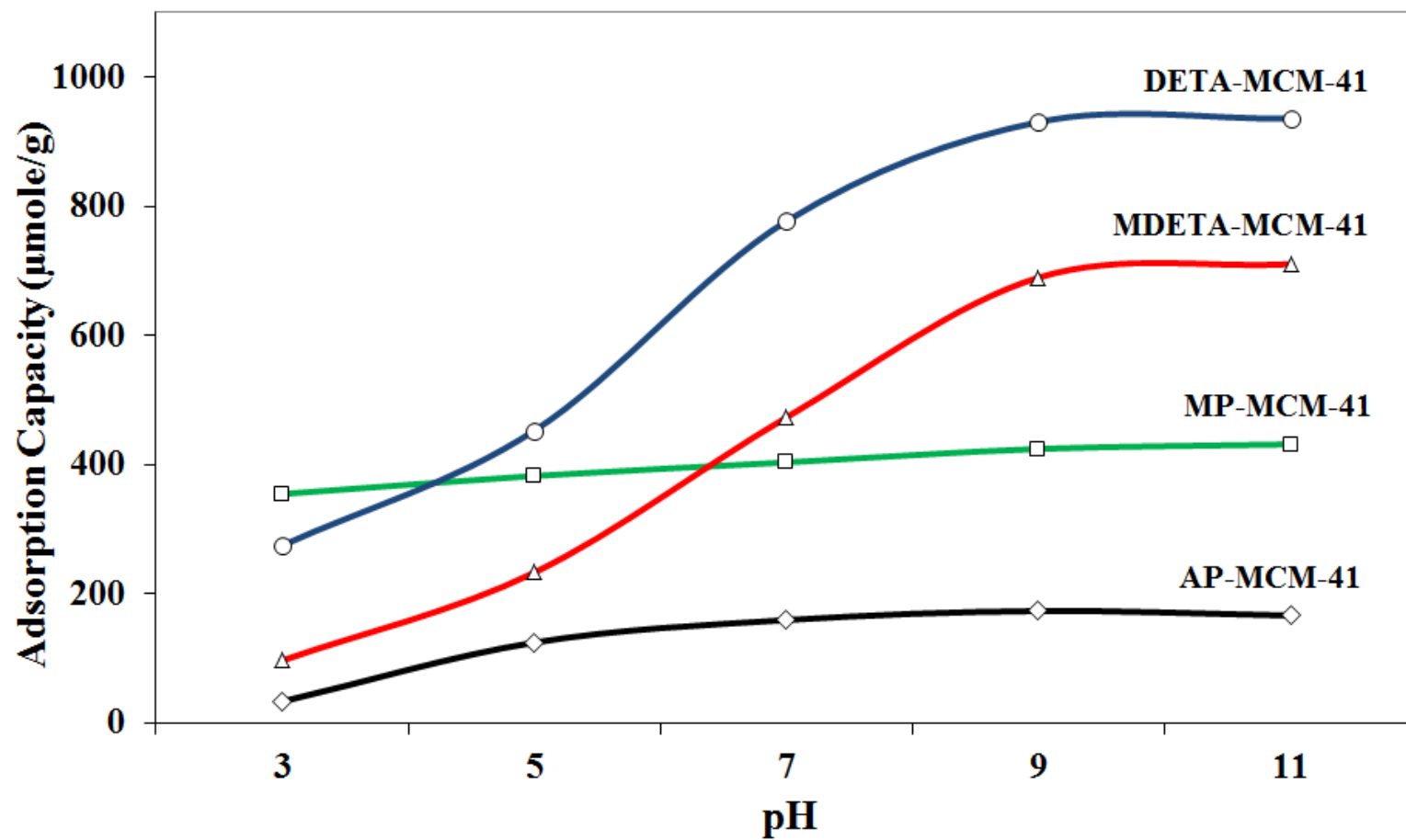


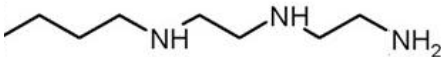
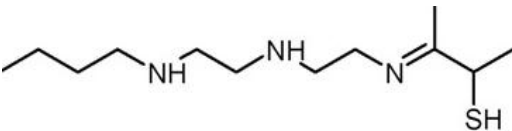
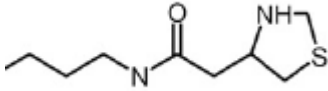
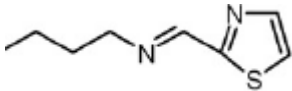
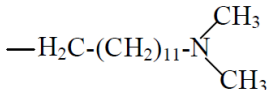
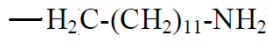

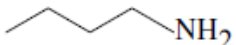



Figure 6.3: Adsorption capacities of functionalised MCM-41 for lead extraction over different pH values.

**Table 6.4: Comparison of alternative sorbents used to extract lead ions from solution.**

Sorbent	Immobilised Ligand	Adsorption Capacity ( $\mu\text{mol/g}$ )	Reference
AP-MCM-41		174	This Work
MP-MCM-41		425	This Work
DETA-MCM-41		931	This Work
MDETA-MCM-41		690	This Work
Silica (Kieselgel 100)		80	[235]
Silica (Kieselgel 100)		49	[235]
MCM-41		410	[236]
MCM-41		250	[236]
SBA-15		342	[228]
MCM-41		408	[228]
MCM-41		493	[237]

### **6.3.4 Reutilisation of DETA-MCM-41 for repeated sorbent use and further removal of Pb (II) from contaminated water**

3 samples of DETA-MCM-41 containing 200  $\mu\text{g}$  of Pb were regenerated by washing the solid in 10  $\text{cm}^3$  of 1 M HCl. The acid washings were analysed by FAAS using matrix matched calibration solutions and it was shown that Pb (II) was successfully removed from the ligand (average measured concentrations were  $19.7 \pm 0.5 \mu\text{g cm}^{-3}$ , indicating 99 % recovery of lead ions). The solid sorbents were filtered and washed with distilled water before exposure to a second 10  $\text{cm}^3$  solution containing 20  $\mu\text{g cm}^{-3}$  of Pb (II). Once again the extraction was efficient with > 99 % of Pb (II) removed from solution using the regenerated sorbent materials. The sorbents were acid washed for a second time and extraction was again successful with > 97 % recovery values. The sorbents were then exposed to a third contaminated solution: extraction performance was 100 %.

These experiments demonstrated that there was no significant loss in sorbent performance after it had been washed with HCl to recover extracted Pb (II) ions. Indeed regeneration of the material was achieved at the same time allowing the materials to be easily reused. The acid treatment did not appear to remove the ligand from the silica which was used in subsequent mitigation treatments, making the material competitive with other adsorbents that are cheaper to produce but that cannot be regenerated. Although further work is required to determine the number of times the sorbents can be reused before extraction efficiency is altered, this initial experiment demonstrates the potential reuse of DETA-MCM-41.

### **6.3.5 Assessment of DETA-MCM-41 extraction efficiencies in real water samples**

To examine the performance of DETA-MCM-41 to extract Pb (II) ions in the presence of other cations the sorbent was added to 20  $\text{cm}^3$  samples of distilled, tap or river water; each was spiked with Pb (II) to a solution concentration of 25  $\mu\text{g cm}^{-3}$ . The results given in Table 6.5 indicate that Pb (II) was removed equally well from real samples as extractions values were within 100 % for tap water and 98 % for river water. The sorbents were acid washed and Pb recovery values of 101 and 90 % were obtained for the sorbents applied to spiked, tap or river water, respectively.

In spite of the high concentrations of Ca and Mg ions measured in the river water sample ( $43.6 \mu\text{g cm}^{-3}$  and  $6 \mu\text{g cm}^{-3}$ , respectively, Pb (II) adsorption and recovery values were only slightly less than those obtained for the spiked tap water sample, which implied that the Pb-DETA co-ordination was not appreciably hindered by presence of other co-ordinating ions at reasonably high concentration.

**Table 6.5: The Performance of DETA-MCM-41 in real samples.**

Sample	Spiked ( $\mu\text{g cm}^{-3}$ )	Extraction (%)	Recovered ( $\mu\text{g cm}^{-3}$ )	Recovery (%)
Distilled water	25	$100 \pm 2$	24.83	$99.3 \pm 2$
Tap water	25	$100 \pm 1$	25.31	$101.2 \pm 1$
River water	25	$98 \pm 3$	22.57	$90.3 \pm 3$

### 6.3.6 Assessment of DETA-MCM-41 extraction efficiencies in multi-elements samples

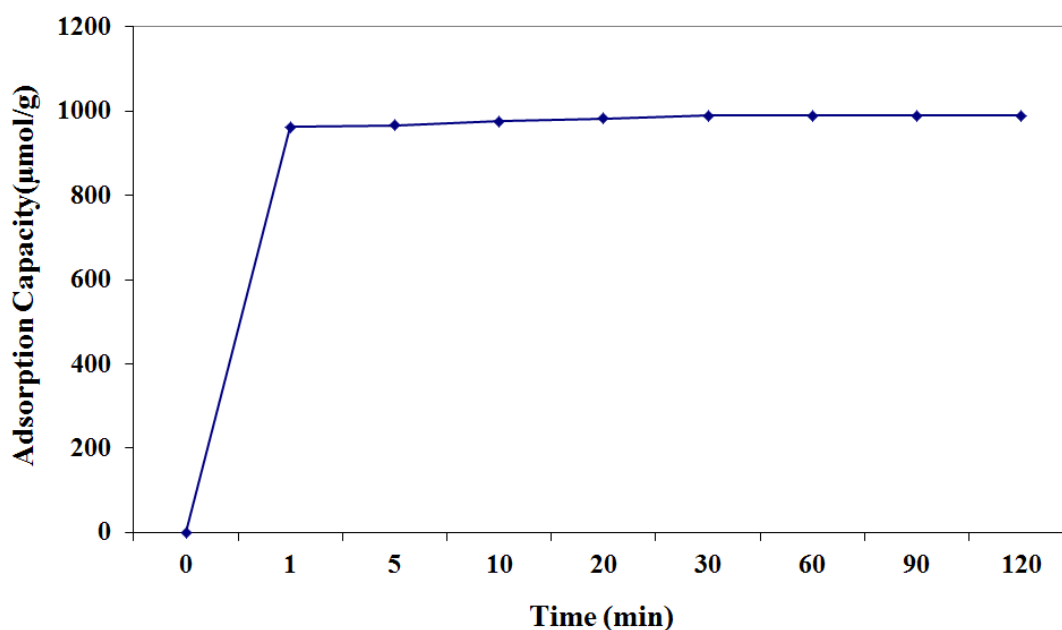
The ability of DETA-MCM-41 to extract Pb (II) in the presence of other metal ions was also assessed by adding the sorbent to a multi-element solution containing  $1 \mu\text{g cm}^{-3}$  each of Cd, Co, Cr, Cu, Fe, Hg, Mn, Ni, Pb, or Zn. The extraction and recovery values for all ions in the standard solution were calculated (see Table 6.6). As expected each metal ion had a different response to the DETA ligand however in general the metal ion concentrations were reduced to  $< 0.2 \mu\text{g cm}^{-3}$ .

This ligand appears to be more suited to the extraction of Pb, Mn, Fe, Cr and Cd; less so for Hg, Co, Cu and Ni. However it should be pointed out that the main aim was to produce and optimised ligand performance for Pb (II) extraction and the ability to completely remove other ions from solution at 100 % was a distinct advantage. Although these tests were by no means exhaustive they did highlight the merits of DETA-MCM-41 as a scavenger of Pb (II) from aqueous solution, giving higher extraction efficiencies than previously found.

**Table 6.6: The efficiency of DETA-MCM-41 to extract Pb in multi elements sample.**

Heavy Metals	Initial concentration ( $\mu\text{g cm}^{-3}$ )	Concentration after extraction ( $\mu\text{g cm}^{-3}$ )	Concentration of metal recovered from loaded sorbent ( $\mu\text{g cm}^{-3}$ )	% of metal ion extracted from original solution	% of metal ion recovered from loaded sorbent
Cd	1.000	0.003	0.791	99.7	79.3
Co	1.000	0.159	0.498	84.1	59.2
Cr	1.000	0.009	0.833	99.1	84.1
Cu	1.000	0.119	0.875	88.1	99.3
Fe	1.000	0.021	1.085	97.9	110.8
Hg	1.000	0.200	0.052	80.0	6.5
Mn	1.000	0.005	0.865	99.5	86.9
Ni	1.000	0.072	0.899	92.8	96.9
Pb	1.000	0.005	0.752	99.5	75.6

Although these experiments are laboratory based and preliminary, the results obtained here for DETA-MCM-41 suggest that the material could be a successful sorbent for environmental or industrial applications. For example, the ability of the DETA ligand to hold onto Pb (II) ions at higher temperatures was confirmed by repeating the extraction experiments at 60 °C where > 98 % extraction efficiencies were observed. The resulting metal ion-ligand chelate was also shown to be stable for at least 4 weeks (the period of time examined here) and this could potentially be for even longer. Moreover, even although these experiments were initiated with an extraction time of 2 hours based on conditions outlined in a previous publication [153], experiments in research undertaken in this work have demonstrated that the time required to reach an extraction maximum is far shorter.



**Figure 6.4: Time required reaching the adsorption capacity of DETA-MCM-41 when the sorbent is stirred in a solution containing 200 µg cm<sup>-3</sup> lead ions.**

One minute after placing the sorbent into a 20 cm<sup>3</sup> solution containing 200 µg cm<sup>-3</sup> Pb (II) ions, 97.2 % of the maximum adsorption capacity had been reached which increased slowly to 100 % in 30 min (see Figure 6.4). Should the sorbent be capable of extracting potentially toxic metals (PTMs) from aqueous solutions where stirring or agitation of the water was not possible (e.g. in a well), experiments were



conducted with no stirring and 90 % Pb was removed from a 20 cm<sup>3</sup> solution containing 200 µg cm<sup>-3</sup> Pb in just 2 hours. Therefore stirring is an important factor to consider when accelerated adsorption is required but in situations where stirring is not possible, longer exposure times will lead to efficient extraction.

## 6.4 Conclusions

MCM-41 prepared by a room temperature procedure with template removal by MWD produced a material with unique properties: 760 m<sup>2</sup> g<sup>-1</sup> and 6.7 nm surface area and pore size respectively. These properties combined allowed the MCM-41 to be functionalised to a much greater extent than has been reported previously; this feature particularly significant for DETA-MCM-41. With this material larger multi-site chelate groups were available to co-ordinate with Pb (II) ions in its preferred trigonal geometry. Although further work is required to test the DETA-MCM-41 sorbent in the field, this research undertaken here, on the characterisation and extraction efficiency of DETA- MCM-41, strongly suggests that this material has tremendous potential to extract Pb (II) from aqueous solutions in industrial or environmental remediation applications. The ion-ligand co-ordination was strong enough that the sorbent can work in static solutions where the ion is driven to the ligand by a concentration gradient alone and can work in contaminated river water samples. This will be of particular significance if the material is to be used in a remote location where stirring or agitation of the contaminated solution is not possible.

**Chapter 7: Selective extraction of mercury (II) from water  
using mercapto functionalised-MCM-41 and regeneration  
of the sorbent using microwave digestion**

## 7.1 Introduction

Mercury ions, Hg (II) are one of the most hazardous substances included in the US Environmental Protection Agency's (EPA) list of priority pollutants. Numerous extraction processes have been assessed to reduce the concentration of Hg (II) in aqueous solution including; ion exchange [106, 166, 238], solvent extraction [151, 168, 239], adsorption [240, 241], precipitation [242, 243] and membrane separation [244, 245] methods. These conventional extraction processes are generally useful but they have certain limitations such as: they are less effective when used to extract Hg (II) from dilute solutions, they are costly and, more importantly, they show little-no selectivity. To improve the selectivity of sorbents for Hg (II) removal, chelating resins have been used but results indicate they have limited applicability due to factors including; poor hydrophilicity, small surface areas, slow rates of adsorption and expense (due to lack of regeneration methods) [246].

The direct interaction of Hg (II) with mercaptopropyl (MP) groups has been proposed previously for adsorption on functionalised mesoporous silica [86]. Several research groups have studied the selectivity of mercapto functionalised MCM-41 to extract the Hg (II) from aqueous media and results indicate reasonably high adsorption capacities and selectivity towards mercury [86, 179, 247]. However, there are still limitations of these materials including the length of time required to prepare MCM-41, difficulties incurred when trying to produce larger batch sizes of material and the inability to remove Hg (II) from loaded sorbents preventing sorbent reuse (thus drastically increasing cost).

MCM-41 based materials will only be useful as metal ion scavengers if they can be economically regenerated whilst maintaining high adsorption capacities for the analyte of interest after multiple uses. It has been previously demonstrated that the regeneration of MP- MCM-41 materials after mercury adsorption cannot be carried out under thermal treatment and acidic conditions [248]. Some research groups worked with similar mercapto-modified MCM-41 reporting effective regeneration of loaded materials by treatment with hydrochloric acid or hydrobromic acids. However, high concentrations (12 M) are used and that could lead to damage of the silica mesostructure [222, 249].

This work presents an assessment of MP-MCM-41 for the selective extraction of Hg (II) from contaminated aqueous solution. Further, a new regeneration method is reported which allows 100 % recovery of Hg (II) ions from loaded MP-MCM-41 without disruption of the chelating agent. MP-MCM-41 can be reused after removal of Hg (II) without the need for surface reactivation and the Hg (II) is selectively recovered from contaminated water. Extraction results for MP-MCM-41 are compared to those obtained by DETA-MCM-41.

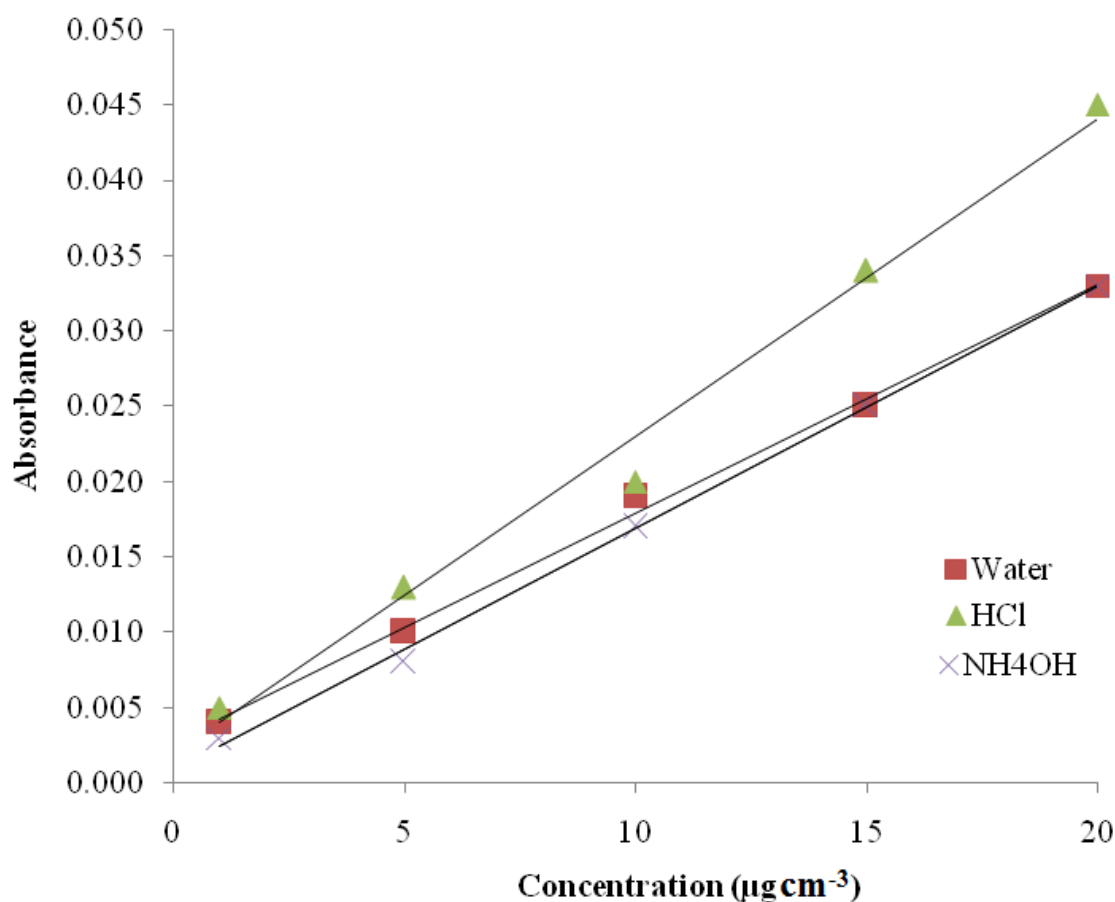
## **7.2 Experimental**

### **7.2.1 Preparation of MCM-41 and functionalised-MCM-41**

The prepared MCM-41 which outlined in section 4.2 and functionalised as summarised in section 3.4.1. Briefly, in a typical experiment, approximately 5 g of microwave digested (MWD) MCM-41 was pre-treated at 140 °C for 2 h and then immersed into 50 cm<sup>3</sup> toluene and 10 cm<sup>3</sup> MPTMS or DETA-TMS in a 250 cm<sup>3</sup> flask. The mixture was refluxed for 4 h and the solid produced was filtered, washed with 100 cm<sup>3</sup> ethanol, and oven-dried at 80 °C for 1 h to produce a mercapto-functionalised (MP-MCM-41) or diethylenetriamine-functionalised (DETA-MCM-41) MCM-41 sorbent, respectively.

### **7.2.2 Calibration data**

Extraction experiments were to be performed in acidic and alkaline conditions; with measurement of Hg (II) in solution by FAAS. Instrumental conditions are given in Section 3.4.4, p. 79. Therefore it was deemed necessary to prepare 3 sets of standard solutions; in water, (1 M) hydrochloric acid or (1 M) ammonium hydroxide, to determine if the matrix of the standard solution effected the Hg (II) measurement by FAAS. Standard solutions in all 3 matrices were prepared between a concentration range of 1 – 20 µg cm<sup>-3</sup> and the regression lines obtained are given in Figure 7.1.



**Figure 7.1: Regression lines for Hg (II) prepared in; water, HCl or NH<sub>4</sub>OH.**

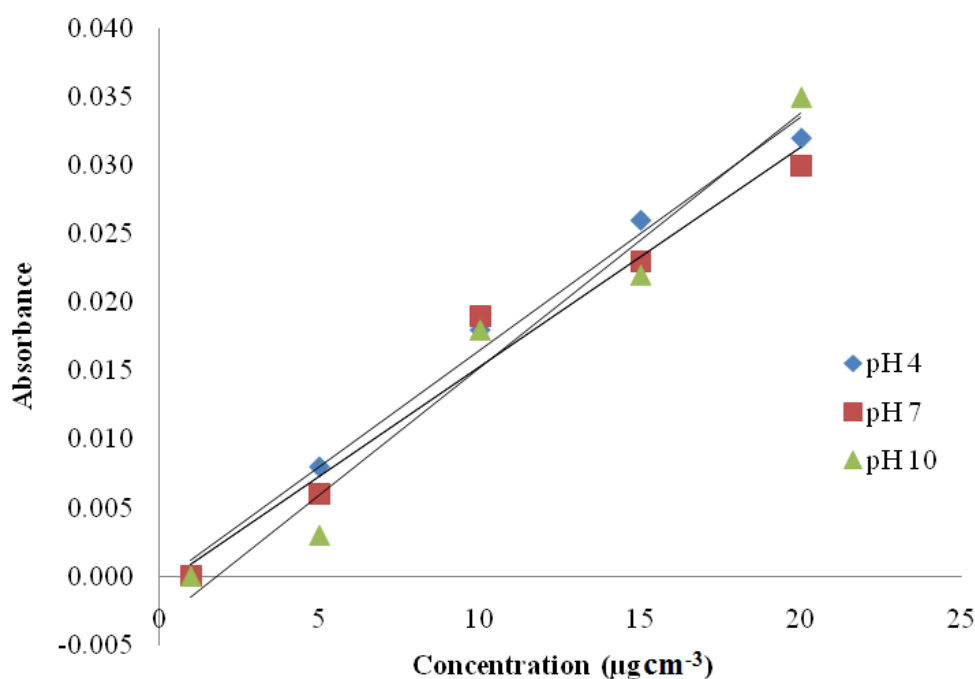
The results obtained indicated that linear correlations were achieved for the 3 regression lines with  $r^2$  values being greater than 0.9891. Examination of regression slopes (Table 7.1) indicated that the regression results obtained for water and NH<sub>4</sub>OH matrices were not significantly different to each other, however the calibration for Hg (II) in acid solution was.

These results suggested that it would be necessary to carry out calibrations both in water and HCl, when extreme acid conditions are used to analyse Hg (II) in acidic solution.

**Table 7.1: Results of linear regression analyses and corresponding to Hg (II) prepared in water, HCl or NH<sub>4</sub>OH.**

Matrix	$r^2$ value	Slope	Intercept	Error on slope	Error on intercept
Water	0.9970	0.0015	0.0027	0.00004819	0.000591
HCl	0.9891	0.0021	0.0019	0.00012771	0.001565
NH <sub>4</sub> OH	0.9982	0.0016	0.0008	0.00003945	0.000484

However, in the extraction experiments studied within this research, solutions were prepared in water and the pH was then adjusted using drop wise addition of either HCl or NH<sub>4</sub>OH, resulting in much lower concentrations of HCl and NH<sub>4</sub>OH in solution with resultant pH value of 4 or 10. In order to determine whether different regression lines would be obtained with these pHs modified solutions, further calibration experiments were examined.



**Figure 7.2: Regression lines for Hg (II) standard solutions, prepared at pH 4, 7 or 10.**

In this set of experiments, the calibration solutions were prepared in water and the pH of the solutions was then adjusted by the drop wise addition of HCl or NH<sub>4</sub>OH, consistent with the extraction experiments that were to be conducted. The regression lines obtained (Figure 7.2) indicated a positive correlation for each set of calibration solutions, with  $r^2$  values being greater than 0.9681 in all cases; see Table 7.2.

**Table 7.2: Linear regression analyses results for Hg (II) calibration solutions at pH 4, 7 or 10.**

pH	$r^2$ value	Slope	Intercept	Error on slope	Error on intercept
4	0.9898	0.001704	-0.00058	0.0001	0.001226
7	0.9705	0.001601	-0.00073	0.000161	0.001974
10	0.9681	0.00186	-0.00338	0.000195	0.002389

The results obtained indicated that regression slopes were very similar regardless of the solution pH (4, 7 or 10). It was concluded that the regression lines were not appreciably different and so in future experiments one set of calibration solutions were used to determine the Hg (II) concentration in extraction solutions regardless of the solution pH. For ease, calibration solutions for Hg (II) were prepared in distilled water.

### 7.2.3 Extraction of Hg (II) from solution using functionalised-MCM-41

To assess the applicability of MP-MCM-41 as a suitable adsorbent for Hg (II) from solution; experiments were conducted as discussed in Section 3.4.2, p.77. The extraction procedure was also performed using non-functionalised MCM-41 at pH 7 as a control experiment. In the absence of mercapto-groups on the surface of MCM-41, no Hg (II) was removed from solution.

This experiment confirmed that removal of Hg (II) would not be due to encapsulation of the metal ion in the pores of the meso-silica. Indeed Hg (II) was only removed from solution by the functionalised material and this implied chelate-ion coordinating bonds were involved in the extraction process.

#### **7.2.4 Experiments used to assess the selectivity of MP-MCM-41 towards Hg (II) in contaminated water samples**

To demonstrate the potential selectivity of MP-MCM-41 for Hg (II) when present in solutions containing other mixed metal ions, a 25 cm<sup>3</sup> non-buffered water solution containing (20 µg cm<sup>-3</sup>) of selected metals (Cd, Cr, Hg, Mn, Pb, or Zn) was prepared. In each experiment 25 mg of MP-MCM-41 was added to the solution and stirring commenced immediately after addition of the sorbent. Additionally, the performance of MP-MCM-41 in real samples was evaluated by adding 25 mg of sorbent to a river water sample (collected from the Bothlin River in Glasgow) and a tap water sample (taken from a building in the Drygate campus in Glasgow). The tap and river water samples were known to contain high concentrations of metal ions, but not Hg (II) and so they were spiked to produce solutions containing 25 µg cm<sup>-3</sup> of Hg (II). To assess extraction performance, aliquots were removed from stirring solutions at known time points, filtered (Fisherbrand QL100) and the presence of metal ions in solution was determined by FAAS.

#### **7.2.5 Recovery of Hg (II) from loaded sorbents using microwave digestion**

A 1 g sample of mercaptopropyl-MCM-41 (MP-MCM-41) was added to a 40 cm<sup>3</sup> aqueous solution containing 1000 µg cm<sup>-3</sup> Hg (II) to pre-load the sorbent with analyte. A reduction in Hg (II) concentration measured after sorbent addition was used to provide evidence that the target analyte was extracted by the sorbent. The loaded sorbent was removed from the solution by filtration and dried in air. Approximately 0.125 g of loaded sorbent was immersed in 20 cm<sup>3</sup> of 1% HNO<sub>3</sub>, and the resulting suspension was placed in a 50 cm<sup>3</sup> capacity Teflon microwave vessel.



To assess the ability to recover Hg (II) ions from the MP-MCM-41 two different conditions were used with the microwave. The first set of conditions examined the use of high energy to break the Si-C<sub>3</sub>H<sub>6</sub>-S-Hg bonds ensuring that all the Hg (II) could be taken back into solution. The second set of experiments was to decrease the energy of the microwave so that the S-Hg bonds would be disrupted whilst leaving the chelating agent on the surface of the silica. Table 7.3 summarises parameters used in high or low energy microwave digestion experiments. The efficiency of the regeneration process was evaluated by calculating the percentage of mercury desorbed as the ratio of the amount of mercury in solution after low energy microwave digestion (LE-MWD) to the mass of mercury removed by high energy conditions (HE-MWD):

$$\% \text{ Regeneration} = \frac{\text{Mass of Hg}_{\text{LE-MWD}}}{\text{Mass of Hg}_{\text{HE-MWD}}} \times 100 \quad \text{Equation 7.1}$$

**Table 7.3: Operation conditions used in Hg (II) recovery experiments.**

	Low Energy MWD	High Energy MWD
Working frequency	2450MHz	2450MHz
Power applied to the sample	800 W	1600 W
Heating Rate	Ramped to 80 °C for 5 min held 85 °C for 10 min	Ramped to 180 °C for 15 min held 180 °C for 5 min
Solvent	1% HNO <sub>3</sub>	10% HNO <sub>3</sub>
Volume of solvent (cm <sup>3</sup> )	20 cm <sup>3</sup>	20 cm <sup>3</sup>
Weight of sample (g)	0.125	0.3 g

## 7.3 Results and discussion

### 7.3.1 Parent Material characterisation

The functionalised samples of MCM-41 were characterised using BET to compare the N<sub>2</sub>-adsorption isotherms, see Figure 7.3. In each case typical Type IV N<sub>2</sub>-adsorption isotherms were obtained with distinct hysteresis loops and steep adsorption/desorption steps indicating a well-ordered array of pores. All samples display parallel and nearly vertical isotherm branches typical of hexagonal mesoporous silica. The type IV isotherm shape is preserved for all samples suggesting the pore structure has been maintained post-functionalisation.

The physicochemical data for the 3 samples are summarised in Table 7.4. As expected significant reductions in surface area and pore volume (calculated from the BJH model) were observed for the modified materials; this is consistent with the longer length of the chelate compared to MP. However the average pore diameter remained similar post-modification. The degrees of functionalisation ( $L_0$ ) were high indicating that materials were successfully functionalised with both chelates.

**Table 7.4: Physicochemical data recorded for the MCM-41, MP-MCM-41 and DETA-MCM-41 samples.**

Sample Name	BET Surface Area (m <sup>2</sup> g <sup>-1</sup> ) <sup>a</sup>	Pore Size (nm) <sup>b</sup>	Pore Volume (cm <sup>3</sup> g <sup>-1</sup> ) <sup>c</sup>	$L_0$ (mmol/g) <sup>d</sup>
MCM-41	760	6.7	0.9868	---
MP-MCM-41	449	6.7	0.5924	2.96
DETA-MCM-41	238	5.5	0.409	7.19

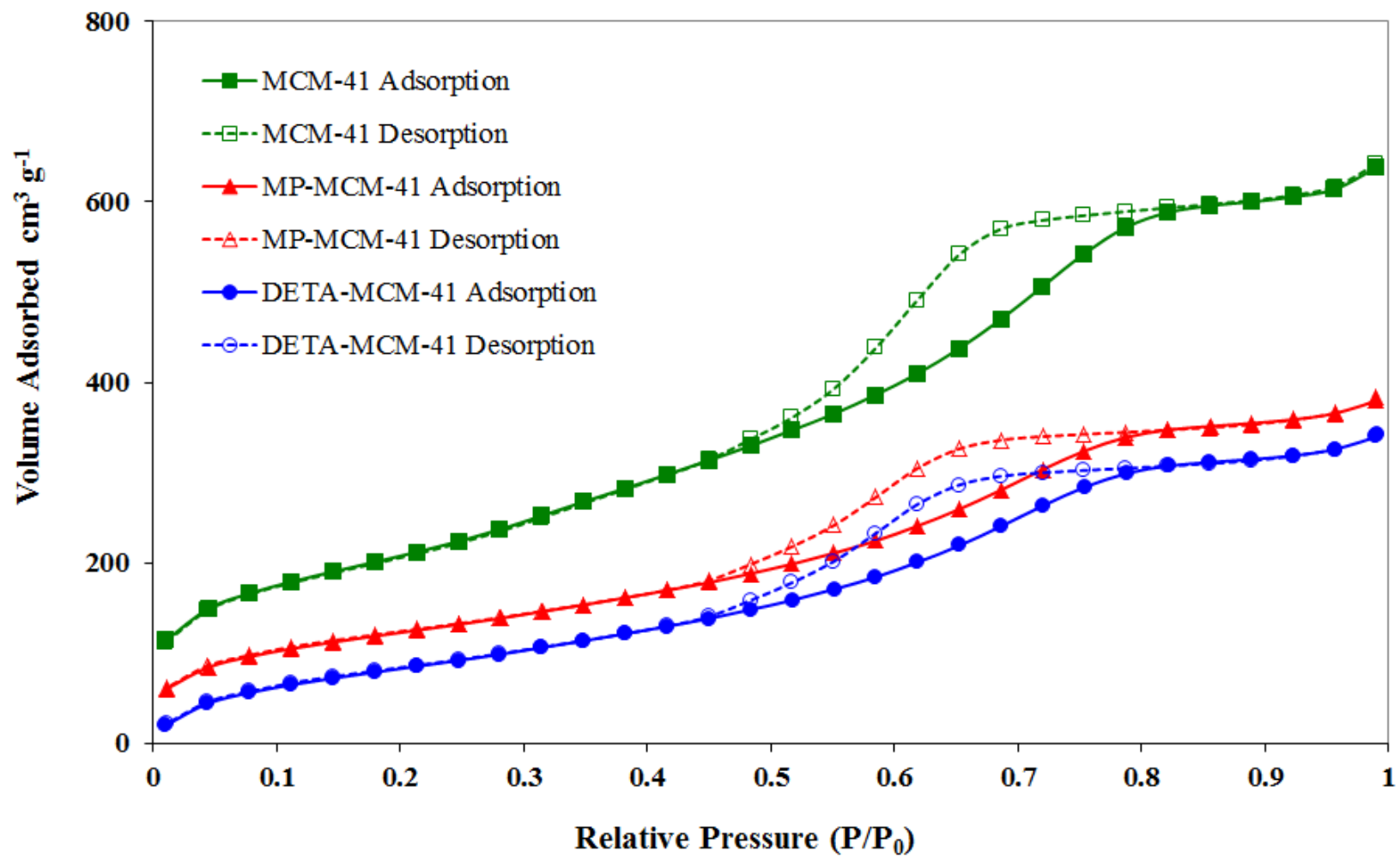
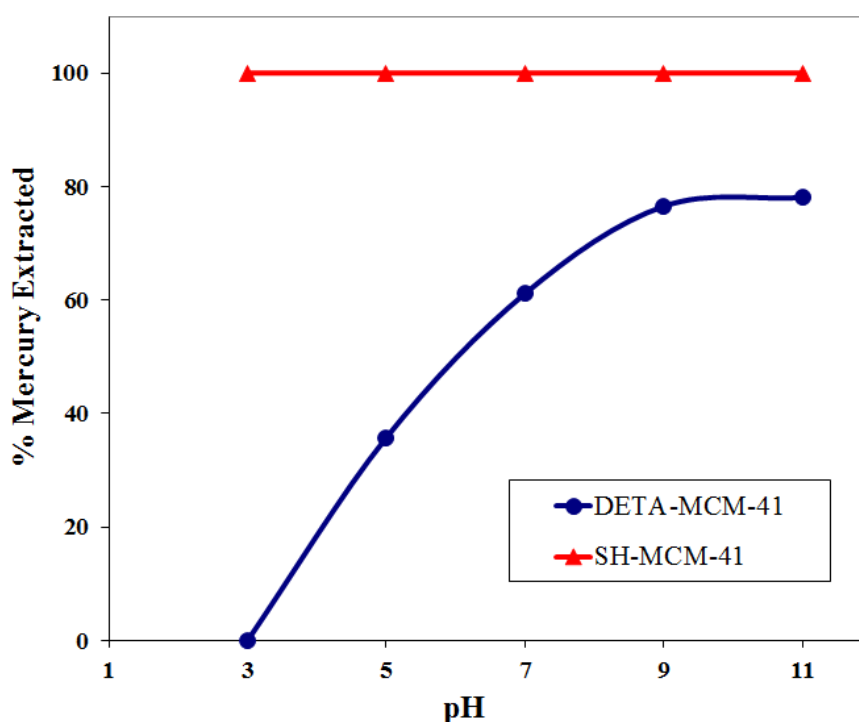


Figure 7.3: BET isotherm patterns of MCM-41, MP-MCM-41 and DETA-MCM-41.

### 7.3.2 Mercury (II) extraction and adsorption capacities using spiked solutions of distilled water

Samples of MCM-41 and functionalised MCM-41 (MP-MCM-41 and DETA-MCM-41) were each added to aqueous solutions containing known amounts of Hg(II) ions at solution pHs of 3, 5, 7, 9 or 11. Interestingly, unlike for all other chelating agents tested, the results indicated that there was no effect of changing pH on the efficiency of MP-MCM-41 for Hg (II) extraction from water over the pH range used in this study (Figure 7.4), making it applicable as a sorbent material for a wide range of potential applications.



**Figure 7.4: Effect of pH on the extraction of mercury ions from water using functionalised MCM-41.**

Moreover, the adsorption capacity for Hg (II) was measured resulting in an adsorption capacity value ( $1245 \mu\text{mol g}^{-1}$ ) that was higher than previous, similar studies (see Table 7.5). The high values obtained appeared to be a direct result of the optimised preparation method used for the parent material as other research groups using MP-MCM-41 achieved lower adsorption capacities of 1050 [250] or 590  $\mu\text{mol}$

$\text{g}^{-1}$  [127]. Using FAAS with a LOD of  $1.4 \mu\text{g cm}^{-3}$ , it was possible that best recoveries achieved were 93 % after just one exposure of the sorbent to  $100 \mu\text{g}$  of Hg (II). Therefore to provide evidence that the sorbent was capable of extracting a high mass of Hg (II) with good efficiency the sorbent was introduced to  $5 \text{ cm}^3$  solutions containing Hg (II) at a concentration of  $800 \mu\text{g cm}^{-3}$ . Hg (II) was measured in the extracted aliquot only after the sorbent was introduced to the 3<sup>rd</sup> solution containing a high mass of Hg (II). Overall the sorbent was exposed to  $10000 \mu\text{g}$  of Hg (II) and  $90 \mu\text{g}$  of Hg (II) was measured in the solution indicating an extraction efficiency of approximately 99.1 %.

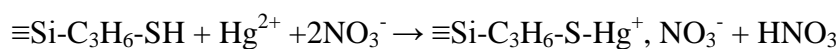
**Table 7.5: A list of maximum adsorption capacities for Hg (II) using modified adsorbents.**

Material	Ligand	Adsorption capacity ( $\mu\text{mol g}^{-1}$ )	Ref.
MCM-41	2-(3-(2-Aminoethylthio) propylthio) ethanamine	700	[86]
MCM-41	2-Mercaptothiazoline	700	[179]
HMS	3-mercaptopropyl	550	[251]
Sol-gel silica	1,5-Diphenylcarbazide	29	[130]
Silica gel	Dithizone	320	[252]
MCM-41	2-Mercaptopyridine	120	[232]
MCM-41	3-aminopropyl	400	[80]
MCM-41	3-mercaptopropyl	1050	[250]
MCM-41	3-mercaptopropyl	590	[127]
MCM-41	3-mercaptopropyl	1245	This work

The DETA-MCM-41 sorbent showed a much lower adsorption capacity, of approximately  $50 \mu\text{mol g}^{-1}$ , and also a strong dependence on pH with the highest capacities achieved (80 % that of MP-MCM-41) when the solution pH was adjusted to values of 9 and above (Figure 7.4). The difference in performance between MP- and DETA-MCM-41 over the pH range can be used as an advantage. For example, MP-MCM-41 can be used to extract Hg from contaminated solutions over a wide range of pH values which will expand its use in environmental remediation.

The DETA-MCM-41 material was easily regenerated by lowering the solution pH value to 3; with successful removal of all the encapsulated Hg (II). The regenerated DETA-MCM-41 was then re-used to extract further Hg (II) from aqueous solution and the results highlighted the ease at which this material could be regenerated whilst still performing at approximately 99% of the original extraction efficiency.

The dramatic difference in performance over the pH range studied can be related to the stability of the chelate attached to the silica material. For MP-MCM-41 the –S-Hg- bond has a high stability constant [248] whereas for DETA-MCM-41 the –N-Hg- has much lower stability constant [250]. The high stability of the –S-Hg bond over the observed pH range of 3-11 allowed the chelate to extract Hg (II) at high efficiencies. Indeed the stability of the –S-Hg- bond is higher than those for other divalent metal ions with SH groups [253]. Further explanation of this phenomenon was given by Walcarius and Delacote [247] who reported that the complexation of Hg (II) to thiol groups led to the formation of a positive charge:



The formation of positively charged complexes inside the mesoporous adsorbents could prevent  $\text{Hg}^{2+}$  being replaced by  $\text{H}^+$  at low pH. Note however that there are limits to the use of mesoporous silica at much lower pH values ( $< 1$ ) where damage to the silica meso-structure has been reported [222, 247-250].

### 7.3.3 The selectivity of MP-MCM-41 towards Hg (II) in the presence of other heavy metal ions

A multi-element solution was used to evaluate the selectivity of MP-MCM-41 and DETA-MCM-41 towards Hg (II) ions. Approximately 25 mg of each sorbent was added to an individual solution containing 20  $\mu\text{g cm}^{-3}$  of Cd (II), Cr (III), Hg (II), Mn (II), Pb (II), and Zn (II). The solutions were stirred for 2 h, filtered and the filtrates were analysed by FAAS. Approximately 80 % of Hg (II) was extracted by DETA-MCM-41, with greater than 97 % extraction efficiencies for Cd (II), Cr (II), Mn (II), Pb (II), and Zn (II). This is in contrast with the results obtained for MP-MCM-41 which was almost exclusively selective towards Hg (II) despite the presence of other heavy metals in solution (Table 7.6).

**Table 7.6: The efficiency of DETA-MCM-41 and MP-MCM-41 for Hg (II) in selected multi element water samples.**

Metal	Spiked ( $\mu\text{gcm}^{-3}$ )	Found after 2h stirring ( $\mu\text{g cm}^{-3}$ )	
		DETA-MCM-41	MP-MCM-41
Cd (II)	20	0.7	18.1
Cr (III)	20	0.3	20.5
Hg (II)	20	4.3	< LOD
Mn (II)	20	0.1	19.8
Pb (II)	20	0.3	20.3
Zn (II)	20	0.5	19.4

LOD = 1.4  $\mu\text{g cm}^{-3}$ .

These results reflect the expected performance of amino- and mercapto-ligands based on metal ion-ligand stability constants which are 19.2 [250] and  $> 23$  [127] for amino-ligands with mercury and other metal ions, respectively and 37.3 [248] for sulfur and mercury.

The ability of MP-MCM-41 to extract Hg (II) in the presence of other potentially toxic metals (PTMs) was also assessed by adding the sorbent to a sample of river water and tap water. The water samples were first analysed by ICP-MS to determine the concentration of other heavy metals in each solution before being spiked with mercury ions to produce solution concentrations of  $25 \mu\text{g cm}^{-3}$  of Hg (II), the results are given in Table 7.7.

**Table 7.7: ICP/MS concentration data recorded for heavy metals in river and tap water samples.**

Heavy Metal	River Water (ppb)	Tap Water (ppb)
As	$0.7 \pm 0.1$	$2.5 \pm 0.1$
Ca*	$43,600 \pm 1000$	$11,500 \pm 1000$
Cd	$5.5 \pm 0.1$	$12.7 \pm 0.1$
Cr	$4.3 \pm 0.4$	$14.3 \pm 0.4$
Cu	$12.0 \pm 0.3$	$60.3 \pm 0.3$
Fe	$60.1 \pm 0.2$	$249.9 \pm 0.2$
Mg*	$6,000 \pm 1000$	$8,500 \pm 1000$
Mn	$3.4 \pm 0.1$	$9.9 \pm 0.1$
Ni	$12.0 \pm 0.2$	$50.4 \pm 0.2$
Pb	$3.1 \pm 0.1$	$54.8 \pm 0.1$
Zn	$2.7 \pm 1$	$353.9 \pm 1$

\*measured by FAAS



In spite of the high concentrations of Ca and Mg in the solutions, Hg (II) removal was 100 % from river water and tap water, which implied that the Hg-S coordinating bond was not appreciably hindered by the presence of other metal ions at high concentration, thus proving further evidence of the high performance, and selectivity, of MP-MCM-41 for Hg (II).

### 7.3.4 Removal of Hg (II) from loaded samples of MP-MCM-41 or DETA-MCM-41 and regeneration of the sorbent

During the filtration procedure step discussed in Section 7.2.5, sorbents were recovered and washed with 20 cm<sup>3</sup> of 1 M HCl in an attempt to remove the encapsulated Hg (II). FAAS analysis of the washings indicated that all metal ions, including Hg (II) were almost fully recovered from the DETA-MCM-41 sample (Table 7.8).

**Table 7.8: The masses of heavy metal ions retained by sorbents after being washed in 1 M HCl samples.**

Metal	Masses ( $\mu\text{g}$ ) of ions in pre-washed (loaded) sorbent		Masses retained ( $\mu\text{g}$ ) by chelate after washing in 1 M HCl	
	DETA-MCM-41	MP-MCM-41	DETA-MCM-41	MP-MCM-41
Hg (II)	314	400	20	400
Cd (II)	386	38	0	0
Zn (II)	390	12	14	0
Mn (II)	398	4	0	0
Cr (III)	394	0	6	0
Pb (II)	394	0	20	0

The selectivity of MP-MCM-41 towards Hg (II) was further evidenced during the 1 M HCl washing procedure where no Hg (II) was removed. As an increase in the concentration of acid used was undesirable, (previous reports suggested high concentrations of protons could damage the silica mesostructure [248-250], a new method was developed to remove Hg (II) from MP-MCM-41 using aqueous 0.2 M nitric acid and low energy microwave assisted digestion (LE-MWD). A second set of conditions, using high energy microwave digestion (HE-MWD), was used to break the chelating group from the surface of the silica so that the exact mass of Hg (II) encapsulated by the sorbent could be measured. Both sets of microwave conditions used are outlined in table 7.3 section 7.2.5.

Samples (40 mg) of MCM-41 and MP-MCM-41 and a functionalised sample loaded with 400 µg of Hg (II); (Hg-MP-MCM-41) were examined by microanalysis and FTIR before and after microwave treatment. The elemental analysis results shown in Table 7.9 indicated a 70 % retention of mercaptopropyl groups on the surface of the silica after LE-MWD treatment.

**Table 7.9: Elemental analysis data recorded for sorbent samples.**

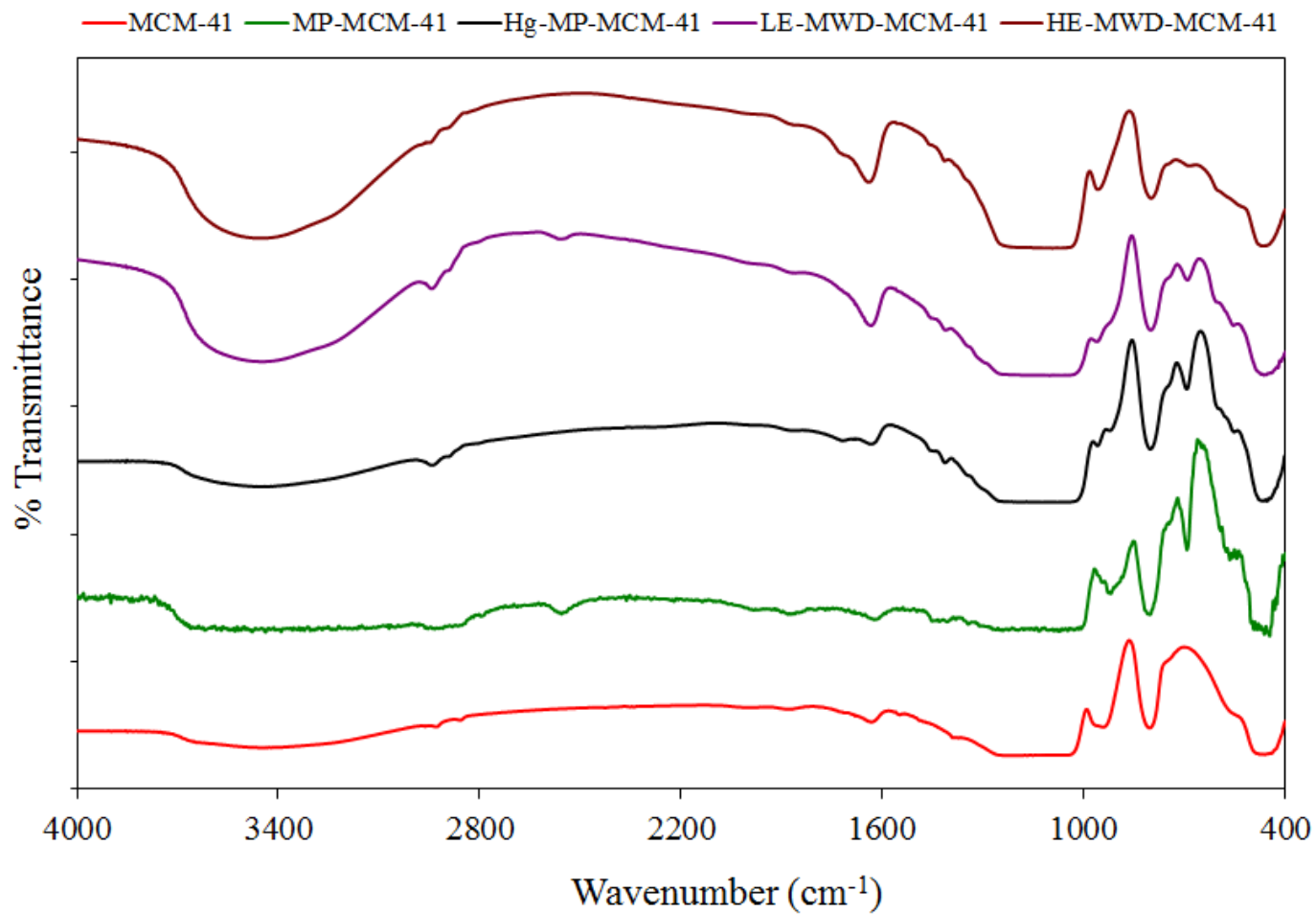
Sorbent	%C	%H	%S
MCM-41	Trace/nil	0.52	Trace/nil
MP-MCM-41	12.33	2.58	9.07
Hg-MP- MCM-41	10.09	2.19	8.56
LE-MWD-MCM-41	7.30	1.84	6.37
HE-MWD-MCM-41	4.18	1.90	1.29

The use of HE-MWD conditions resulted in a loss of almost all mercaptopropyl functional groups from the silica surface. Additionally, analysis of the filtered nitric acid solutions collected after microwave treatment indicated that both LE- and HE-MWD methods led to a recovery of approximately 97 % of Hg (II) from loaded

sorbents. Extraction by MP-MCM-41 followed by LE-MWD treatment would therefore lead to a useful method for the selective recovery of Hg (II) from contaminated waters.

The FTIR spectra of all samples (Figure 7.5) contained similar features expected of a silica containing material associated with the inorganic backbone such as (i) a large broad band between 3500 and 3200  $\text{cm}^{-1}$  which is assigned to the O–H stretching mode of silanol groups and adsorbed water, (ii) several absorption bands at around 1030-1240  $\text{cm}^{-1}$  which can be assigned to the Si–O–Si stretching and (iii) the water bending mode band around 1650  $\text{cm}^{-1}$ . In addition to those peaks, the spectrum of the MP-MCM-41 sample contained extra bands at 2850 and 2930  $\text{cm}^{-1}$  which were assigned to the C-H stretching of  $\text{sp}^3$  carbon and a weak band at 2557  $\text{cm}^{-1}$  was assigned to a SH stretching mode; supporting the theory that MP is present on the surface of the silica. The Hg-MP-MCM-41 spectrum lost the SH stretching mode at 2557  $\text{cm}^{-1}$  presumably because the hydrogen had been replaced with Hg (II). The sample spectrum for LE-MWD-MCM-41 was similar to that of MP-MCM-41 but a reduced intensity of the 2557  $\text{cm}^{-1}$  band was observed, supporting the theory that some mercapto-functionality was lost during treatment. The sample spectrum for HE-MWD-MCM-41 had no band at 2557  $\text{cm}^{-1}$  but very small bands at 2850 and 2930  $\text{cm}^{-1}$  were observed, indicating that the functional groups were destroyed by the high energy microwave conditions.

The results indicated that the new treatment method using nitric acid (0.2 M) and low energy microwave assisted digestion could successfully remove Hg (II) from loaded sorbents without removal of all functionality from MP-MCM-41. To evaluate the efficiency of regenerated MP-MCM-41 its adsorption capacity was re-determined. Using the regenerated sorbent an adsorption capacity of 950  $\mu\text{mol g}^{-1}$  was determined indicating that the material can be successfully re-used after LE-MWD treatment. This method improves on results reported previously where harsher conditions (12 M HCl) were used to remove 90 % of Hg (II) from thiol-functionalised mesoporous silica and on re-use only 40 – 60 % of the original value of Hg (II) was extracted from solution [247].



**Figure 7.5: FT-IR spectra of MCM-41, MP-MCM-41, Hg-MP-MCM-41, LE-MWD-MCM-41 and HE-MWD-MCM-41.**

## 7.4 Conclusions

A new room temperature preparation method, which involved surfactant extraction by MWD, produced a better-prepared MCM-41 base material for chelate functionalisation. This in turn led to a material which had higher adsorption capacities for Hg (II) ions than those reported previously. The sorbent was almost exclusively selective to Hg (II), even in the presence of a wide range of other heavy metal ions, such as those present in contaminated water samples. Removal of Hg (II) from loaded sorbents could also be achieved using a new method involving LE-MWD conditions. All of these features combined provided a highly selective removal and pre-concentration method for Hg (II) from aqueous solutions. Selective recovery (97 %) of Hg (II) from contaminated waters can be economically favourable and provides an alternative application method in addition to environmental mitigation strategies. Regeneration of MP-MCM-41 was presented, for the first time, with mild acid conditions. Examination of the material after treatment suggested that the recovery method proposed will not disrupt the chelate on the surface of the silica and so the material could be reused (with approximately 76 % of the original adsorption capacity).

## **Chapter 8: Removal of Chromium (VI) from aqueous solutions**

## 8.1 Introduction

### 8.1.1 Adsorption of chromium species from water samples

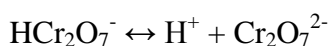
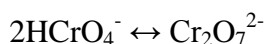
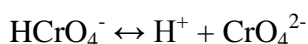
Chromium (Cr) concentration in natural waters is normally at the low  $\text{ng cm}^{-3}$  level and many modern instrumental techniques, such as flame atomic absorption spectrometry (FAAS), graphite furnace atomic absorption spectrometry (GFAAS), inductively coupled plasma-atomic emission spectrometry (ICP-AES) and inductively coupled plasma-mass spectrometry (ICP-MS), can be used to determine the total amount of chromium in solution. When Cr speciation is required separation and preconcentration methods are required before detection [138]. Separation methods reported in the literature are usually based on liquid–liquid extraction [254, 255], solid phase extraction [256-258], co-precipitation [259, 260], or ion chromatography [261].

Removal of Cr from solution is still a topic of environmental interest. Materials are sought that will remove high Cr masses from water using the smallest amount of material, as indicated by the material's adsorption capacity. Moreover, the sorbent should target Cr (VI) in the presence of other heavy metals, in particular show preference for Cr (VI) over Cr (III) ions. Conventional porous materials used for adsorption of Cr (VI) include activated carbon [262, 263], ion exchangers [264, 265], zeolites [266, 267] and clays [268, 269]. However these materials have low adsorption capacities and low selectivity [270]. For example the maximum adsorption capacity of Cr (VI) on activated carbon was reported as 22.29 mg/g [263] and in the case of modified natural clinoptilolite or ZSM-5 zeolites, the Cr (VI) loading capacities were approximately 29.7 or 10.6 mg/g, respectively [271].

To improve adsorption performance mesoporous silica materials have recently been used in a wide range of environmental remediation applications. In recent years the materials have demonstrated high adsorption capacity values for volatile compounds from indoor air [150, 272] and heavy metals from aqueous solution [84, 85]. Adsorption of Cr (VI) by modified mesoporous materials as also been studied [273-277]. The maximum Cr (VI) adsorption capacity value for modified MCM-41 material reported was more than four times higher than for the porous sorbents described above [271].

### 8.1.2 Effect of pH on Cr (VI) adsorption

Examining the extraction efficiency of Cr ions from water it is important to measure the pH of the contaminated solution. This is because alteration of the solution pH can affect Cr speciation and/or the functional group used in the adsorbent. It has been shown that Cr (VI) exists in the following forms depending upon the pH of the aqueous solution that the anion resides in [277].



The distribution of each species depends on total Cr (VI) concentration and the solution pH [277]. In acidic media Cr(III) species are positively charged ( $\text{Cr}(\text{H}_2\text{O})_6^{3+}$ ) whereas at high solution pH values the Cr ion is found in the hydroxylated form of Cr(III) ( $\text{Cr}(\text{OH})(\text{H}_2\text{O})_5^{2+}$ ) [276]. Regarding the sorbent, where amino functional groups are used the pH will also affect extraction efficiency: at low solution pH values the amino group will have a positive charge on the nitrogen atom but at high pH the amino groups will be uncharged.

### 8.1.3 Adsorption kinetics study

A kinetic study was carried out to evaluate the adsorption performance of Cr ions on the surface of AP-MCM-41 and also to determine the rate of Cr (VI) removal by AP-MCM-41. A series of Cr solutions (each with a volume of 25 cm<sup>3</sup>) with concentrations of 10, 50, 100 or 200 µg cm<sup>-3</sup> were stirred at 25 °C in the presence of 50 mg adsorbent for 1, 5, 10, 20, 30 or 40 min. After the appropriate stirring time, solutions were filtered and Cr concentrations measured by ICP-AES.

The study of adsorption dynamics is used to describe the solute uptake rate, which controls the residence time of adsorbate uptake at the solid-solution interface. The kinetics of Cr(VI) adsorption on AP-MCM-41 was analysed using pseudo first-order [200], pseudo second-order [278] or intraparticle diffusion [125, 279] kinetic models. The conformity between experimental data and the model predicted values was expressed by the correlation coefficients ( $r^2$ , values being close or equal to 1). A



relatively high  $r^2$  value indicates that the model successfully describes the kinetics of adsorption.

***The pseudo first-order equation:***

The pseudo first-order equation [200] is generally presented as follows:

$$\log(q_e - q_t) = \log(q_e) - \frac{k_1}{2.303} t \quad \text{Equation 8.1}$$

where  $q_e$  and  $q_t$  are the adsorption capacity at equilibrium and at time  $t$ , respectively ( $\text{mg g}^{-1}$ ),  $k_1$  is the rate coefficient of pseudo first-order adsorption ( $\text{L min}^{-1}$ ). The plot of  $\log(q_e - q_t)$  vs.  $t$  should give a linear relationship from which  $k_1$  and  $q_e$  can be determined from the slope and intercept of the plot, respectively.

***The pseudo second-order equation:***

The pseudo second-order adsorption kinetic rate equation [278] is expressed as:

$$\left(\frac{t}{q_t}\right) = \frac{1}{k_2 q_e^2} + \frac{1}{q_e} t \quad \text{Equation 8.2}$$

where  $k_2$  is the rate constant of pseudo second-order adsorption ( $\text{g mg}^{-1} \text{min}^{-1}$ ). The plot of  $(t/q_t)$  and  $t$ , should give a linear relationship from which  $q_e$  and  $k_2$  can be determined from the slope and intercept of the plot, respectively.

***The intraparticle diffusion model:***

To study the mechanism of the particle diffusion the Morris–Weber equation [125, 279] was applied:

$$q_t = k_{id} \sqrt{t} \quad \text{Equation 8.3}$$

where  $q_t$  is the amount of metal ion sorbed ( $\text{mg L}^{-1}$ ) at time  $t$  and  $k_{id}$  is the intraparticle diffusion rate constant ( $\text{mg L}^{-1} \text{min}^{-1/2}$ ).

### 8.1.4 Adsorption isotherms to study the maximum adsorption capacity

To study the maximum adsorption capacity of Cr(VI) on AP-MCM-41 the Langmuir model [280] and the Freundlich model [281] were applied. Various initial concentrations of Cr (VI) solutions (10, 50, 100 or 200  $\mu\text{g cm}^{-3}$ ), were prepared. The conditions were used for this experiment in addition to stirring speed which was 250 rpm, the temperature was 20  $^{\circ}\text{C}$  and stirring time for 120 min, sorbent weight used was 0.05 g and the pH was 3. The amount of chromium (VI) extracted at equilibrium,  $q_e$  (mg/g) was calculated according to Equation 8.4:

$$q_e = \frac{C_0 - C_e}{W} V \quad \text{Equation 8.4}$$

Where  $C_0$  and  $C_e$  (mg/g) are the liquid phase initial and equilibrium concentrations of Cr (VI) respectively,  $V$  is the volume of the solution ( $\text{cm}^3$ ), and  $W$  is the mass of sorbent (g) used [282]. The sorption equilibrium data of Cr (VI) onto the AP-MCM-41 were analysed according to Langmuir (Equation 8.5) and Freundlich (Equation 8.6) isotherm models [283].

$$\frac{C_e}{q_e} = \left( \frac{1}{q_m b} \right) + \left( \frac{1}{q_m} \right) C_e \quad \text{Equation 8.5}$$

$$\ln q_e = \ln K_f + \left( \frac{1}{n} \right) \ln C_e \quad \text{Equation 8.6}$$

Where  $q_e$  and  $C_e$  are the equilibrium concentrations of Cr ions in the adsorbed and liquid phases in mg/g and mg/L, respectively.  $q_m$  (mg/g) and  $b$  (L/mg) are the Langmuir constants. Whereas the  $q_m$  is the maximum monolayer capacity and  $b$  is the adsorption affinity onto the adsorption.  $K_f$  (mg/g) and  $n$  (L/mg) are the Freundlich constants which are related to the sorption capacity and intensity, respectively. The Langmuir and Freundlich constants can be calculated from the slope and intercept of the linear plot obtained from eq. 8.5 and 8.6 respectively.

For predicting the favourability of an adsorption system, the Langmuir equation can also be expressed in terms of a dimensionless separation factor ( $R_L$ ) by using the Langmuir constant  $b$  and the initial concentrations of the chromium (Equation 8.7).

$$R_L = \frac{1}{1 + C_0 b} \quad \text{Equation 8.7}$$

When,  $R_L > 1$ ,  $R_L = 1$ ,  $0 < R_L < 1$  and  $R_L = 0$ , indicates unfavourable, linear, favourable and irreversible, adsorption isotherms, respectively [134, 284].

In this work, a simple amino functionalised MCM-41 was synthesised and used to selectively extract Cr (VI) from water samples. As functionalised MWD-MCM-41 showed great performance with heavy metals as discussed in the chapters 6 and 7 with Pb and Hg ions. The simple amino functional groups will be examined towards Cr species extraction from water samples in presence of other potentially toxic elements which usually present in real samples. In addition to MWD-MCM-41, two other porous samples of mesoporous silica materials with different porosity parameters were synthesised and amino-functionalised to be evaluated as chromium (VI) adsorbents.

To identify the effect of pore size distribution on the adsorption kinetics as well as to establish accurate predictions of chromium (VI) adsorption onto porous materials which provide the necessary information for predicting the rate limiting step of hexavalent chromium adsorption and postulate the mechanism of Cr(VI) adsorption by porous materials.

## 8.2 Experimental

### 8.2.1 Determination of Cr (VI) in water samples by colourimetry

Six different levels of calibration standards were prepared in the range from  $0.1 \mu\text{g cm}^{-3}$  to  $1.0 \mu\text{g cm}^{-3}$  with reagent blank as first level. A  $1 \text{ cm}^3$  of diphenylcarbazide solution was added to one  $\text{cm}^3$  of the water sample and the pH of the solution was adjusted to be in the range of 1-2 by adding  $0.2 \text{ cm}^3$  hydrochloric acid (1 M) and allowed to stand 15 min for full colour development. An appropriate portion was transferred to a 1 cm absorption cell and measured the absorbance at 540 nm with the blank as a reference. The analysis was carried out using SI Photonics (M-420) CCD Array UV-Vis spectrophotometer.

Regression analysis was used to model the average absorbance values with concentration and the line obtained (Figure 8.1) was positively correlated with an  $r^2$  value of 0.9986 between  $0.1 - 1 \mu\text{g cm}^{-3}$ , with a reagent blank used as the first calibrant.

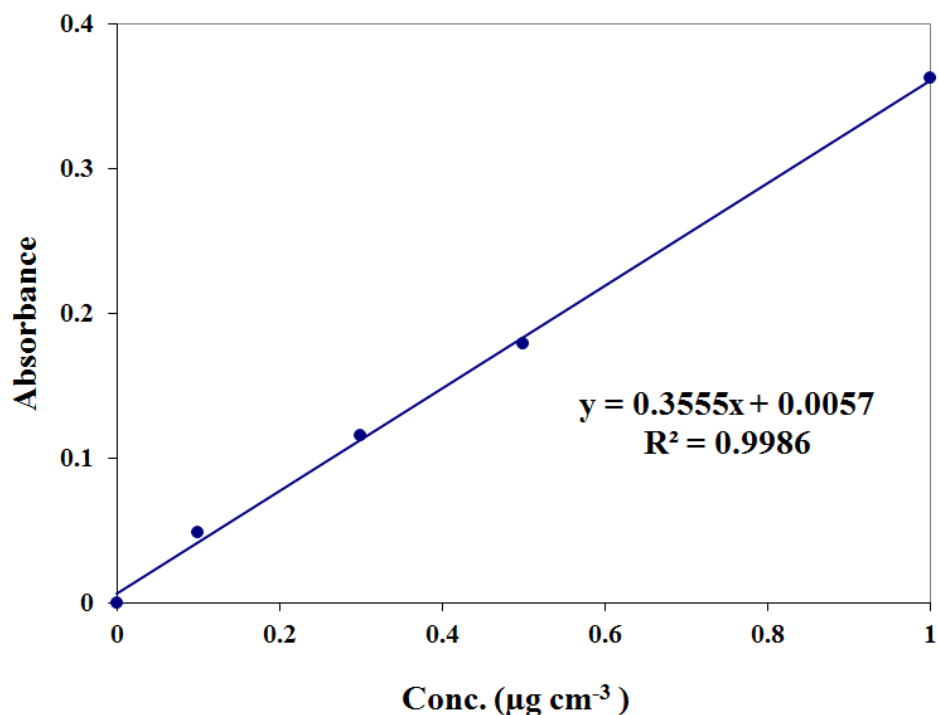


Figure 8.1: Calibration graph for Cr (VI) by colourimetry

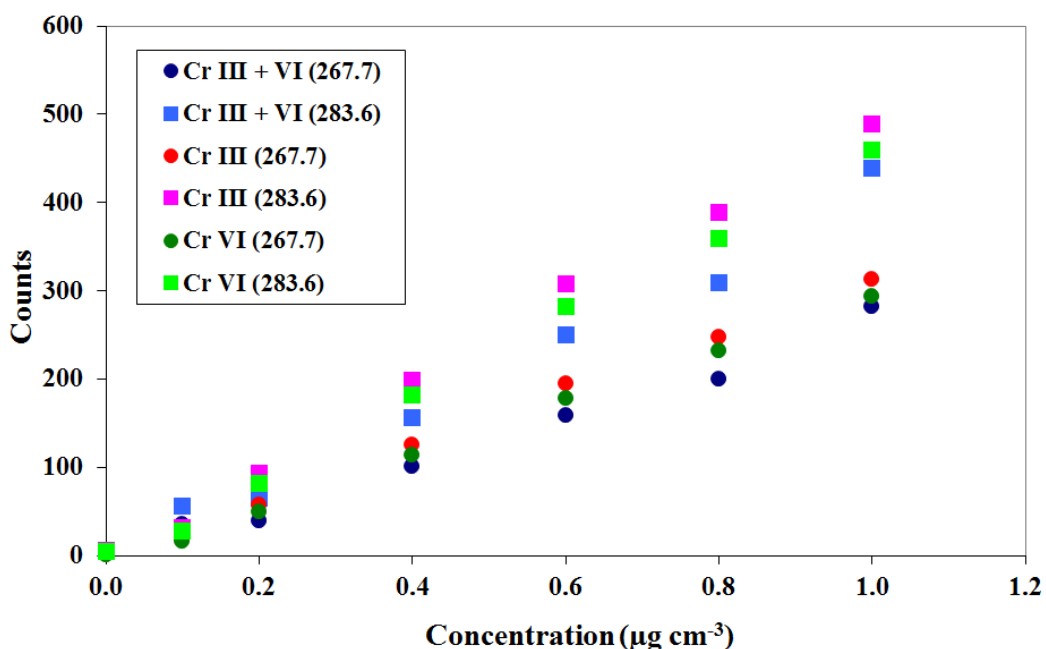
### **8.2.2 Determination of total chromium ( $\text{Cr}_{\text{Total}}$ ) in water samples using ICP-AES**

As discussed in Section 3.10.2, p. 82, a Thermo Scientific iCAP 6200 ICP-AES was used for the analysis of Cr solutions. Calibration standards were prepared in 5 %  $\text{HNO}_3$  at the following concentrations: 0.1, 0.5, 1, 5, or 10  $\mu\text{g cm}^{-3}$ . A quality control (QC) check solution was prepared at 1  $\mu\text{g cm}^{-3}$  to check recovery and test the stability of the method. The QC solution was repeatedly analysed after each 20 samples to ensure the instrument response did not drift during the analysis. Instrumental operating conditions are given in chapter 3, Table 3.7.

To determine the total Cr in water samples, it was first necessary to study the calibration differences for Cr (III) or Cr (VI) standard solutions. Different sets of standard solutions of both Cr species were prepared at the range 0.1-1  $\mu\text{g cm}^{-3}$  and a third set of solutions contained both Cr (III) and Cr (VI) at the same total concentration. The 3 calibration solution sets were measured at two different wave lengths (267.7 or 283.6 nm) to find the most sensitive wavelength for detection of Cr. The regression lines obtained were studied to determine whether the slopes were appreciably different and thus confirming the need to standardise the instrument using 3 different calibration solutions every analysis. Using the 3 regression lines the concentration of a sample (at 0.50  $\mu\text{g cm}^{-3}$ ) was measured according to the 3 calibration curves obtained (Figure 8.2) the regression lines were most sensitive using a detection wavelength of 283.6 nm. Anova was applied to examine the validity of using one calibration curve for all samples (See Table 8.1). The results obtained showed that there was no significant different in the results when different Cr (III) regression lines were used to calculate the concentration of a sample.

In contrast, a significant different in the results was observed when Cr (VI) calibration curves were used to determine the concentration of Cr (VI) in solution; although F-test failed by a small difference ( $F_{\text{critical}} = 3.1059$  and  $F_{\text{calculated}} = 3.5820$ ). By examination of all regression lines given in Figure 8.2, a decision was made to use Cr (VI) calibration solutions for future calibrations. This regression line lies

between the Cr (III) and mixed Cr (III+VI) calibration curves hence will give minimum error if used to calibration curve both species of Cr.



**Figure 8.2: A graph of concentration ( $\mu\text{g cm}^{-3}$ ) versus counts for the Cr (III), (VI) or mixed Cr (III) + (VI) standard solutions using ICP-AES.**

From the statistical results obtained it was concluded that either detection wavelength could be used to determine Cr in solution; with 283.6 nm giving slightly higher sensitivity. The method detection limits (MDL) were  $0.004 \mu\text{g cm}^{-3}$  or  $0.003 \mu\text{g cm}^{-3}$  using wave lengths of 267.7 or 283.6 nm, respectively.

The ICP-AES method is used to determine the concentration of  $\text{Cr}_{\text{Total}}$  in solution. The colorimetric method, described in Section 8.2.1 is used to determine the concentration of Cr (VI) in solution. And so the Cr (III) concentration was calculated by subtraction:  $\text{Cr}_{\text{(III)}} = \text{Cr}_{\text{Total}} - \text{Cr}_{\text{(VI)}}$ .

**Table 8.1: The Anova-test for three different Cr standard solutions.**

0.5 ppm of Chromium sample	Concentration found (ppm) according to different calibration curves						F-test		
	Cr III + VI (267.7)	Cr III + VI (283.6)	Cr III (267.7)	Cr III (283.6)	Cr VI (267.7)	Cr VI (283.6)	F <sub>calc</sub>	F <sub>crit</sub>	Result
Cr (III) Replicate 1	0.5529	0.5565	0.5368	0.5529	0.5242	0.5285			
Cr (III) Replicate 2	0.5476	0.5480	0.5394	0.5346	0.5474	0.5501	1.3906	3.1059	Pass
Cr (III) Replicate 3	0.5517	0.5463	0.5422	0.5384	0.5431	0.5410			
Cr (III) Average	0.5508	0.5503	0.5395	0.5420	0.5382	0.5399			
Cr (VI) Replicate 1	0.5096	0.5177	0.4962	0.4930	0.4949	0.5004			
Cr (VI) Replicate 2	0.5074	0.5146	0.5005	0.4945	0.4965	0.5079	11.2029	3.1059	Failed
Cr (VI) Replicate 3	0.5114	0.5138	0.4969	0.5041	0.5019	0.4978			
Cr (VI) Average	0.5094	0.5154	0.4979	0.4972	0.4978	0.5020			
Cr (III) +(VI) Replicate 1	0.4752	0.4897	0.4797	0.4761	0.4776	0.4773			
Cr (III) +(VI) Replicate 2	0.4843	0.4831	0.4770	0.4762	0.4783	0.4816	3.5820	3.1059	Failed
Cr (III) +(VI) Replicate 3	0.4786	0.4926	0.4838	0.4598	0.4809	0.4844			
Cr (III) +(VI) Average	0.4794	0.4885	0.4802	0.4707	0.4789	0.4811			

### 8.2.3 Extraction of Cr from polluted water and regeneration of sorbent

The general procedure for extraction of Cr ions from water can be summarised as follows. Approximately 25 mg samples of AP-MCM-41 or DETA-MCM-41 were suspended in 25 cm<sup>3</sup> solutions containing 100 µg cm<sup>-3</sup> Cr (III) or Cr (VI) at various pH values (between 1 and 11) and the solution was stirred (250 rpm) for approximately 2 hours. After this time the solution was filtered (Fisherbrand QL100) and the filtrate was analysed using ICP/AES.

To recover the extracted Cr ions, and regenerate the sorbent for future work, the loaded material was washed with 25 cm<sup>3</sup> of water at pH 3 to recover Cr (III) or 25 cm<sup>3</sup> of water at pH 9 for recovery of Cr (VI) (water pH was adjusted using 1 M HCl or 1M NH<sub>4</sub>OH).

Preconcentration experiments were carried out using 100 cm<sup>3</sup> of 3 different concentrations of Cr (VI) (0.01, 0.1 or 1 µg cm<sup>-3</sup>) and 1000 cm<sup>3</sup> of 0.01 µg cm<sup>-3</sup>. The solutions were stirred with 25 mg of AP-MCM-41 for 2 hours then the solutions were filtered and analysed by ICP-AES. The sorbent that remained in the filter paper was washed with 10 cm<sup>3</sup> water at pH 9 and this 10 cm<sup>3</sup> solution was analysed by ICP-AES after filtration.

Water samples (a river water sample collected from the Bothlin river in Glasgow and a tap water sample taken from a building in the Drygate campus in Glasgow) were spiked with Cr (VI) to produce solution concentrations of 25 µg cm<sup>-3</sup>. Then approximately 25 mg of AP-MCM-41 was added and the solution was stirred (250 rpm) for approximately 2 hours. Then the solution was filtered and the filtrate was analysed using ICP-AES. Analyte recovery, and sorbent regeneration, was carried out using 25 cm<sup>3</sup> of water at pH 3.



## 8.3 Results and discussion

### 8.3.1 Extraction of Cr (III) and Cr (VI) from water: the effect of solution pH on the extraction efficiency

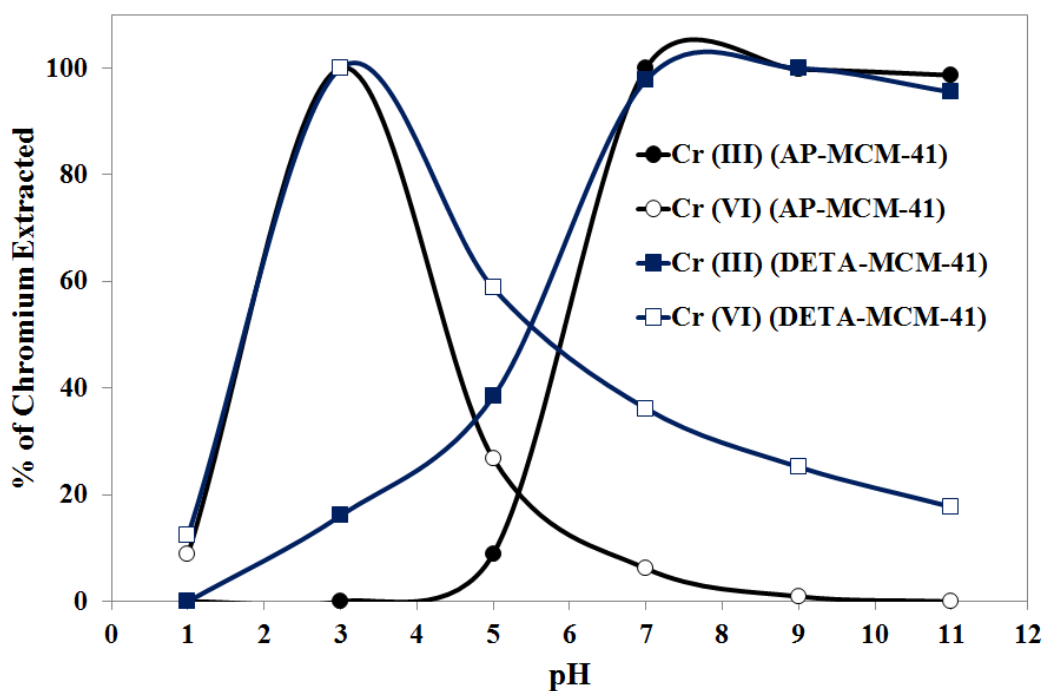
To study the effect of solution pH on the extraction efficiency of Cr ions from water using AP-MCM-41 a number of experiments were performed as described in Section 8.2.3.

The results, shown in Figure 8.3, confirm a strong pH dependence of the extraction of both Cr (III) and Cr (VI) with AP-MCM-41. Examination of the Cr (III) data indicated decreasing extraction efficiencies at low pH. This was expected due to the increased  $H^+$  species in solution which compete with Cr (III) for adsorption sites. Amino-functionalised mesoporous silica (AP-MCM-41) is likely to immobilise Cr (III) due to favourable co-ordination interaction between  $Cr(H_2O)_6^{3+}$  and amino groups at high pH. This was confirmed here with efficient extraction being observed once the solution pH increases above 7.

Contrasting pH dependence was also observed for the removal of Cr (VI) by AP-MCM-41. Cr (VI) had favourable electrostatic interaction at low solution pH because the amino group is positively charged, which in turn neutralise the negatively charged hydroxyl group (OH) on the sorbent surface, thereby reducing the hindrance to the diffusion of negatively charged dichromate ions. At higher pH values, the reduction in Cr (VI) adsorption may be due to the presence of more  $OH^-$  ions causing increased hindrance to diffusion of dichromate ions [285]. Maximum adsorption capacity values were measured at pH 3 for Cr (VI) and pH 9 for Cr (III). Interestingly, similar pH trends were measured for Cr (III) and (VI) adsorption onto DETA-MCM-41.

After sorbents were loaded with Cr ions, attempts were made to recover them and regenerate the sorbent for future extractions. The procedure used is described in Section 8.2.3. The recovery results (Table 8.2) confirm that Cr (III) and Cr (VI) were recovered completely (more than 99.9%) when the loaded sorbent was washed with water at pH 3 or 9, respectively. In contrast when DETA-MCM-41 was washed in a similar way, the percentage recovery values decreased to less than 85 %. Overall, because AP-MCM-41 can be used for exclusive extraction of Cr (VI) at pH 3,

leaving all Cr (III) in solution, combined with the possibility of full ion recovery by simple washing methods, the AP-MCM-41 material was chosen as the sorbent of choice for future extraction experiments with Cr (VI).



**Figure 8.3: The effect of pH on extraction of Cr (III) and Cr (VI) ions from contaminated water.**

**Table 8.2: Efficiency of adsorbents to extract 2500 µg of Cr (III) or Cr (VI) from water.**

Sorbent	Mass (µg) of Cr (III) extracted		Mass (µg) of Cr (VI) extracted	
	3	9	3	9
AP-MCM-41	trace/nil	2461.5	995.3	trace/nil
DETA-MCM-41	400.2	2487.5	1754.0	311.3

### 8.3.2 Kinetic study of Chromium (VI) adsorption onto AP-MCM-41

Kinetics studies were performed to understand the mechanistic steps of the adsorption process and the rate of kinetics for the adsorption of Cr (VI) ions onto AP-MCM-41. Experiments were performed as described in Section 8.1.3.

The concentrations of Cr in water samples at equilibrium  $C_e$  were demonstrated in table 8.3.

**Table 8.3: Chromium, initial concentrations ( $C_0$ ) and equilibrium concentration ( $C_e$ ) in water.**

Time (min)	$C_0$ ( $\mu\text{g cm}^{-3}$ )		$C_e$ ( $\mu\text{g cm}^{-3}$ )			
	1	5	10	20	30	40
10	5.2	2.1	0.08	0.07	0.06	0.05
50	26	1.2	0.55	0.53	0.47	0.4
100	71	42	19	7	1.1	1
200	139	85	43	11	8.1	8

Then the adsorption capacity at equilibrium  $q_e$  and the adsorption capacity at time  $t$   $q_t$  can be calculated from  $C_e$  values obtained in table 8.3, and apply those values in equation 8.4. The adsorption capacities  $q_e$  and  $q_t$  ( $\text{mg g}^{-1}$ ) results demonstrated in Table 8.4:

**Table 8.4: Then the adsorption capacity at equilibrium ( $q_e$ ) and the adsorption capacity at time  $t$  ( $q_t$ ).**

$q_t$ at 1 min	$q_t$ at 5 min	$q_t$ at 10 min	$q_t$ at 20 min	$q_t$ at 30 min	$q_e$ at 40 min
2.4	3.95	4.96	4.97	4.97	4.98
12	24.4	24.7	24.74	24.77	24.8
14.5	29	40.5	46.5	49.45	49.5
30.5	57.5	78.5	94.5	95.95	96

Those values of  $q_e$  and  $q_t$  ( $\text{mg g}^{-1}$ ) then can be applied into the relations expressed in equation 8.1 and 8.2 and then the conformity between experimental data and the model predicted values was expressed by the correlation coefficients ( $r^2$ , values being close or equal to 1). A relatively high  $r^2$  value indicates that the model successfully describes the kinetics of adsorption.

Using the calculations given above, the pseudo first-order models, and pseudo second-order models, were applied to the experimental data to assess the rate of chromium adsorption. The results are given in Figures 8.4 and 8.5, together with the regression and correlation coefficients. According to the correlation coefficients the experimental data was not best explained by the pseudo first-order rate equation. Better correlation was demonstrated in the pseudo second-order models. These results confirm that the adsorption process of Cr (VI) onto AP-MCM-41 is more complicated than can be explained by the pseudo first-order model, despite what has been previously reported in the literature [281, 285, 286].

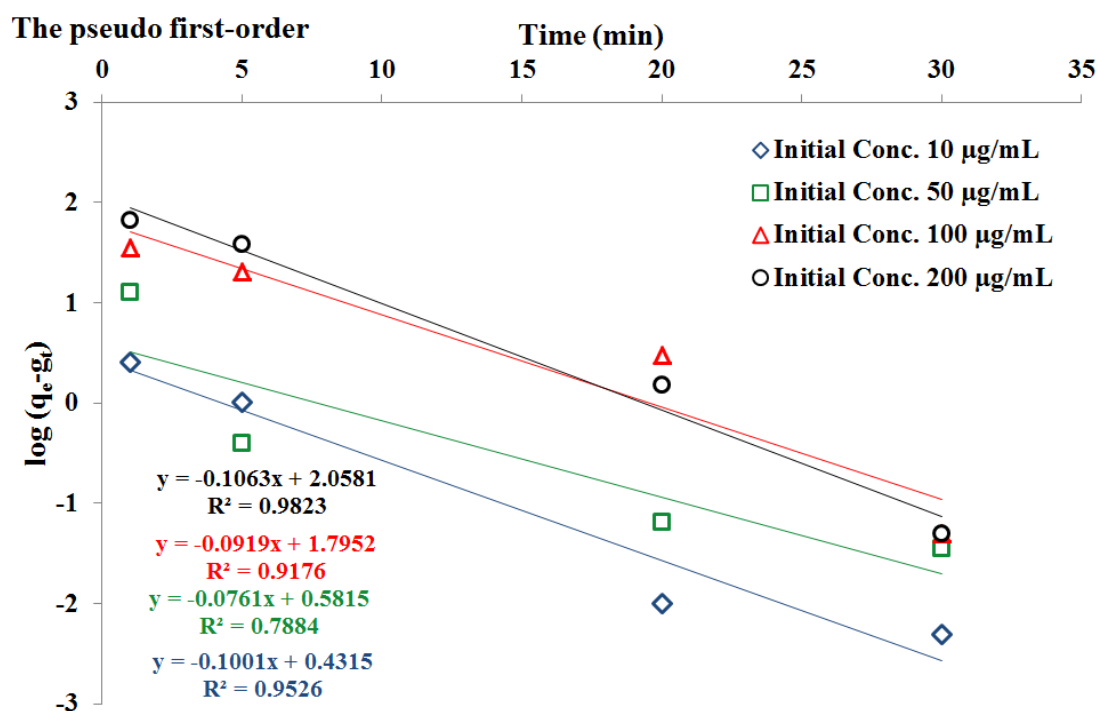
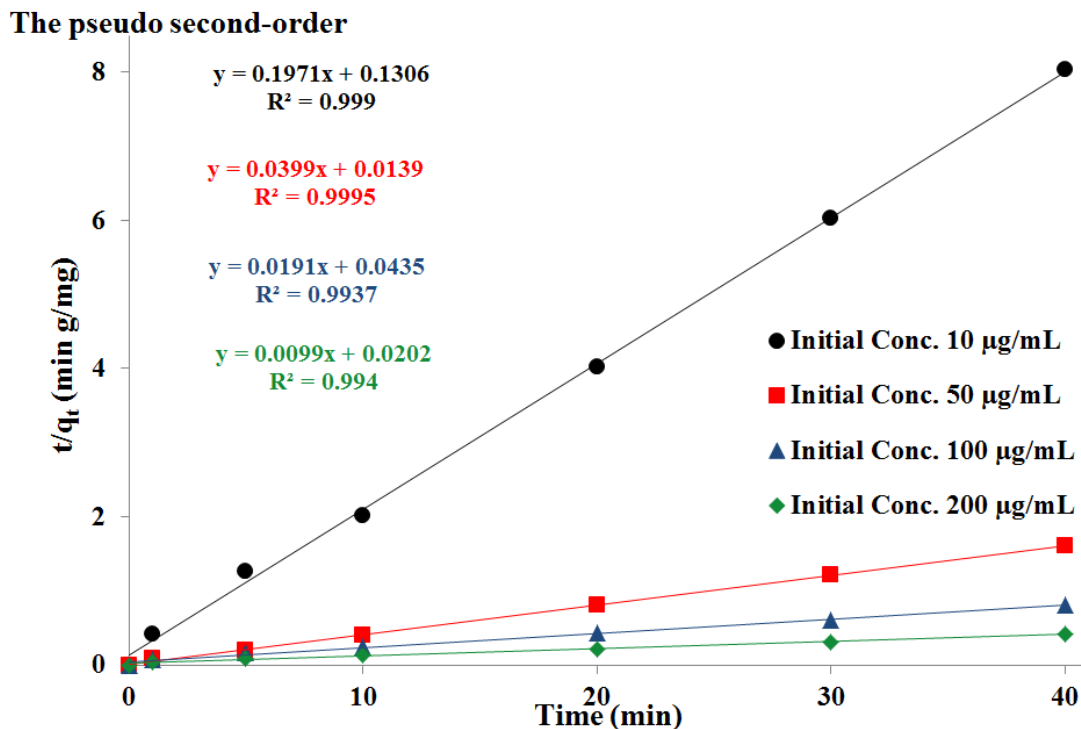


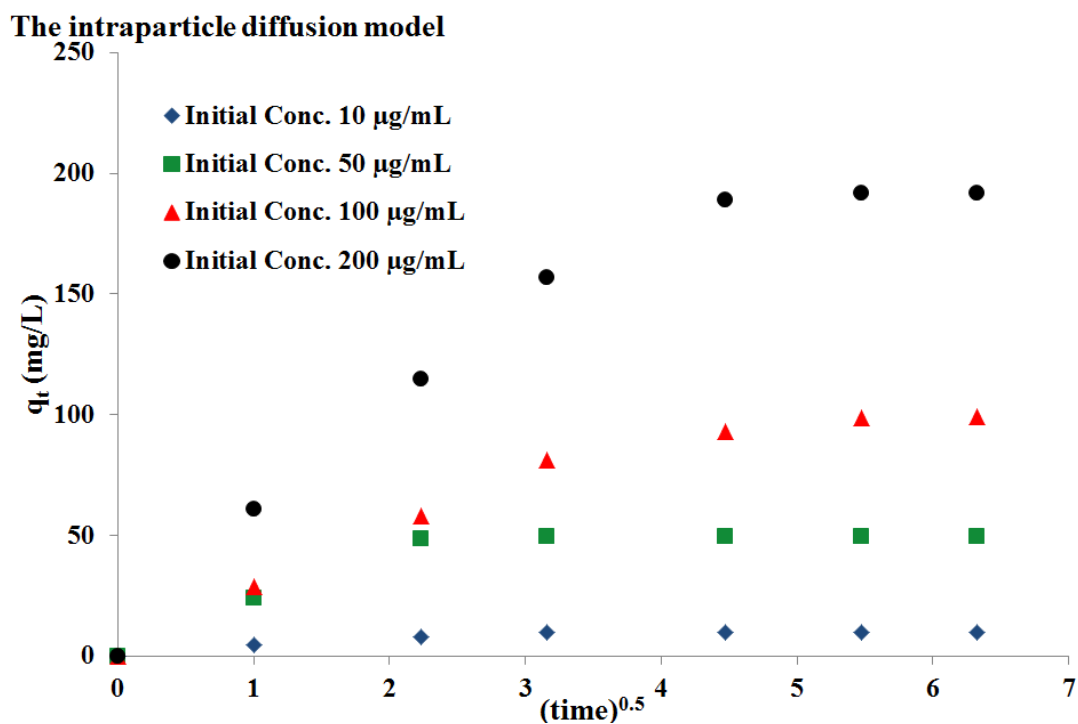
Figure 8.4: Pseudo-first order kinetics models of Cr (VI) onto AP-MCM-41.



**Figure 8.5: Pseudo-second kinetic model of Cr (VI) onto AP-MCM-41.**

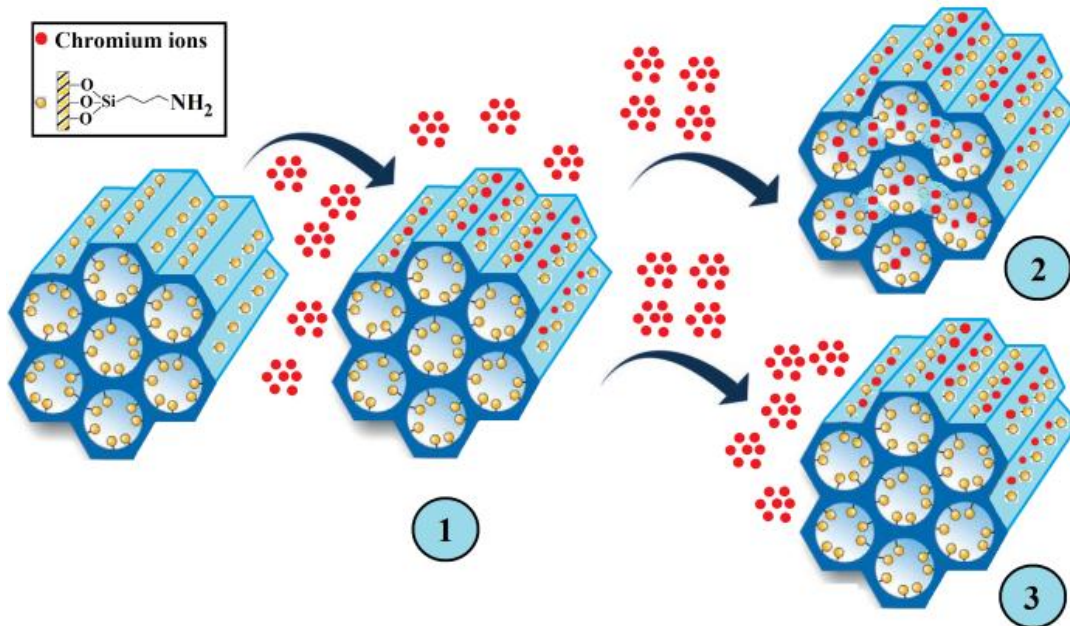
To better understand the adsorption behaviour of Cr (VI) with AP-MWD-MCM-41, the intraparticle diffusion model was applied to the experimental data. The resultant model, which plots mass of Cr (VI) on AP-MCM-41 vs.  $(\text{time})^{1/2}$  is shown in Figure 8.6. The curve observed was of great interest as 2 kinetic effects were observed. The first section of the curve ( $t=0$  to  $t=10$  min) was attributed to mass transfer effects (slope =  $K_{id(1)}$ ) taking place due to boundary layer diffusion, while a second linear rate curve was thought to indicate intraparticle diffusion (slope  $K_{id(2)}$ ). This data, for the first time, provides evidence that there were 2 types of adsorption occurring between Cr (VI) and AP-MWD-MCM-41.

The mechanism of Cr(VI) adsorption onto the microwave-treated AP-MCM-41 sorbent was complex and appeared to involve both surface as well as intra-particle adsorption. Both reactions mechanisms contributing to the rate determining step of adsorption kinetics.



**Figure 8.6: Intraparticle diffusion sorption kinetic model of Cr (VI) onto AP-MCM-41.**

In other words the adsorption mechanism of Cr (VI) onto AP-MCM-41 follows two steps: film diffusion and intraparticle transport (pore diffusion). It is most likely that pore diffusion will be the rate determining step in the adsorption process. Previously published results report that the adsorption of Cr (VI) onto functionalised silica is according to the pseudo first-order model. Clearly this was not the case here as the measured data demonstrated. It was postulated that the different adsorption behaviour given by this material was influenced by the method used to remove the surfactant from the pores of the silica. There are 2 key proposed advantages to surfactant removal by microwave digestion: (i) that there is a higher degree of functionalisation due to the production of more silanol groups on the surface of the material and (ii) that larger pores are created and functionalisation occurs inside the pores as well as on the surface of the material. These results may be used to support the theory, with rates of adsorption being demonstrated by both surface adsorption (the faster initial rate of reaction) and chelation of metal ions in the larger pores (the second slower rate of reaction). This is illustrated in Figure 8.7 steps 1 and 2, with the conventional adsorption process illustrated in step 3.



**Figure 8.7: Illustrates three different adsorption processes: the first is film diffusion which is the initial adsorption process, the second is intraparticle transport (pore diffusion) which occurs only when the pores of MCM-41 are large enough to allow Cr (VI) to be bound to the inner surface. The third adsorption process would occur for most other MCM-41 material with smaller pores (and pseudo first order kinetic would occur).**

The diffusion rate parameters  $K_{id(1)}$  and  $K_{id(2)}$  (the slope of equation 8.3) obtained are shown in Table 8.5. The value of  $K_{id(1)}$  indicated that the intraparticle diffusion process occurred at high Cr (VI) concentrations, whereas at low concentration, Cr (VI) ions were extracted by amine groups on the outer surface of the material. The diffusion rate parameters indicated that intraparticle diffusion controlled the adsorption rate; which was the slowest step. Moreover, sorption of Cr (VI) in pores of AP-MCM-41 was concentration dependent. The results obtained by these kinetic models suggested that the reaction of Cr (VI) with AP-MWD-MCM-41 was defined by a sequence of processes that contributed towards the overall adsorption rate: mass transfer of ions through the liquid surrounding the surface of sorbent particle and diffusion of ions through the particle pores. The slowest step was considered to be

diffusion of ions through the sorbent pores which was observed at high Cr (VI) concentration.

**Table 8.5: Rate constants of the pseudo-first order pseudo second-order and the intraparticle diffusion kinetic models.**

Conc. (ppm)	The pseudo first-order		The pseudo second-order		The intraparticle diffusion model		
	$k_1$	$r^2$	$k_2$	$r^2$	$k_{id(1)}$	$k_{id(2)}$	$r^2$
10	0.23	0.9526	0.30	0.9990	3.06	---	0.9662
50	0.18	0.7884	0.11	0.9995	16.30	---	0.9182
100	0.21	0.9176	0.08	0.9937	25.34	3.32	0.9980
200	0.24	0.9823	0.05	0.9440	48.91	1.66	0.9940

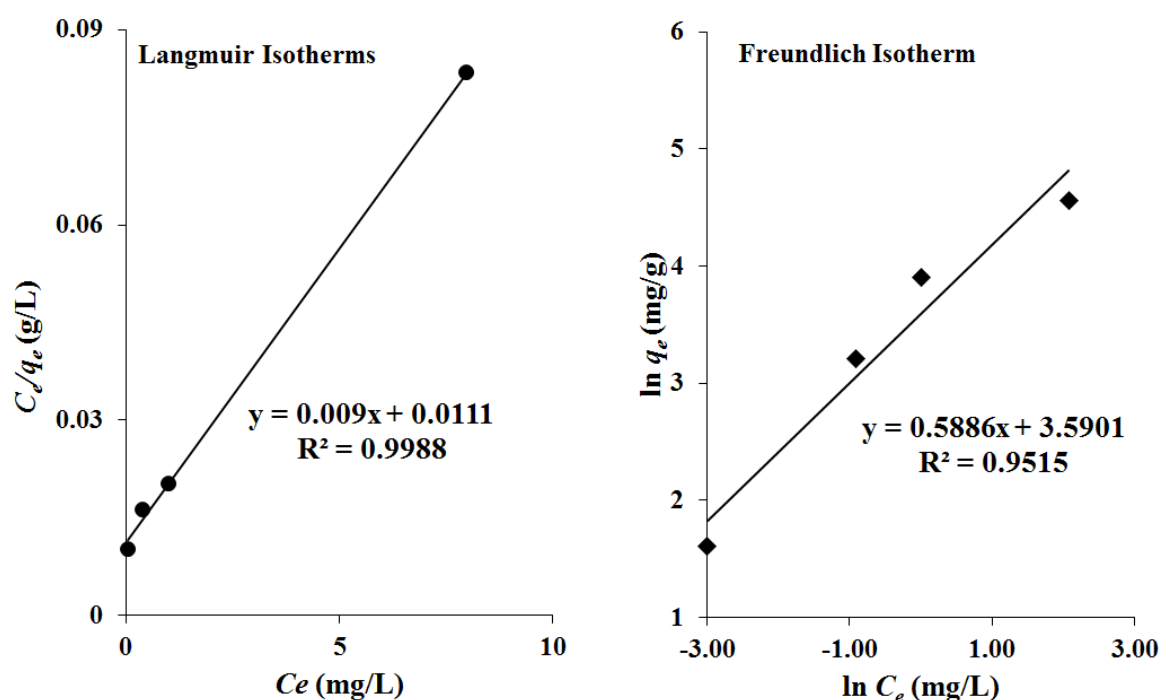
### 8.3.3 Adsorption isotherms

To study the relationship between the mass of Cr (VI) adsorbed per unit mass of AP-MWD-MCM-41 at constant temperature, and its concentration in the equilibrium solution, Langmuir and Freundlich adsorption isotherms were examined using the experimental data.

The concentration of Cr in water at equilibrium  $C_e$  and the adsorption capacities  $q_e$  and  $q_t$  ( $\text{mg g}^{-1}$ ) which calculated in tables 8.3 and 8.4 applied those values into the relations expressed in equations 8.5 and 8.6 to calculate the maximum adsorption capacities according to Langmuir isotherm and Freundlich model respectively. As can be seen from the isotherms and regression coefficients given in Figure 8.8 the distribution of Cr (VI) between the liquid phase and the solid adsorbent phase at equilibrium, was best described by the Langmuir isotherm more than the Freundlich model.



This implied that the mechanism of adsorption onto AP-MWD-MCM-41 was onto a homogeneous adsorbent surface. Using the linear model according to Langmuir, the maximum adsorption capacity was calculated as is  $111.1 \text{ mg g}^{-1}$ , whereas application of the Freundlich model gave a value of  $36.2 \text{ mg g}^{-1}$ . The results suggested that Cr (VI) was adsorbed by a 1:1 mechanism (monolayer sorption). The dimensionless parameter ( $R_L$ ) value, defined in Equation 8.7 was calculated by substituting the values of  $b$  and  $C_0$  to the equation. The  $R_L$  value was 0.86 which being in the range of 0 to 1, indicated a favourable adsorption mechanism of Cr (VI) onto AP-MWD-MCM-41. The Langmuir isotherm model fitting the experimental data provides further evidence, also obtained by the kinetics model, that monolayer sorption occurred indicating a homogenous functionalised surface was produced by the new synthesis method.



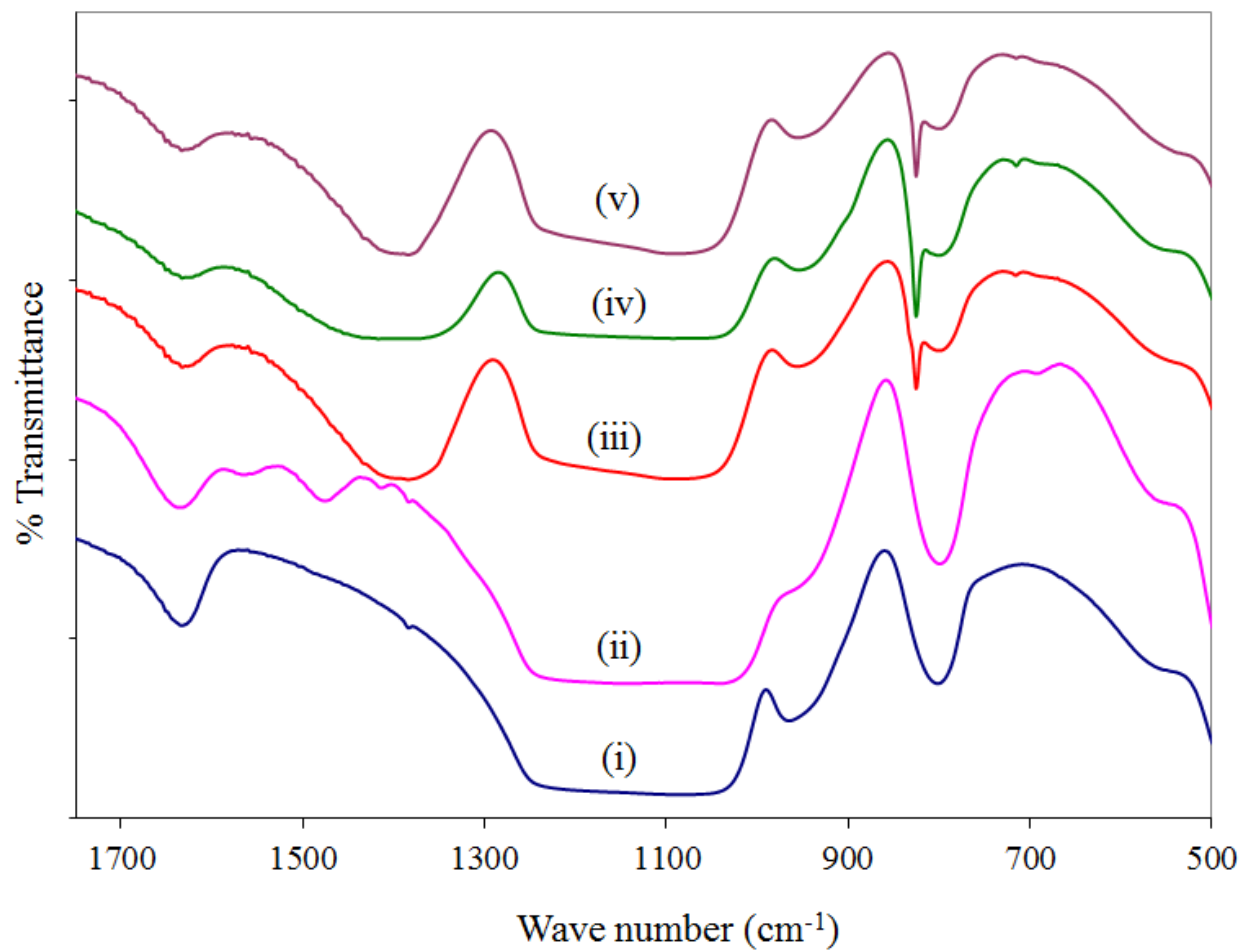
**Figure 8.8: Langmuir and Freundlich isotherms for Cr (VI) adsorption onto AP-MWD-MCM-41.**

### 8.3.4 Fourier-transform infrared spectroscopy

Samples of MCM-41 and AP-MCM-41 (before and after Cr extraction) were analysed by FTIR (Infrared spectra of all samples were obtained in KBr pellets in the 4000–400  $\text{cm}^{-1}$  region with a resolution of 4  $\text{cm}^{-1}$ , by accumulating 64 scans using an ATI Mattson FTIR spectrophotometer); spectra are illustrated in Figure 8.9. The wide bands at 1240-1030  $\text{cm}^{-1}$  are typically regarded as Si-O-Si bands of the condensed silica network, the peak at 1630  $\text{cm}^{-1}$  (attributed to the bending vibration of adsorbed water) and the peak at 806  $\text{cm}^{-1}$  can be assigned to the symmetric stretching vibration of Si-O are present in all samples analysed. When comparing MWD-MCM-41 (spectrum i) with AP-MWD-MCM-41 (spectrum ii) the peak at 1470  $\text{cm}^{-1}$  indicates successful incorporation of the amine functionality as this peak (assigned to N-H stretch) is absent in the MCM-41 spectrum. There is also a weak band at 693  $\text{cm}^{-1}$  for AP-MCM-41 and as a N-H bending vibration provides further evidence of incorporation of the amine functional group onto the silica surface.

Differences were also observed between the spectra obtained for AP-MWD-MCM-41 before loading with chromium ions (spectrum ii) and after loading with hexavalent chromium (spectrum iii), trivalent chromium (spectrum iv) and both species of chromium (spectrum v). Specifically the N-H stretch at 1470  $\text{cm}^{-1}$  disappeared and lower wavenumber and a broad band appeared in the range 1340-1400  $\text{cm}^{-1}$  which can be assigned as secondary C-N stretch [287]. The Si-OH stretch at 970  $\text{cm}^{-1}$  was also shifted to 950  $\text{cm}^{-1}$ ; illustrating the influence of the associated anion with the chelate. A sharp peak at 823  $\text{cm}^{-1}$  also appeared in all AP-MCM-41 samples after loading with chromium.

The appearance of these peaks provide evidence of chromium loading as previous work has assigned the broad band at 1340-1400  $\text{cm}^{-1}$  to a Cr-N stretch and the sharp peak at 823  $\text{cm}^{-1}$  to a Cr-O vibration [288]; thus both would appear when chromate ions co-ordinate with amine groups on the surface of the silica adsorbent. The FTIR analyses demonstrate the use of optical spectroscopy to quickly establish the success of functionalisation and of sorbent loading.



**Figure 8.9: FTIR spectra of (i) MWD-MCM-41, (ii) AP-MWD-MCM-41, (iii) Cr (III)-AP-MWD-MCM-41, (iv) Cr (VI)-APMWD-MCM-41 and (v) Cr (III)+Cr (VI)-AP-MWD-MCM-41.**

### 8.3.5 Preconcentration of Cr (VI) removed from water samples

To check the ability of AP-MWD-MCM-41 to preconcentrate Cr ions from water samples experiments were performed as described in Section 8.2.3.

Water samples (100 or 1000 cm<sup>3</sup>) were spiked with different concentrations of Cr (VI) (0.01, 0.1 or 1 µg cm<sup>-3</sup>). A known mass (25 mg) of sorbent was added to each water sample and the solutions were stirred for 2 hours after which time the sorbents were collected by filtration and washed with 10 cm<sup>3</sup> of 0.1 M ammonium hydroxide.

The solutions were filtrated again and the filtrates were analysed by ICP-AES. The results (Table 8.6) indicated that using this simple method of extraction and recovery, preconcentration of Cr (VI) was possible with an enrichment factor of 10.

Moreover, preconcentration was achieved with accuracy even when the concentration of Cr (VI) was as low as 0.01 µg cm<sup>-3</sup>. It was, however, observed that the preconcentration procedure did not produce accurate results when working with solutions at a concentration of 0.001 µg cm<sup>-3</sup>, presumably due to the detection limit of the ICP-AES.

An enrichment factor of 100 was also measured and with a percentage recovery value of 77 %. Considering the low concentration (0.01 µg cm<sup>-3</sup>) of Cr (VI) in solution and the high enrichment factor achieved (100); this recovery value was deemed to be acceptable.

This method of preconcentration could be used when Cr (VI) is determined by instrumental methods with higher limits of detection, for example FAAS. Equally, this method of preconcentration could be used for the determination of trace amounts of Cr (VI) in environmental samples.

**Table 8.6: Preconcentration of Cr(VI) from water samples.**

Sample	Cr Conc. ( $\mu\text{g cm}^{-3}$ )	Added	Found	Found after washed the extracted Cr on sorbent by 0.1M $\text{NH}_4\text{OH}$ ( $10 \text{ cm}^3$ )	Enrichment factor	% Recovery
Distilled Water ( $100 \text{ cm}^3$ )	ND*	0.001	ND*	ND*	10	---
Distilled Water ( $100 \text{ cm}^3$ )	ND*	0.010	0.011	0.1116	10	111.6
Distilled Water ( $100 \text{ cm}^3$ )	ND*	0.100	0.107	1.089	10	108.9
Distilled Water ( $100 \text{ cm}^3$ )	ND*	1.000	1.002	9.703	10	97.03
Distilled Water ( $1000 \text{ cm}^3$ )	ND*	0.010	0.013	0.7709	100	77.09

\*ND: not detected.

### 8.3.6 Adsorption of Cr (VI) from real water samples

The ability of AP-MWD-MCM-41 to extract Cr (VI) in the presence of other potentially toxic metals (PTMs) that will be present in environmental samples was assessed by adding the sorbent to a river and tap water samples of river water and tap water spiked with Cr (VI). The water samples were first analysed by ICP-AES to determine the concentration of Cr (VI) in each solution before being spiked with Cr (VI) ions to produce solution concentrations of  $1 \mu\text{g cm}^{-3}$  of Cr (VI); the results are given in Table 8.7. In spite of the presence of other metal ions in solution, particularly excessively high concentrations of Ca (II) and Mg (II) (See table 7.7, p. 164). Cr (VI) removal was more than 99.9 % for both the river and tap water samples. These results implied that the Cr-N co-ordinating bond was not appreciably hindered by the presence of other co-ordinating ions at high concentration, thus proving further evidence of the high performance, and selectivity, of AP-MWD-MCM-41 for Cr (VI). The percentage recovery of Cr (VI) from loaded sorbents was more than 97 % with slightly higher recovery values being calculated for the tap water sample.

**Table 8.7: Performance of AP-MCM-41 for Cr (VI) selection from real water samples.**

Sample	Conc. Cr ( $\mu\text{g cm}^{-3}$ )	Added ( $\mu\text{g cm}^{-3}$ )	Found before sorbent added ( $\mu\text{g cm}^{-3}$ )	Found after sorbent added ( $\mu\text{g cm}^{-3}$ )	Found after washed 0.1M $\text{NH}_4\text{OH}$ ( $\mu\text{g cm}^{-3}$ )	% Recovery
Tap Water	0.008	1.000	1.011	0.008	0.9872	98.72
River water	0.007	1.000	1.005	0.011	0.9714	97.14
Distilled Water	0.004	1.000	1.001	0.005	0.9948	99.48

### 8.3.7 Selectivity of AP-MCM-41 towards Cr (VI) in the presence of other heavy metal ions

To demonstrate the potential environmental performance of the sorbent when exposed to solutions containing mixed metal ions, multi-elements experiments were carried out using standard solutions containing selected metals (Al, As, Ba, Cd, Co, Cr (III), Cr (VI), Mn, Ni, Pb, and Zn). A known weight (50 mg) of AP-MWD-MCM-41 was added to solutions containing  $10 \mu\text{g cm}^{-3}$  of each element at 3 different pH values (1, 3 or 9). All solutions were stirred for 2 hours at ambient temperature, and then solutions were removed and filtered prior to analysis by ICP-AES. The results obtained are given in Figure 8.10.

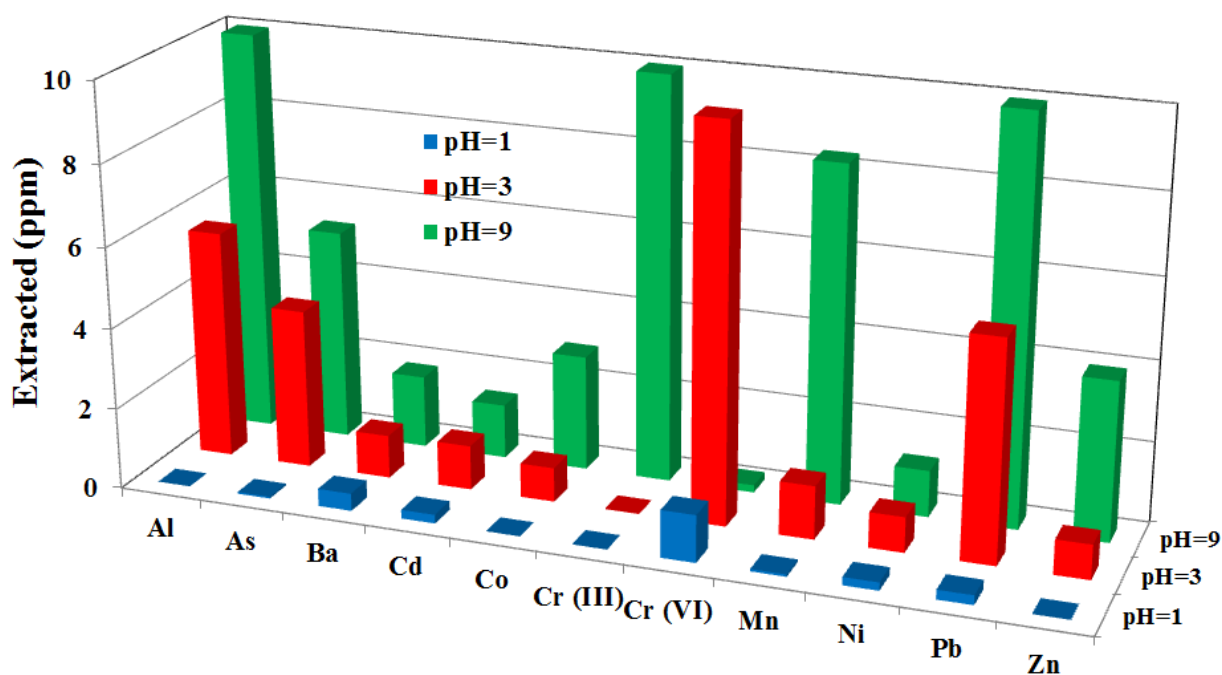


Figure 8.10: Effect of pH for extraction of potentially toxic metals from water using AP-MWD-MCM-41.

## **8.4 Effect of meso-silica pore size distribution on extraction of Cr (VI)**

As noted in Section 8.3.2 and 8.3.3. Adsorption of Cr (VI) onto mesoporous silica was not described by a simple adsorption process. Moreover Skipper et al.[289] reported recently that the in chromium (VI) adsorption could demonstrate unusual enthalpy behaviour, which rise on surface coverage, suggests that physisorption in these systems is accompanied by a second mechanism; one that likely involves weak chemisorption. Although the previous study of kinetics gave an insight into the possible mechanisms of Cr (VI) adsorption, along with possibly reaction pathways and solute residence time on the adsorbent surface, is important to determine whether the adsorption process will go to completion or not. Kinetic adsorption models normally used to describe Cr (VI) adsorption onto porous materials are represented a simplistic approximation of the pore diffusion kinetics without considering the possible impact of pore dimensions to date, no detailed studies of the impact of pore diffusion processes on metal ion uptake have been reported, and in particular, the effects of pore radius and pore size distribution on the sorption kinetics. Current literature reporting on kinetics studies of Cr (VI) adsorption onto different sorbents give conflicting results. Some authors conclude that the adsorption process shows compliance with the first order model of kinetics [290-294]. Others note an adsorption process that follows a second order kinetic model [285, 295-299].

To examine the adsorption process in more detail the previous results obtained for Cr (VI) adsorption onto AP-MWD-MCM-41 were compared with two other mesoporous silica materials with different porosity parameters: AP-Calcined-MCM-41 and SBA-15. Both materials were prepared as described in Section 4.2, p. 88 and Section 3.1.2, p. 63 respectively.

### **8.4.1 Material characteristics**

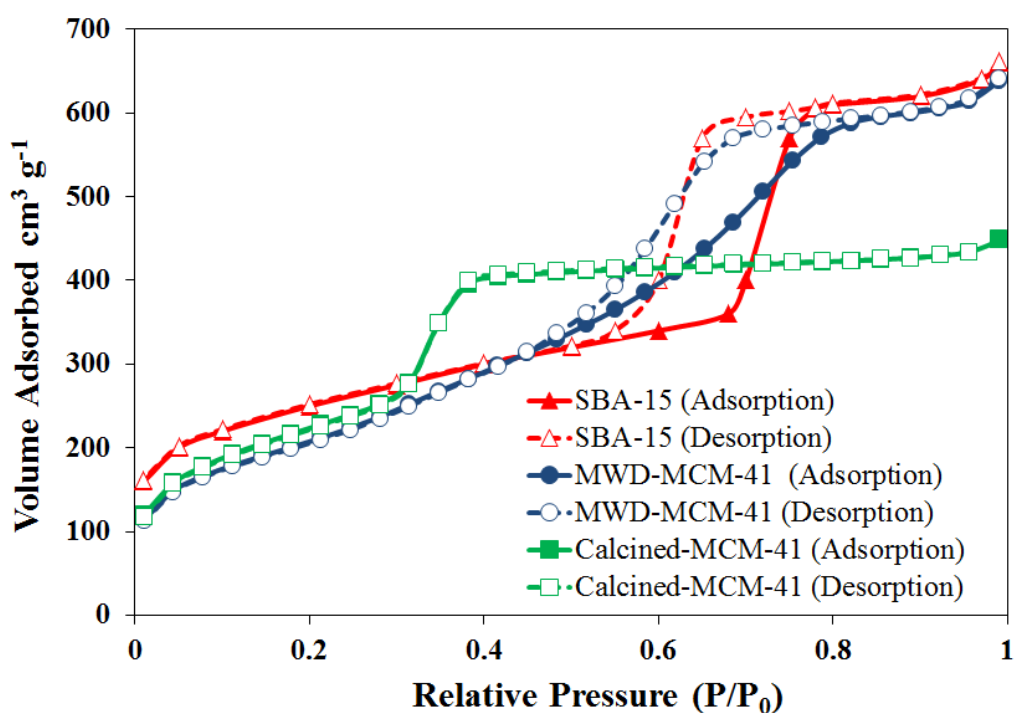
The 3 materials were characterised using BET to examine their pore size and pore distribution. The physicochemical properties of each material are summarised in Table 8.8.



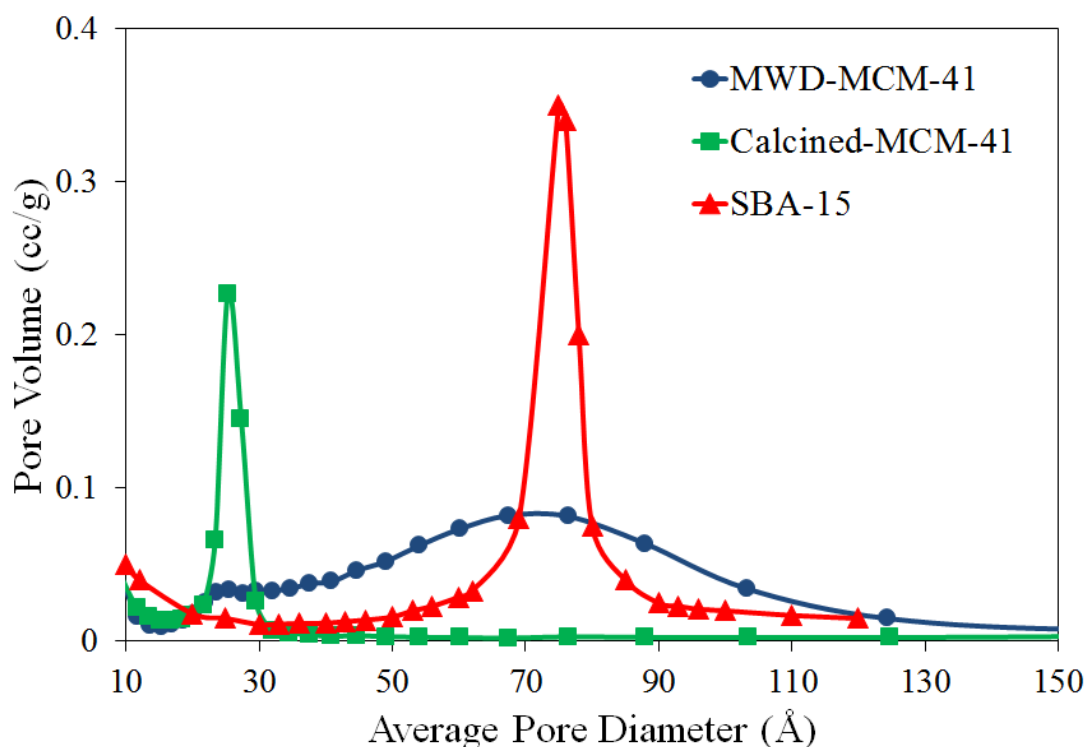
**Table 8.8: Physicochemical properties of mesoporous silica materials used.**

Sorbent	BET Surface Area ( $\text{m}^2 \text{g}^{-1}$ )	Pore Size (nm)	Pore Volume ( $\text{cm}^3 \text{g}^{-1}$ )
MWD-MCM-41	760	6.7	0.99
Calcined-MCM-41	813	2.53	0.69
SBA-15	850	7.18	1.01

The  $\text{N}_2$  sorption isotherms (Figure 8.11) were type IV for all samples confirming their mesoporous natures, however slightly different capillary condensation steps were noted at higher relative pressures for SBA-15 and MWD-MCM-41 compared with Calcined-MCM-41, suggesting larger average pore size for these 2 samples. The hysteresis loop was also broader for SBA-15 and MWD-MCM-41 suggesting that these materials contained pores with different shapes and size. In contrast the calcined material demonstrated no hysteresis loop indicating a well-defined, narrow pore size of regularly shaped pores.

**Figure 8.11: Nitrogen adsorption isotherm of the mesoporous silica sorbents.**

This was confirmed when the pore distribution plots were examined (Figure 8.12). It was clear that the MCM-41 sample subjected to MWD had a broad pore size distribution (approx. from 2 - 12 nm) compared with the calcined MCM-41 and SBA-15 samples.



**Figure 8.12: BET pore size distribution patterns of the mesoporous silica sorbents.**

Surface modification of the three materials was carried out by post synthesis grafting using aminopropyltrimethoxy-silane (AP-TMS); experimental details are summarised in section 3.4.1, p. 76. After the materials were dried elemental analysis was used to estimate the degree of functionalisation ( $Lo$ ) of the materials. The  $Lo$  values were approximately 2 for AP-MWD-MCM-41, 1.3 for AP-Calcined-MCM-41 and 1.6 for AP-SBA-15 respectively. Highest functionalisation was achieved for the MWD MCM-41 sample. As mentioned previously this was attributed to the unique preparation process which used hydrogen peroxide and nitric acid during the microwave digestion step. Two key features produced included larger pores and a higher number of silanol groups on the surface of the material. Both features

combined led to a material with the ability to co-ordinate with a larger number of amino groups.

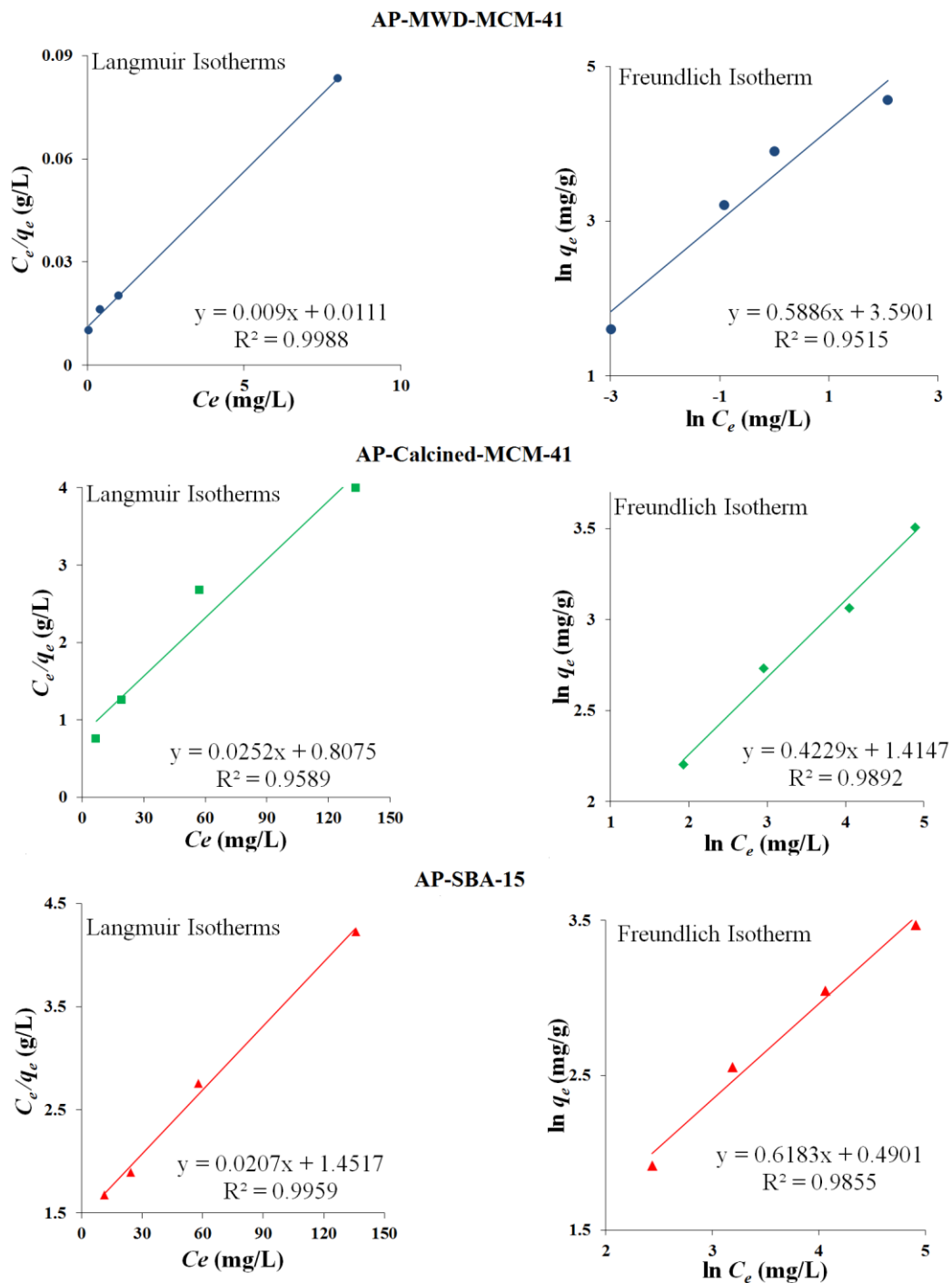
#### 8.4.2 Adsorption study

The equilibrium isotherm results were calculated using Langmuir [280] and Freundlich models [281]. The results (Figure 8.13) demonstrated that the Langmuir model described the adsorption process for AP-MWD-MCM-41 and AP-SBA-15; indicating homogeneous distribution of active sites on the surface of these 2 sorbents with monolayer surface coverage with Cr (VI). The sample of MCM-41 that had been calcined was better described by the Freundlich model. The linearised Langmuir and Freundlich equations were used to fit the equilibrium isotherms for these chromium-sorbent systems and the maximum adsorption capacities according to those models are summarised in Table 8.9.

**Table 8.9: Isotherm parameters for Cr (VI) sorption on amino-functionalised mesoporous silica.**

Sample	Langmuir		Freundlich		
	$q_m$ (mg/g)	$b$ (L/mg)	$R_L$	$K_f$ (mg/g)	$n$ (L/mg)
AP-MWD-MCM-41	111.1	0.811	0.110	36.24	1.70
AP-Calcined-MCM-41	39.68	0.031	0.763	4.115	2.36
AP-SBA-15	48.31	0.014	0.877	1.632	1.62

The adsorption capacity of the AP-MWD-MCM-41 material at 111.1 mg/g was significantly higher than for AP-Calcined-MCM-41 or AP-SBA-15. AP-MWD-MCM-41's  $b$  constant was also significantly higher which implies that this material had a higher affinity of adsorption than both other sorbents. The results of both AP-MWD-MCM-41 and AP-SBA-15 suggested that Cr (VI) was adsorbed by a 1:1 mechanism (monolayer sorption). The dimensionless parameter ( $R_L$ ) [300] values were the range of 0 - 1, pointing out favourable adsorption of Cr (VI) onto all 3 sorbents used in this study.



**Figure 8.13: Adsorption isotherms of Cr (VI) onto AP-mesoporous sorbents.**

### 8.4.3 Kinetic study

The kinetics of Cr (VI) adsorption were analysed using pseudo first-order, pseudo second-order and intraparticle diffusion kinetic models. The results of the kinetics studies are also presented in Figure 8.14. Examination of the pseudo-first order rate plots, and the calculated correlation coefficients, confirmed that the adsorption kinetics did not fit well with this model.

The calculated correlation coefficients for AP-MWD-MCM-41, AP-calcined-MCM-41 or AP-SBA-15, were 0.7613, 0.0099 and 0.0415 respectively. Indeed the correlation coefficients increased to 0.9990, 0.9998 or 0.9999, for AP-MWD-MCM-41, AP-calcined-MCM-41 or AP-SBA-15 respectively when the pseudo second-order model was used. Most kinetic information was obtained by application of the intraparticle diffusion model (Figure 8.14 (c)). The adsorption of Cr (VI) onto AP-Calcined-MCM-41 or AP-SBA-15 involved one fast kinetic process ( $9.2$  and  $9.7 \text{ mg L}^{-1} \text{ min}^{-1/2}$ ) explained as a one-step adsorption until the adsorption capacity of the material was reached. In contrast there were 2 distinct kinetic regions of the AP-MWD-MCM-41 plot. A faster adsorption process ( $4.8 \text{ mg L}^{-1} \text{ min}^{-1/2}$ ) occurred up to 1 min after addition of the sorbent to the Cr (VI) solution, after which time a slower second reaction rate ( $2.52 \text{ mg L}^{-1} \text{ min}^{-1/2}$ ) was measured until the adsorption capacity was reached. These results provide the first experimental evidence that AP-MWD-MCM-41 has pores large enough to permit functionalisation and co-ordination with metal ions inside the pore. For the first time, experimental results are presented that confirm the theory previously presented.

If the intraparticle diffusion plots are examined in more detail it could be said that, in case of AP-MWD-MCM-41, the adsorption rate decreased with increasing adsorption time. This observation was not observed for the other 2 sorbents. This result suggested that for Cr (VI) adsorption pore diffusion was not the rate-controlling step for sorbents with smaller pore size distribution (AP-SBA-15 and AP-Calcined-MCM-41) but it was the rate-controlling step for AP-MWD-MCM-41 which contained large pores and a a broad pore size distribution.

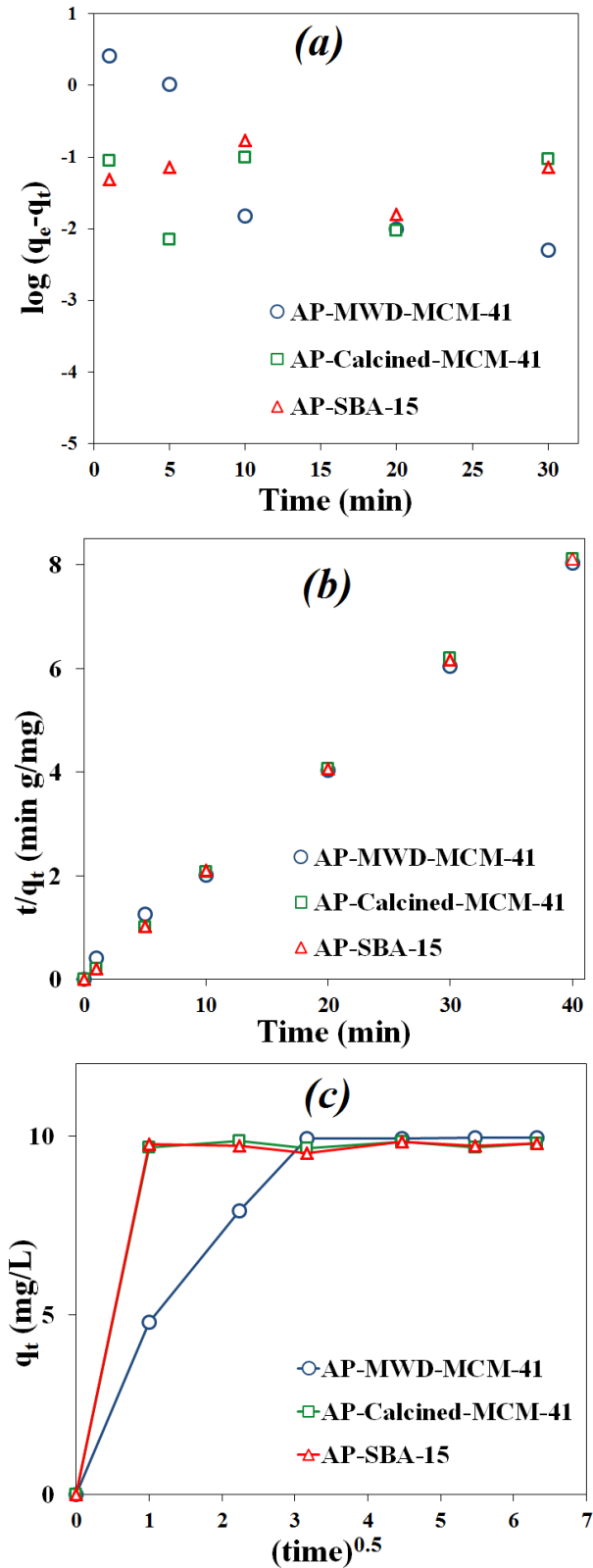
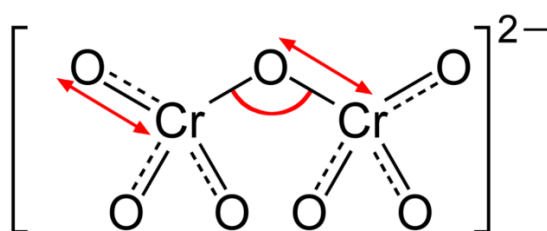


Figure 8.14: Pseudo first-order (a), pseudo second-order (b) and intraparticle diffusion (c) kinetic models.

A complicated adsorption process for extraction of Cr (VI) from the liquid phase is expected as its behaviour is poorly understood. In the liquid phase a range of coordination numbers are expected, and can be even up to 7 [301]. In the main, the dichromate dianion ( $\text{Cr}_2\text{O}_7^{2-}$ ) is reported as the most abundant species when solution pH is in the range 2 – 6 [302, 303] and in some cases the dichromate dianion may form a trimer, as found, e.g. in rubidium trichromate or even a tetramer as found in  $\text{K}_2\text{Cr}_4\text{O}_{13}$  [304]. In addition to the different species found in solution the dichromate dianion dimensions were found to vary due to the varieties of bonds length and angles possible in the molecule [304] (see Figure 8.15). Bearing in mind the presence of larger Cr species and the ability of the molecule to ‘stretch’, the AP-MWD-MCM-41 may be the only material capable of adsorbing the analyte both on the surface of the material, and within the pores, thus providing the significantly higher adsorption capacity and increased performance towards Cr (VI) compared to sorbents with narrow pore size distributions.

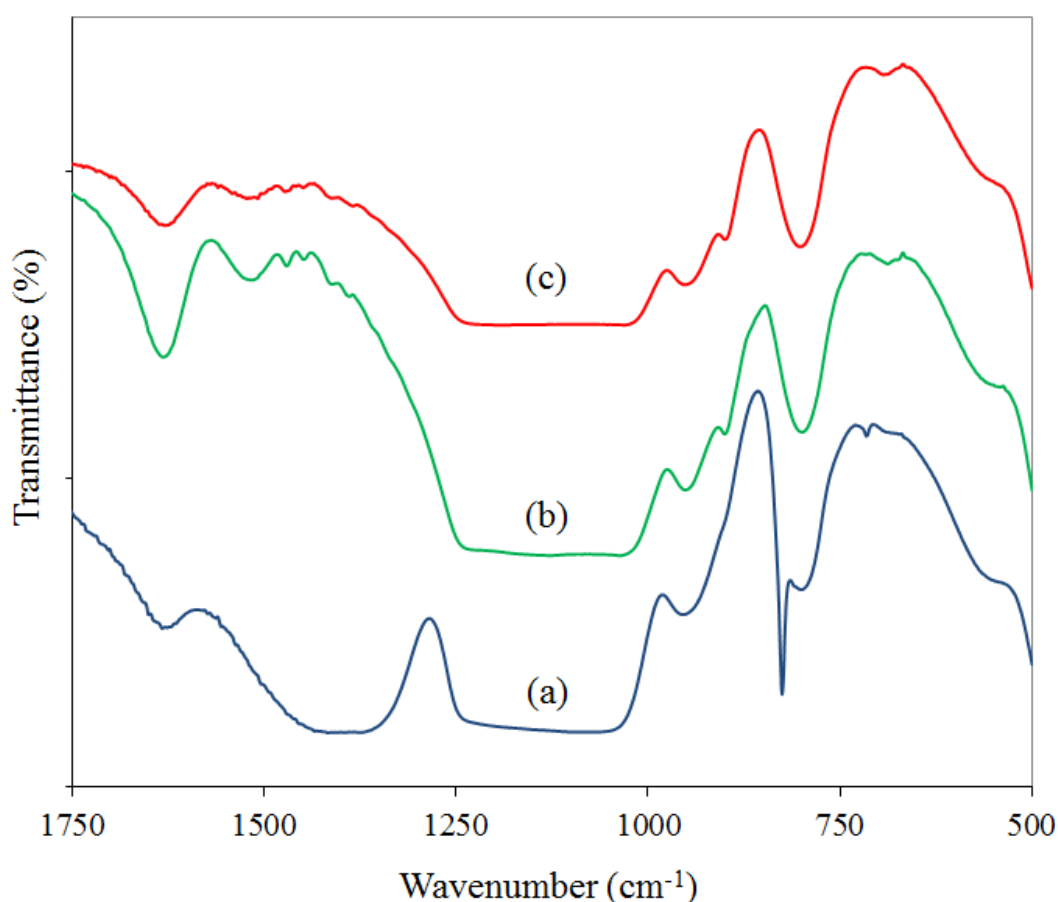


**Figure 8.15: The theoretical structure of dichromate dianion: The Cr–O–Cr angle varies between 116.2° and 162.1°. The range for the Cr–O(terminal) bond lengths is between 1.469 and 1.777 Å. The range for the Cr–O(bridging) is 1.622–1.956 Å. [304]**

#### 8.4.4 FTIR study

After sorbents extraction Cr (VI) from solution they were examined by FTIR spectroscopy. The spectra obtained are given in Figure 8.16. The N-H stretch at  $1470\text{ cm}^{-1}$  disappeared from the spectrum of AP-MWD-MCM-41 loaded with Cr (VI) and a broad band appeared in the range  $1340\text{--}1400\text{ cm}^{-1}$ ; which can be assigned as a secondary C-N stretch [305]. Interestingly the N-H stretch at  $1470\text{ cm}^{-1}$  was still evident in both spectra of Cr loaded AP-Calcined-MCM-41 and AP-SBA-15.

This implied that some of the aminopropyl functional groups were not involved in the adsorption process. It is postulated that these NH- groups would be present in the pores of the material. As the pores are smaller they could not accommodate Cr species and thus remained not attached to the surface. A sharp peak at  $823\text{ cm}^{-1}$  in the AP-MWD-MCM-41 spectrum alone. This was assigned to a Cr-O vibration. A weak band appeared with AP-Calcined-MCM-41 and AP-SBA-15 at  $893\text{ cm}^{-1}$  which can be assigned to an N-O vibration. The appearance of these peaks with AP-MWD-MCM-41 provided evidence of Cr loading with different co-ordination geometries.



**Figure 8.16: FTIR spectra of chromium loaded (a) AP-MWD-MCM-41, (b) AP-Calcined-MCM-41 and (c) AP-SBA-15.**

In summary, the results obtained (adsorption isotherms, kinetic models and FTIR spectra) combined to suggest that different adsorption behaviours will be obtained for Cr (VI) depending on the material's pore size distribution. With narrow pore size distribution (AP-Calcined-MCM-41 or AP-SBA-15) the reaction can be defined as a



one-step adsorption process, which means very fast adsorption until the adsorption capacity of the material is reached. A completely different behaviour was observed when the adsorbent had a broad pore size distribution (AP-MWD-MCM-41). The adsorption process was dictated by a sequence of processes that gave different rates of adsorption: mass transfer of ions through the liquid surrounding the surface of sorbent particles and diffusion of ions through the particle pores. The slowest step (that is the rate determining step) was considered to be due to diffusion of ions through the sorbent pores.

## 8.5 Conclusions

AP-MCM-41 was assessed for removal of Cr (VI) from aqueous solution. Removal involved monolayer interaction with the chelate on the silica surface and the functionalisation, and loading, could be tracked using FTIR spectroscopy. The adsorption capacity was extremely high when AP-MCM-41 produced using a MWD method was used (compared to a production method which used calcinations) or even compared to SBA-15. Almost exclusive removal of Cr (VI) was achieved at pH 3 and moreover, the sorbent could be used to extract a wide range of other metal ions from water if its pH was modified above 7. No reduction in performance was observed even when removing Cr (VI) from water which contained other metal ions (e.g.  $\text{Ca}^{2+}$  and  $\text{Mg}^{2+}$ ) at significantly higher concentration. The ease, at which AP-MCM-41 was synthesised, tuned and regenerated all combined well to suggest that this sorbent could be used for environmental remediation, recovery of Cr (VI) from contaminated water, solid phase extraction or pre-concentration processes. Examination of the effect of pore size distribution on adsorption provided evidence that the material's extremely high adsorption capacity was due to the larger pores and surface activation. With the Cr (VI) concentration range studied here, within 10 min more than 99 % of Cr (VI) was removed from solution.

## **Chapter 9: Conclusions and further work**

## 9.1 Extraction of VOCs from indoor air

The results obtained during this research demonstrated successful generation of a steady stream of contaminated air using a laboratory built dynamic air sampling system. Permeation vials were shown to provide constant mass loss of selected VOCs for up to 6 weeks. Direct injection of VOCs onto sampling tubes was shown to be a good method for introduction of VOCs onto calibrant tubes as indicated by the internal standard calibration graphs. The calibration method was shown to be repeatable and reproducible. However, the need to use different sorbents for calibration has not been well understood and needs further work. The same mass of analyte was injected onto each sorbent and the analytical method of detection was exactly the same. However, different calibration slopes were generated indicating that different masses were desorbed (or adsorbed) by each sorbent. It appeared that some of the analytes were retained by SBA-15 and more for MCM-41; both calibrations were less sensitive than for Tenax-TA. As the calibrations were linear and repeatable it was thought that the silica sorbents could still be used to perform air sampling as long as Tenax-TA was used for calibration if methanolic solutions are used to spike calibrant sampling tubes

A complicated relationship was observed between the effect of humidity and sampling flow rate, especially for Tenax TA, on the collection of VOCs onto meso-silica samples. The effect of relative humidity to adsorb VOCs onto Tenax was completely different when the sampling flow rate was altered from 50 to 100 cm<sup>3</sup> min<sup>-1</sup>. On the other hand the mesoporous silicate sorbents (SBA-15 and MCM-41) showed the same behaviour during trapping the VOCs from indoor air at different RH and sampling flow rates. The presence of water vapour (H-RH) decreased the masses trapped on SBA-15 and MCM-41, and when the sampling flow rates were increased the VOC masses trapped onto SBA-15 and MCM-41 has been slightly increased.

Breakthrough experiments confirmed that at high relative humidity the commercial sorbent (Tenax TA) had the best adsorption capacity for VOCs studied here. But at low relative humidity SBA-15 trapped the greatest masses compared. MCM-41 showed lowest performance in adsorption capacity but the highest performance for

dynamic adsorption capacity. The laboratory prepared sorbents (SBA-15 and MCM-41) showed better performance than Tenax when collecting VOCs from dry air (25 % RH).

In general, it was shown that calibration experiments using spiked methanolic solutions need to be conducted using Tenax-TA as the sorbent, regardless of which sorbent is used for air sampling. At high relative humidity Tenax-TA should be the chosen sorbent of choice for collection of VOCs from air, however at lower humidity, higher adsorption performance was demonstrated by the silica adsorbents.

## **9.2 New method of MCM-41 preparation**

To ensure environmental and/or industrial application of silica adsorbents, better production methods are required. Therefore, the key aims of this section of the PhD were to develop a method of MCM-41 production which was faster, more economical and provided larger sample quantities in batch production. Moreover, as the target application areas were adsorption studies, it was also important to provide material which could support a larger proportion of adsorption sites for heavy metals. Hence the ultimate aims of this section of the research were: (i) the ability to synthesis large quantities (100 g) of material in a simple batch process, (ii) to produce large mesopores which favour functionalisation, (iii) to have a wide pore size distribution, (iv) to have a long range order of the pores and (v) the ease at which the material can be prepared without expensive laboratory kit. A new method of MCM-41 production using room temperature hydrolysis and condensation conditions together with microwave and nitric acid/hydrogen peroxide digestion of the organic template resulted in achieving all these goals. A mesoporous silica was produced with a larger number of silanol group available for functionalisation and a larger pore distribution. These suspected characteristics, (supported by BET, microanalysis and FTIR spectroscopic results), favoured derivatisation; specifically allowing larger multi-site chelate groups to co-ordinate around the metal ion of interest.

### **9.3 Extraction of heavy metals from water using MWD-MCM-41**

The results obtained in this thesis conclusively demonstrated that MCM-41 functionalised sorbents, prepared using the new MWD method) had the potential to be extremely efficient sorbents for the removal of selected heavy metals, Pb (II), Hg (II) and Cr (VI), from aqueous solution.

Amino functionalised MCM-41 (DETA-MCM-41) was the most efficient material to extract Pb (II) from solution. The ion-ligand co-ordination was strong enough for the sorbent to work in static solutions, where the ion was driven to the ligand by a concentration gradient alone. This will be of particular significance if the material was to be utilised in a remote location where stirring or agitation of the contaminated solution was not possible.

Mercapto functionalised MCM-41 (MP-MCM-41) was used to extract mercury from water samples. The sorbent was almost exclusively selective to Hg (II), even in the presence of a wide range of other heavy metal ions, such as those present in contaminated water samples. Removal of Hg (II) from loaded sorbents was also achieved using a new method involving MWD. All of these features combined to provide a highly selective removal and pre-concentration method for Hg (II) from aqueous solutions. Selective recovery (97 %) of Hg (II) from contaminated waters was economically favourable and provided an alternative application method in addition to environmental mitigation strategies. Regeneration of MP-MCM-41 was presented, for the first time, with mild acid conditions. Examination of the material after treatment suggested that the recovery method proposed did not disrupt the chelate on the surface of the silica and so the material was reused (with approximately 76 % of the original adsorption capacity).

A simple amino functionalised MCM-41 (AP-MCM-41) has prepared and assessed for removal of Cr (VI) ions from aqueous solution. Removal involved monolayer interaction with the chelate on the silica surface and the functionalisation and loading was tracked by FTIR spectroscopy. The adsorption capacity was higher than previously reported for competitive sorbents and pre-treatment of solution permitted

either exclusive removal of Cr (VI) or a sorbent that can be used to extract a wide range of other PTMs from water.

Also the kinetics of Cr (VI) removal from aqueous solutions over a wide range of pore distribution was tested under ambient condition using pseudo-first order, pseudo-second order, and intraparticle diffusion kinetic models. The results obtained showed that the adsorption adhered to the pseudo-second order model since theoretical and experimental sorption capacities were in excellent agreement when a broad pore size distribution material was used. The intraparticle diffusion model revealed that pore diffusion was not the rate-controlling step with narrow pore size distribution sorbents. On the other hand pore diffusion was the rate-controlling step when a broad pore size distribution material was used. The intraparticle model demonstrated here provides the first evidence of Cr (VI) adsorption in the pores of MCM-41. The equilibrium isotherm study showed the best suitability of Langmuir model for AP-MWD-MCM-41 and AP-SBA-15, indicating homogeneous distribution of active sites on the surface of sorbents and monolayer sorption but was not the case with AP-Calcined-MCM-41.

The work presented here demonstrated that functionalised MCM-41 had the potential to be an extremely useful sorbent for heavy metal extraction from aqueous phase. The work focused on a batch method, which involved stirring the contaminated solution with the material for 2 h.

#### **9.4 Future work**

Some areas of this project need more investigation. MCM-41 produced with high pore size and pore size distributions showed excellent performance to extract heavy metals from water samples. It is suggested however that this material should be tested in a variety of adsorption and/or catalytic applications.

In this work, MCM-41 was used to extract VOCs from indoor air. The MCM-41 used was produced according to a conventional preparation method. Although the results were encouraging, the material was only tested at 2 relative humidity values. Since the effect of changing the humidity (%RH) was found to have a significant impact on VOC extraction efficiency a larger range of humidity values should be

examined to evaluate the impact on sorbent performance. Additionally, the target VOCs used in this project were monoaromatic hydrocarbons (MAHCs) and mesoporous silicate was used without functionalisation. Investigation of more complicated compounds like polycyclic aromatic hydrocarbon (PAHs) with non-polar surface (C16 organic functionalised-MCM-41) could be used to test the ability of functionalised MCM-41 to extract polar hydrocarbons and estimate the ability of sorbent regeneration.

The incorporation of various functional groups into the MWD-MCM-41 framework has thus been attempted in order to produce surface properties suitable for desired functionalities such as selective-adsorption activity for target molecule and acidity for catalysis. Acid catalytic activity satisfies one of the most important applications of porous solids, especially mesoporous silica which provides a larger reaction space compared to proton type zeolites. The MWD-MCM-41 could be used as catalyst support in liquid phase reactions because of its well-defined mesoporous structure in combination with a large pore size distribution, which makes varies size of organic molecules to diffuse relatively easily to the catalytically active sites located inside the pores. Therefore testing the ability of MCM-41 produced in this work as a catalyst should be a main focus of future work.

The ability of functionalised MCM-41 to extract heavy metals from water samples especially in distilled, tap and river waters samples have been studied in this project. The material showed great performance in adsorption process with high adsorption capacities. But estimation of the behaviour of the materials in harsher environments like sea water and sewage is important for the global heavy metals pollution problem.

According to the international atomic energy agency (IAEA) standard, the main disposal wastes in the nuclear plants are the low-level radioactive wastewater (LLRW) which contain low concentration of radioactive activated corrosion products such as  $^{60}\text{Co}(\text{II})$  and  $^{56}\text{Mn}(\text{II})$ . The treatment of these waste liquids is actually the removal of the radioactive metal ions. Due to the low adsorptive capacity of the traditional adsorbents and their weak combination with metal ions. Amino-functionalised MCM-41 could be the best choice for removal of these ions from

water samples. That could be one of the future works of using MCM-41 to treat water samples.

Purification of liquids with low-concentration of heavy metals using mesoporous silica in the case of dynamic flow (column modes) is important for the design of an industrial scale process. Functionalised-MCM-41 will efficiently applied for heavy metal removal in column mode. The diffusion rate of the aqueous heavy metal ions into the pores can be estimated and compared their sorption affinity and capacity with batch adsorption results (results in chapters 6, 7 and 8).



## References:

- [1] J. Rouquerol, D. Avnir, D.H. Everett, C. Fairbridge, M. Haynes, N. Pernicone, J.D.F. Ramsay, K.S.W. Sing, K.K. Unger, Guidelines for the Characterization of Porous Solids, in: F.R.-R.K.S.W.S. J. Rouquerol, K.K. Unger (Eds.) Stud. Surf. Sci. Catal., Elsevier, 1994, pp. 1-9.
- [2] R.K. Iler, The Chemistry of Silica, John Wiley & Sons, New York, 1979.
- [3] V. Boonamnuayvitaya, C. Tayamanon, S. Sae-ung, W. Tanthapanichakoon, Chem. Eng. Sci., 61 (2006) 1686-1691.
- [4] A. Karout, C. Chopard, A.C. Pierre, J. Mol. Catal. B: Enzym., 44 (2007) 117-127.
- [5] P. Kuśtrowski, R. Janus, A. Kochanowski, L. Chmielarz, B. Dudek, Z. Piwowarska, M. Michalik, Mater. Res. Bull., 45 (2010) 787-793.
- [6] J.Y. Ying, J.B. Benziger, Colloids and Surfaces A: Physicochemical and Engineering Aspects, 74 (1993) 23-31.
- [7] N.L. Dias Filho, D.R. Do Carmo, Adsorption at silica, alumina and related surfaces, in: Encyclopedia of Surface and Colloid Science, Marcel Dekker, New York, 2004, pp. 1–20.
- [8] F. Quignard, C. Lecuyer, C. Bougault, F. Lefebvre, A. Choplin, D. Olivier, J.M. Basset, Inorg. Chem., 31 (1992) 928-930.
- [9] R. Baxter, P. Reinhardt, N. López, F. Illas, Surf. Sci., 445 (2000) 448-460.
- [10] R. Ströbel, J. Garcke, P.T. Moseley, L. Jörissen, G. Wolf, J. Power Sources, 159 (2006) 781-801.
- [11] S.M. Auerbach., A.C. Kathleen, K.D. Prabir, Handbook of Zeolite Science and Technology, M. Dekker, New York, 2003.
- [12] J. Garcia-Martinez, Nanotechnology for the Energy Challenge, John Wiley & Sons, Weinheim (1st Ed.), 2010.
- [13] C.T. Kresge, M.E. Leonowicz, W.J. Roth, J.C. Vartuli, J.S. Beck, Nature, 359 (1992) 710-712.
- [14] J.S. Beck, J.C. Vartuli, W.J. Roth, M.E. Leonowicz, C.T. Kresge, K.D. Schmitt, C.T.W. Chu, D.H. Olson, E.W. Sheppard, J. Am. Chem. Soc., 114 (1992) 10834-10843.
- [15] X.S. Zhao, G.Q. Lu, G.J. Millar, Ind. Eng. Chem. Res., 35 (1996) 2075-2090.

- [16] J.S. Beck, J.C. Vartuli, *Current Opinion in Solid State and Materials Science*, 1 (1996) 76-87.
- [17] G.S. Attard, J.C. Glyde, C.G. Goltner, *Nature*, 378 (1995) 366-368.
- [18] K. Holmberg, B. Jönsson, B. Kronberg, B. Lindman, *Surfactants and polymers in aqueous solution*, 2nd Ed., John Wiley & Sons, Ltd, England, 2003.
- [19] J.N. Israelachvili, D.J. Mitchell, B.W. Ninham, *Journal of the Chemical Society, Faraday Transactions 2: Molecular and Chemical Physics*, 72 (1976) 1525-1568.
- [20] J.N. Israelachvili, *Intermolecular and Surface Forces*, 2nd Edition, Academic Press, London, 1992.
- [21] V. Chiola, J.E. Ritsko, C.D. Vanderpool, US Patent No. 3 556 725 1971.
- [22] F. Di Renzo, H. Cambon, R. Dutartre, *Microporous Materials*, 10 (1997) 283-286.
- [23] V. Meynen, P. Cool, E.F. Vansant, *Microporous Mesoporous Mater.*, 125 (2009) 170-223.
- [24] F. Hoffmann, M. Cornelius, J. Morell, M. Fröba, *Angewandte Chemie International Edition*, 45 (2006) 3216-3251.
- [25] H. Kosslick, G. Lischke, H. Landmesser, B. Parlitz, W. Storek, R. Fricke, *J. Catal.*, 176 (1998) 102-114.
- [26] C. Liu, S. Wang, Z. Rong, X. Wang, G. Gu, W. Sun, *J. Non-Cryst. Solids*, 356 (2010) 1246-1251.
- [27] D. Chen, Z. Li, C. Yu, Y. Shi, Z. Zhang, B. Tu, D. Zhao, *Chem. Mater.*, 17 (2005) 3228-3234.
- [28] L. Sierra, S. Valange, J. Barrault, J.-L. Guth, *Microporous Mesoporous Mater.*, 113 (2008) 352-361.
- [29] A. Sayari, *J. Am. Chem. Soc.*, 122 (2000) 6504-6505.
- [30] M. Dubois, T. Gulik-Krzywicki, B. Cabane, *Langmuir*, 9 (1993) 673-680.
- [31] M. Ogawa, *J. Am. Chem. Soc.*, 116 (1994) 7941-7942.
- [32] P.T. Tanev, T.J. Pinnavaia, *Science*, 271 (1996) 1267-1269.
- [33] Y. Zhu, W. Shen, X. Dong, J. Shi, *J. Mater. Res.*, 20 (2005) 2682-2690.
- [34] J. Sun, D. Ma, H. Zhang, C. Wang, X. Bao, D.S. Su, A. Klein-Hoffmann, G. Weinberg, S. Mann, *J. Mater. Chem.*, 16 (2006) 1507-1510.
- [35] G. Zhou, Y. Chen, J. Yang, S. Yang, *J. Mater. Chem.*, 17 (2007) 2839-2844.

- [36] Y.-Q. Yeh, B.-C. Chen, H.-P. Lin, C.-Y. Tang, *Langmuir*, 22 (2005) 6-9.
- [37] V.R.K. Iler, *The Chemistry of Silica. Solubility, Polymerization, Colloid and Surface Properties, and Biochemistry*, John Wiley & sons, USA, 1979.
- [38] C.J. Brinker, G.W. Scherer, *Sol-Gel Science*, Academic Press, New York, 1990.
- [39] C.-Y. Chen, S.L. Burkett, H.-X. Li, M.E. Davis, *Microporous Materials*, 2 (1993) 27-34.
- [40] B. Hatton, K. Landskron, W. Whitnall, D. Perovic, G.A. Ozin, *Acc. Chem. Res.*, 38 (2005) 305-312.
- [41] F. Kleitz, W. Schmidt, F. Schüth, *Microporous Mesoporous Mater.*, 65 (2003) 1-29.
- [42] N. Alam, R. Mokaya, *J. Mater. Chem.*, 18 (2008) 1383-1391.
- [43] D. Gu, F. Zhang, Y. Shi, F. Zhang, Z. Wu, Y. Deng, L. Zhang, B. Tu, D. Zhao, *J. Colloid Interface Sci.*, 328 (2008) 338-343.
- [44] F. Bérubé, S. Kaliaguine, *Microporous Mesoporous Mater.*, 115 (2008) 469-479.
- [45] M. Kruk, M. Jaroniec, C.H. Ko, R. Ryoo, *Chem. Mater.*, 12 (2000) 1961-1968.
- [46] A.G.S. Prado, C. Airoidi, *J. Mater. Chem.*, 12 (2002) 3823-3826.
- [47] R. Mokaya, W. Jones, *J. Mater. Chem.*, 8 (1998) 2819-2826.
- [48] C.-Y. Chen, H.-X. Li, M.E. Davis, *Microporous Materials*, 2 (1993) 17-26.
- [49] E. Ihara, K. Koyama, H. Yasuda, N. Kanehisa, Y. Kai, *J. Organomet. Chem.*, 574 (1999) 40-49.
- [50] D. Zhao, Q. Huo, J. Feng, B.F. Chmelka, G.D. Stucky, *J. Am. Chem. Soc.*, 120 (1998) 6024-6036.
- [51] D. Zhao, J. Feng, Q. Huo, N. Melosh, G.H. Fredrickson, B.F. Chmelka, G.D. Stucky, *Science*, 279 (1998) 548-552.
- [52] S. Kawi, *Chem. Commun. (Cambridge, U. K.)*, (1998) 1407-1408.
- [53] R. van Grieken, G. Calleja, G.D. Stucky, J.A. Melero, R.A. García, J. Iglesias, *Langmuir*, 19 (2003) 3966-3973.
- [54] M. T. J. Keene, R. Denoyel, P. L. Llewellyn, *Chem. Commun. (Cambridge, U. K.)*, (1998) 2203-2204.
- [55] X.-B. Lu, W.-H. Zhang, J.-H. Xiu, R. He, L.-G. Chen, X. Li, *Ind. Eng. Chem. Res.*, 42 (2003) 653-656.

- [56] B. Tian, X. Liu, C. Yu, F. Gao, Q. Luo, S. Xie, B. Tu, D. Zhao, *Chem. Commun.* (Cambridge, U. K.), (2002) 1186-1187.
- [57] C. Cai, H. Wang, J. Han, *Appl. Surf. Sci.*, 257 (2011) 9802-9808.
- [58] W. Lin, Q. Cai, W. Pang, Y. Yue, B. Zou, *Microporous Mesoporous Mater.*, 33 (1999) 187-196.
- [59] M. Grün, K.K. Unger, A. Matsumoto, K. Tsutsumi, *Microporous Mesoporous Mater.*, 27 (1999) 207-216.
- [60] D. Kumar, K. Schumacher, C. du Fresne von Hohenesche, M. Grün, K.K. Unger, *Colloids and Surfaces A: Physicochemical and Engineering Aspects*, 187-188 (2001) 109-116.
- [61] A. Monnier, F. Schüth, Q. Huo, D. Kumar, D. Margolese, R.S. Maxwell, G.D. Stucky, M. Krishnamurty, P. Petroff, A. Firouzi, M. Janicke, B.F. Chmelka, *Science*, 261 (1993) 1299–1303.
- [62] C. Liu, L. Wang, W. Ren, Z. Rong, X. Wang, J. Wang, *Microporous Mesoporous Mater.*, 106 (2007) 35-39.
- [63] S. Jana, B. Dutta, H. Honda, S. Koner, *Appl. Clay Sci.*, 54 (2011) 138-143.
- [64] T. Yasmin, K. Müller, *Journal of Chromatography A*, 1217 (2010) 3362-3374.
- [65] S.-E. Park, D.S. Kim, J.-S. Chang, W.Y. Kim, *Catal. Today*, 44 (1998) 301-308.
- [66] A. Marcilla, M. Beltran, A. Gómez-Siurana, I. Martinez, D. Berenguer, *Chem. Eng. Res. Des.*, 89 (2011) 2330-2343.
- [67] H. Ji, Y. Fan, W. Jin, C. Chen, N. Xu, *J. Non-Cryst. Solids*, 354 (2008) 2010-2016.
- [68] L. Huang, Q. Huang, H. Xiao, M. Eić, *Microporous Mesoporous Mater.*, 98 (2007) 330-338.
- [69] Z. Huang, L. Huang, S.C. Shen, C.C. Poh, K. Hidajat, S. Kawi, S.C. Ng, *Microporous Mesoporous Mater.*, 80 (2005) 157-163.
- [70] L. Huang, S. Kawi, C. Poh, K. Hidajat, S.C. Ng, *Talanta*, 66 (2005) 943-951.
- [71] Y. Wan, D. Zhang, N. Hao, D. Zhao, *International Journal of Nanotechnology*, 4 (2007) 66-99.
- [72] D. Bruhwiler, *Nanoscale*, 2 (2010) 887-892.
- [73] T. Yokoi, H. Yoshitake, T. Tatsumi, *J. Mater. Chem.*, 14 (2004) 951-957.

- [74] A.M. Tope, N. Srinivas, S.J. Kulkarni, K. Jamil, *J. Mol. Catal. B: Enzym.*, 16 (2001) 17-26.
- [75] S. Udayakumar, Y.-S. Son, M.-K. Lee, S.-W. Park, D.-W. Park, *Applied Catalysis A: General*, 347 (2008) 192-199.
- [76] D.J. Macquarrie, S.J. Tavener, M.A. Harmer, *Chem. Commun. (Cambridge, U. K.)*, (2005) 2363-2365.
- [77] J.L. Blin, C. Gérardin, L. Rodehüser, C. Selve, M.J. Stébé, *Chem. Mater.*, 16 (2004) 5071-5080.
- [78] R. Ryoo, C.H. Ko, M. Kruk, V. Antochshuk, M. Jaroniec, *The Journal of Physical Chemistry B*, 104 (2000) 11465-11471.
- [79] Z. Luan, J.A. Fournier, J.B. Wooten, D.E. Miser, M.J. Chang, *Stud. Surf. Sci. Catal.*, 156 (2005) 897-906.
- [80] A.M. Liu, K. Hidajat, S. Kawi, D.Y. Zhao, *Chem. Commun. (Cambridge, U. K.)*, (2000) 1145-1146.
- [81] G. Li, Z. Zhao, J. Liu, G. Jiang, *J. Hazard. Mater.*, 192 (2011) 277-283.
- [82] X. Chen, K.F. Lam, K.L. Yeung, *Chem. Eng. J. (Lausanne)*, 172 (2011) 728-734.
- [83] M. Algarra, M.V. Jiménez, E. Rodríguez-Castellón, A. Jiménez-López, J. Jiménez-Jiménez, *Chemosphere*, 59 (2005) 779-786.
- [84] S.A. Idris, S.R. Harvey, L.T. Gibson, *J. Hazard. Mater.*, 193 (2011) 171– 176.
- [85] S.A. Idris, C.M. Davidson, C. McManamon, M.A. Morris, P. Anderson, L.T. Gibson, *Journal of Hazardous Materials*, 185 (2011) 898-904.
- [86] M. Puanngam, F. Unob, *J. Hazard. Mater.*, 154 (2008) 578-587.
- [87] D. Pérez-Quintanilla, A. Sánchez, I. del Hierro, M. Fajardo, I. Sierra, *J. Colloid Interface Sci.*, 313 (2007) 551-562.
- [88] Y. Wang, R.T. Yang, J.M. Heinzl, *Chem. Eng. Sci.*, 63 (2008) 356-365.
- [89] A. Vinu, M. Hartmann, Adsorption of cytochrome c on MCM-41 and SBA-15: Influence of pH, in: M.C. E. van Steen, L.H. Callanan (Eds.) *Stud. Surf. Sci. Catal.*, Elsevier, 2004, pp. 2987-2994.
- [90] K.-Z. Hossain, C.M. Monreal, A. Sayari, *Colloids and Surfaces B: Biointerfaces*, 62 (2008) 42-50.
- [91] X.S. Zhao, Q. Ma, G.Q. Lu, *Energy Fuels*, 12 (1998) 1051-1054.

- [92] J. Zhao, F. Gao, Y. Fu, W. Jin, P. Yang, D. Zhao, *Chem. Commun. (Cambridge, U. K.)*, (2002) 752-753.
- [93] X. Liu, L. Zhou, X. Fu, Y. Sun, W. Su, Y. Zhou, *Chem. Eng. Sci.*, 62 (2007) 1101-1110.
- [94] A. Corma, A. Martinez, V. Martinezsoria, J.B. Monton, *J. Catal.*, 153 (1995) 25-31.
- [95] G.F. Zheng, W. Zhang, Z. Shi, M. Gross, A.B. Sproul, S.R. Wenham, M.A. Green, M. Morey, A. Davidson, G. Stucky, *Microporous Materials*, 6 (1996) 99-104.
- [96] A. Tuel, S. Gontier, R. Teissier, *Chem. Commun. (Cambridge, U. K.)*, (1996) 651-652.
- [97] P. Selvam, S.E. Dapurkar, *Applied Catalysis A: General*, 276 (2004) 257-265.
- [98] G. Maged Samir, *Microporous Mesoporous Mater.*, 97 (2006) 107-113.
- [99] Z. Luan, J. Xu, H. He, J. Klinowski, L. Kevan, *The Journal of Physical Chemistry*, 100 (1996) 19595-19602.
- [100] U. Ciesla, F. Schüth, *Microporous Mesoporous Mater.*, 27 (1999) 131-149.
- [101] M. Mamak, N. Coombs, G.A. Ozin, *Chem. Commun. (Cambridge, U. K.)*, (2002) 2300-2301.
- [102] T.T. Emons, J. Li, L.F. Nazar, *J. Am. Chem. Soc.*, 124 (2002) 8516-8517.
- [103] T. Yamada, H.S. Zhou, H. Uchida, M. Tomita, Y. Ueno, T. Ichino, I. Honma, K. Asai, T. Katsube, *Adv. Mater. (Weinheim, Ger.)*, 14 (2002) 812-815.
- [104] H. Li, M. Nogami, *Adv. Mater. (Weinheim, Ger.)*, 14 (2002) 912-914.
- [105] M.H. Huang, A. Choudrey, P. Yang, *Chem. Commun. (Cambridge, U. K.)*, (2000) 1063-1064.
- [106] J.M. Monteagudo, M.J. Ortiz, *J. Chem. Technol. Biotechnol.*, 75 (2000) 767-772.
- [107] K.S.W. Sing, D.H. Everett, R.A.W. Haul, L. Moscou, R.A. Pierotti, J. Rouquerol, T. Siemieniewska, *Pure Appl. Chem.*, 57 (1985) 603-619.
- [108] P.I. Ravikovitch, D. Wei, W.T. Chueh, G.L. Haller, A.V. Neimark, *The Journal of Physical Chemistry B*, 101 (1997) 3671-3679.
- [109] M. Kruk, M. Jaroniec, A. Sayari, *Langmuir*, 13 (1997) 6267-6273.
- [110] H. Naono, M. Hakuman, T. Tanaka, N. Tamura, K. Nakai, *J. Colloid Interface Sci.*, 225 (2000) 411-420.

- [111] S. Brunauer, P.H. Emmett, E. Teller, *J. Am. Chem. Soc.*, 60 (1938) 309-319.
- [112] A.K. Ladavos, A.P. Katsoulidis, A. Iosifidis, K.S. Triantafyllidis, T.J. Pinnavaia, P.J. Pomonis, *Microporous Mesoporous Mater.*, 151 (2012) 126-133.
- [113] E.P. Barrett, L.G. Joyner, P.P. Halenda, *J. Am. Chem. Soc.*, 73 (1951) 373-380.
- [114] W. Thomson (Lord Kelvin), *Philos. Mag.*, 42 (1871) 448-452
- [115] S. Lowell, J.E. Shields, M.A. Thomas, M. Thommes, *Characterization of Porous Solids and Powders: Surface Area, Pore Size and Density*, Kluwer Academic Publishers, Corr, 2004.
- [116] P.W. Atkins, *Physical Chemistry*, 6th ed., Oxford University Press, Oxford, 1998.
- [117] B.E. Warren, *X-ray Diffraction*, Dover Publication, New York, 1990.
- [118] M. Kruk, M. Jaroniec, J.M. Kim, R. Ryoo, *Langmuir*, 15 (1999) 5279-5284.
- [119] M. Jaroniec, M. Kruk, H.J. Shin, R. Ryoo, Y. Sakamoto, O. Terasaki, *Microporous Mesoporous Mater.*, 48 (2001) 127-134.
- [120] A. Zukal, M. Thommes, J. Čejka, *Microporous Mesoporous Mater.*, 104 (2007) 52-58.
- [121] E. Brennan, (2009) <http://eoin-brennan.com/Content/GraphicDesign.html>.
- [122] S. Besson, T. Gacoin, C. Ricolleau, C. Jacquioid, J.-P. Boilot, *Nano Lett.*, 2 (2002) 409-414.
- [123] N.B. Colthup, L.H. Daly, S.E. Wiberley, *Introduction to Infrared and Raman Spectroscopy*, 3rd ed., Academic Press, Boston, 1990.
- [124] J.M. Hollas, *Modern Spectroscopy*, 4th ed., John Wiley & Sons Ltd, Chichester, 2005.
- [125] S. Srivastava, R. Tygir, N. Pant, *Water Res.*, 23 (1989) 1161- 1165.
- [126] I. Antal, Á.Z. Dávid, *Fundamentals and pharmaceutical applications of near-infrared spectroscopy* <http://www.glatt.com>, 2007.
- [127] M. Malandrino, O. Abollino, A. Giacomino, M. Aceto, E. Mentasti, *J. Colloid Interface Sci.*, 299 (2006) 537-546.
- [128] M. Thompson, *CHNS Elemental Analysers*, The Royal Society of Chemistry, Analytical Methods Committee, 2008.
- [129] H. Martin, *Journal of Chromatography A*, 885 (2000) 129-151.

- [130] A. Khan, F. Mahmood, M.Y. Khokhar, S. Ahmed, *Reactive and Functional Polymers*, 66 (2006) 1014-1020.
- [131] G.M. Message, *Practical Aspects of Gas Chromatography/Mass Spectrometry*, John Wiley & Sons, New York, 1984.
- [132] D.A. Skoog, D.M. West, F.J. Holler, *Fundamentals of Analytical Chemistry*, 7th ed., Saunder College Publishing, Philadelphia, 1996.
- [133] H.M. McNair, J.M. MILLER, *Basic Gas Chromatography* John Wiley & Sons, New York 1997.
- [134] T.Y. Guo, Y.Q. Xia, G.J. Hao, M.D. Song, B.H. Zhang, *Biomaterials*, 25 (2004) 5905-5912.
- [135] W. Jennings, E. Mittlefehldt, P. Stremple, *Analytical Gas Chromatography* Second ed., J & W Scientific Folsom, California, 1996.
- [136] E. De Hoffman, J. Charette, V. Stroobant, *Mass Spectrometry, Principles and Applications*, John Wiley & Sons Ltd, Chichester, UK, 1996.
- [137] K.L. Busch, G.L. Glish, S.A. McLuckey, *Mass Spectrometry/Mass Spectrometry: Techniques and Applications of Tandem Mass Spectrometry*, VCH Publishers, New York, USA, 1988.
- [138] V. Gómez, M.P. Callao, *TrAC Trends in Analytical Chemistry*, 25 (2006) 1006-1015.
- [139] J. Kenkel, *Analytical Chemistry for Technicians*, Lewis Publishers, Boca Raton, 1994.
- [140] X. Long, M. Miró, E.H. Hansen, *Anal. Chem.*, 77 (2005) 6032-6040.
- [141] D. Littlejohn, *Atomic Spectrometry Course (CH520)*, The University of Strathclyde, Glasgow UK, 2010.
- [142] L. Ebdon, E.H. Evans, A.S. Fisher, S.J. Hill, *An Introduction to Analytical Atomic Spectrometry*, John Wiley & Sons Ltd, Chichester, 1998.
- [143] C.B. Boss, K.J. Fredeen, *Concepts, Instrumentation and Techniques in Inductively Coupled Plasma Optical Emission Spectrometry*, 2nd ed., The Perkin-Elmer Corporation, USA, 1997.
- [144] T.J. Maning, W.R. Grow, *Inductively Coupled Plasma - Atomic Emission Spectrometry*, 1st ed., Springer-Verlag New York, 1997.
- [145] G.W. Dickinson, V.A. Fassel, *Anal. Chem.*, 41 (1969) 1021-1024.



- [146] P. Allain, Y. Mauras, *Anal. Chem.*, 51 (1979) 2089-2091.
- [147] T.J. Tredwell, *Handbook of Optics (Visible Array Detectors) Chapter 22*, The McGraw-Hill Companies, New York, 2004.
- [148] Y. Xia, R. Mokaya, *J. Mater. Chem.*, 14 (2004) 2507-2515.
- [149] C. Robertson, *Novel Mesoporous Silicates as Indoor Air Pollutant Scavengers*, in: Department of Pure and Applied Chemistry, University of Strathclyde, Glasgow, 2008.
- [150] S.A. Idris, C. Robertson, M.A. Morris, L.T. Gibson, *Analytical Methods*, 2 (2010) 1803-1809.
- [151] K.N. Brewer, R.S. Herbst, I.Y. Glagolenko, T.A. Todd, *Solvent Extr. Ion Exch.*, 16 (1998) 487-504.
- [152] T.-M. Wu, G.-R. Wu, H.-M. Kao, J.-L. Wang, *Journal of Chromatography A*, 1105 (2006) 168-175.
- [153] A.M. Burke, J.P. Hanrahan, D.A. Healy, J.R. Sodeau, J.D. Holmes, M.A. Morris, *J. Hazard. Mater.*, 164 (2009) 229-234.
- [154] M. Anbia, M. Lashgari, *Chem. Eng. J. (Lausanne)*, 150 (2009) 555-560.
- [155] J. Li, H. Wei, S. Guo, E. Wang, *Anal. Chim. Acta*, 630 (2008) 181-185.
- [156] M. Grün, K.K. Unger, A. Matsumoto, K. Tsutsumi, *Microporous Mesoporous Mater.*, 27 (1999) 207-216.
- [157] S. Inagaki, Y. Aratani, Y. Sekine, E. Kikuchi, M. Matsukata, *Rapid crystallization of Si-MCM-41 under Na-free conditions*, in: N.Ž. J. Čejka, P. Nachtigall (Eds.) *Stud. Surf. Sci. Catal.*, Elsevier, 2005, pp. 533-540.
- [158] X. Tang, S. Liu, Y. Wang, W. Huang, E. Sominski, O. Palchik, Y. Koltypin, A. Gedanken, *Chem. Commun. (Cambridge, U. K.)*, (2000) 2119-2120.
- [159] X. Liu, H. Sun, Y. Yang, *J. Colloid Interface Sci.*, 319 (2008) 377-380.
- [160] H. Ritter, M. Nieminen, M. Karppinen, D. Brühwiler, *Microporous Mesoporous Mater.*, 121 (2009) 79-83.
- [161] Y. Wan, D. Zhang, N. Hao, D. Zhao, *International Journal Nanotechnology*, 4 (2007) 66-99.
- [162] S.M. Evangelista, E. DeOliveira, G.R. Castro, L.F. Zara, A.G.S. Prado, *Surf. Sci.*, 601 (2007) 2194-2202.
- [163] A. Sayari, P. Liu, M. Kruk, M. Jaroniec, *Chem. Mater.*, 9 (1997) 2499-2506.

- [164] D. Méhn, Z. Kónya, J. Halász, J.B. Nagy, B. Rác, A. Molnár, I. Kiricsi, *Applied Catalysis A: General*, 232 (2002) 67-76.
- [165] J.S. Choi, D.J. Kim, S.H. Chang, W.S. Ahn, *Applied Catalysis A: General*, 254 (2003) 225-237.
- [166] M.C. Dujardin, C. Cazé, I. Vroman, *Reactive and Functional Polymers*, 43 (2000) 123-132.
- [167] B. Berglund, U. Berglund, G. Lindvall, Assignment of discomfort and irritation from the indoor air, in: *Indoor Air Quality (86)*, American Society of Heating, Refrigeration, and Air-conditioning Engineers, Atlanta, 1986, pp. 138-149.
- [168] D. Sevdíć, H. Meider, D. Pavković, *Solvent Extr. Ion Exch.*, 8 (1990) 643-658.
- [169] L. Møhlhave, G. Clausen, B. Berglund, J. De Ceaurriz, A. Kettrup, T. Lindvall, M. Maroni, A.C. Pickering, U. Risse, H. Rothweiler, B. Seifert, M. Younes, *Indoor Air*, 7 (1997) 225-240.
- [170] P. Pluschke, *The Handbook of Environmental Chemistry (Indoor air pollution)*, Springer, Berlin Heidelberg, 2004.
- [171] D. Crump, I. Madany, Daily variations of volatile organic compound concentrations in residential indoor air, in: *Proceedings of Indoor Air 93*, Helsinki, 1993, pp. 15-20.
- [172] P. Wolkoff, *Indoor Air*, 5 (1995) 5-73.
- [173] B. Seifert, D. Ullrich, *Atmospheric Environment* (1967), 21 (1987) 395-404.
- [174] A. Kumar, I. Víden, *Environmental Monitoring and Assessment*, 131 (2007) 301-321.
- [175] M.-L. Mattinen, J. Tuominen, K. Saarela, *Indoor Air*, 5 (1995) 56-61.
- [176] F.J. Santos, M.T. Galceran, D. Fraisse, *Journal of Chromatography A*, 742 (1996) 181-189.
- [177] S.K. Brown, M.R. Sim, M.J. Abramson, C.N. Gray, *Indoor Air*, 4 (1994) 123-134.
- [178] S. Li, S. Chen, L. Zhu, X. Chen, C. Yao, X. Shen, *Sci. Total Environ.*, 407 (2009) 2004-2011.
- [179] D. Pérez-Quintanilla, I.d. Hierro, M. Fajardo, I. Sierra, *J. Hazard. Mater.*, 134 (2006) 245-256.

- [180] R.D. Edwards, J. Jurvelin, K. Saarela, M. Jantunen, *Atmos. Environ.*, 35 (2001) 4531-4543.
- [181] Y. Tsuchiya, J. Kanabus-kaminska, Pilot study on indoor air quality (IRC-P-3001), in: NATO/CCMS (Committee on the Challenges of Modern Society), Quebec, 1990.
- [182] M.R. Winkle, P.A. Scheff, *Indoor Air*, 11 (2001) 49-64.
- [183] S.K. Brown, *Indoor Air*, 12 (2002) 55-63.
- [184] C.Y. Chao, G.Y. Chan, *Atmos. Environ.*, 35 (2001) 5895-5913.
- [185] Y.M. Kim, S. Harrad, R.M. Harrison, *Environ. Sci. Technol.*, 35 (2001) 997-1004.
- [186] S. Kubo, K. Kosuge, *Langmuir*, 23 (2007) 11761-11768.
- [187] J. Izumi, VOC Recovery Process, Mitsubishi Heavy Industries, Ltd., 1996.
- [188] T.-M. Wu, G.-R. Wu, H.-M. Kao, J.-L. Wang, *Journal of Chromatography A*, 1105 (2006) 168-175.
- [189] C.W. Purnomo, *Asean Journal of Chemical Engineering*, 7 (2007) 43-48.
- [190] M. Jaroniec, Design, Synthesis and Characterization of Ordered Mesoporous Materials for Environmental Applications Combined and Hybrid Adsorbents, in: J. Loureiro, M. Kartel (Eds.), Springer Netherlands, 2006, pp. 23-36.
- [191] R. Serna-Guerrero, A. Sayari, *Environ. Sci. Technol.*, 41 (2007) 4761-4766.
- [192] B.L. Newalkar, N.V. Choudary, U.T. Turaga, R.P. Vijayalakshmi, P. Kumar, S. Komarneni, T.S.G. Bhat, *Chem. Mater.*, 15 (2003) 1474-1479.
- [193] D.P. Serrano, G. Calleja, J.A. Botas, F.J. Gutierrez, *Ind. Eng. Chem. Res.*, 43 (2004) 7010-7018.
- [194] Q. Hu, J.J. Li, Z.P. Hao, L.D. Li, S.Z. Qiao, *Chem. Eng. J. (Lausanne)*, 149 (2009) 281-288.
- [195] Q. Hu, J. Li, S. Qiao, Z. Hao, H. Tian, C. Ma, C. He, *J. Hazard. Mater.*, 164 (2009) 1205-1212.
- [196] Y. An, J.S. Zhang, C.Y. Shaw, *International Journal of Heating, Ventilating, Air-Conditioning and Refrigerating Research*, 5 (1999) 297-316.
- [197] J.C.S. Chang, Z. Guo, *Indoor Air*, 4 (1994) 35-39.
- [198] S. Kirchner, P. Karpe, P. Rouxel, Adsorption/desorption processes of organic pollutants on indoor material areas, CSTB Report EAE/SB-96059, 1996.

- [199] B.A. Tichenor, Z. Guo, J.E. Dunn, L.E. Sparks, M.A. Mason, *Indoor Air*, 1 (1991) 23-35.
- [200] S. Lagergren, *Handlingar*, 24 (1898) 1-39.
- [201] H. Huang, F. Haghghat, P. Blondeau, *Indoor Air*, 16 (2006) 236-247.
- [202] R.L. Corsi, D. Won, M. Rynes, The interaction of VOCs and indoor materials: an experimental evaluation of adsorptive sinks and influencing factors, in: *Proceedings of Indoor Air'99*, 1999, pp. 390-395.
- [203] J. Zhang, J.S. Zhang, Q. Chen, Effects of environmental conditions on the VOC sorption by building materials, in: *ASHRAE Transactions*, 2002, pp. 273-282.
- [204] K. Kosuge, S. Kubo, N. Kikukawa, M. Takemori, *Langmuir*, 23 (2007) 3095-3102.
- [205] H. Martin, *Journal of Chromatography A*, 885 (2000) 129-151.
- [206] The Agency for Toxic Substances and Disease Registry (ATSDR), *ATSDR CEP Site Count Report*, 2007
- [207] R. Rubio, J. Huguet, G. Rauret, *Water Res.*, 18 (1984) 423-428.
- [208] M. Zougagh, A.G.a. de Torres, J.M. Cano Pavón, *Talanta*, 56 (2002) 753-761.
- [209] K. Jankowski, J. Yao, K. Kasiura, A. Jackowska, A. Sieradzka, *Spectrochimica Acta Part B: Atomic Spectroscopy*, 60 (2005) 369-375.
- [210] G.Z. Tsogas, D.L. Giokas, A.G. Vlessidis, *J. Hazard. Mater.*, 163 (2009) 988-994.
- [211] S.B. Sarmani, *Hydrobiologia*, 176-177 (1989) 233-238.
- [212] S. Obiri, *Environmental Monitoring and Assessment*, 130 (2007) 455-463.
- [213] H. Ciftci, H. Yalcin, E. Eren, A. Olcucu, M. Sekerci, *Desalination*, 256 (2010) 48-53.
- [214] Z. Dong, *Energy Procedia*, 11 (2011) 2953-2958.
- [215] O.D. Uluozlu, M. Tuzen, M. Soylak, *Food Chem. Toxicol.*, 47 (2009) 2601-2605.
- [216] C. Duran, A. Gundogdu, V.N. Bulut, M. Soylak, L. Elci, H.B. Sentürk, M. Tüfekci, *J. Hazard. Mater.*, 146 (2007) 347-355.
- [217] K.G. Bhattacharyya, S.S. Gupta, *Adv. Colloid Interface Sci.*, 140 (2008) 114-131.
- [218] P.K. Jal, S. Patel, B.K. Mishra, *Talanta*, 62 (2004) 1005-1028.

- [219] H.H. Tran, F.A. Roddick, J.A. O'Donnell, *Water Res.*, 33 (1999) 2992-3000.
- [220] K. Mohanty, D. Das, M. Biswas, *Adsorption*, 12 (2006) 119-132.
- [221] Z. Gu, B. Deng, J. Yang, *Microporous Mesoporous Mater.*, 102 (2007) 265-273.
- [222] X. Feng, G.E. Fryxell, L.-Q. Wang, A.Y. Kim, J. Liu, K.M. Kemner, *Science*, 276 (1997) 923-926.
- [223] Y.J. Chen, T.S. Hwang, X.H. Hwnag, H.K. Liao, C.H. Lin, Sialic Acid Synthase from *Escherichia coli* - Structural Characterization by Mass Spectrometry, *The Proceedings of the International Symposium on Biomolecular Chemistry*, Tokyo, 2003.
- [224] H. Yoshitake, T. Yokoi, T. Tatsumi, *Chem. Mater.*, 15 (2003) 1713-1721.
- [225] J. Kecht, A. Schlossbauer, T. Bein, *Chem. Mater.*, 20 (2008) 7207-7214.
- [226] Y.-H. Liu, H.-P. Lin, C.-Y. Mou, *Langmuir*, 20 (2004) 3231-3239.
- [227] H. Lee, J. Yi, *Sep. Sci. Technol.*, 36 (2001) 2433-2448.
- [228] H. Yang, R. Xu, X. Xue, F. Li, G. Li, *J. Hazard. Mater.*, 152 (2008) 690-698.
- [229] K. Wei, L. Shu, W. Guo, Y. Wu, X. Zeng, *Chin. J. Chem.*, 29 (2011) 143-146.
- [230] E. Da'na, N. De Silva, A. Sayari, *Chem. Eng. J. (Lausanne)*, 166 (2011) 454-459.
- [231] M.V. Lombardo, M. Videla, A. Calvo, F.G. Requejo, G.J.A.A. Soler-Illia, *J. Hazard. Mater.*, in press.
- [232] D. Pérez-Quintanilla, I. del Hierro, M. Fajardo, I. Sierra, *Microporous Mesoporous Mater.*, 89 (2006) 58-68.
- [233] Y.-K. Lu, X.-P. Yan, *Anal. Chem.*, 76 (2003) 453-457.
- [234] M. Anbia, M. Lashgari, *Chem. Eng. J. (Lausanne)*, 150 (2009) 555-560.
- [235] G. Grigoropoulou, P. Stathi, M.A. Karakassides, M. Louloudi, Y. Deligiannakis, *Colloids and Surfaces A: Physicochemical and Engineering Aspects*, 320 (2008) 25-35.
- [236] A. Benhamou, M. Baudu, Z. Derriche, J.P. Basly, *J. Hazard. Mater.*, 171 (2009) 1001-1008.
- [237] S. Wu, F. Li, R. Xu, S. Wei, G. Li, *Journal of Nanoparticle Research*, 12 (2010) 2111-2124.
- [238] S. Chiarle, M. Ratto, M. Rovatti, *Water Res.*, 34 (2000) 2971-2978.

- [239] S.K. Fiskum, B.M. Rapko, G.J. Lumetta, *Solvent Extr. Ion Exch.*, 19 (2001) 643-657.
- [240] I.L. Lagadic, M.K. Mitchell, B.D. Payne, *Environ. Sci. Technol.*, 35 (2001) 984-990.
- [241] D. Mohan, V.K. Gupta, S.K. Srivastava, S. Chander, *Colloids and Surfaces A: Physicochemical and Engineering Aspects*, 177 (2000) 169-181.
- [242] S.A. Idris, O.A. Mkhathresh, F. Heatley, *Polymer International*, 55 (2006) 1040-1048.
- [243] J.W. Patterson, R. Passino, *Metals Speciation Separation and Recovery*, Lewis Publishers, New York, 1990.
- [244] Y. Terashima, H. Ozaki, M. Sekine, *Water Res.*, 20 (1986) 537-545.
- [245] K.A. Larson, J.M. Wiencek, *Ind. Eng. Chem. Res.*, 31 (1992) 2714-2722.
- [246] M. Yu, W. Tian, D. Sun, W. Shen, G. Wang, N. Xu, *Anal. Chim. Acta*, 428 (2001) 209-218.
- [247] A. Walcarius, C. Delacôte, *Anal. Chim. Acta*, 547 (2005) 3-13.
- [248] A. Arencibia, J. Aguado, J.M. Arsuaga, *Appl. Surf. Sci.*, 256 (2010) 5453-5457.
- [249] B. Lee, Y. Kim, H. Lee, J. Yi, *Microporous Mesoporous Mater.*, 50 (2001) 77-90.
- [250] M.A. Ebadian, Marshall Allen and Yong Cai, *Mercury Contaminated Material Decontamination Methods*. HCET Final Report U.S.E.P.A. HCT-2000-D053-002-04.
- [251] L. Mercier, T.J. Pinnavaia, *Environ. Sci. Technol.*, 32 (1998) 2749-2754.
- [252] A.R. Cestari, E.F.S. Vieira, E.C.N. Lopes, R.G. da Silva, *J. Colloid Interface Sci.*, 272 (2004) 271-276.
- [253] E.F.S. Vieira, A.R. Cestari, A.S.J. de, C. Airoidi, *Thermochim. Acta*, 328 (1999) 247-252.
- [254] Z.-H. Wang, M. Song, Q.-L. Ma, H.-M. Ma, S.-C. Liang, *Microchim. Acta*, 134 (2000) 95-99.
- [255] Á. Béni, R. Karosi, J. Posta, *Microchem. J.*, 85 (2007) 103-108.
- [256] H.F. Maltez, E. Carasek, *Talanta*, 65 (2005) 537-542.
- [257] S. Pramanik, S. Dey, P. Chattopadhyay, *Anal. Chim. Acta*, 584 (2007) 469-476.

- [258] M. Tuzen, M. Soylak, *J. Hazard. Mater.*, 147 (2007) 219-225.
- [259] L. Wang, B. Hu, Z. Jiang, Z. Li, *Int. J. Environ. Anal. Chem.*, 82 (2002) 387–393.
- [260] P. Gopi Krishna, J. Mary Gladis, U. Rambabu, T. Prasada Rao, G.R.K. Naidu, *Talanta*, 63 (2004) 541-546.
- [261] P.M. Paquet, J.-F. Gravel, P. Nobert, D. Boudreau, *Spectrochimica Acta Part B: Atomic Spectroscopy*, 53 (1998) 1907-1917.
- [262] D. Park, Y.-S. Yun, J.M. Park, *Ind. Eng. Chem. Res.*, 45 (2006) 2405-2407.
- [263] D. Mohan, K.P. Singh, V.K. Singh, *Ind. Eng. Chem. Res.*, 44 (2005) 1027-1042.
- [264] D. Petruzzelli, R. Passino, G. Tiravanti, *Ind. Eng. Chem. Res.*, 34 (1995) 2612-2617.
- [265] D. Zhao, A.K. SenGupta, L. Stewart, *Ind. Eng. Chem. Res.*, 37 (1998) 4383-4387.
- [266] G.M. Haggerty, R.S. Bowman, *Environ. Sci. Technol.*, 28 (1994) 452-458.
- [267] Z. Li, R.S. Bowman, *Environ. Sci. Technol.*, 32 (1998) 2278-2282.
- [268] B.S. Krishna, D.S.R. Murty, B.S. Jai Prakash, *Appl. Clay Sci.*, 20 (2001) 65-71.
- [269] S.A. Khan, R. Riaz ur, M.A. Khan, *Waste Management*, 15 (1995) 271-282.
- [270] L. Mercier, C. Detellier, *Environ. Sci. Technol.*, 29 (1995) 1318-1323.
- [271] M. Ghiaci, R. Kia, A. Abbaspur, F. Seyedeyn-Azad, *Sep. Purif. Technol.*, 40 (2004) 285-295.
- [272] P. Delaney, R.M. Healy, J.P. Hanrahan, L.T. Gibson, J.C. Wenger, M.A. Morris, J.D. Holmes, *J. Environ. Monit.*, 12 (2010) 2244-2251.
- [273] J. Qiu, Z. Wang, H. Li, L. Xu, J. Peng, M. Zhai, C. Yang, J. Li, G. Wei, *J. Hazard. Mater.*, 166 (2009) 270-276.
- [274] D. Pérez-Quintanilla, I. del Hierro, M. Fajardo, I. Sierra, *Mater. Res. Bull.*, 42 (2007) 1518-1530.
- [275] J. Li, X. Miao, Y. Hao, J. Zhao, X. Sun, L. Wang, *J. Colloid Interface Sci.*, 318 (2008) 309-314.
- [276] N. Shevchenko, V. Zaitsev, A. Walcarius, *Environ. Sci. Technol.*, 42 (2008) 6922-6928.

- [277] H.-J. Park, L.L. Tavlarides, *Ind. Eng. Chem. Res.*, 47 (2008) 3401-3409.
- [278] Y. Ho, G. McKay, D. Wase, C. Foster, *Adsorption Science and Technology* 18 (2000) 639-650.
- [279] W. Weber, J. Morris, *Am. Soc. Civ. Eng.*, 89 (1963) 31-60.
- [280] I. Langmuir, *J. Am. Chem. Soc.*, 40 (1918) 1361-1403.
- [281] J.-u.-R. Memon, S.Q. Memon, M.I. Bhangar, M.Y. Khuhawar, *J. Hazard. Mater.*, 163 (2009) 511-516.
- [282] G. Purna Chandra Rao, S. Satyaveni, A. Ramesh, K. Seshaiyah, K.S.N. Murthy, N.V. Choudary, *Journal of Environmental Management*, 81 (2006) 265-272.
- [283] G. Zolfaghari, A. Esmaili-Sari, M. Anbia, H. Younesi, S. Amirmahmoodi, A. Ghafari-Nazari, *J. Hazard. Mater.*, 192 (2011) 1046-1055.
- [284] J. Pan, X. Zou, X. Wang, W. Guan, Y. Yan, J. Han, *Chem. Eng. J. (Lausanne)*, 162 (2010) 910-918.
- [285] A.K. Bhattacharya, T.K. Naiya, S.N. Mandal, S.K. Das, *Chem. Eng. J. (Lausanne)*, 137 (2008) 529-541.
- [286] N.K. Hamadi, X.D. Chen, M.M. Farid, M.G.Q. Lu, *Chem. Eng. J. (Lausanne)*, 84 (2001) 95-105.
- [287] J. Coates, *Interpretation of Infrared Spectra, A Practical Approach*, in: *Encyclopedia of Analytical Chemistry*, John Wiley & Sons Ltd, Chichester, 2000, pp. 10815–10837.
- [288] N.I. Kapakoglou, D.L. Giokas, G.Z. Tsogas, A.G. Vlessidis, *Anal. Chem.*, 80 (2008) 9787-9796.
- [289] C.V.J. Skipper, A. Hamaed, D.M. Antonelli, N. Kaltsoyannis, *Journal of the American Chemical Society*, 132 (2010) 17296-17305.
- [290] V.K. Gupta, M. Gupta, S. Sharma, *Water Res.*, 35 (2001) 1125-1134.
- [291] B. Sushanta, I. Aminul, B. Snigdha, *The Regulatory Roles of Estrogen in Carcinogenesis*, in: *Phytopharmaceuticals in Cancer Chemoprevention*, CRC Press, 2004.
- [292] Y. Huang, X. Ma, G. Liang, Y. Yan, S. Wang, *Chem. Eng. J. (Lausanne)*, 138 (2008) 187-193.
- [293] C.-H. Weng, Y.C. Sharma, S.-H. Chu, *J. Hazard. Mater.*, 155 (2008) 65-75.
- [294] J. Zolgharnein, A. Shahmoradi, *J. Chem. Eng. Data*, 55 (2010) 3428-3437.



- [295] A. Sari, M. Tuzen, *Sep. Sci. Technol.*, 43 (2008) 3563-3581.
- [296] S. Debnath, U.C. Ghosh, *The Journal of Chemical Thermodynamics*, 40 (2008) 67-77.
- [297] P. Yuan, M. Fan, D. Yang, H. He, D. Liu, A. Yuan, J. Zhu, T. Chen, *J. Hazard. Mater.*, 166 (2009) 821-829.
- [298] P. Yuan, D. Liu, M. Fan, D. Yang, R. Zhu, F. Ge, J. Zhu, H. He, *J. Hazard. Mater.*, 173 (2010) 614-621.
- [299] D.D. Maksin, A.B. Nastasović, A.D. Milutinović-Nikolić, L.T. Suručić, Z.P. Sandić, R.V. Hercigonja, A.E. Onjia, *J. Hazard. Mater.*, 209–210 (2012) 99-110.
- [300] N. Li, X.-M. Lei, *J. Inclusion Phenom. Macrocyclic Chem.*, (2012) 1-10.
- [301] M. Cieślak-Golonka, M. Daszkiewicz, *Coord. Chem. Rev.*, 249 (2005) 2391-2407.
- [302] P. Gili, P.A. Lorenzo-Luis, *Coord. Chem. Rev.*, 193–195 (1999) 747-768.
- [303] F. Brito, J. Ascanio, S. Mateo, C. Hernández, L. Araujo, P. Gili, P. Martín-Zarza, S. Domínguez, A. Mederos, *Polyhedron*, 16 (1997) 3835-3846.
- [304] M.R. Sundberg, J. Valo, R. Uggla, M. Melnik, *Inorg. Chim. Acta*, 383 (2012) 164-168.
- [305] J. Coates, *Interpretation of Infrared Spectra, A Practical Approach*, in: *Encyclopedia of Analytical Chemistry*, John Wiley & Sons, Ltd, 2006.

## **Publications from this work**

There are seven papers will be published from this work. Three are already published:

[1] S.A. Idris, C. Robertson, M.A. Morris, L.T. Gibson, A comparative study of selected sorbents for sampling of aromatic VOCs from indoor air, *Analytical Methods*, 2 (2010) 1803-1809.

[2] S.A. Idris, C.M. Davidson, C. McManamon, M.A. Morris, P. Anderson, L.T. Gibson, Large pore diameter MCM-41 and its application for lead removal from aqueous media, *Journal of Hazardous Materials*, 185 (2011) 898-904.

[3] S.A. Idris, S.R. Harvey, L.T. Gibson, Selective extraction of mercury(II) from water samples using mercapto functionalised-MCM-41 and regeneration of the sorbent using microwave digestion, *Journal of Hazardous Materials*, 193 (2011) 171-176.

### **Two papers have been already submitted:**

[1] Salah A. Idris, Khalid M. Alotaibi, Michael A. Morris and Lorraine T. Gibson, Effect of pore size distribution of mesoporous silica materials on extracting hexavalent chromium from water samples.

[2] Salah A. Idris, Khalid Alotaibi, Tanya A. Peshkur, Peter Anderson and Lorraine T. Gibson, Preconcentration and selective extraction of chromium species in water samples using amino modified mesoporous silica.

### **Two papers are under preparation:**

[1] Salah A. Idris, Khalid Alotaibi, Tanya A. Peshkur, Peter Anderson M. Morris and Lorraine T. Gibson, Adsorption kinetics for the removal of hexavalent chromium from aqueous solutions: investigation in affecting pore size distribution of mesoporous silicate on the rate of chromium (VI) uptake.

[2] The last paper will discuss the preparation method in this thesis for MWD-MCM-41 and the ability for the first time to tune the pore size and pore size distribution by using microwave digestion. This paper will be submitted to one of the high impact factor journal as novel material has produced.